The structural organisation of collagen in the corneas of primates and other mammals and the stromal changes associated with the disease keratoconus.

Thesis submitted to Cardiff University, University of Wales
for the degree of

Doctor of Philosophy
in the discipline of Biophysics

Sally Hayes (BSc)

The Structural Biophysics Group,
School of Optometry and Vision Sciences,
Cardiff University
2005

ProQuest LLC
789 East Eisenhower Parkway
P.O. Box 1346
Ann Arbor, MI 48106-1346

Acknowledgements

There are many people that I would like to thank for their help and support during the course of my PhD. In particular, I wish to thank my co-supervisors, Keith Meek and Andrew Quantock, for their exciting project ideas, their constant enthusiasm and their easily approachable manner. I am also extremely grateful to Craig Boote for his patience and friendship whilst teaching me the principles of x-ray diffraction and also for his help in analysing the data.

I must also thank the staff at the Synchrotron Radiation Source (Daresbury, UK), especially Gunter Grossman, Mike Mc Donald, Steve Buffy and Robert Kehoe, for their kind assistance during data collection.

I greatly appreciate the help of Stephen Tuft (Moorfields Eye Hospital, London), Yifei Huang (Great Wall Hospital, Beijing), Nick Hawksworth (Royal Glamorgan Hospital), Val Smith (Bristol Eye Bank), Tom Kelly (Manchester Eye Hospital), Arun Brahma (Manchester Eye Hospital), Beatrice Yue (University of Illinois), Masayoshi Tachibana (Kyoto Prefectural University) and Stuart Judge (Oxford University), for providing me with tissue samples required for my research.

I am also grateful to Jemma Finlayson, a final year degree student who during the course of her research project, assisted in the preparation of specimens and the collection of the data presented in Chapter 4. In addition, I would like to thank Richard Newton and Hina Puri for their contribution to the collection of the human x-ray diffraction data shown in Chapter 3.

Finally, I would like to thank my friends, my family and my husband Enda, for their constant support, motivation and encouragement throughout the course of my study.

Summary

X-ray diffraction was used to determine the ultrastructural arrangement of collagen in the normal human, monkey and bovine cornea. Using the same technique, the ultrastructural organisation of collagen in human keratoconus corneal buttons and in the corneas of mice with a murine specific keratopathy (SKC), in which the males develop a cone shaped cornea, was also examined.

Collagen fibrils were found to be most closely packed in the prepupillary region of the normal human cornea, suggesting an optimisation of tissue strength and transparency in the main optical zone. In humans and marmoset monkeys, fibril size and interfibrillar spacing increased rapidly at the limbus to provide additional tensile strength at the point where the cornea meets the less curved sclera.

A difference in the preferred orientation of collagen fibrils was observed between human and bovine corneas. Throughout the human corneal stroma, (and predominantly in the posterior stroma), collagen fibrils are preferentially aligned in the superior-inferior and nasal-temporal directions; this alignment coincides with the insertion points of the rectus muscles. The proportion of aligned collagen mass (relative to the total collagen mass), which increases in all four quadrants of the peripheral human cornea, is highest in the superior-nasal and inferior-temporal regions, revealing a symmetry between the left and right cornea in terms of collagen mass distribution.

Abnormalities in collagen orientation and mass distribution were seen in the majority of keratoconus corneal buttons examined. A relationship between the size and shape of the cone and the extent of the structural alterations was seen in some cases; however a large variation existed between corneas. These results are consistent with a theoretical mechanism of keratoconus progression which involves enzyme action and inter-fibrillar and inter-lamellar slippage.

Examination of the structural organisation of collagen in SKC mice corneas, revealed the strain to be an unsuitable model for studying human keratoconus.

Chapter 1. Introduction

Using X-ray diffraction (XRD) as the main method of data collection, this thesis examines in detail the structural organisation of collagen fibrils in the stroma of normal human, monkey, bovine and mouse cornea and investigates the extent to which the normal arrangement is altered in the human disease keratoconus and also in a murine specific keratopathy, that in some ways mimics keratoconus. This thesis also aims to form a link between structural alterations and specific keratoconus shape changes by examining XRD data alongside videokeratographic images of corneal shape.

1.1 Structure and function of the cornea

The outer tunic of the eye is made up of a transparent cornea (7%) and an opaque sclera (93%) (Figure 1.1). The cornea is a highly organised group of cells and proteins, which, due to the absence of any blood vessels, obtains its nourishment from both the aqueous humour in the chamber behind it and from the tear film covering its anterior surface. The absence of blood vessels is crucial for corneal transparency as it enables light to be transmitted onto the retina with minimum scattering, so producing a clear image.

To function efficiently the cornea must be tough enough to withstand external damage and to resist intraocular pressure. It must also be of a sufficient curvature to refract incoming light onto the retina; the cornea is responsible for about 70% of the refractive power of the eye, the remainder is performed by the lens.

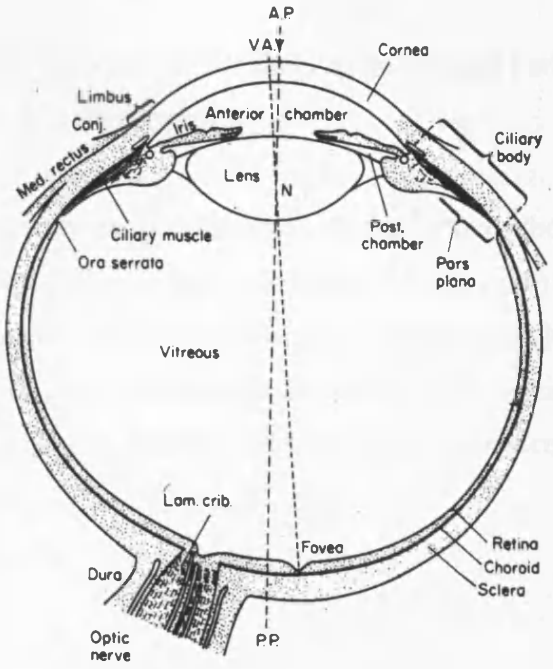

Figure 1.1. Cross section of the human eye. The posterior pole (PP), anterior pole (AP) and visual axis (VA) are labelled. Reproduced from Wolfe (1968).

An adult human cornea is approximately 11.7mm horizontally by 10.6mm vertically and 0.52mm thick in the central region, increasing slightly towards the limbus (Hogan *et al.* 1971). Due to the change in tissue thickness across the cornea, the anterior surface has a higher radius of curvature (typically 7.7mm) than the posterior surface (typically 6.9mm) (Snell and Lemp 1998).

The elliptical anterior profile of the cornea is due to the greater extension of limbal tissue in the superior and inferior aspects of the anterior cornea. However, the posterior central edge of the limbus presents a circular profile of diameter 11.7mm (Hogan *et al.* 1971). The structure of the limbus is discussed in Section 1.8.

The central third of the cornea, commonly referred to as the prepupillary region or the corneal cap, is considered to be the optical zone (Waring III 1989) and is responsible for most of the cornea's refractive power. The remaining peripheral cornea is less curved and serves mainly as a refractive surface for peripheral vision. The prepupillary region of the cornea has a radius of curvature of between 7.2 and 7.8mm; this increases in the peripheral region as the cornea flattens towards the limbus (Saude

1993). Figure 1.2 schematically shows the prepupillary and peripheral regions of the cornea as well as the posterior limbal region.

For anatomic purposes the peripheral cornea can be further subdivided into two concentric zones: the paracentral zone (or mid-peripheral zone) and the perilimbal zone (or peripheral zone). The paracentral zone forms an annulus of approximately 4-8mm in diameter. The perilimbal zone is an annulus of approximately 9-11mm in diameter and is the region of greatest flattening in the normal cornea (Waring III 1989).

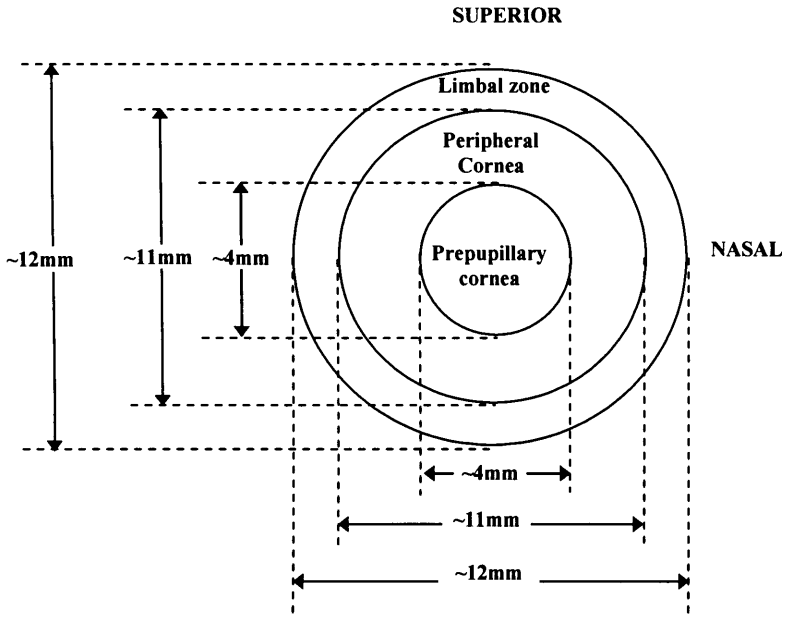

Figure 1.2. Conventional designation of the prepupillary, peripheral and posterior limbal zones of the human cornea. Adapted from Waring III (1989).

Figure 1.3 shows the five distinct layers that make up the mammalian cornea. From anterior to posterior the layers are:

- Epithelium - comprises about 10% of corneal thickness (50-60μm) and consists of 5-6 organised cell layers (columnar basal cells, wing cells and flattened surface cells). The epithelium is continuous with the conjunctiva at the limbus and forms

a protective layer against external damage and bacterial ingress, whilst also providing a smooth surface for optimal light transmission and nutrient absorption. A pre-corneal tear film which consists of a lipid layer, an aqueous layer and a mucin layer, coats the outer surface of the cornea.

- Bowman's layer – an acellular layer (8-12μm thick) which is secreted by the epithelium. Bowman's layer, which terminates at the limbus, consists of fine randomly arranged collagen fibrils (20-30nm diameter) and offers resistance to trauma and deformation. It has been suggested that the insertion of some anterior stromal lamellae into Bowman's layer may play a role in maintaining the shape and stability of the anterior corneal surface (Bron 2001; Muller *et al.* 2001).

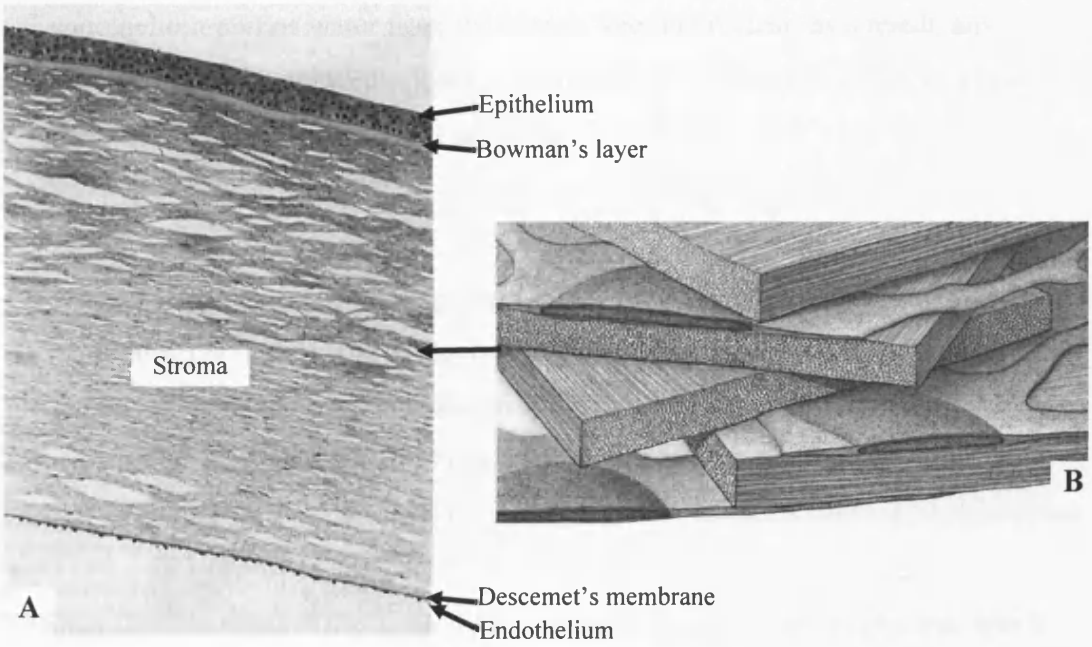

Figure 1.3. Full thickness view of the cornea as seen by light microscopy (A) and a schematic diagram showing the arrangement of lamellae and keratocytes within the stroma. Adapted from Smith *et al.* (2002).

- Stroma - the thickest of the layers (measuring 500μm), it comprises 90% of the total corneal thickness. Consisting of water (78%), collagen (15%), other proteins (5%), proteoglycans (1%) and salts (1%) (Maurice 1984), it provides the cornea with strength, elasticity and form. Collagen fibrils of uniform diameter lie parallel

to each other in layers (lamellae) which are parallel to the surface of the cornea and form approximate right angles between fibres of successive lamellae. In the peripheral cornea there are approximately 500 of these layers whilst in the central cornea there are far fewer (approximately 300) (Hamada 1974). As this thesis is concerned solely with stromal ultrastructure it will be discussed in more detail at a later stage.

- Descemet's Membrane - the basement membrane (8-12μm thick) of the endothelium. It consists of glycoproteins and collagen.

- Endothelium – a single mosaic layer (18-20 μm thick) of simple squamous cells. The endothelium acts as a semi-permeable membrane, through which nutrients are absorbed from the aqueous humour and waste products are removed. The endothelium pumps water from the cornea, keeping it clear; as a result, any damage to this layer rapidly leads to corneal swelling and subsequently a loss of tissue transparency (Steimke *et al.* 1992).

1.2 Ultrastructure of the corneal stroma

As mentioned previously, the corneal stroma consists primarily of water; however of the dry components the protein collagen is the most abundant. Collagen provides the cornea with the strength needed to resist intraocular pressure and maintain correct corneal curvature for optimal light refraction.

The non-fibrillar extra-cellular matrix is composed mainly of proteoglycans, which play an important role in maintaining the hydration, ultrastructure and transparency of the cornea.

1.2.1 Collagen

Collagens are a family of proteins that constitute a quarter of the total protein in mammalian tissue and form 71% of the dry weight of the cornea (Miller and Gay 1982). The function and location of various types of collagen is highly specific due to

their chemical and structural differences; it is these differences that enable collagen types to be grouped according to their characteristics.

Some types of collagen, such as IV, VI and VII are non-fibril forming whilst others, including XII and XIV are collectively referred to as fibril-associated collagens with interrupted triple helices (FACIT collagens). Another group of collagens exist which take the form of fibrils (such as Types I, II, III and V) and interact at their surface with other non-fibril forming and FACIT collagens. Despite the differences between collagen types, they all share the same triple-helix structure which is composed of three polypeptides of amino acid sequences rich in either proline or hydroxyproline and with glycine as every third residue.

Type I collagen is a major component in both the cornea (68% of dry weight) and the sclera (50-70% of dry weight) (Maurice 1984) and provides the tissues with strength. Type V collagen accounts for approximately 10% of the dry weight of the cornea (Newsome *et al.* 1982) and has been implicated in the maintenance of collagen fibril diameter (Birk *et al.* 1986). The distribution of collagen types within the mammalian cornea are summarised in Table 1.

Collagen Types	Bowman's layer	Stroma	Descemet's membrane
I	+ve Ben-Zvi *et al.* (1986) - ve Nakayasu *et al.* (1986)	Ben-Zvi *et al.* (1986); Marshall *et al.* (1991b); Nakayasu *et al.* (1986)	
III	+ve Marshall *et al.* (1991b) -ve Ben-Zvi *et al.* (1986)	Ben-Zvi *et al.* (1986); Marshall *et al.* (1991b); Nakayasu *et al.* (1986)	
IV	Ben-Zvi *et al.* (1986); Nakayasu *et al.* (1986)		Nakayasu *et al.* (1986)
V	Marshall *et al.* (1991a)	Nakayasu *et al.* (1986); Tsuchiya *et al.* (1986)	
VI	Marshall *et al.* (1991a)	Marshall *et al.* (1991a)	+ve Marshall *et al.* (1991a) -ve Zimmermann *et al.* (1986)
VIII			Sawada *et al.* (1990)
XII		Wessel *et al.* (1997)	
XIII		Sandberg-Lall *et al.* (2000)	
XVII	Lin *et al.* (2001)		Lin *et al.* (2001)

Table 1. The distribution of collagen types in the human cornea. Discrepancies between studies regarding the presence of various collagen types are indicated (present (+ve), absent (-ve)).

Striated collagen fibrils (such as Type I) are formed by an extra cellular assembly of tropocollagen molecules. The triple stranded helices of tropocollagen, each consisting of three pro-α chains, are formed within the cell, after which they are packaged into secretory vesicles and released into the extra cellular environment to undergo a process of proteolytic conversion to form collagen (1.4).

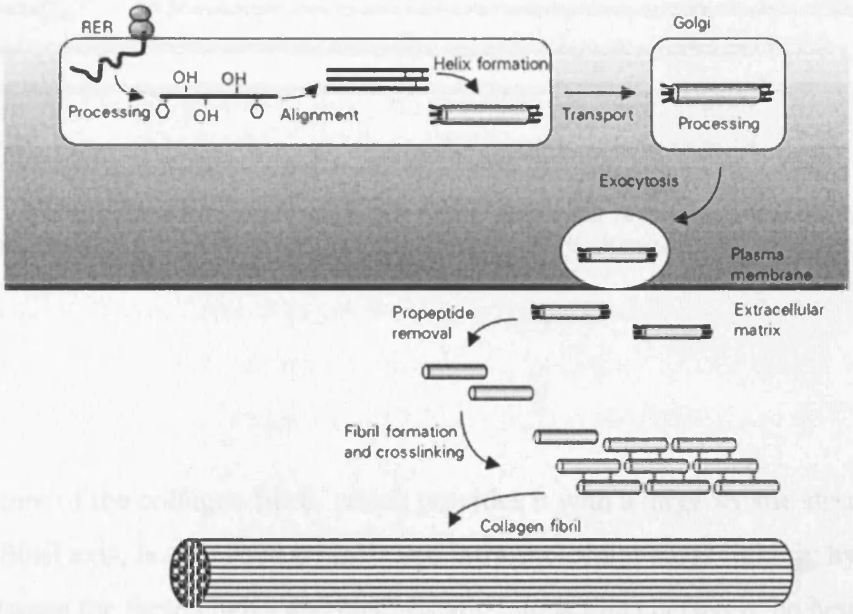

Figure 1.4. Biosynthesis of fibrillar collagens. Modifications of the procollagen peptide in the rough endoplasmic reticulum (RER) include hydroxylation, glycosylation, and disulfide bond formation. Interchain disulfide bonds between the C-terminal peptides align the three chains and initiate formation of the triple helix. The process propagates towards the N-terminus of the molecule end. N-linked oligosaccharides are transferred to the propeptides in the RER and processed in the Golgi apparatus. Upon secretion, propeptides are cleaved, allowing lateral alignment and cross linking. Reproduced from Michelacci (2003).

The specific staggered arrangement of triple-helical molecules in fibrillar collagen gives rise to a striking 67nm pattern of banding (Figure 1.5). Scleral collagen exhibits this 67nm D-period (Yamamoto *et al.* 2000); however, a lower D-period of 65nm is seen in corneal collagen (Marchini *et al.* 1986; Meek *et al.* 1981). The reason for the lower D-periodicity in corneal collagen is thought to be due to the slight tilt of the

corneal collagen molecules with respect to the fibril axis (Bigi and Roveri 1991; Marchini *et al.* 1993).

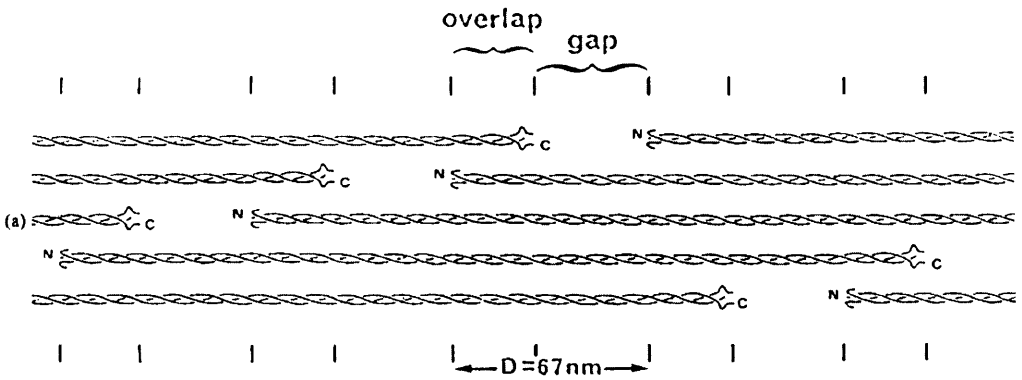

Figure 1.5. Axial structure of D-periodic collagen fibrils. Schematic representation of the axial packing arrangement of triple helical collagen molecules in a fibril. Reproduced from Chapman *et al.* (1990).

The structure of the collagen fibril, which provides it with a large tensile strength along its fibril axis, is stabilised by inter and intra-molecular cross linking, hydrogen bonds between the three chains and electrostatic interactions between the helices (Comper 1996; Hay 1981).

1.2.2 Proteoglycans

Proteoglycans consist of glycosaminoglycans attached to a relatively small protein core. Glycosaminoglycans are highly sulphated acid mucopolysaccharides that give the proteoglycans an overall negative charge. The implications of their negative charge on corneal hydration are briefly discussed in Section 1.4.

The most common glycosaminoglycans in the cornea are keratan sulphate (about 65%), chondroitin-4-sulphate and dermatan sulphate (Soriano *et al.* 2000; Axelsson and Heinegard 1978). Keratan sulphate binds to three separate protein cores to form three unique proteoglycans: lumican (Blochberger *et al.* 1992), keratocan (Corpuz *et*

al. 1996) and mimecan (Funderburgh *et al.* 1997). Chondroitin sulphate and dermatan sulphate, which are structurally very similar, bind with a protein core to form the most common proteoglycan in the cornea, decorin (Li *et al.* 1992).

Proteoglycans interact with collagen at specific sites along the fibril; dermatan sulphate is located in the gap region and keratan sulphate in the overlap region (Meek *et al.* 1986; Scott and Haigh 1985b).

Experimental evidence indicates that keratan sulphate proteoglycans are involved in the regulation of both collagen fibril diameter (Tasheva *et al.* 2002) and inter-fibrillar spacing (IFS) (Borcherding *et al.* 1975) and therefore play an important role in maintaining corneal transparency (Borcherding *et al.* 1975; Rada *et al.* 1993). Evidence for this is provided by the increased levels of keratan sulphate during the development of corneal transparency in chick corneas (Coulombre and Coulombre 1958) and also the absence of keratan sulphate (accompanied by changes in chondroitin sulphate and dermatan sulphate) in opaque corneal scar tissue (Cintron *et al.* 1990; Hassell *et al.* 1983). The development of corneal clouding in mice bred with a lumican null mutation further highlights the importance of keratan sulphate proteoglycans in the maintenance of corneal transparency (Chakravarti *et al.* 2000; Quantock *et al.* 2001).

1.3 Corneal transparency

Transparency is an essential property of the cornea, as without it blindness occurs. Over the years, many theories for corneal transparency have been suggested; one of the most basic theories attempted to explain the minimal light scatter in the cornea in terms of a uniform refractive index of all of the corneal components (Leber 1903). However, present knowledge of corneal ultrastructure and the discovery that corneal collagen fibrils have a higher refractive index than the surrounding matrix (Aurell and Holmgren 1953; Bettleheim and Kumbar 1977; Leonard and Meek 1997; McCally and Farell 1982), has since ruled out this theory.

In 1946, with no evidence to support the theory, Cassperson and Engstrom suggested that corneal transparency may be due to the presence of narrow fibres positioned in a regular arrangement. Maurice (1957) later revisited the theory and calculated the light scattering from individual fibrils based on the idea that a lattice arrangement of fibrils act as a diffraction grating. His calculations showed that the regular arrangement of uniformally narrow collagen fibrils in the cornea results in a destructive interference of the light scattered by individual fibrils and as the centre-to-centre spacing of the collagen fibrils is less than the wavelength of visible light, destructive interference occurs in all directions. In this way light passes solely along the primary visual axis and the cornea is transparent.

Goldman and Benedek (1967) questioned the lattice theory of transparency on the basis that it failed to explain the transparency of the dog fish cornea. They found that in the central zone of the dog fish cornea, Bowman's layer occupied 15% of the total thickness of the cornea and within this layer the fibres were neither parallel nor arranged in a lattice and yet it scattered less light than the rest of the corneal stroma. As a result of their findings, they concluded that a lattice arrangement of collagen fibrils was not essential for corneal transparency and that the transparency of Bowman's layer was due to a uniformity of fibril diameters and interfibrillar spacing over distances of approximately half the wavelength of light. In support of this, Hart and Farrell (1969) went on to mathematically prove that for the cornea to be transparent the fibrils don't need to be as regularly spaced as Maurice had originally thought. They proposed instead that only a short-range order of collagen fibrils was necessary for transparency.

A uniform spacing of collagen fibrils (approximately 57nm in the central cornea (Boote *et al.* 2003 - Appendix 4)) is not the only factor required for corneal transparency; fibril diameter is also of great importance. During the early stages of development, both the cornea and sclera are translucent and their constituent collagen fibrils are of a similar diameter. Later in development, the fibril diameter of scleral collagen rapidly increases and the tissue becomes opaque (Smelser 1960). The cornea remains transparent as the collagen fibrils maintain a uniform diameter (approximately 31nm (Boote *et al.* 2003 - Appendix 4; Meek and Leonard 1993)) and

are smaller than the 500nm wavelength of light (Farrell *et al.* 1973). In the congenital disease sclerocornea, the cornea appears opaque (like the sclera) due to the presence of collagen fibrils that are larger and more variable in size than those present in the normal transparent cornea (Kanai *et al.* 1971; Kenyon 1975). Corneal opacity also occurs as a consequence of corneal scarring due to the larger diameter of scar tissue collagen (Jakus 1962; Schwartz and Graf-Keyserlingk 1969) and the poor organisation of fibrillar collagen in the regenerated stroma (Connon *et al.* 2003; Quantock *et al.* 1994; Rawe *et al.* 1994). In 2-week-old scars the proteoglycans are considerably larger than normal and chondroitin sulphate is the predominant glycosaminoglycan synthesised, with the synthesis of keratan sulphate being minimal (Hassell *et al.* 1983). It has been suggested that the high levels of chondroitin sulphate and hyaluronic acid may be responsible for the high water content in 2-week-old scar tissue (Hassell *et al.* 1983), which combined with the larger than normal proteoglycans likely contribute to the increased IFS observed in scar tissue. Recently the direct summation of fields method was used to predict the light scattering from structures depicted by transmission electron microscopy in semi-transparent scars of wounded rabbit corneas. The results showed that the altered arrangement of stromal lamellae in the scar tissue and the presence of collagen-free areas (named 'lakes') were largely responsible for the loss of corneal transparency (McCally *et al.* 2005).

The first attempt to model the effect of altered collagen fibril packing on corneal haze development following penetrating keratoplasty was made by Connon and colleagues (2003) using XRD data, electron microscopy measurements and the direct summation of fields method. The direct summation of fields method revealed that in rabbit corneas subjected to phototherapeutic keratoplasty, with high levels of corneal haze, the wider spacing and disorganisation of collagen fibrils was not the cause of the increased light scattering. In support of this, there is evidence to suggest that the development of corneal haze in humans following phototherapeutic keratoplasty is due primarily to an increased cellular backscatter from the keratocytes present in the stroma (Moller-Pedersen 2004; Moller-Pedersen *et al.* 1998).

Transparency is also lost when the tissue becomes swollen, due to the disordering of the fibrillar arrangement and the formation of 'lakes', which cause increased light

scatter (Benedek 1971; Meek *et al.* 2003b - Appendix 5). Lakes, which are not present in the normal cornea but are found in Fuchs's dystrophy corneas, may be caused by matrix disorder and the presence of dead cells. The direct summation of fields method, when applied to a normal cornea and a Fuchs dystrophy cornea (at an above physiological hydration), showed that the combined effect of a local disorder of fibrils and extra-fibrillar matrix and an increase in corneal thickness, accounted for a 20% increase in light scatter in the Fuchs dystrophy cornea; the additional scatter was caused by the presence of 'lakes' (Meek *et al.* 2003b – Appendix 5).

In Bowman's layer the fibrils are disordered and scatter light independently of one another; however minimal scattering occurs because the layer is thin (8-12μm) and the fibrils have a small diameter (20-30nm), so making them weak scatterers (Freund *et al.* 1995).

The regular arrangement of constituent cellular components also contributes to the overall transparency of the cornea. Keratocytes are thin (approx. 0.6μm), flat fibroblasts that lie between lamellae and secrete proteoglycans and collagen. They present a very small passage for light to pass through and their cytoplasm is transparent due to the organised packing of corneal crystallins, which form a uniform refractive index (Jester *et al.* 1999a). However, the nuclei are not transparent and are responsible for the small amount of residual scattering present in the normal cornea (Jester *et al.* 1999b; Moller-Pedersen 2004). The density of keratocytes is highest in the anterior stroma and lowest in the posterior stroma (Muller *et al.* 1995).

Other factors also contribute to the transparency of the cornea such as a smooth epithelium covered by a layer of tear film and the absence of any blood vessels in the cornea. The tear film helps to smooth the anterior surface of the cornea to minimise light scatter, as any surface irregularities of a size close to the wavelength of light would result in increased light scatter and therefore image degradation. The absence of blood vessels and anything else that absorbs light in the visible spectrum results in the majority (>90%) of incoming light to be transmitted with very little being absorbed by the cornea itself.

1.4 Corneal hydration and stromal swelling

Corneal hydration (H) is defined as the weight of water in the cornea divided by the dry weight of the cornea. At physiological hydration (H = approximately 3.2) (Hodson *et al.* 1991) the cornea is transparent, however when the cornea swells the transmission of incident light is considerably reduced and corneal clouding occurs (Maurice 1984). Stromal swelling is associated with many corneal diseases, often as a result of structural defects in the endothelium and Descemet's membrane, as is the case in Fuchs's dystrophy and corneal hydrops. The force with which the tissue swells is called the swelling pressure and the swelling pressure of the cornea is inversely related to the hydration of the tissue (Hedbys and Dohlman, 1963).

In the normal, undiseased cornea, there are several systems in operation that regulate the hydration of the stroma; these include, the swelling pressure exerted by glycosaminoglycans (Hedbys 1961), the barrier function of the epithelium and endothelium (Smolin and Thoft 1987) and the endothelial water pumping mechanism (Hodson and Wigham 1983). The epithelium and endothelium act as barriers against the excessive flow of fluid into the stroma from the tear film and the aqueous humour, whilst the presence of an endothelial water pumping mechanism balances the swelling pressure of the stroma. The endothelium actively transports HCO_3^- out of the stroma and into the aqueous humour; thus creating an osmotic gradient which passively draws water out of the stroma (Hodson, 1977).

In vitro the cornea has a strong tendency to imbibe water and swell due to the presence of polyanionic proteoglycans in the stromal extracellular matrix (Aakre and Doughty 1997). Their overall negative charge attracts and binds ions, which result in water being drawn into the cornea and causing it to swell (Klyce and Beuerman 1988). As the cornea swells only in the direction of its thickness, a linear relationship exists between corneal thickness and tissue hydration (Hedbys and Mishima 1962; 1966). The reason for this unidirectional swelling lies in the structure of the corneal stroma, which consists of parallel arrays of lamellae in which the collagen fibrils lie parallel to each other and to the plane of the cornea. When bovine corneas at a hydration of below H=1 are swollen, water is distributed both within and between the fibrils (Meek *et al.* 1991), however, above this hydration the fibrils themselves swell

very little and most of the additional water goes into the interfibrillar spaces (Meek *et al.* 1991). As water enters the interfibrillar space, tissue expansion is restricted within the plane of the tissue by the fibrils themselves, however, in the direction of tissue thickness there is a lack of fibrils to restrain stromal swelling (Mishima 1968).

The distribution of water across the cornea is non-uniform (Kikkawa and Hirayama 1970; Maurice 1957; Turss *et al.* 1971) and in the bovine cornea this has been shown to correlate with changes in proteoglycan composition throughout the thickness of the tissue (Castoro *et al.* 1988). It is plausible that the higher ratio of keratan sulphate to dermatan sulphate in the posterior stroma is largely responsible for the positive gradient of water between the epithelium and endothelium, since keratan sulphate proteoglycans have a larger water sorptive capacity than dermatan sulphate proteoglycans (Castoro *et al.* 1988). Structural differences between the anterior and posterior stroma may also explain the restricted swelling of the anterior stroma. In the anterior stroma lamellar branching occurs between layers to form an interwoven lamellar structure (Komai and Ushiki 1991; Polack 1961; Radner et al. 1998a); this interwoven structure of lamellae is thought to limit the ability of the anterior stroma to swell (Muller et al. 2001), in much the same way as the presence of 'sutural' fibres in the corneas of cartilaginous fish, which connect the basal lamina of the corneal epithelium to a posterior collagenous layer, are thought to limit the swelling of the cornea when immersed in water (Bron 2001; Goldman and Benedek 1967). The differences between the anterior and posterior stroma in terms of structure and ability to swell are discussed further in Section 1.6.

1.5 Collagen fibril orientation in the human cornea

The human cornea is normally subjected to an intraocular pressure of between 10 and 20mmHg, which stretches the tissue in all directions within the plane of the cornea. The force exerted upon the cornea is resisted by the presence of collagenous layers which lie parallel to the corneal surface and offer tensile strength along their long axes. As the tissue is under compression there is an absence of stromal collagen fibrils lying perpendicular to the surface of the cornea.

The ultrastructural arrangement of fibrils in the cornea and sclera has been studied in detail by electron microscopy (Komai and Ushiki 1991); however the results yielded little information regarding the large-scale quantitative orientation of collagen fibrils. In recent years our knowledge of the fibrillar organisation of the cornea, limbus and sclera has greatly advanced through the use of XRD techniques, which have enabled the preferred orientation of collagen fibrils to be determined and mapped (Aghamohamadzadeh *et al.* 2004; Newton and Meek 2001) (Figure 1.6). In-depth studies of collagen fibril orientation in the human cornea have shown collagen fibrils to travel in two preferred directions: nasal-temporal (NT) and superior-inferior (SI) (Daxer and Fratzl 1997; Meek and Boote 2004; Newton and Meek 2001), with the effect being most pronounced in the posterior stroma (Meek *et al.* 1987).

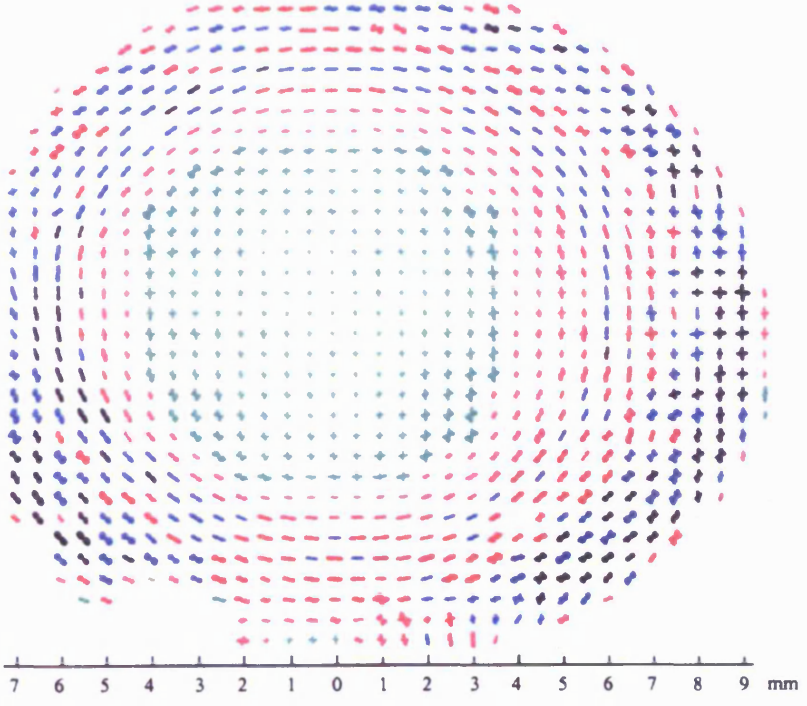

Figure 1.6. Map of preferred collagen fibril orientation in the human cornea, limbus and scleral rim. The preferred fibril direction across the tissue is shown as a montage of polar plots. Each polar plot indicates the preferred direction(s) of the lamellae at that point and the distance from the centre of a polar plot to its edge in any direction is proportional to the total x-ray scatter from only preferentially aligned collagen throughout the thickness of the tissue at that point. As scattering increases from the central cornea to the periphery the polar plots are scaled down by the following factors: green, 1; pink, 2; red, 3; blue, 4; and black, 5. Reproduced from Aghamohamadzadeh *et al.* (2004)

Of the 35 other species studied to date, this orthogonal preferred fibril orientation has only been seen in the primary stroma of chick corneas (Quantock *et al.* 1998). The reason for this arrangement is not yet fully understood but is possibly related to the position at which the four extra-ocular rectus muscles insert into the sclera, offering increased tensile strength to prevent tissue distortion during eye movement (Daxer and Fratzl 1997).

Towards the edge of the cornea, at the limbus, the amount of collagen increases and the preferred orientation becomes circumferential, forming an annulus around the cornea of varying width and fibril density (Aghamohamadzadeh *et al.* 2004; Newton and Meek 1998a, b, 2001). The annulus of collagen around the cornea is thought to absorb the stress caused by the change in curvature at the point where the cornea (7.5mm radius of curvature) meets the less curved sclera (13mm radius of curvature) (Maurice 1984). The cornea, which is approximately spherical in the central 4mm, flattens as it approaches the limbus. It has been suggested that this flattening effect may function to provide a smoother transition between the curvature of the cornea and sclera (Aghamohamadzadeh *et al.* 2004).

The way in which fibrils intermingle at the limbus is as yet unclear but two possible explanations exist. One theory is that cornea collagen fibrils originate in the fibrils that wind around at the limbus of the corneo-scleral junction. The other is that corneal collagen fibrils are continuous with scleral collagen, and the annulus of collagen surrounding the cornea is formed by a second population of fibrils. A recent study using a fine focus beam of x-rays was used to examine in detail the preferred orientation of collagen fibrils in the 1-2mm region of the cornea prior to the limbus (Meek and Boote 2004). The data revealed a gradual change in the preferred orientation of fibrils with increasing proximity to the limbus and a reinforcement of the nasal-temporal lamellae in the peripheral cornea. This led the authors to believe that the effect was achieved by a combined bending of lamellae just before the limbus and the presence of additional lamellae, anchored in the sclera which traverse the peripheral cornea. The suggested arrangement of collagen fibrils in the human cornea is shown schematically in Figure 1.7 (Aghamohamadzadeh *et al.* 2004; Meek and Boote 2004).

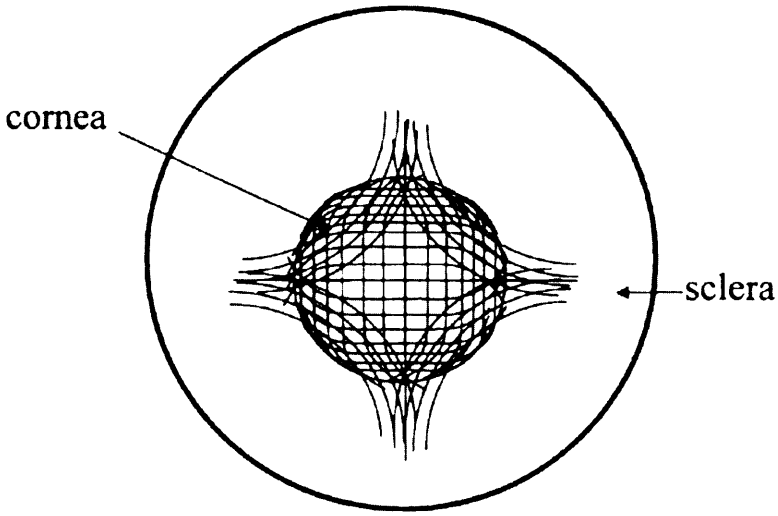

Figure 1.7. Model showing a possible (simplified) arrangement of corneal and limbal lamellae. Reproduced from Aghamohamadzadeh *et al.* (2004).

Recently, Pinsky and colleagues (2005) developed a mechanical model of the cornea. This was done by initially calculating a mathematical model for a typical lamella, taking into account the strain energy of collagen fibrils, extra-fibrillar matrix and proteoglycan cross linking. Lamellar properties were then averaged throughout the thickness of the stroma and combined with XRD derived data of collagen preferred orientation. The model was tested by comparing the predicted induced level of astigmatism for a scleral tunnel incision (which is frequently used in cataract surgery), with published clinical data; the results showed a good agreement between the two. In the future it is hoped that accurate mechanical models of the human cornea, capable of predicting the effects of various surgical procedures and the progression of various diseases such as keratoconus, will be readily available for surgical use.

1.6 A comparison of anterior and posterior stromal ultrastructure

Many structural differences exist between the anterior and posterior stroma, with the most apparent and well researched of these differences being the arrangement of collagen lamellae. In the posterior stroma, lamellae run continuously from limbus to limbus across the cornea (Maurice 1969) and within individual lamellae the fibrils run

approximately parallel to each other, except where lamella branching occurs. In the posterior stroma branching occurs predominantly within the plane of the cornea, however, in the anterior third of the stroma branching also occurs between layers to form an interwoven lamellar structure (Komai and Ushiki 1991; Polack 1961; Radner *et al.* 1998a), as illustrated in Figure 1.8. The lamellae in the posterior stroma are wider and thicker (100-200μm wide and 1.0-2.5μm thick) than the lamellae in the anterior stroma (0.5μm wide and 0.2-1.2μm thick) (Komai and Ushiki 1991). The anterior stroma is less ordered (Freund *et al.* 1995), less hydrated (Turss *et al.* 1971), less easily swollen (Kikkawa and Hirayma 1970), has a higher keratocyte density (Patel *et al.* 2001) and has a higher refractive index than the posterior stroma (Meek *et al.* 2003a - Appendix 6; Patel *et al.* 1995).

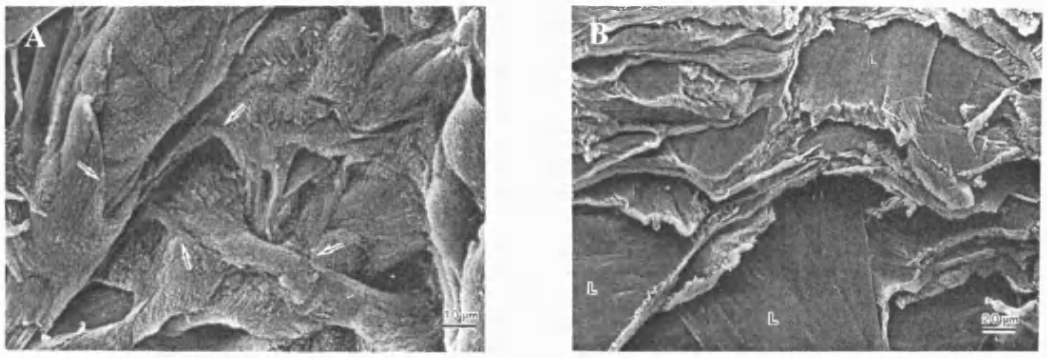

Figure 1.8. A tangential view of the superficial region (x 1100) (A) and deep region (x 580) (B) of the cornea. The lamellae in the superficial region are irregular shaped, run in various directions and often branch out or merge with other lamellae bundles (arrows) (A). Wide plate-like lamellae (L) are regularly stacked in the deep stroma and adjoining lamellae cross at various angles.
Reproduced from Komai and Ushiki (1991).

A transmission electron microscopy and image analysis study of the anterior, middle and posterior stroma of slightly swollen human corneas and unswollen rabbit corneas revealed anterior-posterior variations in fibril size and number density. In both rabbits and humans, the number density of fibrils was greater in the posterior stroma than in the anterior stroma and in humans the number density of fibrils was lower in the mid stroma compared to the anterior stroma (Freund *et al.* 1995). Interference factor calculations showed that in both rabbits and humans destructive interference

effects are greatest in the posterior stroma; the anterior stroma likely scatters approximately twice as much light as the posterior stroma in humans and approximately three times as much in rabbits (Freund *et al.* 1995).

A combination of several factors may be responsible for the variation in swelling properties as a function of stromal depth. The most obvious of these is the interwoven structure of lamellae in the anterior stroma which is thought to limit swelling in this region (Muller *et al.* 2001). Another possible contributing factor is the higher ratio of keratan sulphate to chondroitin sulphate in the posterior stroma compared to the anterior (Castoro *et al.* 1988), as keratan sulphate has a higher water affinity than chondroitin sulphate. A variation in the concentration of proteoglycans between the anterior and posterior cornea may also be partially responsible for the difference in ultrastructure between the regions (Freund *et al.* 1995). As corneal shape is genetically determined and the developmental origin of the anterior third of the stroma is thought to differ from that of the posterior (McTigue 1967), this may help to explain the differences in both the structure and function of the anterior and posterior stroma. The interwoven structure of the lamellae and the anterior cornea's stability under extreme hydration implies that the anterior third of the stroma is involved in maintaining corneal curvature. The insertion of the anterior lamellae into Bowman's layer may also help determine corneal shape by distributing tension equally over the corneal surface (Muller *et al.* 2001), whilst the limbus to limbus arrangement of lamellae in the posterior stroma provides the tissue with strength.

In Chapter 4 of this thesis, the preferred orientation of collagen as a function of stromal depth in bovine and human corneas is examined using XRD.

1.7 Biomechanics of the cornea

The biomechanical stability of the cornea is essential for maintaining good vision and abnormalities in the biomechanical properties of the cornea are associated with much ocular pathology such as keratoconus, keratoglobus and pellucid marginal degeneration. The shape of the cornea is dependent on the intraocular pressure, the thickness of the cornea and the elastic properties of the tissue.

The most accurate and commonly used method for studying the visco-elastic response of the cornea to an increase in intraocular pressure is to calculate Young's Modulus (stress/strain). However, due to differences in experimental techniques and variations in tissue hydration between studies, a large range of values have been reported. Jue and Maurice (1986) calculated Young's Modulus of elasticity for the rabbit cornea ($5x10^6$ Pascals) by placing two small drops of mercury onto the surface of the cornea, applying a stress (an increase in intraocular pressure) and dividing the distance by which the two mercury drops were displaced by their original separation distance. Studies measuring Young's modulus using excised strips of cornea produce much higher measurements than studies of intact corneas (Forster *et al.* 1994). It is thought that this may be due to the fact that when strips of the cornea are used the constituent fibrils are released from their normal attachments, thereby altering the biomechanical properties of the tissue (Jue and Maurice 1986)

The elasticity of the cornea is also dependent upon the hydration of the tissue. Hjørtdal (1995) examined the elasticity of the cornea at normal hydration and found the cornea to be stiffer than the values previously reported for swollen corneas. The author later showed that regional differences exist in the biomechanical properties of the cornea. Meridionally, the cornea is stiffest in the central and peripheral regions, whereas circumferentially the cornea is stiffest at the limbus (Hjørtdal 1996). The increased stiffness at the limbus is likely due to the reinforcement of the tissue by a circum-corneal annulus of collagen. The inter-lamella cohesive strength (the strength with which lamellae adhere to each other), also shows regional variation and is doubled in the periphery compared to the central cornea (Pepose and Ubels 1992). Regional variations in cohesive strength were further characterised by Smolek (1993), who found the cohesive strength to be greatest in the nasal and temporal regions of the cornea ($2.94x10^{-1}$ N/mm), lower in the superior cornea ($2.34x10^{-1}$ N/mm) and even lower in the inferior cornea ($1.96x10^{-1}$ N/mm).

The stroma provides the cornea with the majority of its strength and stability, although the role of Bowman's layer in corneal biomechanical stability has also been investigated in relation to corneal refractive procedures. As Bowman's layer is disrupted in keratoconus there is concern that the removal of Bowman's layer in

photorefractive keratometry may lead to keratoconus like changes. However, a study on strips of cornea showed there to be no difference in the visco-elastic properties of corneas with or without a Bowman's layer (Seiler *et al.* 1992). This suggests that the Bowman's layer does not contribute significantly to the overall mechanical stability of the cornea.

1.8 Structure and function of the limbus

The limbus is a transition zone between the transparent cornea and the opaque sclera, measuring 1.5mm wide horizontally and 2mm wide inferiorally and superiorally (Figure 1.9). The anterior limit of the limbus (corneo-limbal junction) is formed by a plane joining the ends of Bowman's layer and Descemet's membrane, whilst the posterior limit (limbo-scleral junction) is formed by a plane drawn perpendicular to the surface of the eye (at a distance of 1.5mm behind the corneo-limbal junction in the vertical meridian and 2mm behind it in the horizontal meridian), passing through the scleral spur (Hogan *et al.* 1971).

The limbal epithelium, although structurally similar to the corneal epithelium, has a larger number of cell layers (Hogan *et al.* 1971). Below the limbal epithelium the connective tissue is less well organised and the fibrils are of a larger diameter than those found in the corneal stroma (Gipson 1994).

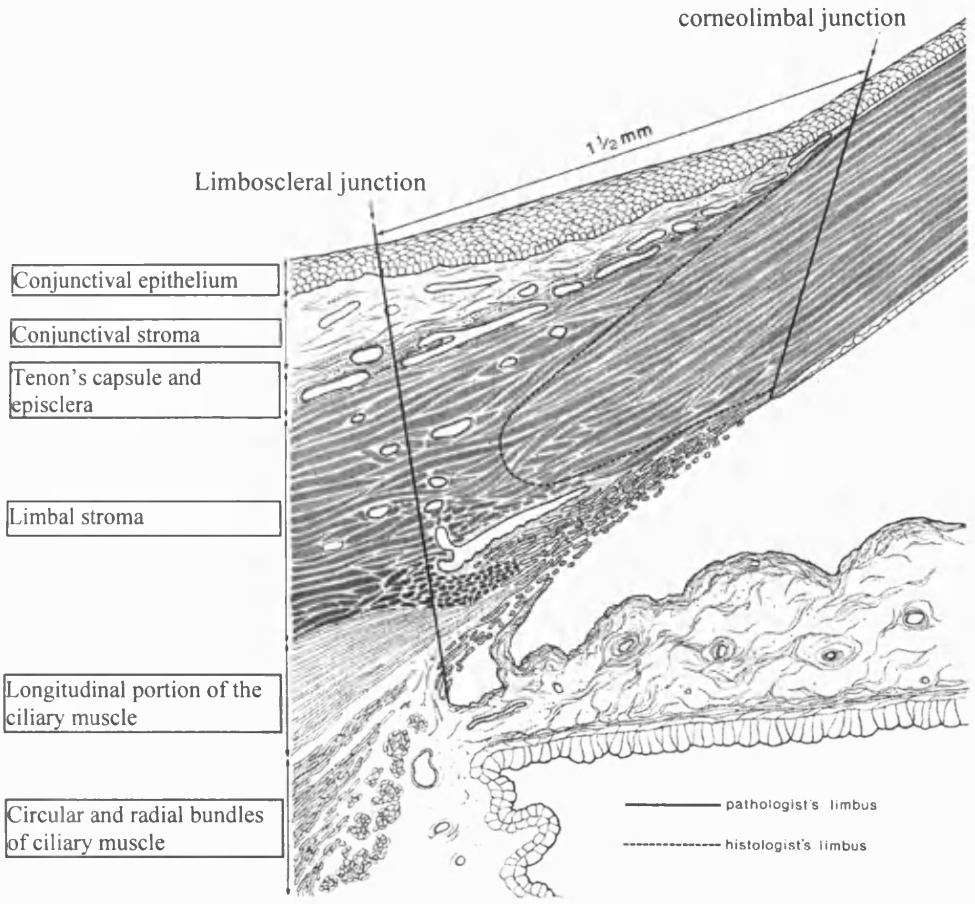

Figure 1.9 A schematic drawing of a meridional section of the limbal area. Adapted from Hogan *et al.* (1971).

Electron microscopy (Borcherding *et al.* 1975) and more recently XRD (Boote *et al.* 2003 – Appendix 4) have shown that the spacing between collagen fibrils and the fibril diameter both increase rapidly at the limbus (Figure 1.10). The XRD study of collagen IFS and fibril diameter across the human cornea and limbus, published by Boote *et al.* ((2003) – Appendix 4), is presented in Chapter 3 along with similar data for adult and embryo marmoset monkey corneas.

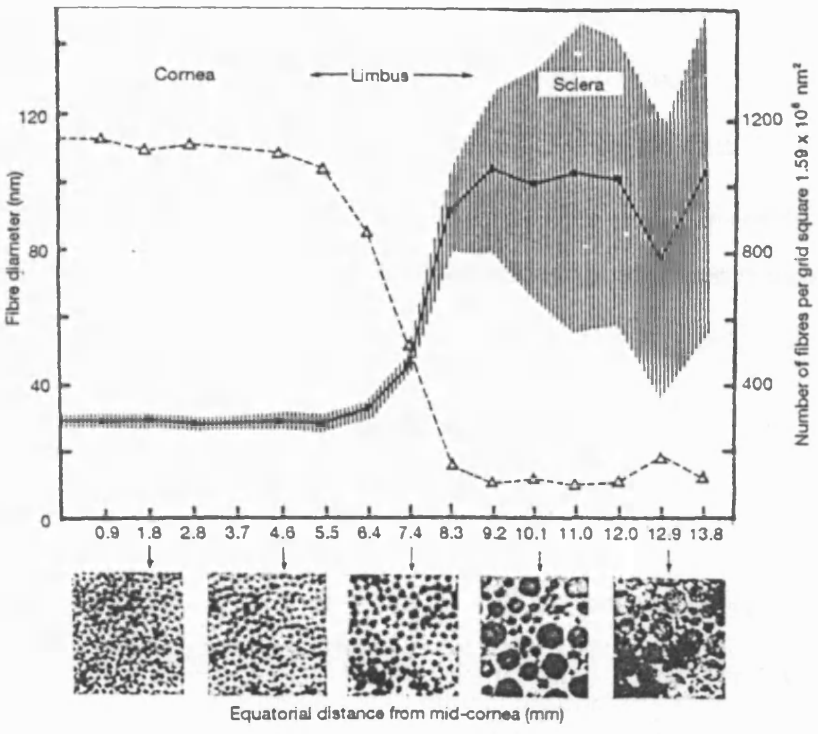

Figure 1.10 Comparison of the average number of collagen fibrils per unit area (open triangles) with the mean fibril diameter (filled circles) +/- 1 s.d. (shaded area) as a function of distance from the centre of the cornea. Arrows indicate the location of electron micrographs along the central vertical axis from the centre of the cornea upward to the sclera (X 40 000). Reproduced from Borcherding *et al.* (1975).

Borcherding *et al.* (1975) noticed a direct correlation between the type and concentration of proteoglycans and the organisation of the collagen fibrils at the limbal region. Hyaluronic acid and dermatan sulphate are present at the limbus and there is a marked increase in the concentration of keratan sulphate (Borcherding *et al.* 1975).

In the human limbal zone there is a change in curvature from a 7.5mm radius of curvature in the cornea to 13mm in the sclera. Maurice (1969) proposed that as a result of the change in curvature, the tension in the limbal zone would be at least twice that in neighbouring regions. This helps to explain the change in preferred collagen orientation at the limbus, whereby the collagen fibrils follow a circular

course to form an annulus around the cornea (Aghamohamadzadeh *et al.* 2004; Meek and Boote 2004; Meek *et al.* 1987).

1.9 Structure and function of the sclera

The sclera forms 93% of the outer fibrous coat of the eye. It consists of distinct concentric layers which, from the outermost surface, are Tenon's capsule, episclera, stroma and lamina fusca. Below the vascularised, loose connective tissue forming the episclera lies the stroma which consists primarily of dense fibrous tissue (mainly collagen Type I) combined with elastic tissue (Forrester *et al.* 2001). The lamina fusca (the innermost layer), is in direct contact with the uvea and is formed of collagen fibres, fibroblasts and pigment-bearing cells.

The visco-elastic properties of the sclera are essential to its structural function, which is to maintain the shape of the globe and to protect the contents of the eye, whilst the opaque nature of the tissue prevents stray light from reaching the retina. The sclera is opaque for the opposite reasons that the cornea is transparent; the fibrils are randomly arranged and have a large and variable diameter (30-300nm), fewer glycosaminoglycans exist on the collagen fibres (a 1/4 of the amount present in the cornea) and the hydration of the sclera (70%) is lower than that of the cornea (78%) (Fatt and Weissman 1992).

1.10 Extraocular muscles

Eye movement is controlled by the combined action of 6 extraocular muscles (Figure 1.11B):

1. Medial rectus – moves the eye towards the nose.
2. Lateral rectus – moves the eye away from the nose.
3. Superior rectus - moves the eye up.
4. Inferior rectus - moves the eye down.
5. Superior oblique – rotates the eye to move the top of the eye towards the nose.
6. Inferior oblique – rotates the eye to move the top of the eye away from the nose.

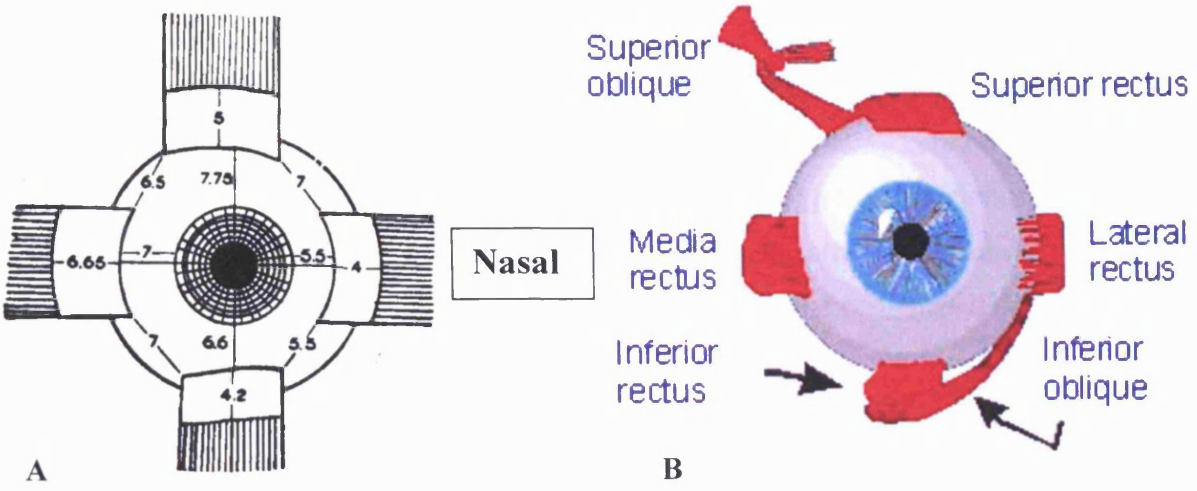

Figure 1.11 Insertion points of the extraocular muscles in the right (A) and left eye (B). Reproduced from (A) Duke-Elder (1932) and (B) http://www.yorku.ca/eye/muscle.htm (Accessed 01/05/05).

The muscles are linked by a complex system of connective tissue. Tenon's capsule surrounds the globe all the way from the optic nerve round to the conjunctiva (located approximately 3mm behind the limbus). Each muscles inserts into the globe through slits in Tenon's capsule and each muscle sheath is connected to adjacent muscle sheaths by a fibrous extension, so forming the intermuscular septum which fuses with the Tenon's capsule 3mm behind the limbus.

The medial, inferior, lateral and superior rectus muscles insert at increasing distances of 5.5mm, 6.5mm, 7.0mm and 7.75mm from the limbus respectively (Figure 1.11A) (Duke-Elder 1932). An imaginary line connecting these insertion points in an anticlockwise direction from the superior rectus creates a configuration known as the 'spiral of Tillaux'. The superior oblique muscle passes through the trochlea before inserting into the globe.

1.11 Keratoconus

The arrangement of collagen in the stroma is of great importance in maintaining both the strength and shape of the cornea. As a result of this, abnormalities in the structural organisation of stromal collagen, which affect the biomechanical stability of the cornea, have been implicated in several corneal diseases including keratoconus (Figure 1.12A), pellucid marginal degeneration (Figure 1.12B) and keratoglobus (Figures 1.12C). Chapter 5 of this thesis focuses solely on the arrangement and distribution of collagen in the stroma of keratoconus corneas and compares it to that of the normal human cornea.

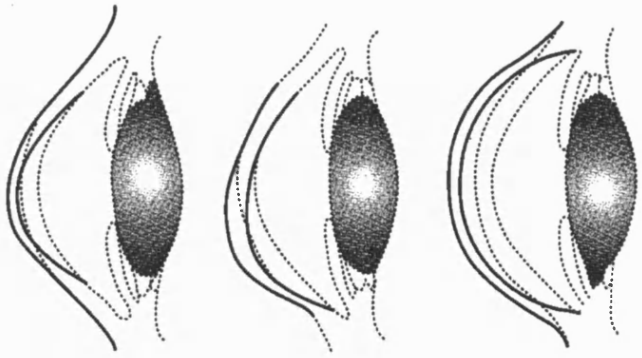

A. Keratoconus

B. Pellucid Marginal Degeneration

C. Keratoglobus

Figure 1.12. Schematic diagrams of keratoconus, pellucid marginal degeneration and keratoglobus.
(A) In keratoconus maximal thinning occurs in the central region of the cornea.
(B) In pellucid marginal degeneration maximal thinning occurs in the inferior cornea.
(C) In keratoglobus the cornea is large, thin and bulbous.
Adapted from Coster (2002)

Keratoconus is a progressive, non-inflammatory, corneal thinning disease that is characterised in advanced cases by a cone-shaped cornea (Figure 1.13A). In a recent study, keratoconus was found to be one of the most common indications for penetrating keratoplasty in the UK (15%), second only to corneal regrafting (41%) (Al-Yousuf *et al.* 2004).

The disease is usually bilateral (99.2% of cases) and in most cases where the disease appears to be unilateral, a closer examination of the other eye or examination of the other eye over a sufficient period of time normally reveals some evidence of the disease (Holland *et al.* 1997). The sub-clinical form is referred to as keratoconus *forme fruste*.

The earliest stages of keratoconus usually become evident during adolescence and young adulthood, with the disease progressing at variable rates over the following 7-20 years (Krachmer *et al.* 1984). Keratoconus is thought to affect between 50 and 230 people per 100,000 (Appelbaum 1936; Hofstetter 1959; Olivares Jimenez *et al.* 1997); the reported prevalence of keratoconus differs between studies due to differences in diagnosis criteria. There is a general agreement between studies that the incidence of keratoconus is far higher in the Asian population than in the Caucasian population (Geogiou *et al.* 2004; Pearson *et al.* 1999).

Various authors have examined the incidence of keratoconus in the male and female populations; some found a higher incidence of keratoconus in males (Lim and Vogt 2002; Owens and Gamble 2003) whilst others found there to be no gender predisposition to the disease (Kennedy *et al.* 1986; Olivares Jimenez *et al.* 1997). A study of 670 keratoconus patients in New Zealand revealed an earlier age of onset and a more rapid rate of disease progression in males (Owens and Gamble 2003). This was also shown to be the case in a more recent study which aimed to characterise the gender differences in the Collaborative Longitudinal Evaluation of Keratoconus (CLEK) Study (Fink *et al.* 2005).

1.11.1 Clinical signs of keratoconus

The detection of keratoconus is aided by the presence of various overt clinical symptoms which include:

1. A decreased visual acuity.
2. Astigmatism.
3. Central corneal thinning (Figure 1.13B).
4. An increased corneal curvature which gives rise to a 'v' shaped profile of the lower lid on the downward gaze (Munson's sign) (Figure 1.13C).
5. Deposition of ferrtin particles, within and between epithelial cells, around the base of the cone (Fleisher's ring) (Figure 1.13D).
6. Small vertical white lines at the apex of the cone in the deep layers of the cornea (Vogt's striae) (Figure 1.13E).

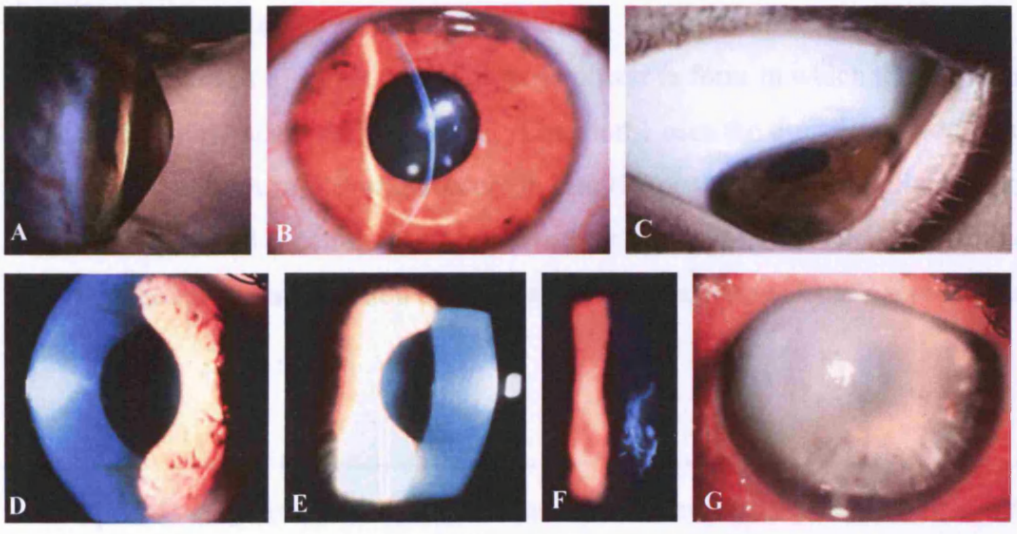

Figure 1.13. Side profile of a keratoconus cornea (A). The clinical symptoms associated with the disease include: central corneal thinning (B), Munson's sign (C), Fleisher's ring (D), Vogt's striae (E), stromal scarring (F) and corneal hydrops (G). Adapted from http://www.kcenter.org.

Other symptoms may also become apparent as the disease progresses, such as stromal scarring (Figure 1.13F) and corneal hydrops (Figure 1.13G). As the cornea thins sub-epithelial scarring may occur due to ruptures in Bowman's layer which are subsequently filled with connective tissue. Scarring may also occur as result of

corneal hydrops which is caused by a rupture in Descemet's membrane and the endothelium. Following the rupture of Descemet's membrane aqueous humour flows into the cornea causing it to swell and scatter more light, resulting in a sudden loss of vision. Although the swelling and opacification normally resolves over a period of 1 to 2 months as Descemet's membrane regenerates, in some cases a scar is formed at the apex of the cone. When scarring occurs the patient experiences a permanent decrease in visual acuity that can only be restored by corneal transplantation.

1.11.2 Diagnosis of keratoconus using videokeratography

In recent years the diagnosis and monitoring of keratoconus has been greatly facilitated by the use of computer-assisted corneal topography analysis (videokeratography), which provides the clinician with information about corneal shape in the form of a colour coded contour map of corneal surface curvature.

Curvature represents the 'rate of change of height' and so forms a sensitive measure of changes in contour across the corneal surface. Maps of corneal curvature are converted into maps of total corneal dioptric power (a form in which the clinician is more familiar) by means of Equation 1. Equation 1 uses the directly proportional relationship between radius of curvature in mm (Rc) and total corneal dioptric power (Cp) (in the paraxial (central 4mm) region of the cornea) and the keratometric index (337.5). The further application of Snell's Law enables corneal surface power to be calculated.

Equation 1: Conversion of corneal curvature to total corneal dioptric power.

$$Cp = \frac{337.5}{Rc}$$

Refractive power is a slightly less accurate measure of contour than curvature, especially in abnormal corneas due to the approximations and assumptions made during its calculation (Arffa *et al.* 1986; Corbett *et al.* 1999). In the peripheral regions of the cornea the paraxial power approximations are no longer valid and as suggested by Roberts (1994), the data should be either treated with caution or ignored.

There are two main computerised corneal topography systems currently in use:

Placido Disc (eg. Eye Sys 2000 (Figure 1.14)) – consists of a cone containing illuminated rings which are projected onto the cornea. The image of the reflected rings is formed behind the cornea and the object rays are gathered by the computer to form a topography map (Figure 1.15). One disadvantage of this system is its limited accuracy in describing the true elevation of the cornea. Also, as the data is obtained from a reflection, consistent precision is required in the alignment of the instrument with the cornea to get reproducible results. A further limitation is that the system measures the reflection from the tear film and so assumes that the tear film is distributed evenly over the corneal surface; variation therefore occurs in cases of dry eye and excessive tearing, as the results are altered after blinking (Bains *et al.* 2000).

Figure 1.14. The Eye Sys 2000 computerized corneal topography system.
Reproduced from http://www.eyesys.com/products

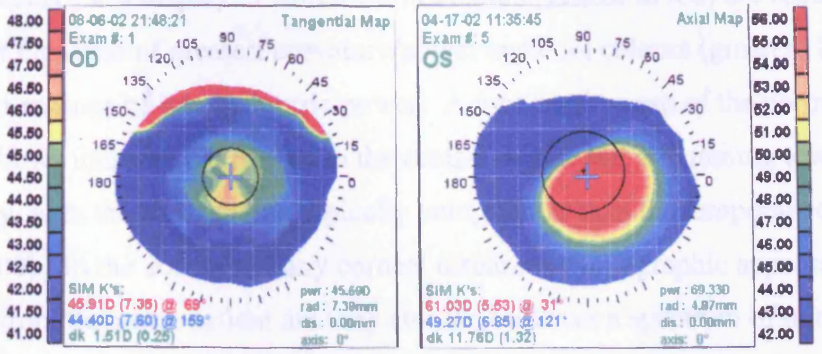

Figure 1.15. Eye Sys topography maps of a normal cornea (A) and a keratoconus cornea (B). Images courtesy of Prof. Y. Huang (Kyoto Prefectural University).

2. Elevation Based Maps (eg.Orbtek Orbscan) – a projection system is used to describe the shape of the cornea (as opposed to the reflective system used in Placido disc technology). Image sensors acquire elevation data from over 9000 points across the cornea by projecting an illuminated ring pattern and a beam of light onto the corneal surface. Elevation based videokeratography is the only system capable of measuring the elevation of both the anterior and posterior surfaces of the cornea (Figure 1.16); this is done by comparing the surface of the cornea to a 'best fit' reference sphere which is calculated using a least squares method. Maps of anterior and posterior surface elevation are especially important in the early diagnosis of keratoconus as posterior surface changes often occur prior to the appearance of anterior surface changes.

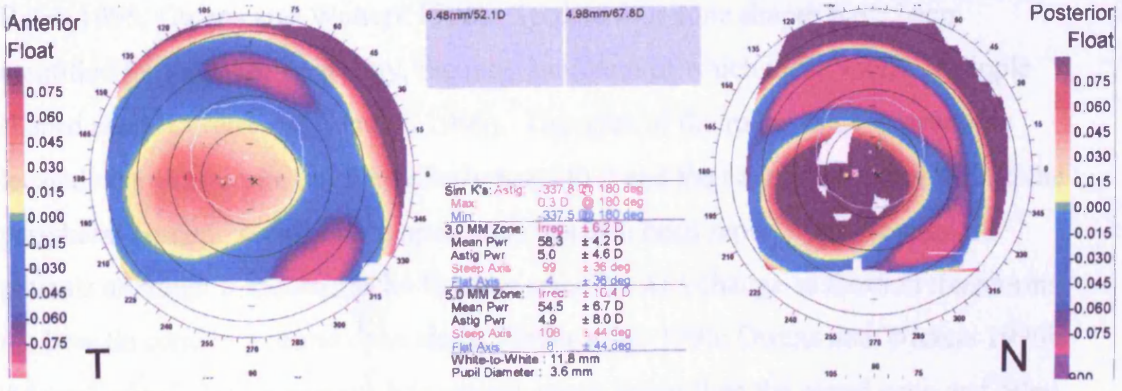

Figure 1.16. Orbscan elevation based videokeratography showing the anterior and posterior floats of a keratoconus cornea. Images courtesy of S. Tuft (Moorfields Eye Hospital).

Both systems use a display in which warm colours (yellow to red) are used to represent the areas of greatest curvature/power and cool colours (green to blue) mark the flatter regions of lower dioptric power. A topography map of the normal human cornea shows increased curvature in the central region and a flattening towards the periphery, with the nasal region typically being flatter than the temporal cornea (Bains *et al.* 2000). In the absence of any corneal disease the topographic appearance of both corneas from the same patient are very similar, however a spectrum of normal topography maps exists between patients.

In keratoconus corneas the highest point of an elevation topography map is the apex of the cone, however, the steepest area is usually on the inferior side of the cone. The contour maps can be likened to climbing a mountain, the steepest part is the climb to the top but once at the top the ground is level (Corbett *et al.* 1999).

The colour coded topography map is extremely useful for the detection of early keratoconus due to the distinct topographical features associated with the disease, which include an increased central corneal curvature (central power > 47D), a larger than normal difference between the central and peripheral corneal curvature, a flatter curve in the superior cornea than in the inferior (>3D difference between points 3mm below and above the corneal vertex) and an asymmetry in the central corneal power (>1.4D) between a set of eyes (Rabinowitz and McDonell 1989). Corneal topography maps of keratoconus patients show a great deal of variation due to differences in the size and shape of the cone and the level of astigmatism. In the majority of keratoconus patients the cone is located in the inferior cornea (Auffarth *et al.* 2000; Baum 1995; Owens and Watters 1996). To date four cone shapes have been identified by videokeratography, the most common of which is the round or nipple shaped cone (Owens and Watters 1996). The apex of the round cone is generally located near the optic axis or inferiorly nasal to it and the cone rarely extends into the peripheral cornea. A bow tie shaped cone has also been reported in keratoconus patients although it appears to be fixation sensitive as a change in fixation transforms the bow tie cone to a round cone shape (Bruce *et al.* 1996; Owens and Watters 1996). An oval cone is less common; it is usually much larger than the round cone and often extends into the peripheral cornea. The oval or sagging cone is most commonly

located in the inferior-temporal cornea (Buxton 1978; Owens and Watters 1996; Perry *et al.* 1980). The least common cone shape is a global cone which occupies approximately 75% of the cornea (Caroline and Norman 1992).

1.11.3 Treatment of keratoconus in early and advanced stages

Once diagnosed, the early stages of keratoconus may be successfully treated and managed through the use of glasses or hard contact lens. However, in advanced stages of the disease surgical correction in the form of a corneal transplant may be required, primarily as a result of contact lens intolerance or due to a loss of best corrected visual acuity caused by corneal scarring (Lim and Vogt 2002). Two methods of corneal transplantation are currently utilised in the treatment of advanced keratoconus. The most frequently used is penetrating keratoplasty, which involves the removal of a full thickness corneal button (usually measuring 7.5mm in diameter) from the diseased host cornea and the replacement with a donor corneal button. Epikeratoplasty, otherwise known as lamella keratoplasty, is an alternative technique which involves a partial thickness corneal graft. In a study of 93 eyes from 78 patients with keratoconus, penetrating keratoplasty resulted in a corrected visual acuity of 20/40 (or better) in 86% of the eyes (Lim *et al.* 2000). The long term success rate of a corneal graft for keratoconus patients is in excess of 95% (Williams *et al.* 1997). The high success rate of corneal transplantation is attributable primarily to the cornea being an immunologically privileged site. It is generally accepted that the immune privilege of corneal allografts is due to the absence of lymphatic and blood vessels in the corneal graft bed. The success rate of corneal transplantation is further enhanced by the effectiveness of immuno-suppressive drugs used to prevent and treat graft rejections. For further information on the immune privilege of corneal allografts the reader is directed towards a review by Niederkorn (1999).

A new technique is currently under development that aims to stop the progression of keratoconus and reduce the need for penetrating keratoplasty. A pilot study, in which riboflavin solution and UVA irradiation were used to increase the level of collagen cross-linking in the corneas of 15 keratoconus patients, was performed to test the effectiveness of the treatment. With a follow up time of 3 years, the progression of

the disease was stopped in all cases and corneal transparency remained unchanged (Wollensak *et al.* 2003). Biomechanical studies of porcine and rabbit corneas treated with the same technique revealed an increased corneal rigidity (Wollensak *et al.* 2003) and an increased resistance to enzymatic digestion by collagenases (Spoerl *et al.* 2004). Although the treatment requires further investigation to assess the long-term maintenance of the induced mechanical stiffness as well as any potential side effects, the technique holds promise for the future treatment of keratoconus.

1.11.4 Keratoconus aetiology

Over the years various associations have been formed between keratoconus and atopic disease (Bawazeer *et al.* 2000; Grewal *et al.* 1999; Owens and Gamble 2003; Peyman *et al.* 1980; Zadnik *et al.* 1998), connective tissue disorder (Robertson 1975; Woodward and Morris 1990), eye rubbing (Bawazeer *et al.* 2000; Grewal *et al.* 1999; Korb *et al.* 1991; McMonnies and Boneham 2003) and hard contact lens wear (Gasset *et al.* 1978).

There is also evidence to suggest a possible genetic origin of keratoconus, such as the bilateralism of the disease (Lee *et al.* 1995), its familial inheritance (Francois 1961), its association with other genetic disorders (Edwards *et al.* 2001), the trend for a higher genetic concordance rate in monozygotic twins compared to dizygotic twins (Rabinowitz 1998) and the fact that the altered expression of particular enzymes and inhibitors, thought to be responsible for the changes in keratoconus, occur at gene level (Whitelock *et al.* 1997). Environmental factors such as eye rubbing and hard contact lens wear may accelerate the progression of keratoconus in genetically susceptible individuals.

Although the condition is more common in some families than others it is not clear whether keratoconus can be inherited and in most cases the condition is sporadic. Based on available information, Krachmer *et al.* (1984) concluded that the chances of a blood relative of a keratoconus patient also having the diseases are less than 1 in 10. The majority of studies suggest an autosomal dominant inheritance of keratoconus (Krachmer *et al.* 1984); however, the irregular dominant pattern suggests that it has a

variable expression or an incomplete penetrance (Biscleglia *et al.* 2005). Genetic analyses are currently underway, investigating the number of genes that influence the disease, the contribution of each gene to keratoconus development, the means of inheritance and the chromosomal location of the gene(s). Loci for keratoconus have been found on chromosomes 3 (Brancati *et al.* 2004), 15 (Hughes *et al.* 2003), 16 (Tyynismaa *et al.* 2002) and 20 (Hayashi *et al.* 2000; Semina *et al.* 2000). Mutations in the visual system homeobox 1 (VSX1) gene, which has been mapped to chromosome 20, have been found in both Italian and Canadian keratoconus patients (Biscleglia *et al.* 2005; Heon *et al.* 2002).

1.11.5 Structural changes associated with keratoconus

Keratoconus, prior to the development of corneal hydrops and scarring, does not affect the transparency of the cornea; it does however affect tissue strength. As the exact origin and mechanism of the disease is not yet fully understood, the structural changes associated with each region of the keratoconus cornea will be discussed individually:

Epithelium – in the early stages of the disease there is an alteration in the size and shape of the squamous cells. As the disease progresses the cells become elongated and spindle-shaped at the base of the cone (Leibowitz 1984; Polack 1976; Somodi *et al.* 1996) and arrange themselves in a whorl around the apex (Somodi *et al.* 1996). An accumulation of iron particles between epithelial cells leads to the appearance of Fleisher's ring (Iwamoto and DeVoe 1976).

Bowman's layer – in some cases of keratoconus this layer thins, becomes fibrillated and eventually ruptures at the apical region of the central cornea, resulting in direct contact between the epithelium and the stroma (Polack 1976; Sawaguchi *et al.* 1998). Slit lamp examination has revealed that ruptures in Bowman's layer are filled with scar tissue (Sawaguchi *et al.* 1998).

Prior to the appearance of scarring in Bowman's membrane, visible dehiscences at this level may be seen with the slit lamp, which appear as 'fine dark rents in an opalescent background' (Bron 1988).

Stroma – thinning of this layer is one of the major clinical signs of the disease. The number of lamellae is significantly lower in the centre of keratoconus corneas (80-140) compared to the normal cornea (about 300) (Patey *et al.* 1984) and it has been suggested that the adhesion between lamellae may also be reduced, based on the observation that the stromal oedema of corneal hydrops is much greater than that associated with Descemet's membrane rupture in buphthalmos (Bron 1988). Various studies comparing the fibrillar arrangement of normal and keratoconus corneas have found the normal orthogonal preferred orientation of collagen to be absent in the apical region of keratoconus corneas (Daxer and Fratzl 1997; Meek *et al.* 2005b – Appendix 9; Radner *et al.* 1998b).

Proteoglycan abnormalities have also been reported in keratoconus corneas. Fullwood *et al.* (1990) found there to be fewer than normal proteoglycans in keratoconus corneas and noticed that their arrangement also differed from that of the normal cornea. Other authors have reported proteoglycan abnormalities in keratoconus corneas such as the presence of proteoglycans with fewer than normal keratan sulphate side chains or in which the keratan sulphate has a modified structure (Funderburgh *et al.* 1989). Other reported abnormalities include an over-expression of keratocan (Wentz-Hunter *et al.* 2001) and an increase in the amount of dermatan sulphate (Funderburgh *et al.* 1998; Wollensak and Buddecke 1990).

Several studies have reported abnormalities in the stromal keratocytes of keratoconus corneas. A transmission electron microscopy study revealed cell shape changes, consistent with apoptosis, in keratoconus corneas (Kim *et al.* 1999). In addition, keratoconus keratocytes located near weak regions of Bowman's membrane and in the posterior stroma have increased levels of the lysosomal enzymes Cathepsin B and G (Sherwin *et al.* 2002), are dissociated from the usual interconnected system of keratocytes (Brookes *et al.* 2003), have extremely long processes (Somodi *et al.* 1996) and have four times as many interleukin-1 receptors than normal (Kim *et al.* 1999).

Descemet's membrane and endothelium – structural changes are rarely seen in these layers during the early stages of keratoconus. However, in advanced stages of the disease breaks sometimes occur in Descemet's membrane, which compromise the endothelial barrier and may lead to acute stromal oedema. The breaks in Descemet's membrane, which result in deep scarring, are repaired by the extension of flattened endothelial cells (Laing *et al.* 1979). Due to the fact that changes in this region do not occur until the late stages of the disease, it seems likely that endothelial cell abnormalities are a secondary event caused by changes in the mechanical stress exerted on the tissue (Sturbaum and Peiffer 1993). This concept is consistent with a specular microscopical examination of 12 keratoconus corneas, which revealed the presence of many large, elongated endothelial cells that appeared to be stretched and orientated towards the apex of the cone (Laing *et al.* 1979).

1.11.6 Mechanism of stromal thinning in keratoconus corneas

Despite much research and many theories with regard to the cause of keratoconus and the mechanism by which the disease progresses, the matter still remains unresolved. There are several limiting factors in keratoconus research, such as the lack of biochemical and structural studies showing the changes occurring during the early stages of the disease. This is due to the fact that samples only become available after the need for corneal transplantation. In addition, there is very little known about the structure and biochemistry of keratoconus corneas beyond the central 8.5mm region of the cornea, as the research samples which are normally obtained at the time of penetrating keratoplasty are corneal buttons of less than 8.5mm diameter. The issue is further complicated by the possibility that keratoconus is the phenotypic appearance of more than one disorder and that it may be an end result or a final common pathway of many different pathological processes. A further limitation to keratoconus research is the absence of an animal model for the disease. Although one instance of a cone shaped cornea was reported in the rhesus monkey (Peiffer *et al.* 1987), no detailed examination was performed to confirm whether the abnormality was indeed keratoconus. More recently in Japan an inbred line of spontaneous mutant mice (named SKC) was identified, in which the males (more so than the females),

developed a cone shaped cornea (Tachibana *et al.* 2002). Results of an XRD study performed on the SKC mice corneas in order to assess their suitability as an animal model for human keratoconus are shown in Chapter 6 and Appendix 10.

One of the first theories for the process of corneal thinning in keratoconus was provided by Teng (1963), who suggested that the primary defect of the disease occurs in the epithelium, from which unspecific enzymes are released that progress through the stroma causing collagen degradation. Teng (1963) went on to hypothesise that the thinned, weakened cornea is then pushed outwards by intraocular pressure resulting in a cone shaped cornea. A subsequent electron microscopy study supported this concept, as vast irregularities were found in the epithelium of keratoconus corneas and the changes were found to progress with the disease (Tsubota *et al.* 1995). It was suggested that the centre of the cone (generally in the inferior cornea), coincided with the location of the most senile epithelial cells and that these cells were more likely to release enzymes (Baum 1995). Other studies reported changes in the tear film of keratoconus corneas, adding further weight to the involvement of epithelial cells in the disease (Dogru *et al.* 2003; Smith *et al.* 2001). More evidence for the theory was provided in a recent study of the records of 20 patients who had recurrent ectasia after penetrating keratoplasty. The histopathology of the excised grafts was found to be consistent with the changes observed in keratoconus corneas. The study also revealed that recurrent ectasia after penetrating keratoplasty is frequently bilateral, develops between 5 and 36 years after surgery (average time of 21.4 ± 7.3 years) and is often preceded by a thinning at the inferior graft-host junction (Patel *et al.* 2005).

Some authors believe that the primary defect of keratoconus is located in the stroma and that changes in the epithelium are secondary to this (Galin and Berger 1958; Krachmer *et al.* 1984). One suggestion is that the over-expression of keratocan (Wentz-Hunter *et al.* 2001) and the possible presence of an abnormal form of keratan sulphate (Funderburgh *et al.* 1989) in keratoconus corneas may alter fibrillogenesis, thereby causing structural defects in the corneal stroma which lead to the development of keratoconus. A further possibility is that the presence of defective keratocytes disrupts fibrillogenesis and affects the turnover of the ground substance (Krachmer 1984). As mentioned previously, several studies have reported abnormalities in the

stromal keratocytes of keratoconus corneas (Brookes *et al.* 2003; Kim *et al.* 1999; Sherwin *et al.* 2002; Somodi *et al.* 1996). One theory is that these abnormal keratocytes, which have increased levels of Cathepsin B and G (Sherwin *et al.* 2002), and have four times as many IL-1 receptors than normal(Kim *et al.* 1999), are either activated by nerve cells in response to eye rubbing or undergo imperfect apoptosis (both of which are triggered by IL-1). This would result in a release of Cathepsin B and G, causing localised damage to Bowman's membrane and a degradation or modification of proteoglycans and type VI collagen (Brookes *et al.* 2003).

Increased levels of proteolytic enzymes (Kenney *et al.* 1994; Smith *et al.* 1995) and reduced levels of proteinase inhibitors (Sawaguchi *et al.* 1994; Whitelock *et al.* 1997) in keratoconus corneas are thought by many to be responsible for the tissue thinning associated with the disease. However, an alternate theory was put forward by Polack (1976), in which he suggested that the stromal thinning in the cone region of keratoconus corneas may be due not to a loss of collagen by degradation but to a redistribution of collagen by a mechanism of lamellar sliding. Consistent with this theory is the suggested reduction in inter-lamellar adhesion (Bron 1988), the observed reduction in lamellar interlacing at the apex of keratoconus corneas (Radner *et al.* 1998b) and the altered orientation of the stromal lamellae in the apical region (Daxer and Fratzl 1997; Meek *et al.* 2005 – Appendix 9). In support of this theory, Edmund (1998b) demonstrated that, with the exception of advanced cases of keratoconus, the cross-sectional area of affected corneas did not differ from that of the normal cornea. Owens and Watters (1996) went on to show that keratoconus corneal thickness is reduced outside the cone region. Meek and colleagues ((2005) – Appendix 9) added to Polack's theory and suggested that the redistribution of collagen in keratoconus corneas is 'caused by an unravelling of lamellae along their length and from their limbal anchors, and a teasing apart at points where the lamellae bifurcate and form Bowman's layer'.

1.12 Basic principles of x-ray diffraction

Maurice (1957) recorded the earliest XRD patterns from cornea; however the origins of the reflections were not clear due to the fact that the cornea only weakly scatterers

x-rays and that the diffractometers used at that time took hours to record a single XRD pattern, during which time the sample was deteriorating. The potential of XRD to study the ultrastructure of the cornea was fully realised at a later date by Goodfellow and colleagues (1978), with the discovery that the cornea gives rise to two low-angle patterns, one from the regular axial arrangement of collagen molecules within the fibrils and the other from the interference between fibrils. The advent of synchrotron radiation sources (SRS) which produce a very high intensity beam of x-rays have greatly facilitated XRD studies of the cornea. The high intensity of the SRS enables corneal XRD patterns to be obtained in minutes rather than hours, allowing structural, quantitative data to be gathered in a close to natural tissue state, without the need for lengthy tissue preparation, such as is associated with electron microscopy. A further advantage for using XRD in the current study is that the data gathered from the patterns represents an average of the whole tissue thickness through which the x-rays have passed.

XRD patterns are obtained by focussing a monochromatic beam of x-rays through a specimen. Some x-rays pass straight through the specimen and are absorbed by a lead backstop behind the sample, whilst others are absorbed by the specimen itself. The remaining x-rays are scattered by the constituents of the sample and form a pattern on a detector placed behind the specimen.

A fibril placed vertically in an x-ray beam causes x-rays to be scattered both parallel to the fibril axis to form a meridional reflection and at right angles to the fibril axis to produce an equatorial reflection (Figure 1.17). In the cornea, collagen fibrils lie in all directions within the plane of the tissue causing both equatorial and meridional reflections to appear as a series of concentric circles. Due to the fact that equatorial reflections are broader than meridional reflections and much more sensitive to increases in tissue hydration, the two are easily distinguishable (Meek and Quantock 2001).

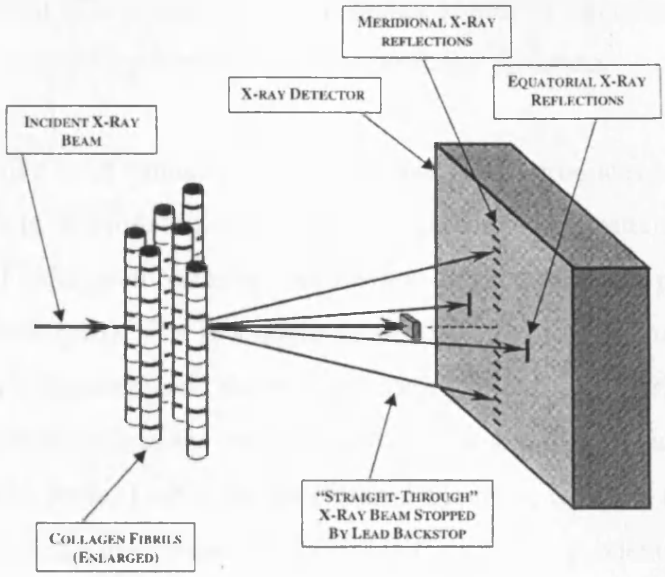

Figure 1.17. Schematic diagram showing the equatorial and meridional reflections arising from an array of collagen fibrils positioned vertically in an x-ray beam. From (Meek and Quantock 2001).

The angle through which the x-rays are scattered is called the scattering angle; the greater the scattering angle, the greater the radial distance (R) from the centre of the pattern. When the x-rays are scattered at large angles (generally defined as greater than 2 degrees) high-angle patterns are recorded using a short specimen to detector distance (approximately 15-20cm); when the x-rays are scattered through small angles (less than 2 degrees) low-angle patterns are recorded using a much larger specimen to detector distance of several metres (Meek and Quantock 2001).

Low-angle meridional reflections produced by corneal collagen are caused by the 65nm D-periodicity along the fibril axis, whilst high-angle equatorial reflections arise from the lateral packing of the molecules within the stromal collagen fibrils. As the collagen molecules are aligned roughly parallel to each other and scatter x-rays at right angles to the direction of their long axis, the orientation of the molecules can therefore be said to reasonably represent the direction of the collagen fibrils at that position within the corneal stroma. This principle is used throughout this study to examine how the preferred orientation of collagen varies within an individual cornea and also how the orientation is altered in keratoconus corneas. The intensity of the reflection provides quantitative information regarding the number of molecules lying

in a certain direction. Therefore, regions of higher scattering intensity on the XRD pattern indicate more collagen travelling in a particular direction.

The cornea is unlike most connective tissues in that it also produces a low-angle equatorial pattern in addition to the usual high-angle equatorial pattern (from the lateral packing of collagen molecules) and the low-angle meridional pattern (from the D-periodicity of collagen). The low-angle equatorial reflection is caused by the uniformity of fibril diameters and the regular spacing of collagen fibrils (over a short range), within each lamella of the corneal stroma. The low-angle equatorial reflection is comprised of two parts. One is the interference function, which is caused by the scattering from an array of collagen fibrils and is therefore dependent on the position of the fibril centre; the other arises from the scattering of a single fibril and so is dependent upon the fibril radius (Goodfellow *et al.* 1978).

1.13 Aims of the thesis

This thesis aims to characterise the ultrastructure of the normal human cornea using both high and low-angle XRD to gain quantitative information about the arrangement and distribution of collagen in the stroma (Chapters 3, 4 and 5). As bovine corneas are frequently used as animal models for corneal research their stromal arrangement of collagen will also be investigated and compared to the human cornea (Chapter 4). In addition, marmoset monkey corneas will also be examined in order to compare the structure of the human cornea to that of another primate (Chapter 3). The structural arrangement and distribution of collagen in keratoconus corneas will be studied with the aim of learning more about the mechanism by which the disease progresses and understanding the relationship between stromal ultrastructure and corneal stability (Chapter 5). An attempt will be made to form a link between corneal structure and specific keratoconus shape changes by examining structural data from a range of keratoconus corneal buttons alongside videokeratographic images of the same corneas. Finally, the corneas of mice with a murine specific keratopathy resulting in a cone shaped cornea (SKC mice) will be examined using XRD to assess the potential of the SKC mouse strain as an animal model for keratoconus (Chapter 6).

Chapter 2. General Materials and Methods

2.1 Introduction

In this section only the materials and methods relevant to the whole thesis are presented. Details of materials and methods specific to individual experiments are shown in their appropriate chapters.

All XRD work was carried out at the Council for the Central Laboratory of the Research Councils (CCLRC) Synchrotron Radiation Source (SRS), Daresbury Laboratory, Cheshire, UK. Due to scheduled beam time it was necessary for samples to be stored prior to data collection. Samples used for low-angle XRD were either wrapped tightly in clingfilm (to minimise dehydration) and frozen at -80°C or stored in silicon oil. Previous XRD findings have shown that although the interfibrillar spacing (IFS) and fibril diameter is reduced in frozen tissue, upon thawing the normal structural parameters of the cornea are restored (Fullwood and Meek 1994). Silicon oil is frequently used in endothelial studies due to the fact that it doesn't penetrate the tissue.

In the case of samples used for high-angle XRD, in which the preferred orientation of collagen and the distribution of tissue mass was under investigation, samples were either frozen at -80°C or fixed in 2.5% formalin or 4% paraformaldehyde, in order to preserve their structure.

2.2 Sample preparation for x-ray diffraction

In the case of frozen corneas, they were slowly defrosted and then placed (whilst still wrapped in clingfilm) into an airtight transparent sample holder (enclosed between two sheets of Mylar (Dupont-Teijin, UK)). Silicon grease was then smeared around the edge of the sample holder to further reduce the possibility of tissue dehydration during data collection. Samples stored in formalin or paraformaldehyde were removed from their fixative solution, wrapped tightly in clingfilm and treated in the same way as frozen corneas. In the case of corneas stored in silicon oil, it was not possible to wrap them in clingfilm, so instead damp cotton wool was placed in the sample holder alongside the sample to minimise dehydration.

2.3 Measuring corneal hydration

As IFS is highly sensitive to corneal hydration (Meek *et al.* 1991) it was necessary to know the hydration of the tissue during the collection of low-angle XRD data. In order to calculate corneal hydration the sample was weighed before and after data collection to calculate an average wet weight during data collection. The sample was then placed in an oven at 60°C for approximately 3 days until a constant dry weight was reached. Tissue hydration was calculated using Equation 2.

Equation 2: Calculation of tissue hydration

$$\text{Hydration (H)} = \frac{\text{(average wet weight – dry weight)}}{\text{dry weight}}$$

2.4 Low-angle x-ray diffraction

2.4.1 Locating the position of the x-ray beam

Prior to data collection, the exact position of the beam was located by exposing a piece of x-ray sensitive paper (mounted on a piece of graph paper the same size and shape as the sample holder), to the x-ray beam for 10 seconds. A red mark was formed on the green x-ray sensitive paper at the point through which the x-ray beam passed. By placing the transparent sample holder over the graph paper (on which the beam position was marked), the cornea was carefully positioned to ensure that the beam passed though the cornea in the antero-posterior direction at the desired location according to the requirements of the experiment.

2.4.2 Data collection

Low angle XRD patterns were obtained using an evacuated camera of length 6.25, 8, 8.25 or 9 metres (as specified in each experiment) and a focussed monochromatic x-ray beam (λ=0.154nm) at SRS Station 2.1.

Corneal samples were prepared and positioned in the sample holder as described previously (Section 2.2). The shutters were opened to allow a timed x-ray exposure of the sample and the resulting pattern was recorded on a gas filled wire detector. A lead backstop was positioned between the cornea and the detector to stop any undeviated x-rays. The average intensity of the x-rays during each exposure was recorded by an ion chamber located between the incident x-ray beam and the specimen.

For calibration purposes, an XRD pattern from a vertically positioned piece of rat tail tendon (which has a known 67nm D-periodicity) was recorded at the start of each experiment. To account for any spatial variation in the sensitivity of the detector a single detector response pattern from a 420-minute exposure to a radioactive source (Fe^{55}) was also recorded for each data set

2.4.3 Data analysis

The XRD patterns were analysed using Unix based image analysis software (Fit2d, produced by Dr. A. Hamersley, ESRF, Grenoble, France) and Windows based statistics (Statsoft Statistica) and spreadsheet (Microsoft Excel) packages to obtain values for the fibril diameter and the IFS of the corneas studied.

To account for beam current decay during data collection each data file was normalised against the appropriate ion chamber reading. The detector response pattern was then subtracted from each normalised image to account for any spatial variation in the sensitivity of the detector. Next, a vertical transect was taken through the centre of the pattern and integrated horizontally, to produce an intensity profile of the x-ray pattern (Figure 2.1 A and B). As x-ray scattering patterns are intrinsically symmetrical, the pattern was folded about the centre to produce an average intensity profile of the two halves, thereby increasing the signal to noise ratio (Figure 2.1C). At this stage the intensity distribution is described as a function of radial distance (R) from the centre of the pattern. The scattering angle and hence R are inversely related to the size of the structure causing the scattering. This parameter, the reciprocal space co-ordinate, is designated by the symbol Q. The intensity distribution is given by Equation 3.

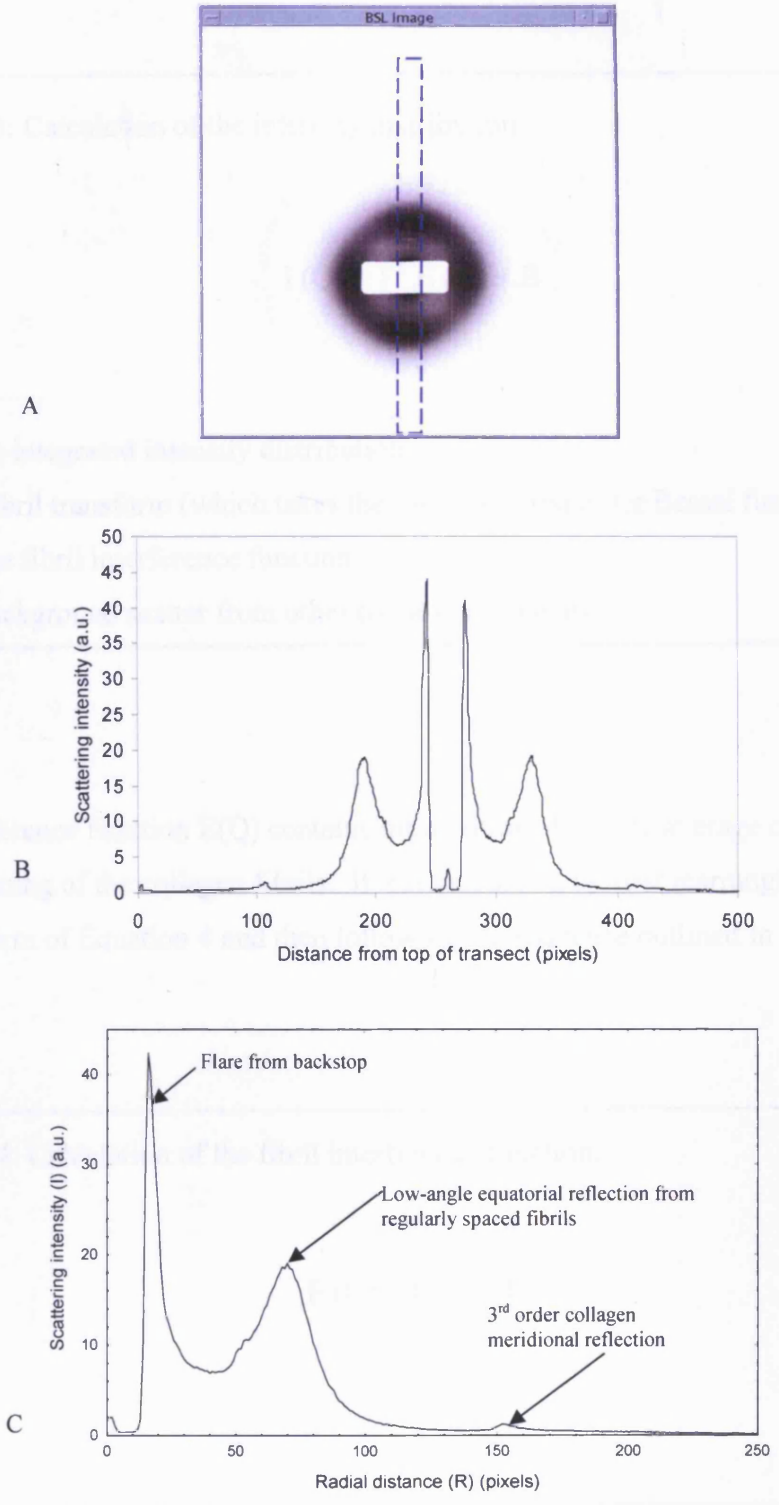

Figure 2.1. (A) Low-angle x-ray scattering pattern from the centre of a normal human cornea. A vertical transect (dashed blue line) was taken through the centre of the pattern to form an intensity profile of the x-ray pattern (B). The data was then folded about the centre to produce an average intensity profile of the two halves (C).

Equation 3: Calculation of the intensity distribution.

$$I(Q) = F^2 E(Q) + B$$

Where,

I (Q) = the integrated intensity distribution

F^2 = the fibril transform (which takes the form of a first order Bessel function)

E (Q) = the fibril interference function

B = the background scatter from other tissue components

The interference function E(Q) contains information about the average centre to centre spacing of the collagen fibrils. It was calculated by first rearranging Equation 3 in the form of Equation 4 and then following the sequence outlined in Steps 1-3.

Equation 4: Calculation of the fibril interference function.

$$E(Q) = \frac{I(Q) - B}{F^2}$$

Step 1: Remove background scatter (B) caused by other tissue components

The scatter intensity (I) was multiplied by the radial position (R) to correct for the use of a linear scan across a circular x-ray pattern, thereby taking into account the fact that only a small sample of the pattern was used to form the integrated intensity distribution profile. A linear background (LOGBK) was generated for the natural log graph of IR against R (Figure 2.2A). The linear background was then anti-logged (ANTILOGB) and subtracted from the image profile graph of R against IR to form a new background-subtracted intensity profile (IR_B). After the removal of diffuse x-ray scatter only the peaks associated with the low-angle x-ray reflections of the cornea remained (Figure 2.2B).

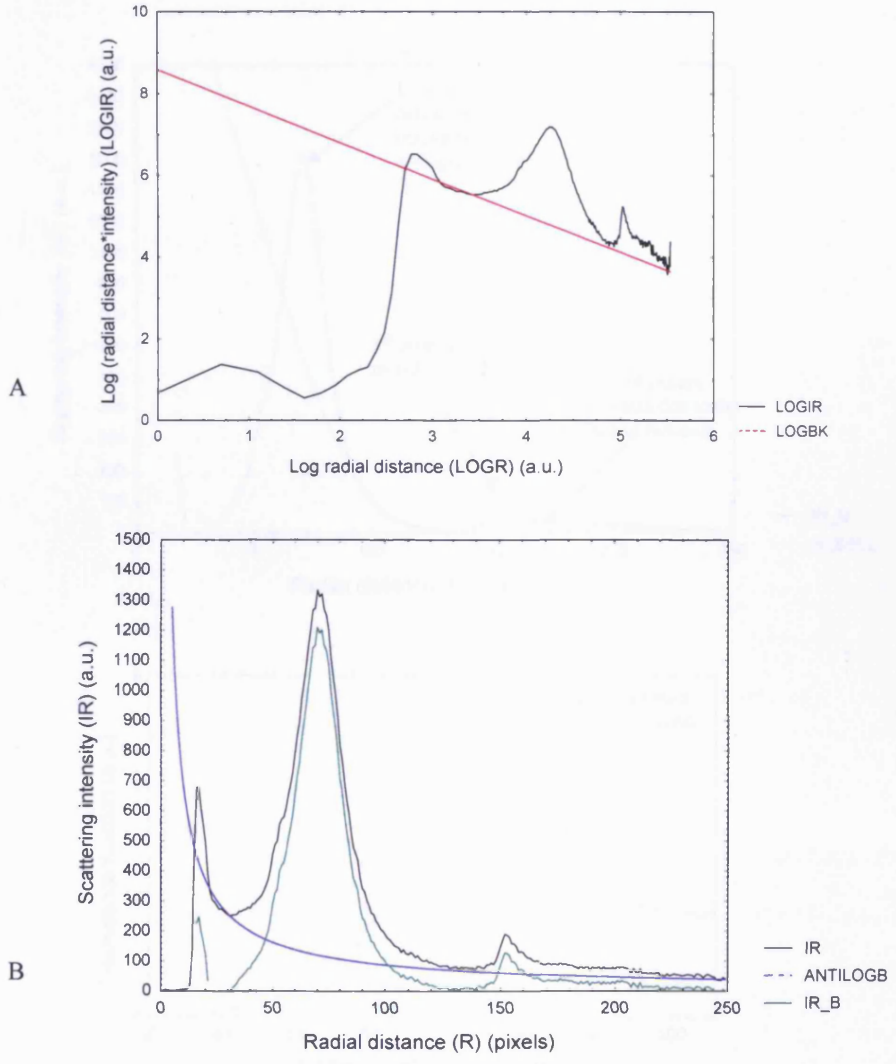

Figure 2.2. (A) A linear background was generated (LOGBK) for the log graph of scattering intensity against radial position (LOGIR). (B) The background scatter (ANTILOGB) was then removed from the profile of scattering intensity against radial position (IR) to leave only the low-angle reflections of the cornea (IR_B).

Step 2: Removal of the fibril transform (F^2)

The fibril transform (which is described in more detail in Step 4), takes the form of a first order Bessel function (BESSEL). The transform has a maximum that produces a low, broad peak near the 3rd order of the collagen meridional reflection. The Bessel function was fitted to this peak in the image profile (IR_B) (Figure 2.3A). The interference function, E(Q), was obtained by dividing the image profile by the fibril transform (Figure 2.3B). This interference function represents the probability of finding a fibril centre at a given distance from another fibril centre. It rises to a peak corresponding to the average nearest neighbour centre to centre spacing of the collagen fibrils then oscillates at about the value of 1 (short range order). In order to determine the Bragg interfibrillar spacing, the radial distance (R) must be calibrated.

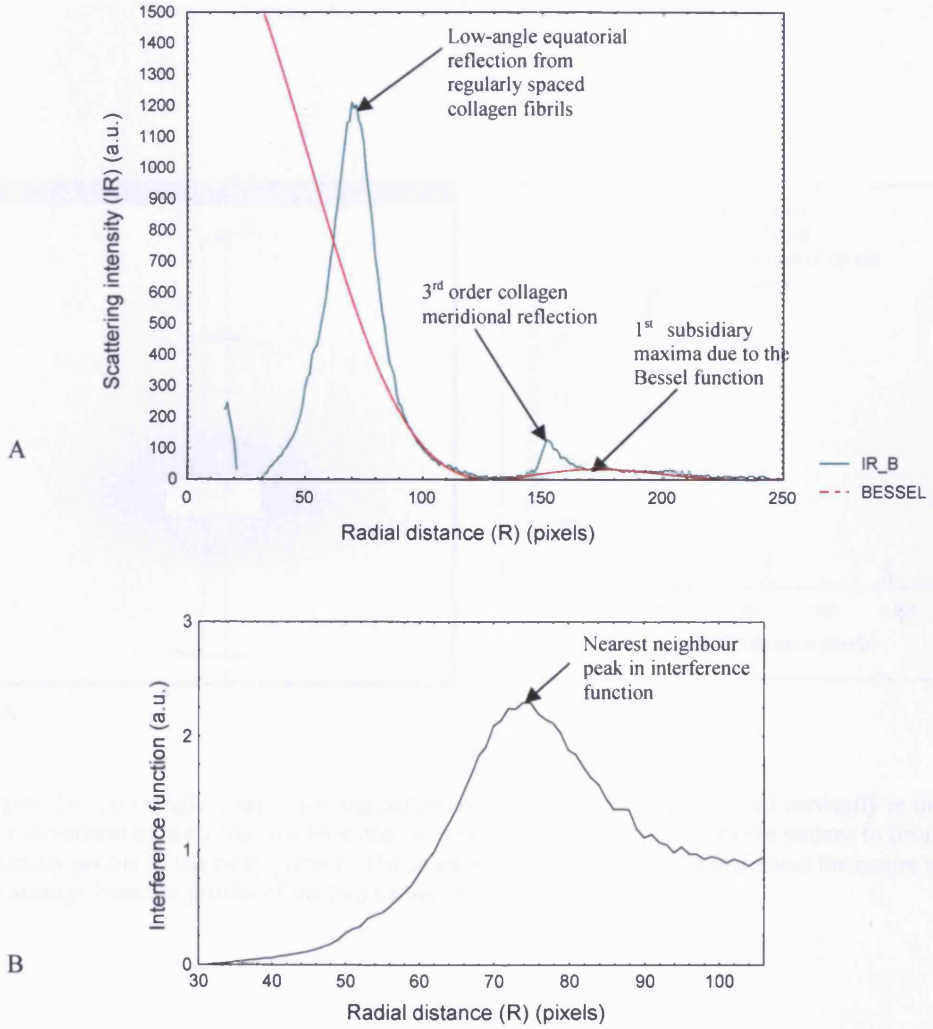

Figure 2.3. (A) The fibril transform (BESSEL) is fitted to the profile of the scattering intensity (from collagen alone) multiplied by radial position (IR_B). (B) The scattering intensity profile is then divided by the fibril transform to produce the interference function.

Step 3: Calculating the Bragg interfibrillar spacing of corneal collagen

The radial distance was calibrated using the position of the sharp meridional 1st order x-ray reflection and known 67nm D-periodicity of rat tail tendon (Figure 2.4). The Bragg interfibrillar spacing of corneal collagen was calculated by first dividing the position of the 1st order reflection of rat tail tendon (Figure 2.4B) by the position of the low-angle equatorial reflection of the corneal collagen (after the removal of background scatter and division by the fibril transform) (Figure 2.3) and then multiplying the resulting number by 67 (the D-period of rat tail tendon). Bragg spacing can be converted to actual interfibrillar spacing using a multiplication factor of 1.12, based on the assumption that the cornea has a liquid-like packing arrangement (Worthington and Inouye 1985). The term IFS used throughout this thesis refers to the actual interfibrillar spacing of collagen fibrils.

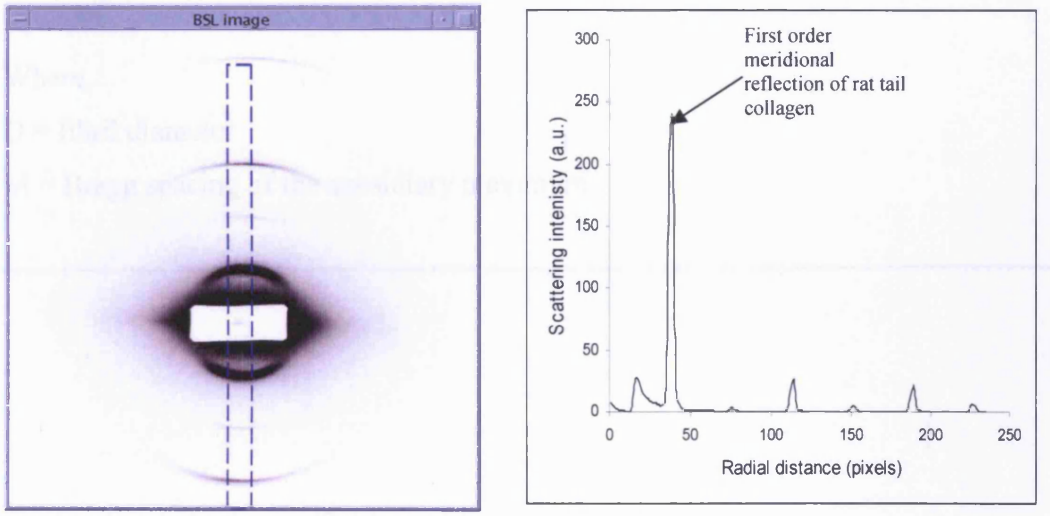

Figure 2.4. Low-angle x-ray scattering pattern from rat tail tendon positioned vertically in the beam (A). A vertical transect (dashed blue line) was taken through the centre of the pattern to form an intensity profile of the x-ray pattern. The intensity profile was then folded about the centre to produce an average intensity profile of the two halves (B).

Step 4: Calculating fibril diameter

Individual collagen fibrils may be well approximated as infinitely long cylinders. Scattering from such cylinders takes the mathematical form of a 1st order Bessel function. The first maxima in a Bessel function occurs at a distance that is inversely related to the diameter (D) of the cylinder. Since the distance is itself inversely proportional to the Bragg spacing (M) of this maximum, there is a simple relationship between M and D (Equation 5).

Equation 5: Calculation of collagen fibril diameter (Worthington and Inouye 1985).

$$D = 2 \times \frac{5.14M}{2\pi}$$

Where,

D = fibril diameter

M = Bragg spacing of the subsidiary maximum

2.5 High-angle x-ray diffraction

2.5.1 Data collection

High-angle XRD patterns were obtained using a focused x-ray beam (λ = 0.1488nm) of dimensions 200x200μm at SRS Station 14.1.

Corneal samples were prepared as described in Section 2.2 and the position of the beam located in the manner described in Section 2.4.1. The resulting x-ray scatter pattern was recorded on a Quantum 4R CCD detector positioned 15cm behind the sample (Figure 2.5). A lead backstop was positioned between the sample and the detector to stop any undeviated rays. The average intensity of the x-rays during each exposure was recorded by an ion chamber located between the incident x-ray beam and the specimen. After normalisation of the x-ray scatter pattern against the intensity of the beam (at the time the pattern was recorded), the intensity of the scattered x-rays is proportional to the amount of collagen in the path of the x-ray beam – the more collagen, the greater the intensity of x-ray scatter. The intensity of the scattered x-rays is therefore a good measure of the collagen mass at a particular location in the tissue.

As x-rays are scattered at right angles to the fibril axis, the distribution of x-ray scatter intensity around the reflection is quantitatively related to the amount of collagen lying in a particular direction within the tissue (Figure 2.5C).

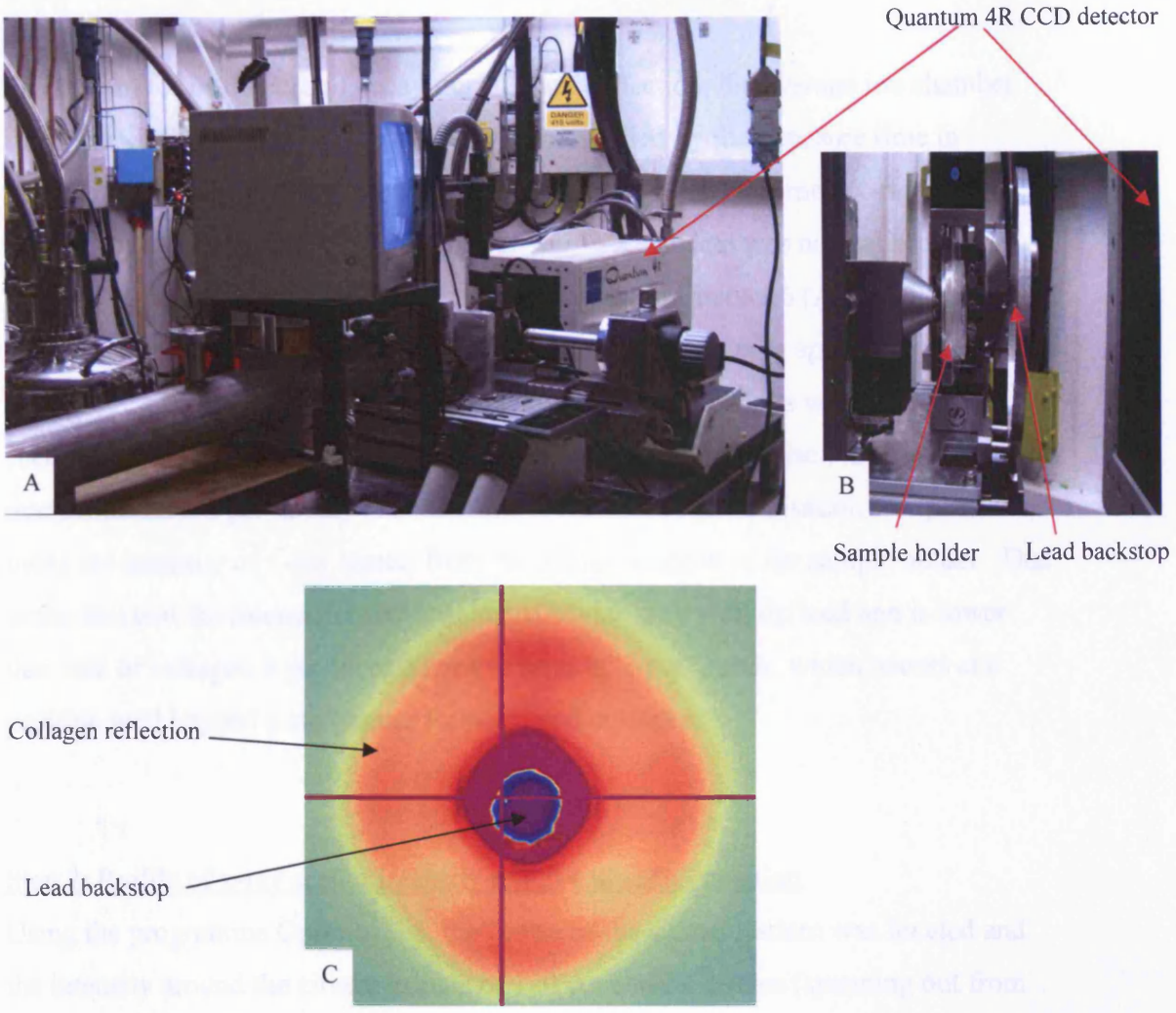

Figure 2.5. (A) Station 14.1, Daresbury SRS, UK. (B) The pattern of x-ray scatter from the specimen is recorded on a Quantum 4R CCD detector; any undeviated x-rays are absorbed by a lead backstop positioned between the sample and the detector. The detector is comprised of four small detectors pieced together. (C) An example of a high-angle x-ray diffraction pattern from the central region of a normal human cornea is also shown. Notice the four orthogonal lobes of increased scatter intensity due to the preferred orientation of collagen in the nasal-temporal and superior-inferior directions.

2.5.2 Data analysis

The aim of the data analysis is to measure (1) the total x-ray scatter and hence the relative collagen mass and (2) the angular distribution of x-ray scatter to produce a fibril orientation function.

The scattering patterns were analysed using Unix based software (Fit2d) and Windows based spreadsheet (Microsoft Excel) and image analysis (Optimus 6.5, Media Cybernetics) packages.

Step 1: Image normalisation

To account for beam current decay during data collection, the average ion chamber reading recorded during each exposure was multiplied by the exposure time in seconds to provide an x-ray intensity value against which the corneal x-ray scatter pattern could then be normalised. All high-angle XRD data was normalised in this way with the exception of the experiment described in Chapter 6 (A study of corneal ultrastructure in normal mice and in mice corneas with a murine specific keratopathy). During the collection of data for this study ion chamber readings were not successfully recorded, therefore making it impossible to normalise the data in the manner described previously. An alternative method of normalisation was performed using the intensity of x-ray scatter from the Mylar window of the sample holder. Due to the fact that the intermolecular spacing of Mylar is so well defined and is lower than that of collagen it produces a narrow band of x-ray scatter, which occurs at a position well beyond x-ray scatter from corneal collagen.

Step 2: Profile of x-ray scatter intensity relative to radial position

Using the programme Optimus 6.5, the centre of the scatter pattern was located and the intensity around the circumference of 120 concentric circles (spanning out from the centre of the pattern to just beyond the ring of collagen scatter), was measured. In the study of the mice corneas with a murine specific keratopathy (Chapter 6), for normalisation purposes, the intensity of scatter was measured around 180 concentric circles so as to include the scatter from Mylar in the resulting intensity profile. The intensity of x-ray scatter around each circle was then averaged and plotted against radial position (Figure 2.6).

Step 3: Background subtraction

The circumference of each concentric circle was then further divided into 256 sectors and the average intensity was recorded for each. Background caused by flare from the backstop and scattering from non-fibrillar material within the cornea was removed by fitting a power law curve to either side of the collagen peak on the plot of scattering intensity versus radial distance and subsequently subtracting it (Daxer and Fratzl 1997). This was done for all of the 256 radial intensity profiles to account for the

uneven flare from the backstop and the changes in background with radial direction (Figure 2.6).

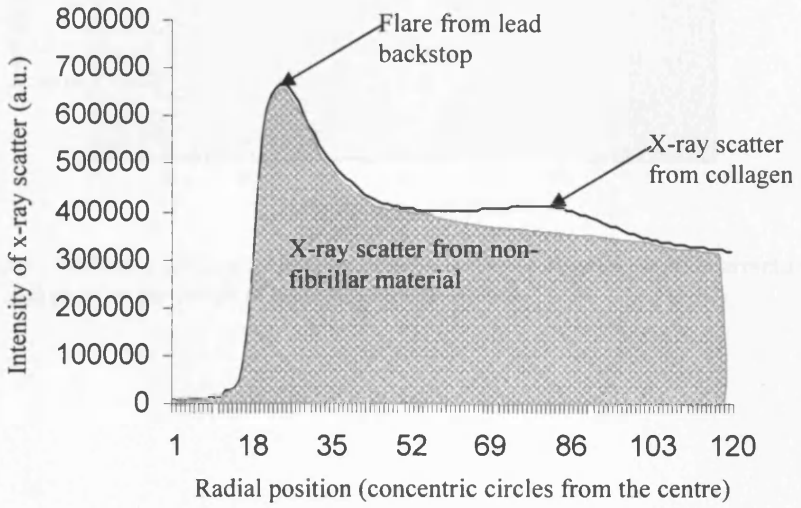

Figure 2.6. Intensity profile of x-ray scatter relative to radial position in the centre of a normal human cornea.

Step 4: Profile of total collagen x-ray scatter intensity relative to radial position

All of the 256 profiles were integrated radially to give a single intensity value for each point on the circumference of the collagen reflection. The profile of collagen x-ray scatter intensity relative to radial position (0-256) was then converted into a profile of collagen x-ray scatter relative to angular position (0-360 degrees) around the XRD pattern (starting at the 3 o'clock position and moving in an anticlockwise direction). The total area under the graph at this stage is proportional to the total collagen mass and is comprised of scatter from collagen lying in all directions (isotropic collagen) and from collagen fibrils with a preferred orientation (aligned collagen) (Figure 2.7).

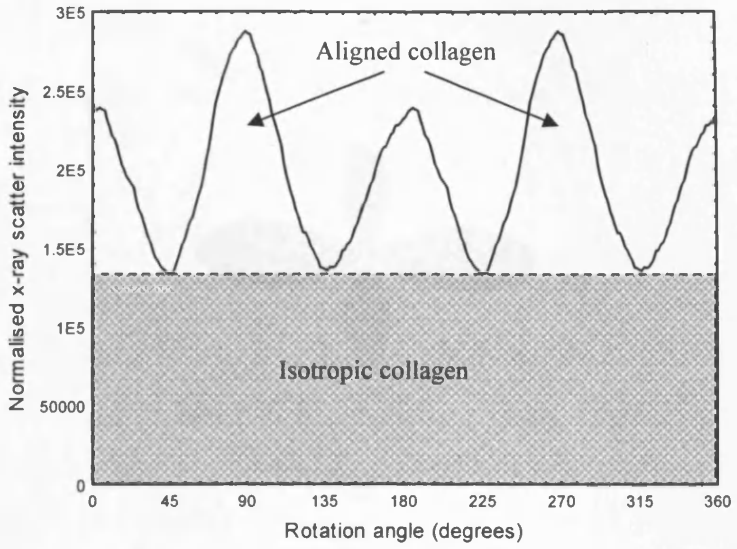

Figure 2.7. Intensity profile of x-ray scatter from collagen relative to angular position around an x-ray diffraction pattern taken from the centre of a normal human cornea.

Step 5: Calculating the index of orientation

A ratio of the scattering from preferentially aligned collagen relative to the total scattering from collagen was generated for each diffraction pattern; this ratio is referred to as the 'index of orientation'.

Step 6: Generation of polar plots to show collagen orientation

A uniform background scatter from isotropic collagen fibrils was removed from the total collagen scatter profile to produce a profile showing only the intensity of aligned collagen scatter relative to angular position (Figure 2.7). As x-rays are scattered at right angles to the direction of the fibril axis the intensity profile was shifted by 90° to produce a new plot showing the relative mass of aligned collagen fibrils as a function of the actual angle at which they occur in the tissue. By plotting this data as a 360° polar plot (Figure 2.8), the distance from the centre of the polar plot in any given direction is representative of the amount of fibrils preferentially orientated in that particular direction at that point in the tissue.

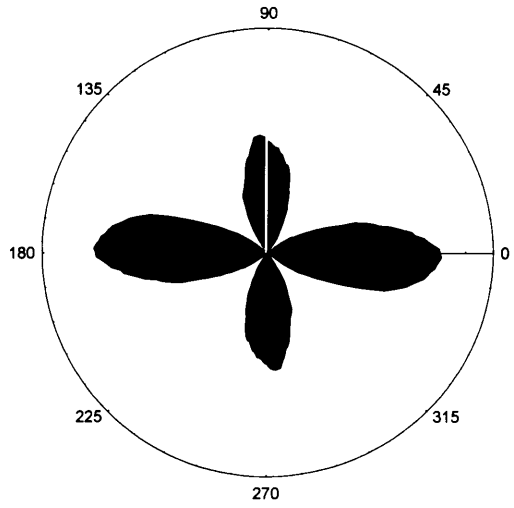

Figure 2.8. A polar plot showing the radial x-ray scatter intensity of preferentially collagen as a function of the angle of orientation in the centre of a normal human cornea. The distance from the centre at any given position is relative to the mass of preferentially aligned collagen travelling in that particular direction.

Chapter 3. A study of collagen interfibrillar spacing and fibril diameter across the human and monkey cornea and limbus.

3.1 Introduction

The biomechanical and optical properties of the cornea are largely governed by the size and organisation of collagen fibrils within the stroma. Corneal transparency requires a certain degree of fibril order (Farrell 1994; Hart and Farrell 1969) and a uniformity of fibril diameter (Farrell 1994; Maurice 1957). The cornea must also have high tissue strength in order to resist the force of intraocular pressure and maintain correct surface curvature for optimum light refraction. Tissue strength is determined by the diameter of the constituent collagen fibrils, their direction in relation to the applied force and the total collagen content (Hukins and Aspden 1985; Jeronimidis and Vincent 1984).

Although many authors have examined IFS and fibril diameter in the centre of the human cornea by means of low-angle XRD (Meek and Leonard 1993) and electron microscopy (Craig and Parry 1981; Freund *et al.* 1995; Kanai and Kaufman 1973), only one has examined the structural changes across the human cornea from limbus to limbus (Borcherding *et al.* 1975). Borcherding (1975) used electron microscopy to study the changes in IFS and fibril diameter across the human cornea and limbus; however, it is known that the tissue preparation required for electron microscopy causes tissue shrinkage (Craig *et al.* 1986; Fullwood and Meek 1993) and is responsible for the considerable variation in IFS and fibril diameter measurements between studies (Borcherding *et al.* 1975; Craig and Parry 1981; Freund *et al.* 1995; Kanai and Kaufman 1973).

Using XRD, it is the primary aim of this study to characterise the changes in fibril diameter and IFS across the human cornea and limbus and to attempt to relate any changes to the properties and functions of the tissue. The same parameters will also be examined across the adult and embryo marmoset monkey cornea and limbus. Factors relating to the biomechanical stability of the monkey cornea are of great interest, as the monkey is widely used as an animal model for human ocular diseases (Fortune *et al.* 2002; Ollivier *et al.* 2003; Peiffer *et al.* 1987) and for studies on the

development and effects of refractive surgery (Melles *et al.* 1998; Petroll *et al.* 1992; Werblin 1992) .

3.2 Materials and Methods

3.2.1 Sample Preparation: human corneas

Five normal human corneas with a 3mm rim of sclera attached (aged 27, 46, 54, 76 and 85 years old), deemed unsuitable for transplantation due to low endothelial cell count were obtained from the UK Corneal Transplant Service Eye bank, Bristol, UK. The corneas were tagged at the time of enucleation with a nylon suture at the 12 o'clock position and stored at the eye bank in mammalian cell culture media (MEM) with 25MM Hepes. On receipt from the eye bank, the samples were rapidly frozen in liquid nitrogen-cooled-isopentane before being wrapped in clingfilm and placed into -80°C storage. The use of isopentane, which is a good cryoconductor, ensures rapid and uniform freezing throughout the tissue, thereby reducing the risk of tissue damage by ice crystal formation. Immediately prior to data collection, the samples were removed from their storage and allowed to thaw at room temperature.

The hydration of the corneas used in this experiment, which was calculated as described in Section 2.3, ranged from H=2 to H=4.

3.2.2 Data collection: human corneas

As described in Section 2.4.2, low-angle XRD patterns were collected on Station 2.1 of the SRS, using a 9m camera, a 0.154nm wavelength and an x-ray beam measuring 0.5mm vertically by 2mm horizontally.

The sample holder was positioned to ensure that the x-ray beam passed through the sample parallel to the optical axis. Using a computer operated stepper system; 180 second exposures were recorded at 0.4mm to 1.0mm intervals along the orthogonal superior-inferior and nasal-temporal meridians. Each sample was rotated through 90 degrees between transects.

3.2.3 Sample preparation: monkey corneas

Two adult (1 male and 1 female) and two foetal (130 days into a 145 day gestation) common marmosets (Callithrix jacchus) were sacrificed by intra-peritoneal injection of a lethal dose of barbiturate at the Department of Physiology, Oxford University, UK. All procedures were carried out in accordance with the Association for Research in Vision and Ophthalmology (ARVO) statement for the use of animals in ophthalmic research.

The eyeballs were removed within 2 hours of death, tagged at the 12 o'clock position using a nylon suture and rapidly frozen in liquid-nitrogen -cooled isopentane. The samples were wrapped in clingfilm and stored at -80°C until required. Immediately prior to x-ray data collection, all of the eyes (with the exception of the adult male right eye and one foetus right eye which were not used in this study), were allowed to thaw at room temperature. Once thawed, a scalpel was then used to remove the cornea with a 0.5mm scleral rim from each sample. Each cornea (with scleral rim) was re-wrapped tightly in clingfilm to prevent dehydration during data collection. Corneal hydration was found to vary very little between samples (H = 2.2 to H = 2.8).

3.2.4 Data collection: monkey corneas

Low-angle XRD patterns were collected as described in Section 2.4.2, using an 8.25m camera, a 0.154nm wavelength and an x-ray beam of dimensions 0.5mm horizontally by 0.5mm vertically. Using the same computer operated stepper system as was used for the human specimens; 120 second exposures were recorded at 0.5mm intervals along the superior-inferior transect of each marmoset cornea.

All data was analysed in the manner outlined in Section 2.4.3.

3.3 Results

3.3.1 Human Cornea: Interfibrillar Spacing

Centre to centre IFS along the superior-inferior and the nasal-temporal transects of each cornea are shown in Figure 3.1.

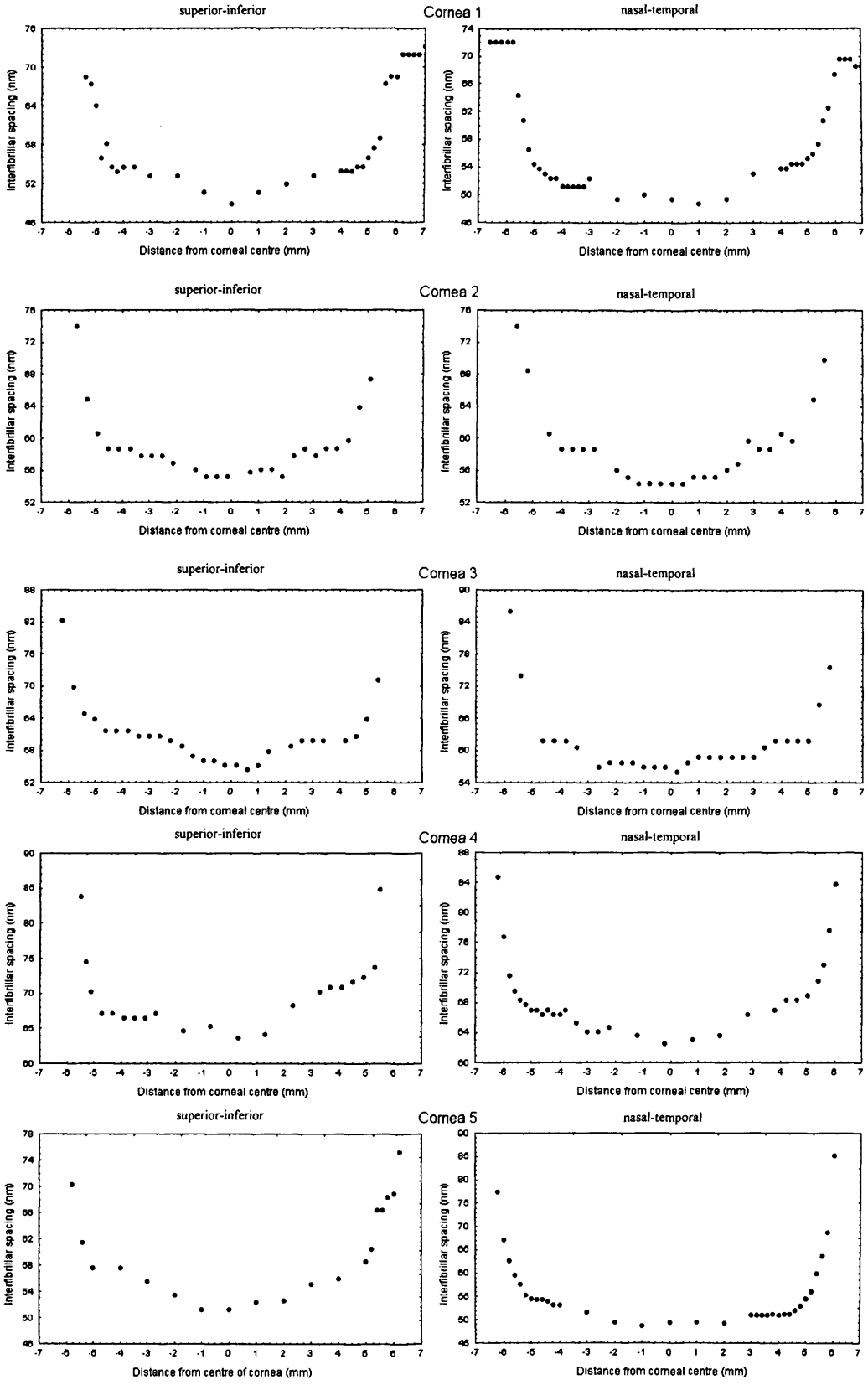

Figure 3.1. Centre-to-centre interfibrillar spacing across orthogonal superior-inferior and nasal-temporal meridians of five normal human corneas.

Table 2 shows the mean IFS within the prepupillary region (the central zone of the cornea responsible for most of corneal refraction) and the peripheral region (the remainder of the cornea) for each of the five corneas studied. In all cases the average IFS was consistently lower (by 7-8%) in the prepupillary region than in the peripheral cornea. A two tailed students T-test revealed the difference in IFS between the prepupillary region and the peripheral cornea to be significant ($P<0.01$). At the limbus the IFS rapidly increases by approximately 25-40%.

Cornea	Hydration	Corneal region	Mean Interfibrillar Spacing (nm) +/- SD.	Significance (P)
1	2.0	Prepupillary	50.2 +/- 1.4	<0.01
		Peripheral	53.8 +/- 2.4	
2	2.7	Prepupillary	55.2 +/- 0.6	<0.01
		Peripheral	60.0 +/- 3.0	
3	2.9	Prepupillary	56.9 +/- 1.4	<0.01
		Peripheral	61.7 +/- 3.6	
4	4.0	Prepupillary	63.8 +/- 0.9	<0.01
		Peripheral	69.0 +/- 4.6	
5	2.0	Prepupillary	50.7 +/- 1.7	<0.01
		Peripheral	55.4 +/- 4.2	

Table 2. Comparison of interfibrillar spacing in the prepupillary and peripheral regions of five human corneas. The statistical significance level (P) between regions is shown.

The results (Figure 3.1 and Table 2) clearly show that differences in corneal hydration between specimens have a similar effect on the IFS in the prepupillary and peripheral regions, with an increase in hydration resulting in an increase in IFS. As additional water appears to be evenly distributed across the cornea a simple equation was formed (Equation 6), based on the linear relationship between hydration and IFS^2 (Meek *et al.* 1991), to normalise the IFS measurements of each cornea to near physiological hydration ($H = 2.9$). It must be remembered however that the linear relationship between hydration and IFS^2 has only been confirmed to exist in the central region of the cornea and this study has assumed that the same relationship also exists in the peripheral cornea and limbus based on the fact that although the IFS values differed between corneas, the same profile of IFS was observed across each cornea despite differences in the hydration of the specimens.

Equation 6: Normalisation of interfibrillar spacing measurements to physiological hydration.

$$D_{norm}^{2} = \frac{d^2 \times H_{phys}}{H_{actual}}$$

Where,

D_{norm}^{2} = Interfibrillar spacing (nm) normalised to near physiological hydration.
d^2 = Interfibrillar spacing (nm) before normalisation to near physiological hydration.
H_{phys} = near physiological hydration (taken to be H = 2.9)
H_{actual} = Actual hydration of cornea.

Figure 3.2 shows the average IFS along the superior-inferior and nasal-temporal transects for the five corneas normalised to near physiological hydration (H = 2.9). The three corneal surface zones: central prepupillary, peripheral cornea and the limbus have been marked onto each transect.

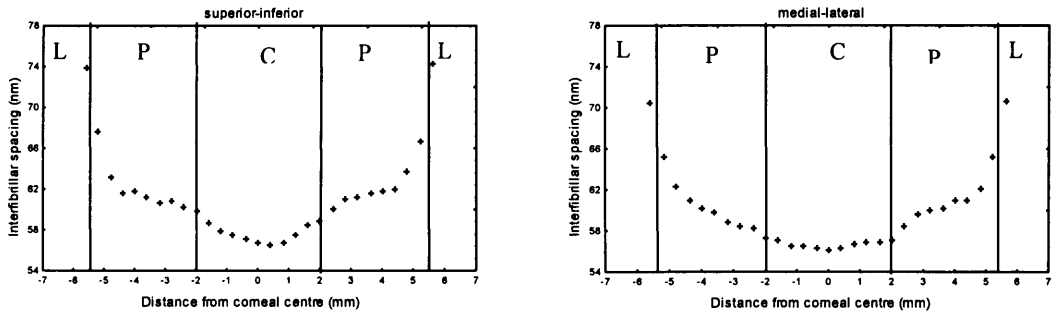

Figure 3.2 Centre to centre interfibrillar spacing, averaged over five corneas normalised to near physiological hydration (H = 2.9). Central (prepupillary), peripheral and limbal zones are denoted by C, P and L, respectively.

Further analysis of the grouped data (from the five human corneas normalised to physiological hydration) using a two tailed Student t-test confirmed IFS to be

significantly lower in the prepupillary region compared to the peripheral regions ($P<0.01$).

3.3.2 Human Cornea: Fibril Diameter

Collagen fibril diameters along the superior-inferior and the nasal-temporal transect of each cornea are shown in Figure 3.3. In all cases fibril diameter was found to be fairly constant across the prepupillary cornea and increase marginally at the periphery. Consistent with the findings of Borcherding (1975), a sharp increase in fibril diameter (of up to 75%) was observed at the limbus.

When compared at the same corneal position there was very little variation in fibril diameter between samples despite differences in tissue hydration; this indicates that fibril diameter is unaffected by changes in tissue hydration within the range studied (H=2 to H=4). This finding is consistent with previous studies (Daxer *et al.* 1998; Meek *et al.* 1991).

Table 3 shows the mean fibril diameter in the prepupillary and peripheral regions for each cornea examined. In each of the five corneas, the fibril diameter was slightly larger and more variable in the peripheral cornea compared to the prepupillary region of the same cornea ($P<0.01$).

Cornea	Hydration	Corneal region	Mean Fibril diameter (nm) +/- SD	Significance (P)
1	2.0	Prepupillary	33.3 +/- 0.3	<0.01
		Peripheral	36.6 +/- 4.2	
2	2.7	Prepupillary	32.8 +/- 0.2	<0.01
		Peripheral	35.4 +/- 4.2	
3	2.9	Prepupillary	32.0 +/- 0.3	<0.01
		Peripheral	33.0 +/- 0.4	
4	4.0	Prepupillary	33.9 +/- 0.1	<0.01
		Peripheral	36.2 +/- 3.3	
5	2.0	Prepupillary	32.9 +/- 0.1	<0.01
		Peripheral	36.4 +/- 3.8	

Table 3. Comparison of fibril diameter in the prepupillary and peripheral regions of five human corneas. The statistical significance level (P) between regions is shown.

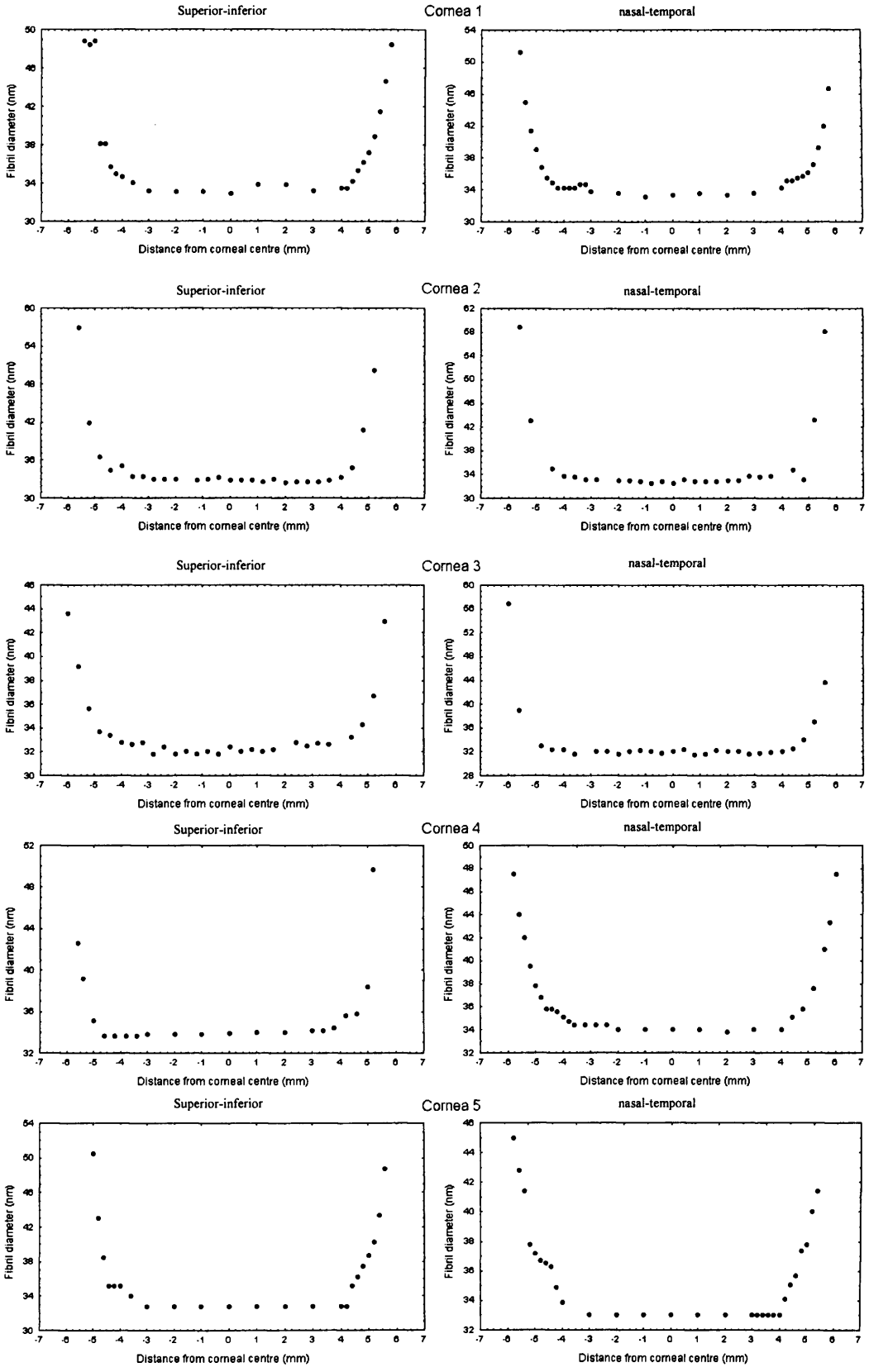

Figure 3.3. Fibril diameter across orthogonal superior-inferior and nasal-temporal meridians of five normal human corneas.

Using Equation 7 and the XRD measurements of Bragg interfibrillar spacing (IFS/1.12) and fibril diameter presented in Tables 2 and 3, the volume fraction of fibrils (VFF) in the stroma was calculated for both the prepupillary and peripheral regions of each cornea, on the basis of a 'unit cell' representing the average volume occupied by each fibril (Meek and Leonard 1993); the results are presented in Table 4. A paired T-test revealed no significant difference in VFF between the prepupillary and peripheral regions of the cornea. An increase in tissue hydration resulted in the VFF in both the prepupillary and peripheral regions decreasing by the same amount; a ratio of 1:1 (prepupillary VFF to peripheral VFF) was maintained at all hydrations between H=2 and H=4 (Table 4).

Equation 7. Calculation of the volume fraction of fibrils in the corneal stroma

$$VFF = \pi diam^2 / (4 \times 1.12 \times BS^2)$$

Where,

VFF = volume fraction of fibrils in the stroma

Diam = fibril diameter (nm) and $\pi diam^2/4$ is the area per unit length of a fibril.

BS = Bragg interfibrillar spacing (nm) and BS^2 is the area per unit length of the 'unit cell'. Multiplication by 1.12 is based on the assumption that fibrils are packed with a liquid–like order (Worthington and Inouye 1985)

Cornea	Hydration	Corneal region	Volume fraction of fibrils (VFF)	Ratio between prepupillary and peripheral VFF
1	2.0	Prepupillary	0.39 +/- 0.03	**1:1**
		Peripheral	0.40 +/- 0.12	
2	2.7	Prepupillary	0.31 +/- 0.01	**1:1**
		Peripheral	0.31 +/- 0.13	
3	2.9	Prepupillary	0.28 +/- 0.03	**1:1**
		Peripheral	0.25 +/- 0.03	
4	4.0	Prepupillary	0.25 +/- 0.01	**1:1**
		Peripheral	0.24 +/- 0.10	
5	2.0	Prepupillary	0.37 +/- 0.03	**1:1**
		Peripheral	0.38 +/- 0.13	

Table 4. The volume fraction of fibrils (VFF) in the prepupillary and peripheral regions of five human corneas.

3.3.3 Monkey Corneas: Interfibrillar spacing and fibril diameter

Fibril diameter and centre-to-centre IFS measurements across the superior-inferior transect of three adult marmoset corneas are shown in Figure 3.4. Figure 3.5 shows the same measurements taken from three foetal marmoset corneas. Noisy data meant that it was not possible to measure fibril diameter and IFS at some positions across the foetal marmoset cornea. The approximate superior-inferior dimensions of the adult marmoset cornea (4mm) and the foetal marmoset cornea (2mm), based on average measurements of 36 marmoset corneas (Troilo *et al.* 1993), have been superimposed onto each respective graph (Figure 3.4 and 3.5 respectively). In both the adult and foetal marmoset corneas the fibril diameter and IFS increase rapidly at the limbus.

Table 5 shows the average IFS and fibril diameter across each cornea. As in the human cornea, an increase in hydration (between H=2.2 and H=2.8) results in an increase in IFS in the adult marmoset cornea, whilst fibril diameter remains relatively constant.

Cornea	Hydration	Mean Interfibrillar Spacing (nm) +/- S.D.	Mean Fibril Diameter (nm) +/- S.D.
Female left	2.2	50 +/- 2.8	34.4 +/- 1.9
Female right	2.9	55.8 +/-2.6	34.9 +/- 1.6
Male left	2.7	53.1 +/- 3.2	35 +/- 2.0
Foetus 1 left	2.8	45.8 +/- 0.5	31.9 +/- 1.0
Foetus 1 right	2.8	60.8 +/- 1.1	32.1 +/- 1.0
Foetus 2 left	2.7	59 +/- 1.9	33.0 +/- 1.5

Table 5. The average IFS and fibril diameter across the adult (n = 3) and foetus (n = 3) marmoset monkey cornea.

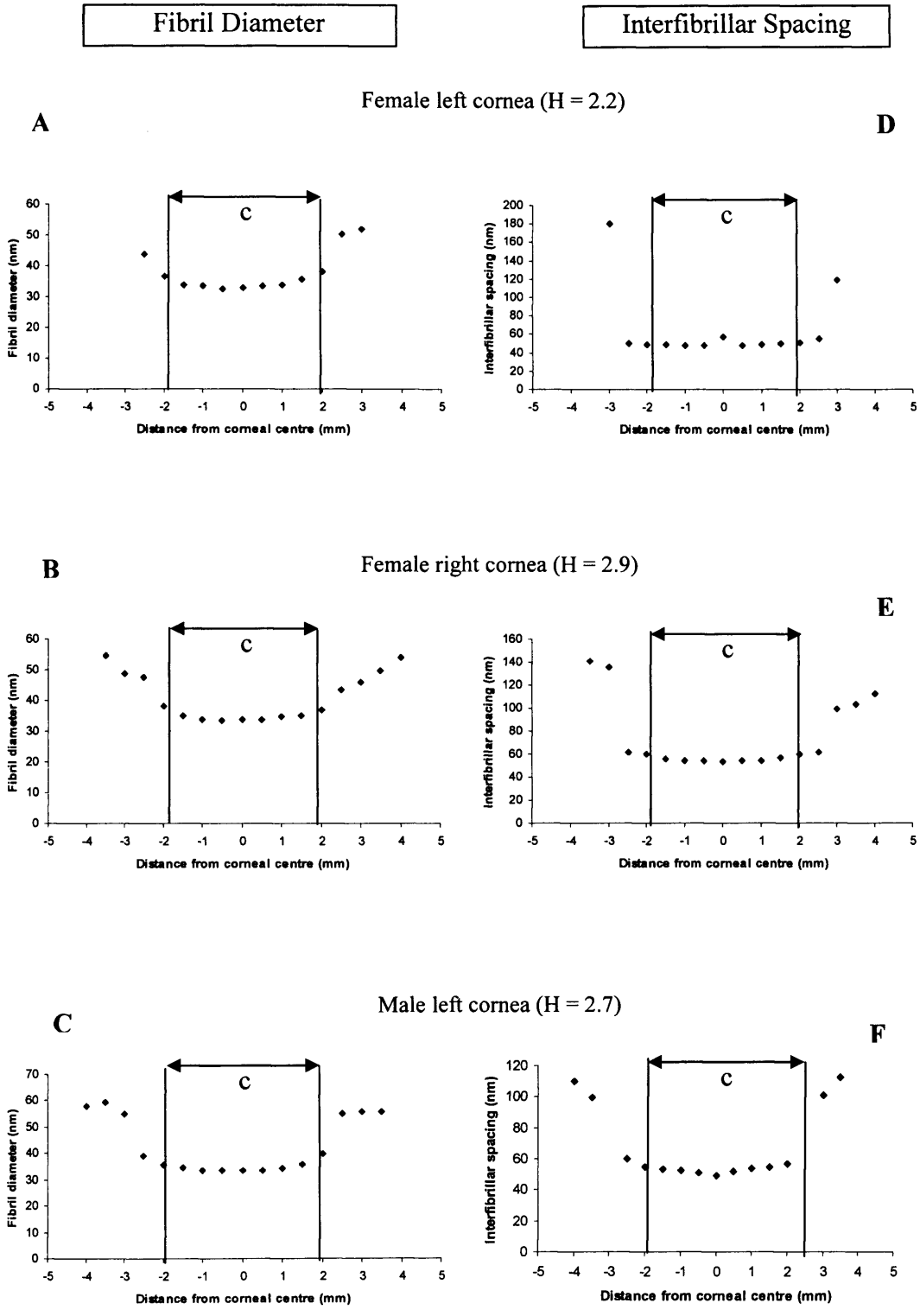

Figure 3.4. Fibril diameter (A, B, C) and centre-to-centre interfibrillar spacing (D, E, F) across the superior-inferior transects of three adult marmoset corneas. The approximate diameter of the cornea (C) is shown on each graph.

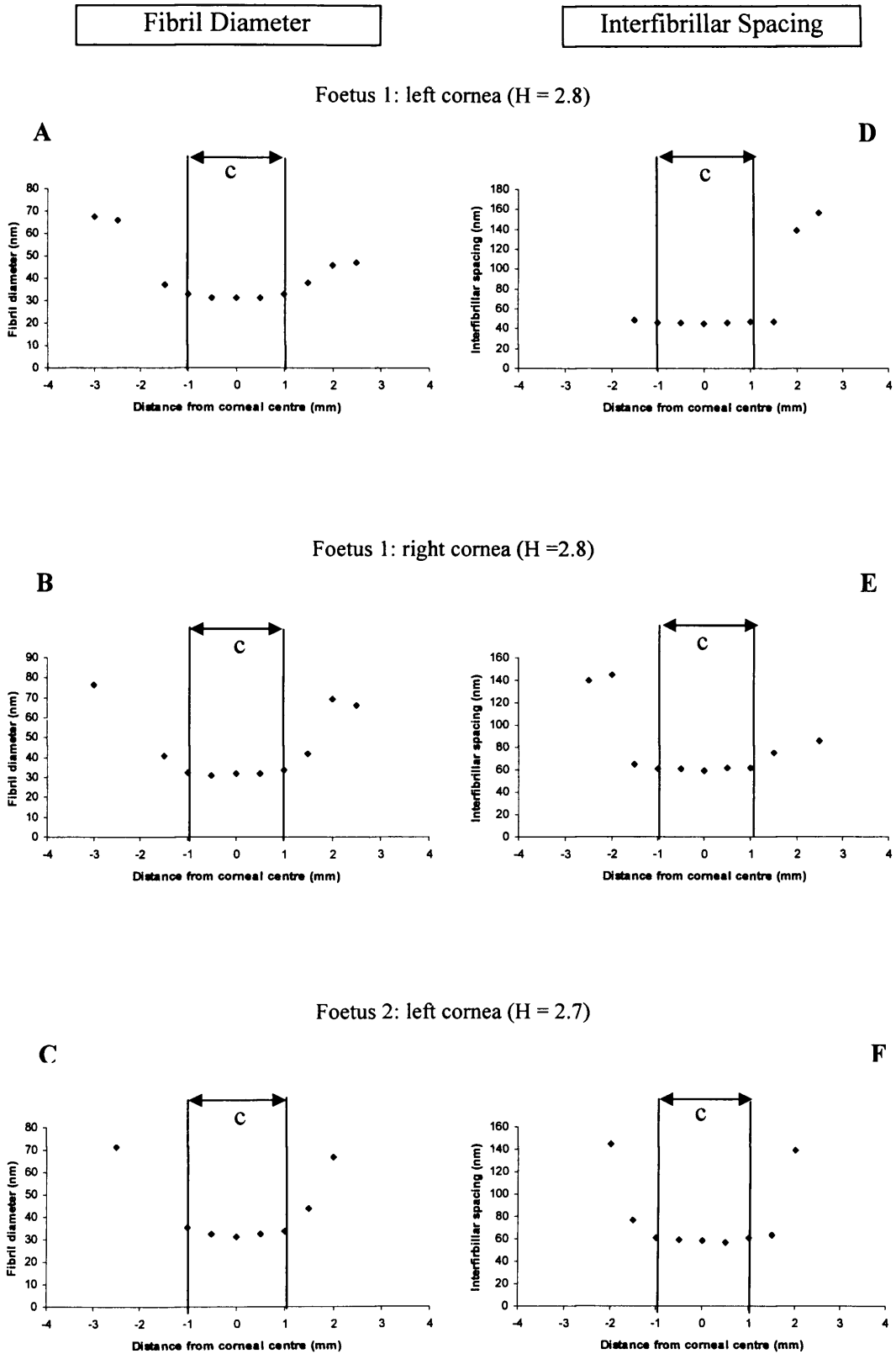

Figure 3.5. Fibril diameter (A, B, C) and centre to centre interfibrillar spacing (D, E, F) across the superior-inferior transects of three foetal marmoset corneas. The approximate diameter of the cornea (C) is shown on each graph.

For comparison purposes with the human corneas, each marmoset cornea was normalised to a hydration of H = 2.9 using Equation 6. The normalised IFS values were then grouped to calculate average IFS across both the adult and foetal cornea. Once normalised against hydration, the results revealed the average IFS across the cornea to be the same in both adult and foetal marmoset (56nm). This suggests that at day 130 of a 145 day gestation period collagen fibril organisation is complete in the marmoset monkey cornea.

Statistical analysis of the normalised IFS measurements using ANOVA found there to be no significant difference in IFS values across individual adult or embryo marmoset cornea. Normalised IFS did not differ between adult marmoset corneas, however, a slight difference in IFS was observed between the three foetal marmoset corneas ($P < 0.05$). Of the three foetal corneas studied, the pair from the same animal also showed a difference in normalised IFS values ($P < 0.05$). This indicates that the variation between foetal corneas in terms of IFS is not likely due to differences in developmental stage but is more likely due to slight inaccuracies in the measurements of the wet and dry corneal weight, caused by the small size of the samples. A slight error in the measurement of the wet weight, the dry weight or both would have a large impact on the determined corneal hydration. As IFS is extremely sensitive to hydration an error in the calculation of corneal hydration may be a possible explanation for the apparent variation in IFS between foetal corneas when normalised to the same hydration.

3.4 Discussion

This study has shown that fibril packing is non-uniform across the human cornea and that the fibril matrix is more compact in the prepupillary region than in the peripheral cornea. The mean IFS in the human cornea was found to be between 7 and 8% lower in the prepupillary region than in the periphery ($P<0.01$). The increase in IFS between the prepupillary and peripheral cornea coincides with a major loss of keratan sulphate and the appearance of more highly sulphated glycosaminoglycans, such as chondroitin sulphate and dermatan sulphate (Borcherding *et al.* 1975). Borcherding and colleagues suggested that the reduced number of fibrils per unit area in the

peripheral cornea may be due to the fact that its sulphated chondroitin molecules extend further into the interfibrillar space than the unsulphated chondroitin molecules present in the central cornea (Borcherding *et al.* 1975). A further explanation may be that the variation in IFS across the cornea is due to localised changes in tissue hydration, whereby a higher hydration in the peripheral cornea might explain the higher IFS.

In agreement with previous work (Borcherding *et al.* 1975), the size of the collagen fibrils remained constant across the prepupillary region of individual corneas, became more variable and increased marginally in the peripheral region and rose rapidly at the limbus. The increase in fibril diameter and IFS at the limbus may provide a smoother transition between corneal and scleral collagen arrangement.

Bearing in mind that corneal thickness is at least 20% lower in the centre of the cornea than at the periphery (Klyce and Beuerman 1988) it seems likely that the closer packing of collagen fibrils in the central cornea serves to increase tissue strength, whilst the thinness of the central cornea compensates for the higher packing density, in terms of tissue transparency (Boote et al. 2003 – Appendix 4). In support of this, research has shown that the cornea is stiffer in the prepupillary region than at the periphery (Hjørtdal 1996).

Calculations by Farrell and McCally (1994) showed that corneal transparency is critically dependent on the total scattering cross section, the fibril density and the thickness of the cornea. The total scattering cross section is determined by the refractive index of the fibrils relative to the ground substance, the size of the collagen fibrils and their mode of packing and the wavelength of the incident light and the angle through which it is scattered. Although the average fibril diameter and IFS vary between the prepupillary and peripheral regions of the cornea, the VFF is the same across both regions. Therefore on the assumption that the ratio of fibril refractive index to ground substance refractive index does not differ between the prepupillary and peripheral regions, one may predict that the total scattering cross section is constant across the cornea. Unfortunately, there appears to be no measurements of refractive index and transparency across the cornea to test this hypothesis.

Between a hydration of H=2 and H=4 additional water appears to be uniformly absorbed across the cornea and limbus, as an increase in corneal hydration resulted in a uniform increase in IFS across the prepupillary, peripheral and limbal regions (Figure 3.1); fibril diameter was unaffected by the change in hydration (Figure 3.3). Within the same hydration range (H=2 to H=4) the VFF did not differ significantly between the prepupillary and peripheral regions of individual corneas ($P<0.01$) (Table 4). Since the VFF is inversely proportional to IFS^2 this supports the existence of a linear relationship between IFS^2 and hydration across all zones of the cornea.

The dimensions of the prepupillary and peripheral regions have yet to be defined for the marmoset cornea. It is clear however, that both fibril diameter and IFS remain fairly constant across the cornea before increasing rapidly at the limbus. The resulting pattern of IFS and fibril diameter across the marmoset cornea is very similar to that of the human cornea. The average fibril diameter across the cornea differs only slightly between foetal and adult marmosets (33 and 34nm respectively) and humans (32nm). When normalised to near physiological hydration (H = 2.9) the average IFS along the superior-inferior transect of both adult and foetal marmoset cornea (56nm) was lower than that of the human cornea (61nm).

Unfortunately, noisy data meant that very few data points were suitable for analysis in the limbal region of the marmoset corneas; however, in both the adult and the embryo marmoset there is clear evidence that, as in the human cornea, fibril diameter and IFS increase rapidly at the limbus (by approximately 50%). It is likely that the increased size of the fibrils at the limbus in both human and marmoset monkey eyes provides the cornea with the high tensile strength required to both maintain corneal curvature at the point where the cornea meets the less curved sclera. The additional strength may also be necessary to prevent tissue distortion during eye movement

It is also notable that at 130 days into a 141-145 day gestation period, fibril diameter and IFS in the foetal cornea are already at adult levels and that the sharp increase in fibril diameter and IFS at the limbus is well established, although it must be acknowledged that due to the limited availability of adult and foetal marmoset corneas for the purposes of this study, the aforementioned conclusions are based on small

sample numbers. However, these findings are consistent with a previous electron microscopy study of marmoset corneal development, in which the average fibril diameter of the anterior and mid stroma was found to change very little between 43 days gestation (29-33nm) and birth (33-41nm) (Ozanics *et al.* 1977).

3.5 Conclusions

Collagen fibrils are more closely packed in the prepupillary region of the human cornea. As the central cornea is thinner than elsewhere, the closer packing of collagen fibrils may serve as a means of increasing tissue strength. The reduced tissue thickness in the central cornea and the closer packing of collagen fibrils indicate an optimisation of both tissue strength and transparency in the main optical zone of the cornea. Changes in corneal hydration (between H=2 and H=4) appear to affect the IFS across the human cornea uniformly, with an increase in hydration resulting in an increase in IFS.

The increase in IFS and fibril diameter seen at the limbus and to a lesser extent between the prepupillary and peripheral regions of the human cornea coincides with a major change in proteoglycan composition.

In the marmoset monkey, both IFS and fibril diameter remain fairly constant across the cornea before increasing rapidly at the limbus. As with the human cornea, the increase in fibril diameter at the limbus likely serves as a means of increasing tissue tensile strength at the point where the cornea meet the less curved sclera. The increase in fibril diameter and IFS at the limbus may also provide a smoother transition between corneal and scleral collagen organisation.

On the basis of IFS and fibril diameter measurements alone, the marmoset monkey cornea appears to be a good animal model for human corneal studies.

3.6 Future study

- Measurements of refractive index and transparency across the cornea would be of great importance to ocular research, however, to date no such measurements have been made.

- In order to either prove or disprove the hypothesis that the variation in IFS across the human cornea is caused by hydration changes, a detailed study measuring corneal hydration across the cornea is also needed.

- The development of mechanical models of the cornea to help predict the outcomes of various surgical techniques requires detailed structural information about the cornea. It would therefore be beneficial to extend this study to examine the IFS and fibril diameter over the entire human cornea, so as to provide further information for the development of such models.

Chapter 4. A study of collagen fibril orientation as a function of tissue depth in the human and bovine cornea

4.1 Introduction

Previous XRD studies of the human cornea have found collagen fibrils to lie in two preferred orthogonal directions (nasal-temporal (NT) and superior-inferior (SI)), with the effect mainly occurring in the posterior stroma (Meek *et al.* 1987). Out of 35 animal species studied to date by XRD, the orthogonal preferred orientation of collagen fibrils has only been seen in the human cornea and the primary chick stroma (Meek *et al.* 1987; Quantock *et al.* 1998).

The present study aims to characterise the preferred orientation of collagen fibrils throughout the thickness of the stroma in both human and bovine cornea in order to identify anterior-posterior differences and to relate any differences to corneal function.

4.2 Materials and methods

4.2.1 Sample preparation: human corneas

Human corneas (n = 6) aged between 48 and 82 years old, deemed unsuitable for transplant due to low endothelial cell count, were donated from the Manchester Eye Bank and the Bristol Eye Bank for the purposes of this study. The details of each sample are shown in Table 6. Corneas A, B, C and D (from the Manchester Eye Bank) were fixed in 4% paraformaldehyde and refrigerated at 4°C until required for data collection. Corneas E and F (from the Bristol Eye Bank) were removed from their culture medium on arrival, wrapped in clingfilm, and transferred to a -80°C freezer. With the exception of one cornea (D), which was tagged at the 12 o'clock position, the orientation of the remaining corneas was unknown.

A silk suture was attached at the edge of each cornea to serve as a point of reference during sectioning to ensure that all the sections taken from an individual cornea would have the same orientation.

Reference	Sample details	Storage before sectioning	Storage after sectioning
Cornea A	Right cornea, 70 year old male	Paraformaldehyde	Paraformaldehyde
Cornea B	Left cornea, 48 yr old male	Paraformaldehyde	Paraformaldehyde
Cornea C	Left cornea, 60 yr old male	Paraformaldehyde	Paraformaldehyde
Cornea D	Right cornea, 79 yr old female	Paraformaldehyde	Paraformaldehyde
Cornea E	Left cornea, 82 yr old male	Frozen	Silicon oil
Cornea F	Left cornea, 77yr old male	Frozen	Silicon oil

Table 6. Sample details for six human corneas used in the study of preferred collagen orientation as a function of tissue depth.

4.2.2 Sample preparation: bovine corneas

Bovine eyeballs (n = 8) were obtained from the abattoir within 3 hours of death. The cornea (with epithelium and endothelium intact) was dissected from each eyeball with a scalpel and a nylon suture was used to tag the corneas at either the 12 o'clock (superior) or 6 o'clock (inferior) position. The oval shape of the cow cornea enabled the SI meridian to be distinguished from the NT meridian. However, due to the previous removal of the extra ocular muscles and optic nerve, it was not possible to determine whether an individual cornea originated from a left or right eye. Therefore, although the SI meridian could be easily determined, it was not possible to distinguish between the *in vivo* 12 o'clock and 6 o'clock positions. The samples were fixed in 4% paraformaldehyde and stored at 4°C for 2 days prior to sectioning and data collection.

4.2.3 Sectioning of corneas

Using a pipette, a dome of ice was formed by dropping water onto the frozen stage of a Mikrom sliding microtome. The stage was maintained at –16°C by means of an adjoining freezer (Figure 4.1). The cornea was moulded over the dome of ice in such a way that the surface of the cornea appeared smooth and curved, mimicking its natural shape. Once the cornea was firmly in position, a beaker was placed over the top of the cornea (to minimise surface evaporation) and the temperature of the stage was rapidly reduced to –40°C; this ensured a rapid freezing of the tissue and a firm attachment of the cornea to the dome of ice. The size and shape of the dome of ice

varied between samples due to human corneas being smaller and having a smaller radius of curvature than bovine corneas.

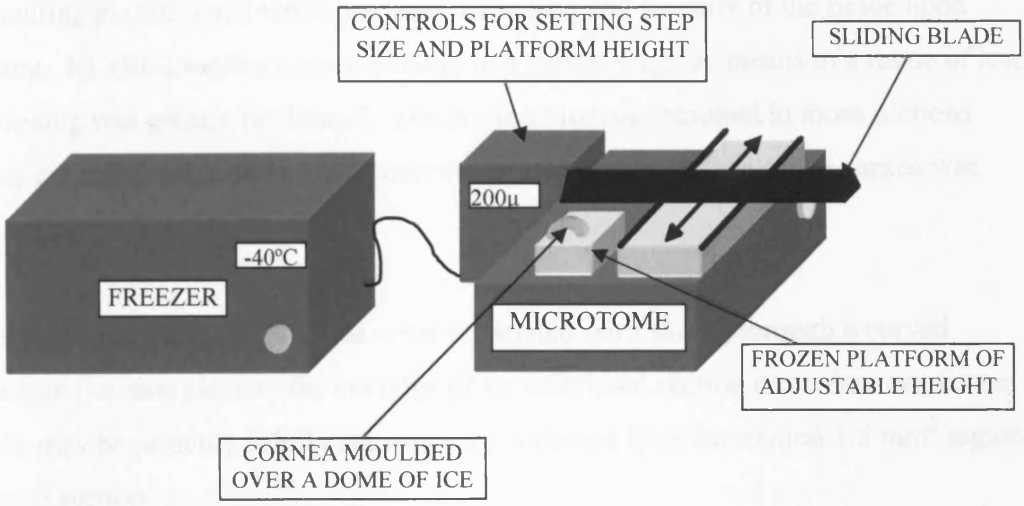

Figure 4.1. Schematic diagram of the sliding microtome and adjoining freezer used for sectioning corneas.

Sections were cut at measured intervals of 150µm in the case of the human corneas and at 200µm for the bovine corneas until the posterior cornea was reached. The posterior section was marked by the subsequent layer having a hole in the centre; the incomplete layer was discarded. A silk suture was used to mark each section taken from an individual cornea at the same position and a knot at the end of the suture was used to mark the anterior (closest to the epithelium) surface.

Sections cut from previously frozen human corneas (E and F) were transferred to vials containing silicon oil. Sections taken from the remaining human and bovine corneas (that were fixed in paraformaldehyde prior to sectioning) were returned to vials containing 4% paraformaldehyde. Two different storage solutions were used (silicon oil and paraformaldehyde) in order to determine the best means of temporary storage

for thin corneal sections (to be used for XRD). All samples were refrigerated at 4°C prior to data collection.

The precise method of corneal preparation and sectioning used in this study was developed following the failure of initial attempts to cut the tissue in its natural unfrozen and unfixed state. Problems were caused by the movement of the cornea on the cutting platform and the subsequent wrinkling and fragility of the tissue upon cutting. By attaching the cornea directly to a frozen stage by means of a dome of ice, sectioning was greatly facilitated. The dome of ice also resulted in more sections being cut from each cornea as the curvature and smooth surface of the cornea was maintained.

In order to minimise the possible error associated with slicing through a curved structure (i.e. that close to the cut edge of an individual section more than one tissue depth may be present), XRD data was only collected from the central 1.5 mm^2 region of each section.

4.2.4 Data collection and analysis

The position of the beam was located by the method described in Section 2.4.1. The corneal section was then carefully positioned into the same sample holder, so that the centre of the sample corresponded to the position of the beam and the most anterior surface of the sample was facing the beam. As it was not possible to wrap the corneal sections in clingfilm, due to their small size and fragility, damp cotton wool was placed along the inside edges of the sample holder to minimise dehydration during data collection. The sample holder was then fixed onto a computer-operated translation stage, and using the beam specifications detailed in Section 2.5.1, high-angle XRD patterns resulting from a 45 second x-ray exposure, were recorded at 0.5mm intervals over the central 1.5mm^2 of each corneal section. The data was analysed as detailed in Section 2.5.2, whereby an x-ray intensity profile of aligned collagen scatter as a function of the angle of orientation was produced for each XRD image and displayed as a polar plot (Figure 2.8). Using Microsoft Excel, the individual polar plots were then arranged onto a grid (relating to corneal position), to

form a map of preferred collagen orientation in the central 1.5mm^2 region of each corneal section. As the amount of x-ray scatter from aligned collagen varied between sections it was necessary for some of the polar plots to be scaled down in size and colour coded so that the orientation of each polar plot could be seen clearly.

In order to examine the distribution of collagen throughout the thickness of the cornea, individual scatter intensities for the total collagen, aligned collagen and the index of orientation were formed from each x-ray scatter intensity profile (Figure 2.7). The individual scatter intensities provide a good measure of the relative amount of fibrillar collagen present at each of the sampling positions.

4.3 Results

4.3.1 Human cornea

Difficulties were experienced whilst sectioning the un-fixed samples that had been stored at -80°C prior to sectioning (E and F) as the tissue tended to wrinkle under the blade during cutting. In addition to this, the cut sections were very fragile and often split when an attempt was made to insert a suture in order to tag the orientation of the section. Further difficulties were encountered during the collection of data from the sections stored in silicon oil (E and F) as they tended to dry out more rapidly than those fixed in 4% paraformaldehyde (A-D). In some cases, the drying out of the un-fixed samples resulted in the shape of the section altering slightly during data collection as the tissue curled up at the edges. Due to the unreliability of the data collected from samples E and F, their results were omitted from the study.

By fixing the tissue in paraformaldehyde the structure of the cornea was preserved and the induced stiffening of the tissue facilitated corneal sectioning and tagging. As a result of tissue fixation, no problems were experienced during the sectioning of corneas A-D or during data collection.

Based on the directly proportional linear relationship between human corneal thickness and hydration (Equation 8) which was established by Hedbys and Mishima (1966), an approximate hydration was calculated for each cornea. As samples A-D

were fixed in 4% paraformaldehyde, the calculated hydration may only be seen to represent an approximation of the actual tissue hydration. The approximate hydration was calculated to be H=3.6 for corneas A, B and C and H=2.5 for cornea D.

Equation 8: Calculation of the relationship between human corneal hydration and tissue thickness.

$$\text{Hydration} = 7.0T - 0.64$$

Where,
T = thickness of tissue (mm)

Figure 4.2 shows a series of polar plot maps of collagen preferred orientation at increasing tissue depth (from epithelium to endothelium) for each of the four paraformaldehyde fixed human corneas (detailed in Table 6). A preferred orthogonal orientation was seen in the anterior, mid and posterior stroma of corneas A and D. However, in corneas B and C a unidirectional preferred orientation was observed in the anterior cornea.

Figure 4.3 shows the average total collagen scatter intensity, aligned collagen scatter and index of orientation in the central 1.5mm^2 of three human corneas (A, B and C) as a function of tissue depth. Corneas A, B and C were selected for averaging as their similar thicknesses (and hydration, H=3.6) ensured that the average intensity of scatter was calculated at each tissue depth from like regions within each cornea. The average intensity of scatter and the average index of orientation at a particular tissue depth were calculated by first averaging the scatter or index for each section of an individual cornea (nine XRD patterns) and then averaging the values between the three corneas at corresponding tissue depths. Total collagen scatter was higher in the posterior half of the cornea than the anterior half (Figure 4.3A), whilst the amount of

x-ray scatter from preferentially aligned collagen showed a gradual increase from the anterior to the posterior (Figure 4.3 B). The proportion of aligned collagen scatter relative to the total collagen scatter, as indicated by the index of orientation, increased from 23% to 41% between the first and second 150μm of the cornea. Throughout the remainder of the mid and posterior stroma the index of orientation remained fairly constant at approximately 0.4 (40% of the total collagen having a preferred orientation) (Figure 4.3C). The apparent regional differences in scattering intensity however failed to be significant due to the small sample size and the variation, (as indicated by the standard error bars), between samples.

Human corneas:

Distance from epithelium:

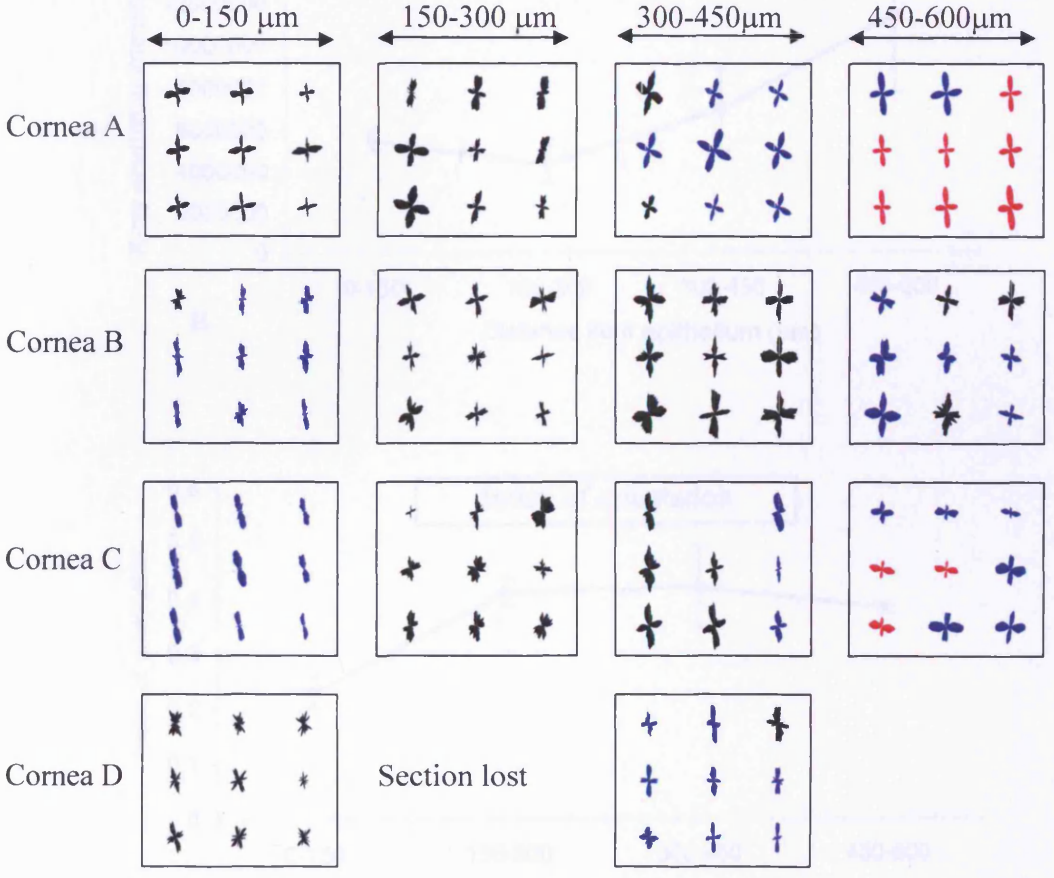

Figure 4.2. Polar plot maps of preferred collagen orientation as a function of corneal depth (from the epithelium to the endothelium) in four human corneas (sample details are shown in Table 6). The polar plots have been scaled according to scattering intensity; red polar plots (highest scattering intensity) have been scaled down by a factor of 3.5, blue plots by a factor of 2 and black (the lowest scattering intensity) by a factor of 1.

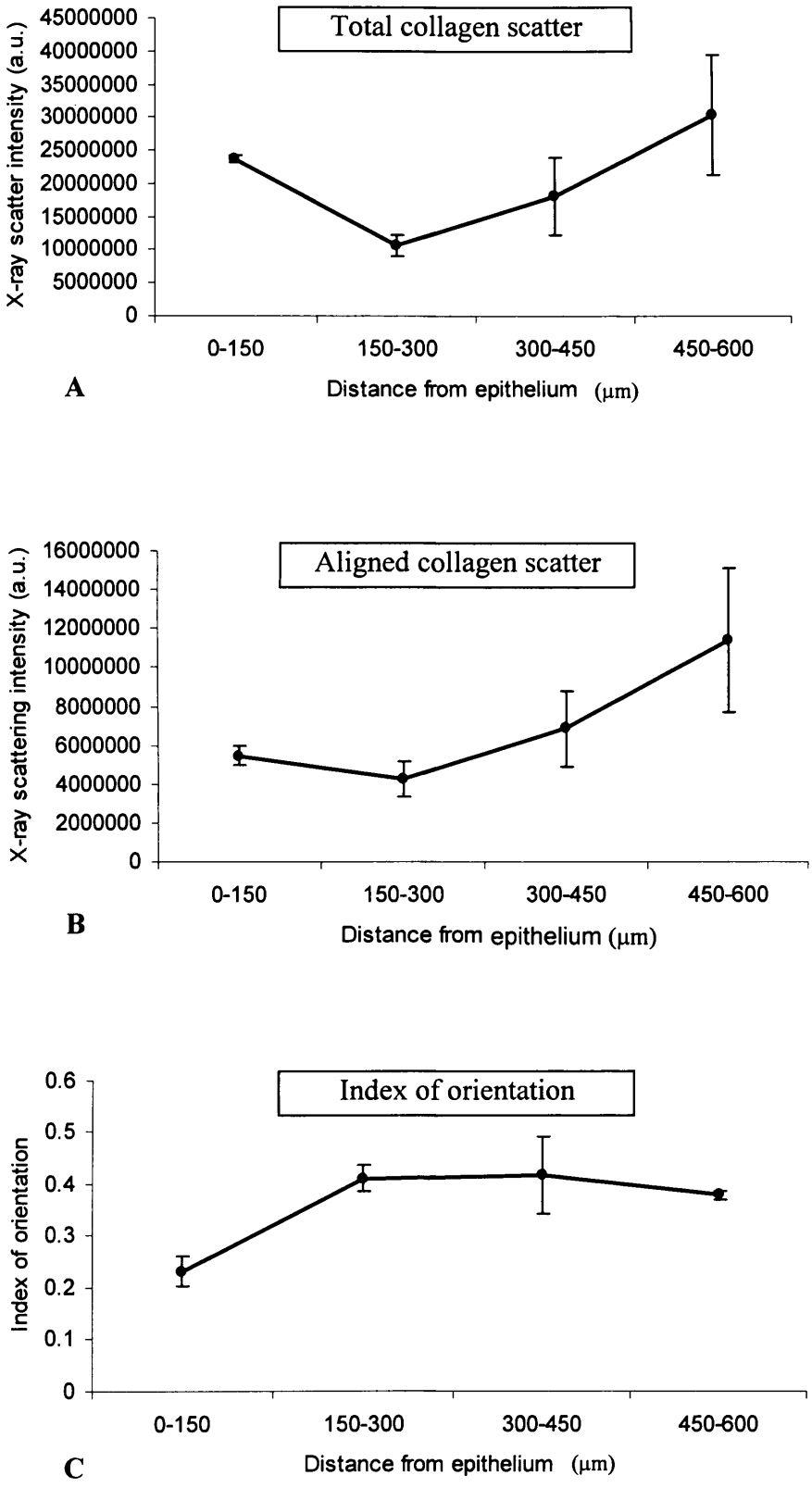

Figure 4.3. The average total collagen scatter (A), aligned collagen scatter (B) and the index of orientation (C) as a function of tissue depth in three normal human corneas at H=3.6. Standard error bars are shown for each data point.

4.3.2 Bovine cornea

Figure 4.4 shows polar plot maps of collagen preferred orientation as a function of tissue depth in eight bovine corneas. In each of the corneas a preferred SI alignment of collagen was seen in the most anterior section of the cornea; this was gradually replaced in the mid stroma by alternating regions of a NT preferred orientation and an orthogonal SI and NT preferred orientation. In the posterior region of most corneas a SI preferred orientation was observed.

As with the human cornea, Hedbys and Mishima (1962) found a directly proportional linear relationship to exist between tissue thickness and hydration in the bovine cornea (Equation 9). Using Equation 9, the approximate hydration of the bovine corneas was calculated to be H = 3.6 for corneas 1-4, H = 4.6 for corneas 5-7 and H = 5.7 for cornea 8.

Equation 9: The relationship between bovine corneal hydration and tissue thickness.

$$\text{Hydration} = 5.3T - 0.67$$

Where,

T = thickness of tissue (mm)

Bovine corneas

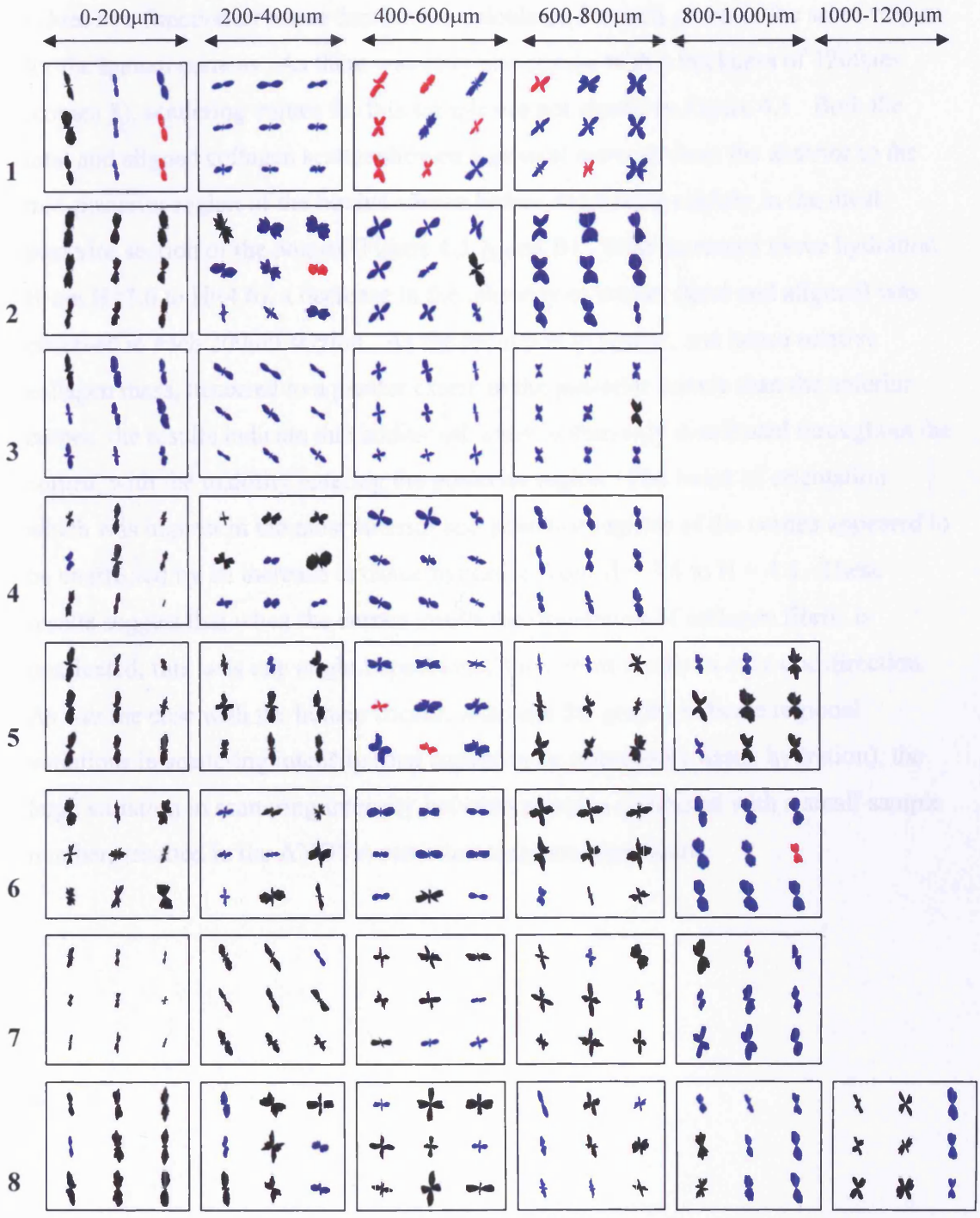

Figure 4.4. Polar plot maps of collagen preferred orientation as a function of tissue depth in eight bovine corneas. The polar plots have been scaled according to scattering intensity, red polar plots have been scaled down by a factor of 3.5, blue plots by a factor of 2 and black plots by a factor of 1.

Figure 4.5 shows the average total collagen x-ray scatter, aligned collagen scatter and index of orientation for 7 out of 8 of the bovine corneas examined. The bovine corneas were grouped according to tissue thickness and the average scatter intensity values as a function of tissue depth were calculated for each group in the same way as for the human corneas. As there was only one cornea with a thickness of 1200μm (cornea 8), scattering values for this sample are not shown in Figure 4.5. Both the total and aligned collagen scatter showed a general increase from the anterior to the mid-posterior region of the bovine cornea before decreasing slightly in the most posterior section of the cornea (Figure 4.5 A and B). With increased tissue hydration (from H=3.6 to H=4.6), a decrease in the intensity of scatter (total and aligned) was observed in each 200μm section. As the reduction in scatter, and hence relative collagen mass, occurred to a greater extent in the posterior cornea than the anterior cornea, the results indicate that additional water is unevenly distributed throughout the cornea, with the majority entering the posterior region. The index of orientation which was highest in the most anterior and posterior regions of the cornea appeared to be unaffected by an increase in tissue hydration from H = 3.6 to H = 4.6. These results suggest that when the cornea swells the orientation of collagen fibrils is unaffected; this is as one might expect since the cornea swells in only one direction. As was the case with the human cornea, although the graphs indicate regional variations in scattering intensity (that appear to be affected by tissue hydration), the large variation in scattering intensity between samples combined with a small sample number, resulted in the ANOVA statistic being non-significant.

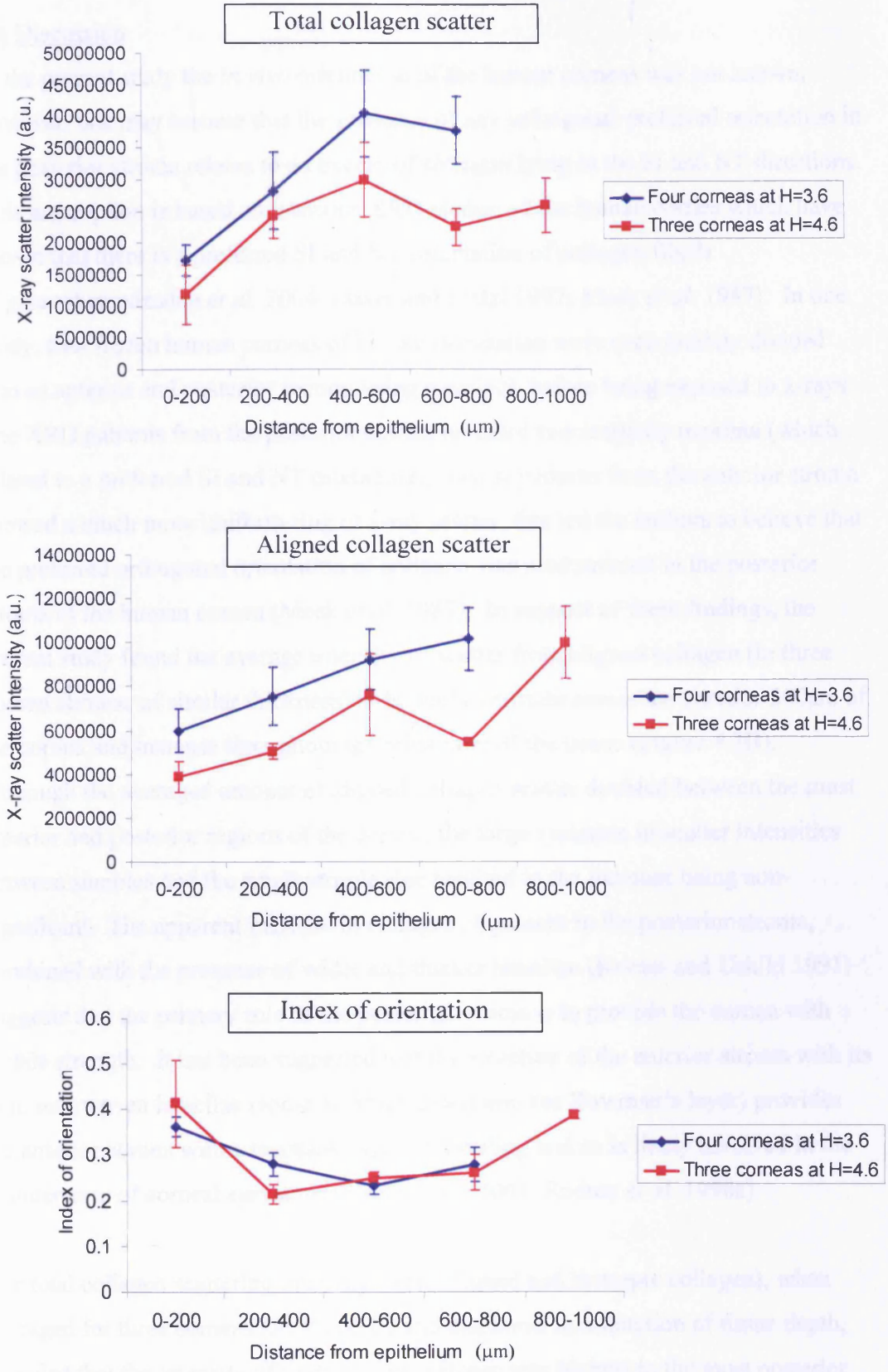

Figure 4.5. The average total collagen scatter (A), aligned collagen scatter (B) and the index of orientation (C) as a function of tissue depth in seven bovine corneas of varying tissue thickness (800 to 1000 microns). Standard error bars are shown for each data point.

4.4 Discussion

In the present study the *in vivo* orientation of the human corneas was not known, however, one may assume that the presence of any orthogonal preferred orientation in the posterior stroma relates to an excess of collagen lying in the SI and NT directions. This assumption is based on previous XRD studies of the human cornea which have shown that there is a preferred SI and NT orientation of collagen fibrils (Aghamohamadzadeh *et al.* 2004; Daxer and Fratzl 1997; Meek *et al.* 1987). In one study, four frozen human corneas of known orientation were each crudely divided into an anterior and posterior section using a scalpel, before being exposed to x-rays. The XRD patterns from the posterior cornea revealed two intensity maxima (which related to a preferred SI and NT orientation), whilst patterns from the anterior stroma showed a much more uniform ring of x-ray scatter; this led the authors to believe that the preferred orthogonal orientation of collagen was predominant in the posterior stroma of the human cornea (Meek *et al.* 1987). In support of these findings, the present study found the average intensity of scatter from aligned collagen (in three human corneas of similar thickness) to be fairly constant across the anterior 300μm of the cornea and increase throughout the remainder of the tissue (Figure 4.3B). Although the averaged amount of aligned collagen scatter doubled between the most anterior and posterior regions of the cornea, the large variation in scatter intensities between samples and the small sample size resulted in the increase being non-significant. The apparent increase in collagen alignment in the posterior stroma, combined with the presence of wider and thicker lamellae (Komai and Ushiki 1991) suggests that the primary role of the posterior stroma is to provide the cornea with tensile strength. It has been suggested that the structure of the anterior stroma with its thin, interwoven lamellae (some of which insert into the Bowman's layer) provides the anterior cornea with a resistance against swelling and so is likely involved in the maintenance of corneal curvature (Muller *et al.* 2001; Radner *et al.* 1998a).

The total collagen scattering intensity (from aligned and isotropic collagen), when averaged for three corneas (A, B and C) and displayed as a function of tissue depth, revealed that the intensity of scatter from collagen was highest in the most posterior section of the human cornea and lowest in the mid stroma (Figure 4.3A). The change in scattering intensity as a function of tissue depth did not however prove to be

significant. The non-significant trends observed in this study do however support a previous electron microscopy study of the human cornea, in which the number density of fibrils in the mid stroma was found to be lower than elsewhere in the cornea (Freund *et al.* 1995). The same study also reported a lower number density of fibrils in the anterior stroma compared to the posterior (Freund *et al.* 1995), which is consistent with the present findings.

As the posterior stroma is known to swell more readily than the anterior stoma (Kikkawa and Hirayma 1970), an increase in hydration would likely result in a greater reduction in fibril packing density (and therefore x-ray scatter) in the posterior stroma. In this way, an increase in tissue hydration would be expected to cause the fibril packing density in the posterior stroma to become increasingly similar to that of the anterior stroma. It was not possible to prove this theory in the present study as only 4 human corneas were examined, one of which had a hydration of approximately H=2.5 and the remaining a hydration of H=3.6. The results did however indicate this to be true for bovine cornea. When bovine corneas were grouped according to tissue thickness, the averaged total and aligned collagen scatter intensity showed a gradual increase from the anterior to the mid-posterior region of the cornea before decreasing slightly in the most posterior section of the cornea (Figure 4.5 A and B). With increased tissue thickness and therefore increased tissue hydration (from H=3.6 to H=4.6), the intensity of scatter in each 200μm section decreased. The total collagen scatter decreased by approximately 30% in the most anterior and posterior sections of the cornea, so maintaining a 1:2.2 (anterior: posterior) ratio of scatter between the two outermost regions. In the remainder of the cornea the increase in hydration resulted in a 74% decrease in total collagen scatter. The reduction in scatter was especially prominent in the posterior portion of the mid stroma suggesting that when tissue hydration increases there is an uneven distribution of additional water throughout the bovine cornea, with the majority going into the mid-posterior stroma. This agrees with the work of Castoro *et al.* (1988) in which a positive water gradient was found to exist from epithelium to endothelium in the bovine cornea which coincided with a change in proteoglycan composition. As the ratio of keratan sulphate to dermatan sulphate proteoglycans increases from epithelium to endothelium (Castoro *et al.* 1988), one would expect the additional water to be drawn predominantly to the

posterior region of the cornea since keratan sulphate proteoglycans have a large water sorbative capacity (Plessy and Bettelheim 1975).

In the bovine cornea the index of orientation which was highest in the most anterior and posterior regions of the cornea, appeared to be unaffected by an increase in tissue hydration from H=3.6 to H=5.7. In support of this, a recent XRD study showed that in the human cornea the preferred orientation of collagen and the index of orientation remained the same when the cornea was examined before swelling and after one hour of free swelling (Meek *et al.* 2005a). The results are as one would expect since an increase in tissue hydration results in a one dimensional increase in tissue thickness (from anterior to posterior) and so the preferred orientation and relative proportion of aligned collagen to total collagen would not be expected to change significantly.

Preferred collagen orientation differed greatly between the human and bovine cornea. In 2 out of 4 paraformaldehyde fixed human corneas (A and D) a preferential orientation of aligned collagen in the SI and NT directions was present not only in the mid and posterior cornea but also in the anterior cornea, albeit to a much lesser extent (Figure 4.2). In the remaining fixed corneas (B and C), a unilateral SI preferred orientation was observed in the anterior stroma and an orthogonal preferred orientation was seen throughout the remainder of the tissue. The reason for the preferred orientation of aligned collagen in the SI and NT directions in the central region of the human cornea is still unknown but as collagen is strongest along its fibril axis an excess of collagen lying in a particular orientation is suggestive of an increased level of stress in that direction. It is a typical property of most soft tissues, including the cornea, that an increased level of stress produces an increased level of stress resistance (Reichel *et al.* 1989). It is important to note therefore that the preferential orientation of collagen in the SI and NT directions corresponds to the insertion points of the four major rectus muscles. It is possible that the presence of excess aligned collagen lying across the cornea between the insertion points of opposing rectus muscles, may provide the cornea with strength to resist tissue distortion during eye movement.

In the most anterior 200μm of each of the eight bovine corneas examined, collagen was found to lie predominantly in the SI direction (Figure 4.4). In the mid stroma the preferred orientation of collagen was found to alternate between regions of NT preferred alignment and regions of orthogonal SI and NT alignment. In the posterior cornea, a further change in the preferred orientation was seen, with an excess of aligned collagen in the majority of cases lying in the SI direction. It must be remembered that the accuracy of the results presented here, showing the changes in the preferred orientation of aligned collagen as a function of tissue depth, are dependent upon the accuracy with which the samples were tagged at the 12 o'clock position and also on the placement of the samples in the sample holder in the correct orientation. The small human error associated with the technique may explain the slight variation between samples in terms of the preferred orientation of aligned collagen.

In contrast to the overall orthogonal preferred orientation of aligned collagen in the human cornea (when the intensity of aligned scatter in each direction is averaged throughout the thickness of the cornea), a SI preferred orientation is seen in the bovine cornea. The reason for this preferred orientation is not at present fully understood. Based on calculations by Maurice (1984) which showed tension to be directly proportional to radius of curvature, one would expect there to be less aligned collagen in the SI direction of the bovine cornea compared to the NT direction, since the radius of curvature in the SI meridian (24mm) is smaller than that of the NT meridian (30mm); however, this is not the case. If a relationship does exist between the preferred orientation of collagen fibrils in the cornea and the insertion points of the major rectus muscles, as suggested previously, then differences between species in the frequency of use of the various extra-ocular muscles may result in differences between the two in terms of the direction and amount of stress exerted on the cornea. If this is the case then an increase in stress in a given direction would require an increase in the level of stress resistance in the same direction. This may explain why the direction of additional aligned collagen differs between human and bovine eyes. If we consider in more detail the differences in ocular demands between the human and cow this may help to shed light on the reason for the difference in corneal collagen arrangement between the two species.

The frontal placement of the primate eye provides a high visual acuity and stereoscopic depth perception as a result of binocular vision. In addition to this humans have the ability to converge their eyes (rotate them medially), so that the light rays from the object reach the same point on both retinas. Convergence is dependent on the action of the extra ocular muscles and the nearer the object is the greater the degree of convergence needed to maintain binocular vision. Humans have a binocular vision of 140° and an orbit convergence of 79.3° (Bruce *et al.* 1996) whilst the cow has a much lower degree of binocular vision (51°) and a much smaller orbital convergence of 32° (Walls 1942). In the case of the cow, which is a prey animal, a large field of view is of more advantage than a high visual acuity. Their large field of view is achieved through a lateral placement of the eyes and a widened cornea which compensates for reduced eye movement. Differences in eye movement between cows and humans such as the degree and frequency of use of ocular convergence may result in differences between the two in terms of the predominant directions of stress acting on the cornea. The differences in corneal shape and ocular demands between the two species may therefore help to explain the differences in the preferred orientation of aligned collagen between the human and cow cornea.

4.5 Conclusions

The preferred orientation of aligned collagen as a function of tissue depth differs between the bovine and human cornea. Throughout the majority of the human cornea, collagen is preferentially aligned in the SI and NT directions and the amount of aligned collagen is far higher in the mid and posterior regions of the cornea than in the anterior. The increased collagen alignment in the posterior stroma which is accompanied by an increase in the width and thickness of lamellae indicates that the posterior cornea is heavily involved in the provision of corneal tensile strength. It has been previously suggested that the preferred directions of corneal collagen alignment may be related to the insertion points of the four major rectus muscles; the excess of aligned collagen may therefore be present to resist tissue distortion during eye movement.

In contrast to the human cornea, the preferred orientation of aligned collagen in the bovine cornea changes with tissue depth. In the majority of cases studied here, an excess of collagen in the SI direction was seen in the anterior stroma, which was followed by a preference for a NT collagen alignment in the anterior mid-stroma, an orthogonal SI and NT alignment in the posterior mid stroma and a SI alignment in the most posterior stroma. In the bovine cornea as a whole, there is a preferential orientation of collagen in the SI direction. The reason for this arrangement is unknown; however differences between humans and cows in the size and shape of the cornea as well as differences in the frequency and direction of eye movement may be responsible for the structural differences observed between the two.

4.6 Future study

- In order to establish whether species differences in the size and shape of the cornea are responsible for differences in the preferred orientation of aligned collagen, it would be interesting to examine a range of animal corneas and relate parameters such as the corneal radius of curvature to the amount and direction of preferentially aligned collagen in the corneal stroma.

- By studying preferred orientation of collagen in the corneas of a range of prey animals (with laterally placed eyes and therefore a large field of vision) and predators (with frontally placed eyes and a high degree of binocular vision), a relationship may also be found between collagen orientation and the direction and extent of ocular movement and convergence.

- Although several studies have examined the variation in corneal strength between the central and peripheral regions of the cornea, no studies to date have characterised corneal strength as a function of tissue depth. This study would be of particular importance to corneal surgery.

Chapter 5. A study of collagen orientation and mass distribution in normal and keratoconus human corneas

5.1 Introduction

Although the exact function of the preferred orthogonal orientation of aligned collagen in the human cornea is unknown, the tensile strength provided by collagen along its fibril axis suggests a likely role in the maintenance of corneal strength and shape. As a result of this, abnormalities in the structural organisation of stromal collagen have been implicated in several corneal diseases, one of which is keratoconus, a condition that is characterised by a progressive thinning and weakening of the stroma, a cone-shaped cornea and severe, irregular astigmatism.

Using both videokeratography and XRD, the aim of this study is to produce a series of maps showing the corneal surface curvature, the distribution of collagen mass and the preferred orientation of collagen fibrils in normal and keratoconus corneas. By combining XRD data with that obtained by videokeratography, this study builds on previous work (Meek *et al.* 2005b – Appendix 9), to examine in detail the interesting relationship between corneal structure and specific keratoconus shape changes and improve our understanding of the mechanism by which the cornea progressively thins in keratoconus.

5.2 Methods

5.2.1 Sample preparation

Three normal human eyeballs, two right (N1 and N3) and one left (N2), were obtained from the Great Wall Hospital, Beijing, China. A further right cornea with scleral rim (S1), which the surgeon deemed to be normal was also received from the Great Wall Hospital. A light microscope examination of sample S1 upon its arrival at Cardiff University (Wales, UK) revealed the presence of an abnormality in the central cornea and a distortion of the limbus in the superior-temporal (ST) quadrant (Figure 5.4).

All samples were removed within one hour post mortem, marked at the 12 o'clock position with either a silk suture or a surgical skin marker pen, placed into a sealed

tube containing either 2.5% or 10% formalin (as stated in Table 7) and sent via air mail to Cardiff University. On arrival the samples were refrigerated at 4°C. Immediately prior to XRD data collection the cornea with a 2mm scleral rim was dissected from each eyeball.

Fourteen keratoconus corneal buttons (K1 to K14) of between 6.5 and 8.5mm diameter were obtained from consenting patients at the time of penetrating keratoplasty from the Great Wall Hospital, Moorfields Eye Hospital (London, UK) and the Royal Glamorgan Hospital (Llantrisant, Wales, UK). In each case, a pre-operative assessment of corneal scarring was made by the operating surgeon; the details are shown in Table 7. At the time of removal, each keratoconus button was either tagged with a 10-0 nylon suture or marked with a surgical marker pen at the 12 o'clock position. Patient details (provided by the operating surgeon) for both normal and keratoconus samples are shown in Table 7. Keratoconus corneal buttons obtained from Moorfields Eye Hospital (K5 to K13) and Royal Glamorgan Hospital (K14) were wrapped tightly in clingfilm immediately after their removal and frozen at -80°C. These samples were transported to Cardiff University on dry ice and transferred to –80°C storage on arrival, where they remained until required for data collection. The tagged keratoconus corneal buttons from Great Wall Hospital (K1 to K4) were placed into sealed tubes containing 2.5% formalin and sent via air mail to Cardiff University. These samples were stored in their original fixative at 4°C until required for data collection.

Table 7. Sample details for normal and keratoconus corneas.

Source	Sample	Details	Age	Gender	Size of sample	Storage
Great Wall Hospital	Normal, right (N1)	No details	-	-	Cornea and 2mm sclera	10% Formalin
Great Wall Hospital	Normal, left (N2)	Ennucleation due to melanoma	24	M	Cornea and 2mm sclera	2.5% Formalin
Great Wall Hospital	Normal, right (N3)	No details	-	-	Cornea and 2mm sclera	2.5% Formalin
Great Wall Hospital	Normal, right (S1) *1	Ennucleation due to choroidal melanoma.	25	F	Cornea and 2mm sclera	2.5% Formalin
Great Wall Hospital	Keratoconus, left (K1)	No corneal scar. Largest curvature is 81.0D	26	M	6.5mm	2.5% Formalin
Great Wall Hospital	Keratoconus, left (K2) *2	No scar. Largest curvature is 72.79D	17	M	6.5mm	2.5% Formalin
Great Wall Hospital	Keratoconus, right (K3) *2	No scar. Largest curvature 62.25D	17	M	7.5mm	2.5% Formalin
Great Wall Hospital	Keratoconus, left (K4)	No significant corneal scar	-	-	7.5mm	2.5% Formalin
Moorfields Eye Hospital	Keratoconus, right (K5)	No significant corneal scar	26	F	7.5mm	Frozen -80°C
Moorfields Eye Hospital	Keratoconus, right (K6)	Graft decentred nasally	37	M	7.5mm	Frozen -80°C
Moorfields Eye Hospital	Keratoconus, right (K7)	No significant corneal scar	32	M	8.0mm	Frozen -80°C
Moorfields Eye Hospital	Keratoconus, left (K8)	No significant corneal scar	20	M	7.5mm	Frozen -80°C
Moorfields Eye Hospital	Keratoconus, left (K9)	Hydrops 15 month previously	24	F	8.0mm	Frozen -80°C
Moorfields Eye Hospital	Keratoconus, right (K10)	Mild axial superficial scar	32	F	8.0mm	Frozen -80°C
Moorfields Eye Hospital	Keratoconus, left (K11)	Slight superficial scar above visual axis	28	M	8.0mm	Frozen -80°C
Moorfields Eye Hospital	Keratoconus, right (K12)	Slight axial superficial scar	32	M	8.0mm	Frozen -80°C
Moorfields Eye Hospital	Keratoconus, right (K13)	Severe keratoconus with minimal scarring	39	M	8.5mm	Frozen -80°C
Royal Glamorgan Hospital	Keratoconus, right (K14)	Splash scar in anterior stroma and scar across centre at Descemet's level	24	M	7.75mm	Frozen -80°C

*1 The cornea was deemed to be normal by the operating surgeon, however, examination of the sample on arrival revealed an abnormality in the central cornea and a distorted limbus.
*2 Left and right keratoconus corneas from the same patient.

5.2.2 Videokeratography

For each sample a videokeratographic image was recorded using either Eye Sys (N1-N3, S1 and K1-K4), Orbscan II (using version v3.12) (K5-K7 and K9-K13) or Visioptic Alcon Eye Map (Visioptic EH-270) (K8 and K14). Videokeratography of all keratoconus corneas was performed *in vivo* (3-5 seconds after blinking), unfortunately however, details of the time gap between videokeratography assessment and surgery were not available. All normal corneas were examined *in vitro* within 2 hours post mortem. In each case the cross at the centre of the recorded image was accurately aligned with the centre of the pupil.

The Eye Sys topography system (used at the Great Wall Hospital) and the Visioptic Alcon Eye Map (used at the Royal Glamorgan Hospital and Moorfields Eye Hospital (for sample K8 only)), provide a single keratometric map of corneal surface dioptric power. In the case of the Eye Sys, a 1x1mm grid is superimposed onto each image. The Orbscan II system, most frequently used at Moorfields Eye Hospital, provides a series of four topography maps showing corneal keratometry, the shape of the anterior and posterior surfaces (anterior and posterior floats) and the thickness of the cornea (pachymetry). The anterior float is determined by fitting a 'best fit' reference sphere (using a least squares method) to the anterior surface of the cornea. The anterior float is therefore the difference between the best fit reference sphere and the anterior surface of the cornea. The posterior float is calculated in a similar way and describes the posterior surface of the cornea.

5.2.3 XRD data collection and analysis

After initially locating the precise position of the x-ray beam using the method described in Section 2.4.1, the cornea was then prepared as described in Section 2.2 and carefully positioned in the sample holder to ensure that the x-ray beam would pass through the top left of the sample, travelling in an antero-posterior direction. The sample holder was then secured onto a computer-operated translation stage positioned 150mm in front of the detector. Using the beam specifications detailed in Section 2.5.1 and an exposure time of between 75 and 120 seconds, high-angle XRD patterns were recorded at regular intervals (0.25mm (K3-K14), 0.4mm (N1-N3 and S1) or

0.5mm (K1-2)) over the entire sample. A 0.25mm interval grid of XRD patterns was produced for the majority of the keratoconus buttons, with the exception of K1 and K2 which were mapped at a 0.5mm resolution. This enabled subtle collagen orientation changes to be observed throughout the button. In the case of each normal human cornea with 2mm scleral rim, the size of the sample was much larger than that of the keratoconus buttons; therefore, due to time restrictions data was collected at 0.4mm intervals over the normal corneal samples (N1-N3).

The exposure time used was dependent upon the intensity of the x-ray beam at the start of data collection; a higher intensity beam meant that a shorter exposure time could be used, whilst still maintaining a good signal to noise ratio. In the initial stage of the analysis (Section 2.5.2, Step 1 of 6), the data was normalised to account for such changes in beam intensity and exposure time between samples. An intensity profile of total collagen x-ray scatter relative to radial position was generated for each of the XRD patterns in Step 4 of the analysis process (Figure 2.7). By dividing the x-ray scatter profile into isotropic scatter and preferentially aligned collagen scatter (Figure 2.7), it was possible to calculate the index of orientation at each sampled position (Section 2.5.2, Step 5). In order to determine the distribution of collagen across a particular sample, individual scatter intensity values were formed for the total collagen, aligned collagen and the index of orientation at each corneal position; these values provide a measure of the relative amount of fibrillar collagen present at each sampling position. Using Microsoft Excel the intensity values were plotted relative to corneal position to form a series of three colour coded contour maps for each sample, showing the distribution of total collagen mass (scattering from both aligned and isotropic collagen), preferentially aligned collagen mass and the index of orientation (aligned scatter/total scatter). By presenting the distribution of aligned collagen mass as an index of orientation (i.e. relative to the total amount of collagen), the reduced thickness of keratoconus corneas is taken into account, so allowing the distribution of collagen mass in normal and keratoconus corneas to be directly compared.

In order to examine the preferred orientation of collagen across the cornea, each profile of aligned collagen scatter as a function of angle of orientation was converted into a polar plot (Section 2.5.2, Step 6). Using a Microsoft Excel spreadsheet, the

individual polar plots were arranged onto a grid (relating to corneal position), to form a map showing the preferred orientation of aligned collagen at regular intervals across the cornea. As the intensity of x-ray scatter from aligned collagen varied across samples due to differences in aligned collagen mass at different positions, it was necessary for some of the polar plots to be scaled down in size and colour coded, so that the orientation of even the lowest intensity polar plots could be seen clearly. The factors by which the polar plots were scaled down and the colour used to represent each factor are shown in the legend below each map.

Due to the large amount of data collected for this study the results will be split into two parts with a separate discussion at the end of each. Data collected for the normal human corneas (N1-N3) and the 'normal' cornea with corneal and limbal abnormalities (S1) will be presented and discussed in Part A (Sections 5.3 and 5.4). Data for the keratoconus corneal buttons (K1-K14) will be shown and discussed in Part B (Sections 5.5 and 5.6).

5.3 Part A: Results

5.3.1 Normal left and right corneas with scleral rim

Figure 5.1 A and B show videokeratographic images of corneal surface dioptric power for a normal right (N1) and left eye (N2) respectively (sample details are shown in Table 7). It also shows corresponding contour maps of total collagen mass distribution (C and D), aligned collagen mass distribution (E and F) and the index of orientation (G and H) in the cornea and scleral rim of the same right and left eye. Similar data is shown for a second normal right cornea with scleral rim (N3) in Appendix 1 (Figure A1.1). The arrangement and distribution of collagen in N3 is very similar to that of N1.

A region of remarkably high scattering intensity (highlighted by the black arrows in Figures 5.1 D and F) was observed just below the centre of the left cornea (N2). It is presumed that this effect is an artefact caused by a slight fold in the tissue (likely produced while preparing the sample for data collection), and that the increased scattering intensity in this region is due to the beam passing through the additional

tissue present at the fold. The chance of producing a fold in the tissue is greatly increased when the sample size is close to that of the sample holder, as is the case when studying a cornea with scleral rim. By the same reasoning it is highly unlikely that a fold in the tissue would be produced in the preparation of a corneal button for XRD due to its smaller size. In any case, the data from the region of the fold should not be considered to represent the normal distribution of collagen mass. Bearing this in mind, the total collagen mass, as indicated by the total collagen scattering intensity, is fairly uniform over the central cornea of both the left and right eye but increases rapidly with proximity to the limbus (highlighted by a dashed blue line) (Figure 5.1 C and D). There is a further increase in collagen mass between the limbus and sclera, which is most pronounced in the inferior aspect of the sclera in both the left and right eye.

There is a non-uniform distribution of aligned collagen scatter in both corneas (Figure 5.1 E and F). Aligned collagen scatter increases in the superior-nasal (SN), superior-temporal (ST), inferior-nasal (IN) and inferior-temporal (IT) quadrants of the peripheral cornea forming a skewed diamond shaped arrangement. This arrangement, which has been previously reported by Aghamohamadzadeh *et al.* (2004), continues into the limbus and sclera. The increase in aligned collagen is most dramatic at the limbus due to the presence of an annulus of collagen which surrounds the cornea.

The index of orientation increases in all four quadrants of the left and right cornea (Figure 5.1 G and H). However, in the normal right cornea (N1) the proportion of aligned collagen is far higher in the SN and IT quadrants (up to 72% of the total collagen is aligned) than in the ST and IN quadrants (36-54% collagen alignment). The left cornea (N2) shows mirror symmetry with the right cornea in terms of this increase in the index of orientation in the four quadrants, which is most pronounced in the SN and IT quadrants of the cornea.

A large variation in the average scattering intensity in the central 4mm was observed between normal corneas (N1-3). When the average total scattering intensity of the central 4mm region of sample N1 was assumed to be 100%, then the total scattering intensity of N3 and N2 in the same region was 83% and 152% respectively. When

calculated in the same manner, the aligned collagen scatter varied between 74% (N3) and 132% (N2). Interestingly, the index of orientation showed only a marginal variation between samples (8%).

Figures 5.2 and 5.3 show the preferred orientation of aligned collagen in the same right (N1) and left (N2) corneas with scleral rim. Once again, the region occupied by the folded tissue in the left cornea (shown by the black arrow) should not be taken to represent normal preferred collagen orientation at that point in the cornea. In the central region of both the left and right corneas, collagen is preferentially aligned in the SI and NT directions; however, approaching the limbus there is a gradual change from an orthogonal preferred collagen orientation to an increasingly tangential orientation. In the perilimbal region, an excess of collagen fibrils lie tangential to the cornea and form an annulus of aligned collagen alignment around it. Beyond the limbus, at the 12, 3, 6 and 9 o'clock positions alone, the preferred orientation of collagen changes to follow a course in line with the insertion point of the closest rectus muscle (superior rectus, lateral rectus, inferior rectus and medial rectus respectively). In the remainder of the anterior sclera there is a circumferential orientation of aligned collagen around the cornea.

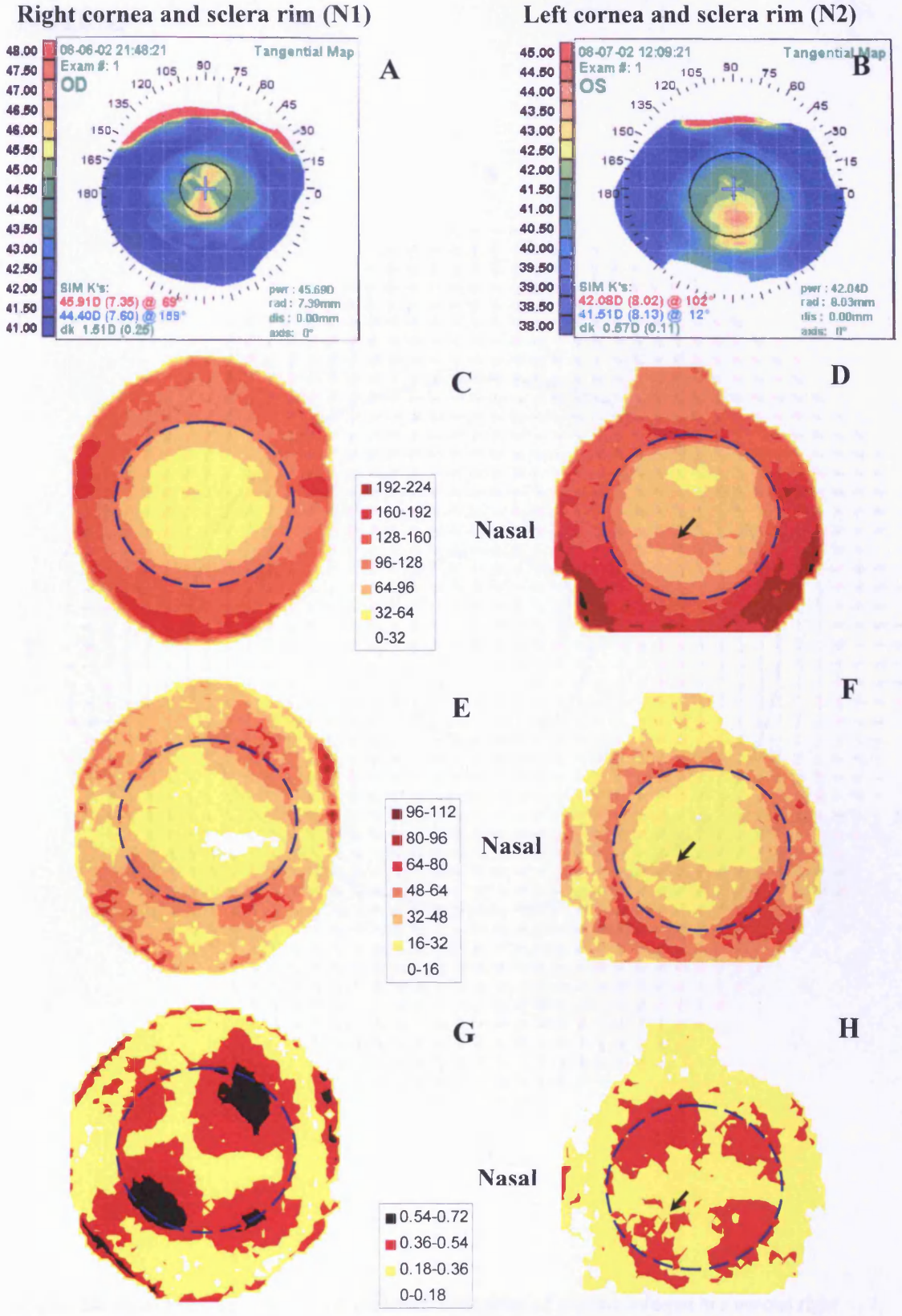

Figure 5.1. Maps showing corneal dioptric power of a right eye (A) and a left eye (B) from different donors. The distribution of total collagen mass (C and D), aligned collagen mass (E and F), and the index of orientation (G and H) are shown for the same right and left corneas with scleral rim. The position of an average human limbus is highlighted by a blue dashed line. A black arrow marks the location of a fold in the left cornea. (Tissues fixed in 10% (N1) and 2% (N2) formalin).

Right (N1)

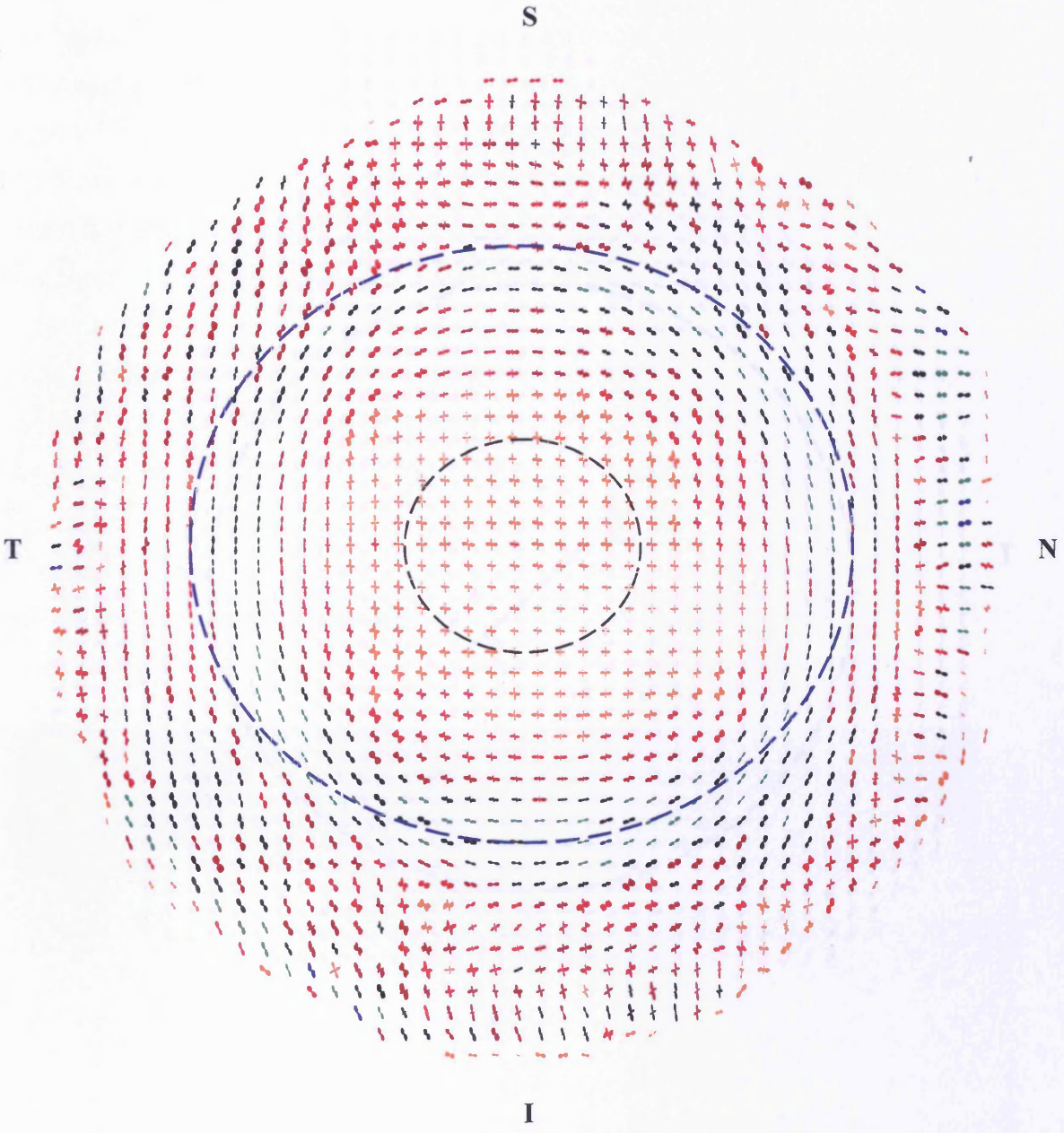

Figure 5.2. Polar plot map showing the preferred orientation of aligned collagen in a normal right human cornea with scleral rim. Due to variations in the mass of aligned collagen throughout the tissue the polar plots have been scaled down by factors of 4.5, 4, 3, 2, 1.5 and 1 and colour coded using the colours blue, green, black, brown, red and orange respectively. The prepupillary region (black dashed line) and the position of an average human limbus (blue dashed line) are highlighted.

Left (N2)

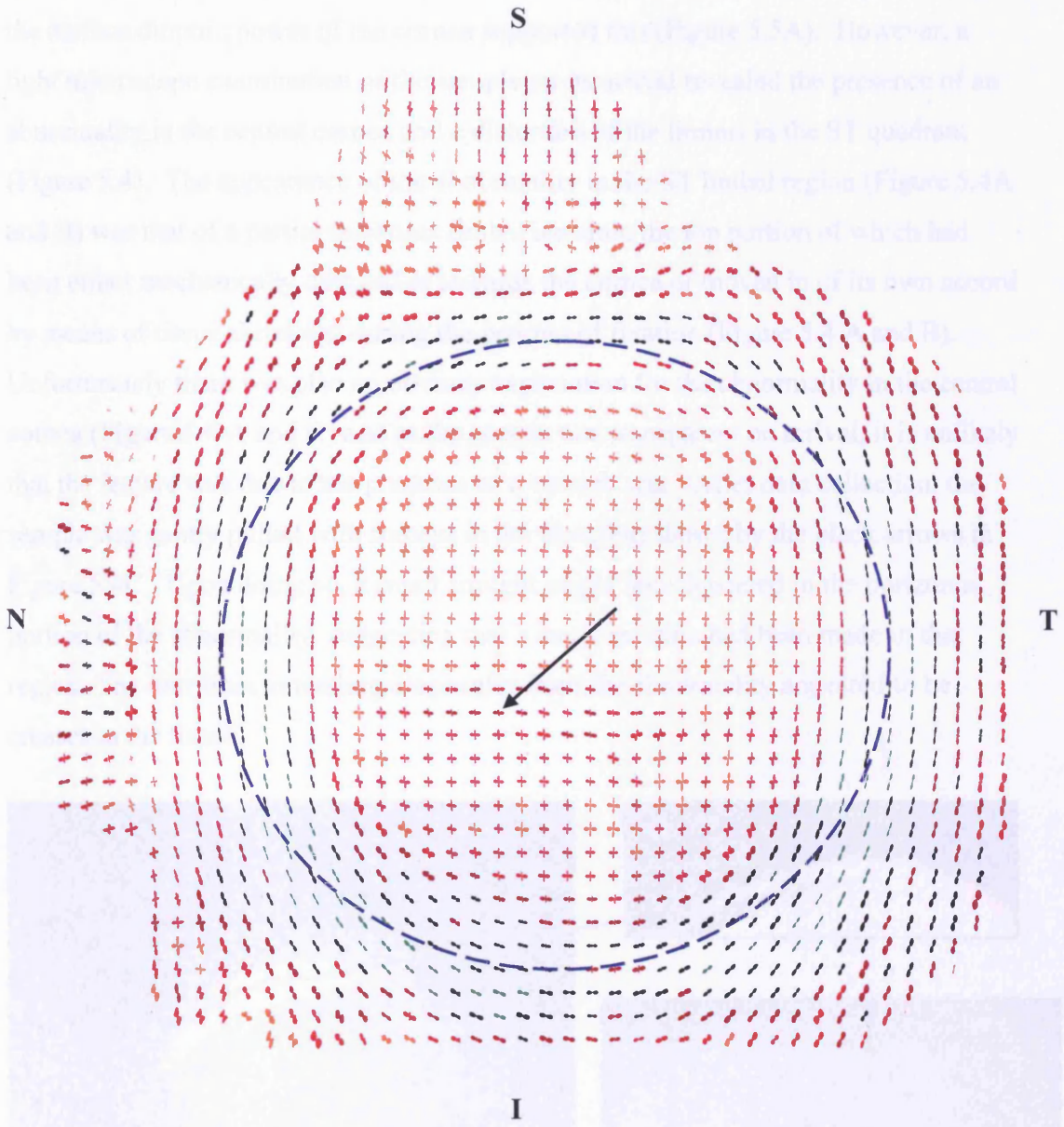

Figure 5.3. Polar plot map showing the preferred orientation of aligned collagen in a normal left human cornea with scleral rim. Due to variations in the mass of aligned collagen throughout the tissue the polar plots have been scaled down by factors of 4.5, 4, 3, 2, 1.5 and 1 and colour coded using the colours blue, green, black, brown, red and orange respectively. The position of an average human limbus is highlighted by a blue dashed line and the black arrow marks the location of a fold in the left cornea.

5.3.2 Right cornea and scleral rim with corneal and limbal abnormalities

Sample S1, which was enucleated due to choroidal melanoma, was deemed by the operating surgeon to be a normal right cornea. A videokeratographic image showing the surface dioptric power of the cornea supported this (Figure 5.5A). However, a light microscope examination of the sample on its arrival revealed the presence of an abnormality in the central cornea and a distortion of the limbus in the ST quadrant (Figure 5.4). The appearance of the abnormality in the ST limbal region (Figure 5.4A and B) was that of a partial thickness limbal incision, the top portion of which had been either mechanically dragged in towards the cornea or moved in of its own accord by means of tissue shrinkage during the process of fixation (Figure 5.4 A and B). Unfortunately there was also no obvious explanation for the abnormality in the central cornea (Figure 5.4 A and C) and as the cornea was transparent on arrival, it is unlikely that the feature was due to the presence of a corneal scar. After data collection, the sample was gently pulled with forceps in the direction shown by the black arrows in Figure 5.4C. Upon doing so, a small straight edged hole appeared in the horizontal portion of the abnormality, suggesting that a small incision had been made in that region. The four lines extending diagonally from the abnormality appeared to be creases in the tissue.

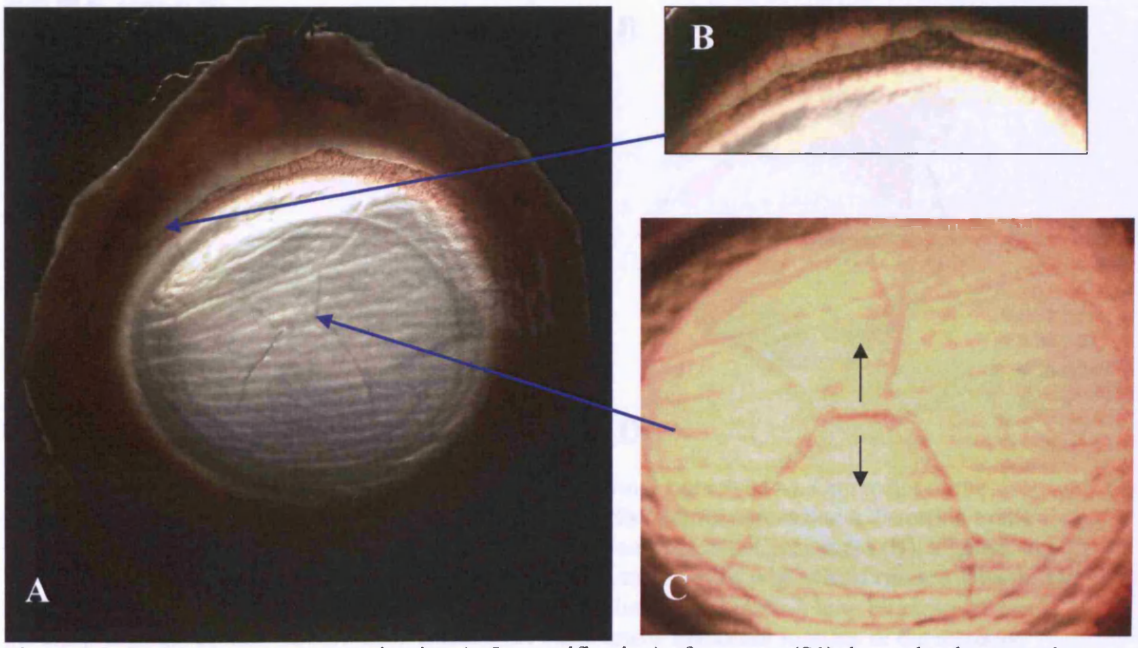

Figure 5.4. Light microscope examination (x 5 magnification) of a cornea (S1) deemed to be normal, which on receipt, showed a distortion to the superior-temporal region of the limbus and an abnormality in the central cornea (A). By colour enhancement and increased magnification (x10), the affected limbal (B) and corneal (C) regions can be seen more clearly. When the tissue was pulled gently in the direction shown by the black arrows a small hole appeared in the centre of the cornea (C).

Figure 5.5 B, C and D show the distribution of total collagen mass, aligned collagen mass and the index of orientation in the same cornea with scleral rim (S1). The normally uniform distribution of total collagen mass is disturbed in the central cornea at the site of the abnormality, and is marked by an increase in collagen mass (Figure 5.5B). A further abnormality in the distribution of total collagen mass was seen in the distorted ST limbal region where the collagen mass was much higher than normal. As in the previous normal corneas studied (Figure 5.1 C and D and Appendix 1), the total collagen scatter increased from the limbus to the sclera, with the increase being most prominent in the inferior aspect of the sclera.

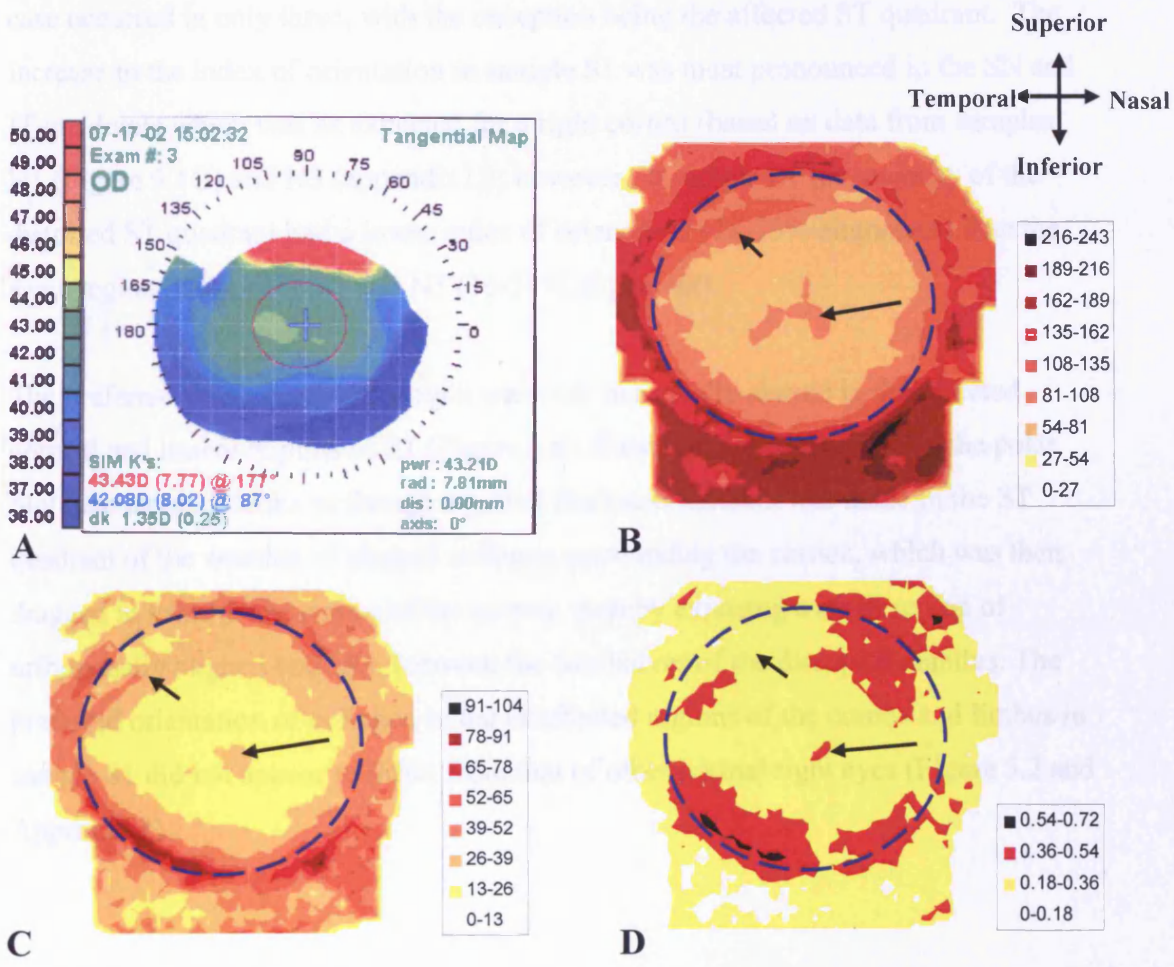

Figure 5.5. Maps showing corneal dioptric power of a normal right eye (A). On receipt of the specimen (S1) there was an unexplainable abnormality in the central cornea and a distortion to the upper limbal region. Contour maps showing the distribution of total collagen mass (B), aligned collagen mass (C), and the index of orientation (D) in the same cornea with scleral rim are shown. The position of an average human limbus is highlighted by a blue dashed line. A long black arrow marks the location of the corneal abnormality and a short black arrow marks the location of the distorted limbus. (Tissue fixed in 2.5% formalin).

The distribution of aligned collagen mass was also abnormal in the affected regions (Figure 5.5C). A slight increase in the amount of aligned collagen mass was observed in the central cornea in the region of the abnormality and the normal diamond shaped arrangement of aligned collagen seen in the periphery of other normal corneas (Figures 5.1 E and F and Appendix 1), was disrupted in the affected ST limbal region. The high index of orientation in the region of the corneal abnormality revealed that the additional collagen present in this region is predominantly aligned collagen (Figure 5.5D). An increase in the index of orientation, which normally occurs in all four quadrants of the peripheral cornea (Figures 5.1 G and H and Appendix 1), in this case occurred in only three, with the exception being the affected ST quadrant. The increase in the index of orientation in sample S1 was most pronounced in the SN and IT quadrants which was as expected for a right cornea (based on data from samples N1 (Figure 5.1G) and N3 (appendix1)); however, in sample S1 the majority of the distorted ST quadrant had a lower index of orientation (18-36% alignment) than the same region in samples N1 and N3 (36-54% alignment).

The preferred orientation of collagen was only marginally altered in the affected corneal and limbal regions of S1 (Figure 5.6). Based on the appearance of the polar plot map alone, it looks as though a partial thickness incision was made in the ST quadrant of the annulus of aligned collagen surrounding the cornea, which was then dragged in towards the centre of the cornea, thereby exposing a small region of orthogonally aligned collagen between the two halves of the disrupted annulus. The preferred orientation of collagen in the unaffected regions of the cornea and limbus in sample S1 did not appear to differ from that of other normal right eyes (Figure 5.2 and Appendix 1).

Right (S1)

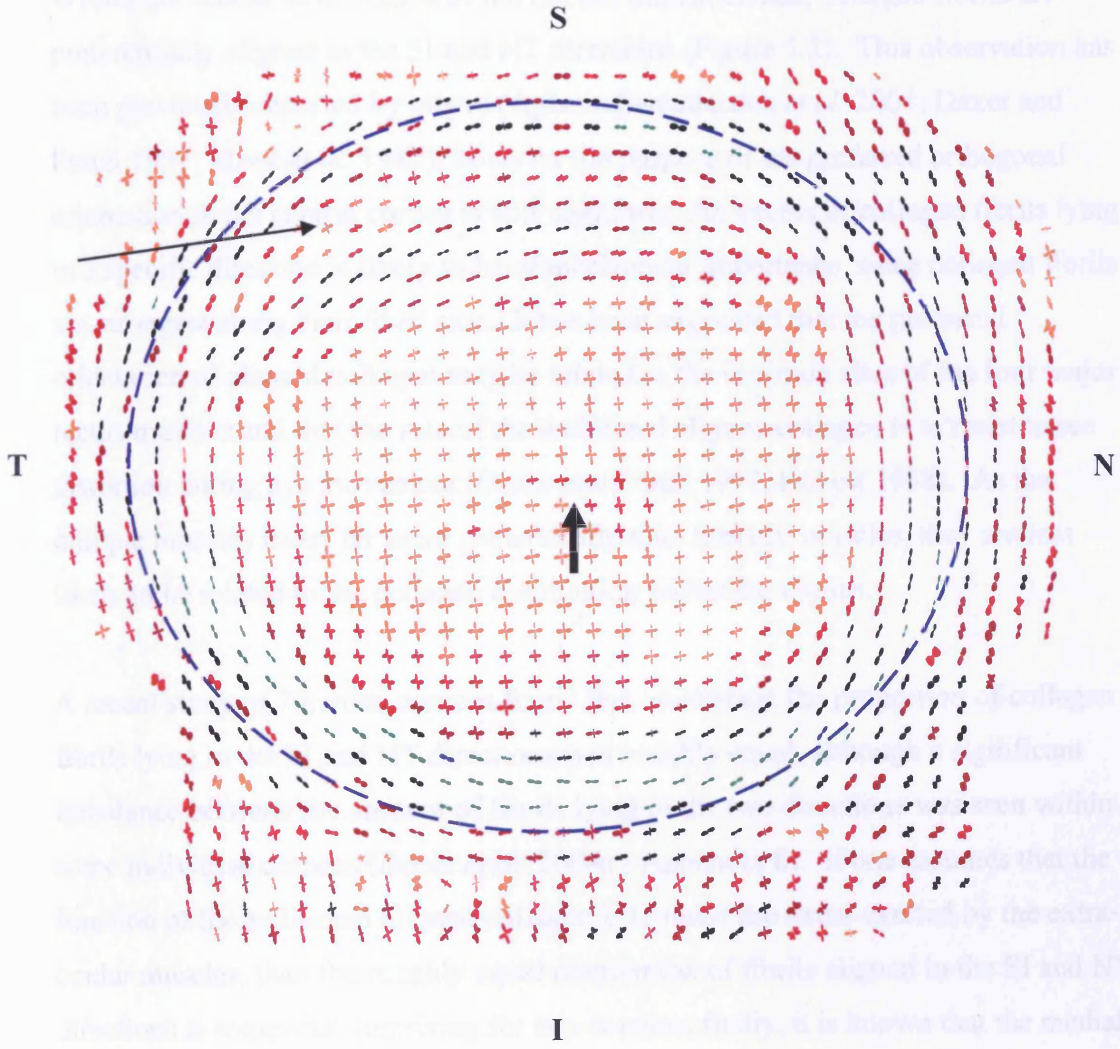

Figure 5.6. Polar plot map showing the preferred orientation of collagen in a right cornea with scleral rim (S1) that had abnormalities in the central region of the cornea (short black arrow) and in the superior-temporal aspect of the limbus (long black arrow). The position of an average human limbus is highlighted by a blue dashed line.

5.4 Part A: Discussion

5.4.1 The arrangement and distribution of collagen in normal left and right human corneas with scleral rims

Within the central 6mm region of the normal human cornea, collagen fibrils are preferentially aligned in the SI and NT directions (Figure 5.2). This observation has been previously reported by others (Aghamohamadzadeh *et al.* 2004; Daxer and Fratzl 1997; Meek *et al.* 1987); however the purpose of the preferred orthogonal orientation in the central cornea is still unknown. An excess of collagen fibrils lying in a specific direction is likely to be of mechanical importance, since collagen fibrils are strongest along their fibril axis. It has been suggested that the preferred orientation of aligned collagen may be related to the insertion sites of the four major rectus muscles and that the role of the additional aligned collagen is to resist tissue distortion during eye movement (Daxer and Fratzl 1997; Kokott 1938). As the oblique muscles insert far more posteriorally than the recti muscles, they are less likely to be related to the collagen distribution within the cornea.

A recent study of 7 human corneas found that on average the proportion of collagen fibrils lying in the SI and NT directions was roughly equal, although a significant imbalance between the amount of fibrils lying in the two directions was seen within some individual corneas (Boote *et al.* 2004a - Appendix 8). If one assumes that the function of the additional aligned collagen is to resist the stress exerted by the extra-ocular muscles, then the roughly equal distribution of fibrils aligned in the SI and NT directions is somewhat surprising for two reasons; firstly, it is known that the medial recti muscles are the most powerful of the extra-ocular muscles and secondly, horizontal eye movements are more frequent than vertical ones (Weale 1982). One might therefore expect there to be more aligned collagen in the NT direction than in the SI direction. However, an understanding of corneal development may provide a possible explanation for the equal amount of collagen alignment in the two directions. During ante-natal development the human cornea is almost circular and at 3-months gestation the ratio of vertical corneal diameter to horizontal diameter is 0.97. At birth, this ratio decreases to 0.93. It has been suggested that the reduced ratio may be due to an increased resistance in the vertical direction during eye growth (Weale 1982).

Additional aligned collagen in the SI direction may also be required to resist the action of the orbicularis (which causes eye lid movement), as its action may contribute to stress along the vertical meridian (Boote *et al.* 2004a – Appendix 8). As the cornea flattens with increasing proximity to the limbus, the orthogonal preferred orientation is gradually lost and is replaced by an excess of collagen lying tangentially to the cornea, so forming an annulus of highly aligned collagen around it. A series of calculations by Maurice (1984) revealed that a circumferential limbal tension of approximately twice that of the radial tension is required to maintain the greater curvature of the cornea, thereby explaining the presence of an annulus of collagen around the cornea. The tangential preferred orientation of collagen around the cornea is maintained in the sclera up to a distance of 1.2mm from the limbus. Beyond this point, there is a major change in the preferred direction of collagen at the 12, 3, 6 and 9 o'clock positions, as it alters its course towards the insertion points of the four major rectus muscles. Between the points of muscle insertion, collagen is aligned circumferentially around the cornea and limbus. This arrangement of collagen in the anterior sclera is likely involved in the resistance of tissue distortion during eye movement.

Total collagen mass is fairly uniform over the central cornea but increases rapidly towards the limbus and continues to increase into the sclera. This increase in collagen mass corresponds to an increase in tissue thickness between the cornea and sclera (0.5mm in the cornea and 0.8mm in the sclera). Collagen mass is higher in the inferior sclera than elsewhere, thus implying that the inferior sclera is stronger than the superior sclera; the reason for this is not clear.

The distribution of aligned collagen mass is also uniform across the central cornea but increases in all four quadrants of the peripheral cornea to form a skewed diamond shaped arrangement. When aligned collagen mass is plotted as a proportion of the total collagen mass, to form an index of orientation, it is evident that the ratio increases dramatically in the periphery of all four quadrants of the cornea. It has been previously suggested that the increased index of orientation is due to the presence of additional aligned collagen lamellae that traverse the peripheral cornea and reinforce the point at which the peripheral cornea flattens (Figure 1.7) (Aghamohamadzadeh *et*

al. 2004). The increase in the index of orientation is most pronounced in the SN and IT quadrants of both the left and right cornea, where up to 72% of the total collagen is preferentially aligned. Attempts to relate these structural features to the strength of the various extra-ocular muscles and the position at which they insert into the sclera have as yet been unsuccessful.

A large variation was observed between normal corneas in terms of the average scattering intensity in the central 4mm region. One would expect there to be some natural variation in scattering intensity between samples since corneal thickness is not uniform throughout the population. A study of 22 corneas examined using ultrasonic pachymetry revealed the average central thickness of the corneas to be 572.0μm +/- 20.6 μm (Patel *et al.* 2001). However, the variation in scattering intensity between the samples used in the present study may be slightly larger than expected due to the presence of small folds in samples N2 and N3. The index of orientation varied very little between samples N1, N2 and N3, suggesting that irrespective of the total collagen mass, the proportion of aligned collagen is fairly constant between normal corneas.

5.4.2 Implications for corneal surgery

This study has shown that in the normal cornea and limbus mirror symmetry exists between the right and left eye, in terms of the arrangement and distribution of preferentially aligned collagen. In addition, the specific arrangement and distribution of preferentially aligned collagen mass in an individual cornea has been shown to vary with angular position around the cornea. It is possible that the anisotropic arrangement of collagen might relate to the differential flattening of the normal cornea along its various meridians (Dingeldein and Klyce 1989) and that the structural symmetry between right and left corneas might in theory help to explain the topographical mirror symmetry seen in fellow corneas (Dingeldein and Klyce 1989; Smolek *et al.* 2002).

Both of these findings are of particular relevance to current surgical practices, as when a corneal transplant operation is performed, no attempt is made to maintain the correct orientation of the donor corneal button. Also a left corneal button may be

transplanted into a right eye and vice versa. Based on the findings of this study, it is suggested that by maintaining the correct orientation of transplant corneas and ensuring that left corneas be grafted into left eyes and likewise for right corneas, it may be possible to further reduce the incidence and level of post-operative astigmatism. However, in practice this may not be feasible due to donor tissue shortages and the additional time required to tag donor corneal tissue (in order to maintain its correct *in vivo* orientation).

A further implication of this study is that if corneal strength and shape are largely determined by the precise organisation of collagen, then data such as is presented here may be of use in aiding the corneal surgeon in their choice of incision site and direction of incision. It is suggested here and elsewhere (Meek and Newton 1999), that incisions following the direction of the preferred orientation of collagen at a specific point may result in less tissue damage and more effective healing than incisions made across the general direction of the collagen fibrils. Bearing in mind the distribution of collagen mass, incisions into areas where there is a reinforcement of collagen (indicating that they are stress bearing regions) such as at the limbus, may have more of an impact on the mechanics and hence the shape of the cornea than incisions made elsewhere. In support of this theory a clinical study by Anders and co-workers (1997) reported that a scleral incision 1mm behind the limbus resulted in a lower post-operative astigmatism than a similar cut made at the limbus.

5.4.3 The arrangement and distribution of collagen in a cornea and scleral rim with corneal and limbal abnormalities.

An examination of one cornea complete with scleral rim (S1), which was deemed by the operating surgeon to be normal and produced normal videokeratography (Figure 5.5A), was found to have abnormalities in the central cornea and in the ST aspect of the limbus that were clearly visible by light microscopy (Figure 5.4). The most likely explanation for the abnormalities is that the cornea experienced some form of mechanical trauma subsequent to its removal from the eye, which was then accentuated by the process of fixation. The abnormality in the central region of the cornea appeared to be due to the presence of a very small horizontal incision from

which creases in the tissue extended above and below. In the region of the abnormality, both the total and the aligned collagen mass were found to be higher than elsewhere in the central cornea (Figure 5.5 B and C). A small fold in the tissue near the incision might explain the increase in collagen mass in the affected region, however, in contrast to the uniaxial preferred orientation of aligned collagen seen in other examples of folded corneal tissue (Figure 5.3 and Appendix1), the orientation of aligned collagen in the central region of sample S1 showed only a slight deviation (Figure 5.6) from that of the normal unfolded cornea (Figure 5.2).
The second abnormality, observed in the ST limbal region of the same sample (S1) was also accompanied by changes in the normal distribution of collagen mass. Light microscopy examination of the region suggested that a partial thickness circumferential limbal incision had been made and the cut tissue then dragged in towards the centre of the cornea. Maps of total collagen scattering supported this, as the normal increase in collagen mass at the limbus was disrupted in the ST aspect. The polar plot map provided further evidence, in that the normal circum-corneal annulus of aligned collagen appeared to be split into two parts in the region of the abnormality, with the corneal side of the disturbed limbal annulus being located well within the cornea. A further interesting point to note is that between the two parts of the disrupted annulus a small region of orthogonally aligned collagen was observed. Although the depth of the incision was unknown, the results suggest that the circum-corneal annulus of collagen at the limbus may only be a feature of the anterior and mid stroma and that the preferred orthogonal (SI and NT) orientation of collagen seen in the cornea, may also be present in the posterior stroma of the limbus. Bearing in mind the mechanical importance of the limbal annulus it would be beneficial to study the orientation of preferentially aligned collagen as a function of tissue depth at the limbus.

Although the exact nature of the abnormalities and the reason for their presence was unclear, sample S1 highlighted the ability of the technique to detect ultrastructural deformations in the cornea that correspond to tissue abnormalities visible by light microscope. These findings indicate that the technique may be capable of detecting characterised structural changes in the cornea such as incisions following cataract surgery.

5.5 Part 2: Results

5.5.1 Keratoconus buttons without corneal scarring

Due to the absence of any folds or abnormalities in sample N1 (normal right cornea) (Figure 5.1 and 5.2) it was used as a control for the keratoconus corneal buttons. The mirror symmetry between the normal left and right cornea (Figure 5.1), enables a comparison to be drawn between a normal right cornea and either a left or right keratoconus button, so long as both the mirror symmetry and the normal variation in mass distribution between individuals is taken into account. For comparison purposes with the majority of the keratoconus corneal buttons used in this study, the distribution and preferred orientation of collagen mass is only shown for the central 8mm region of sample N1 (Figure 5.7). The central 6.4mm region has also been outlined for comparison with the keratoconus buttons K1 and K2 which are of a similar size (6.5mm buttons). Sample details for each cornea are shown in Table 7 (Section 5.2.1).

Within the central 6.4mm region of the normal cornea there is a uniform distribution of total and aligned collagen mass and a preferred orthogonal SI and NT orientation of collagen fibrils. The increase in the index of orientation, which occurs in the periphery of all four quadrants of the normal human cornea, is only evident in the SN and IT quadrants of the central 6.4mm (as it is in these quadrants that the effect is most pronounced). Towards the edge of the central 8mm region of the same cornea there is an increase in both total and aligned collagen mass and although the index of orientation is highest in the SN and IT quadrants a small increase can also be seen in the SI and NT quadrants. The preferred orthogonal orientation of collagen becomes more tangential towards the edge of the 8mm region.

N1 (central 8mm region of a normal right cornea)

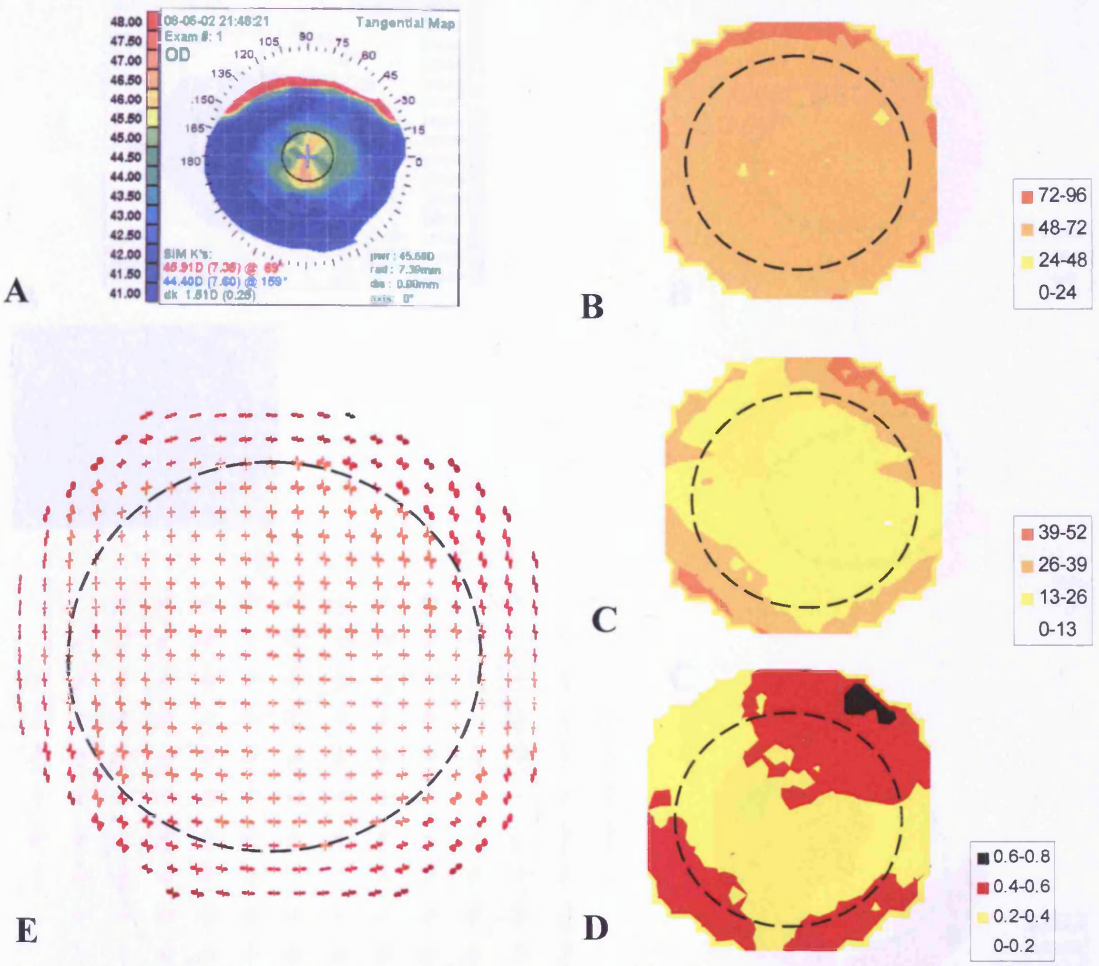

Figure 5.7. Map of corneal dioptric power for a normal right eye (A), accompanied by maps showing the distribution of total collagen mass (B), aligned collagen mass (C), the index of orientation (D) and the preferred orientation of collagen (E), recorded at 0.4mm intervals across the central 8mm region of the same cornea. The 6.4mm region is highlighted by a black dashed circle. (Sample N1 – tissue fixed in 2.5% formalin).

Figures 5.8-5.11 show similar Eye Sys videokeratography, collagen mass distribution and preferred collagen orientation maps for keratoconus buttons K1 to K4 (fixed in 2.5% formalin). Samples K2 (right) and K3 (left) were taken from the same patient. In each case an outline showing the region of highest dioptric power (referred to herein as the apical region) has been superimposed onto the maps of collagen orientation and mass distribution. The para-apical region refers to the remainder of the button outside the marked apical region.

K1 (6.5mm button of a left keratoconus cornea)

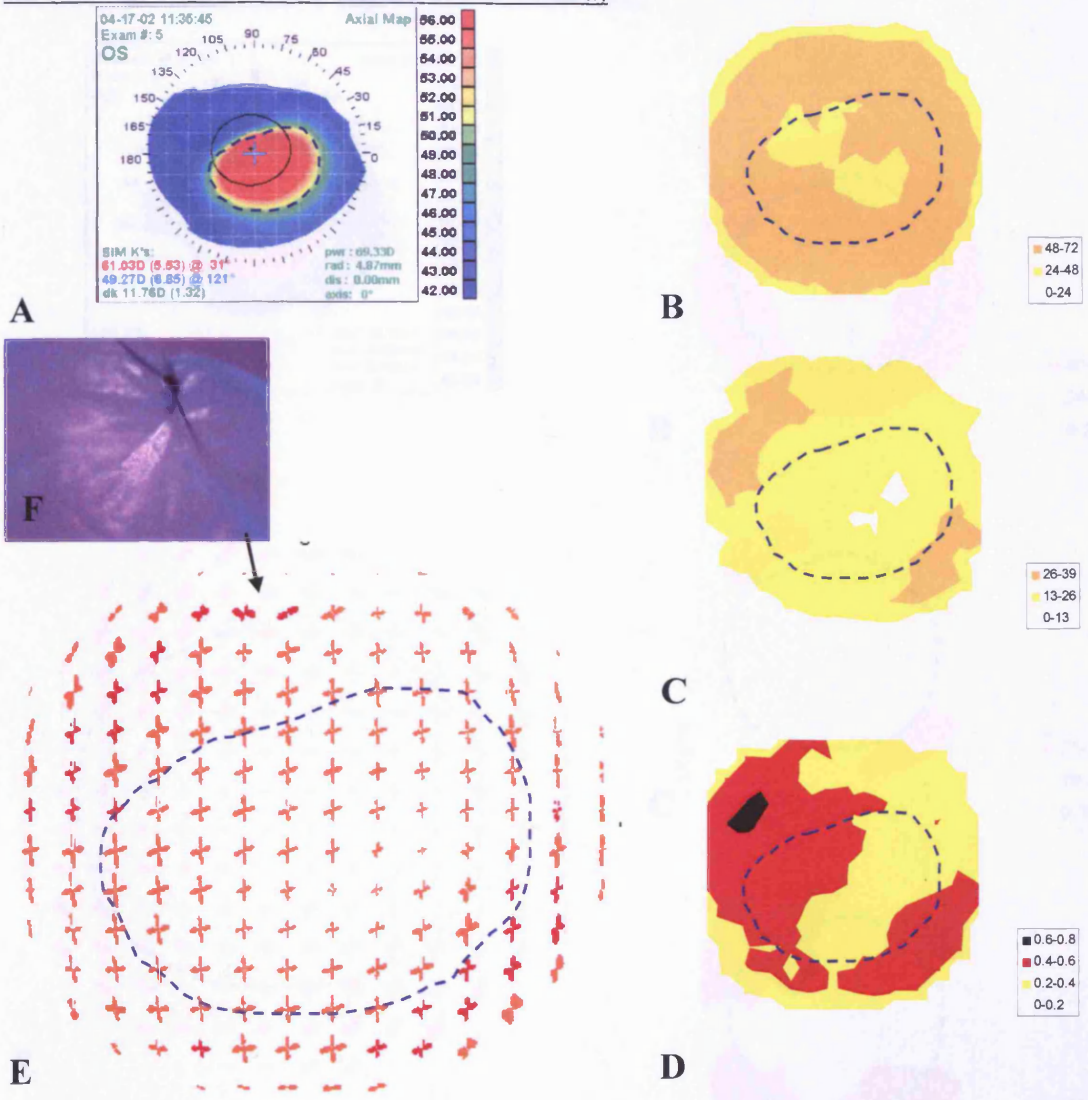

Figure 5.8. Map of corneal dioptric power for a keratoconus left eye (A) accompanied by maps showing the distribution of total collagen mass (B), aligned collagen mass (C), the index of orientation (D) and the preferred orientation of collagen (E) at 0.5mm intervals across a 6.5mm button taken from the same cornea. Due to variations in the amount of aligned collagen across the sample the polar plots have been scaled down by factors of 1.5 and 1 and coloured red and orange respectively. The region of highest dioptric power (as determined by videokeratography) is highlighted by a blue dashed line. The region of the suture, as seen by a light microscope is also shown (F), and a black arrow marks its location on the polar plot map (E). (Sample K1 – tissue fixed in 2.5% formalin).

Total and aligned collagen mass are lower than normal in the apical region of sample K1. However, the index of orientation within the central 6mm region of the cornea is higher than normal, indicating either a preferential loss of isotropic collagen or a redistribution of collagen mass. The preferred orientation of collagen is also altered within the apical region and at the location of the suture.

K2 (6.5mm button from a left keratoconus cornea)

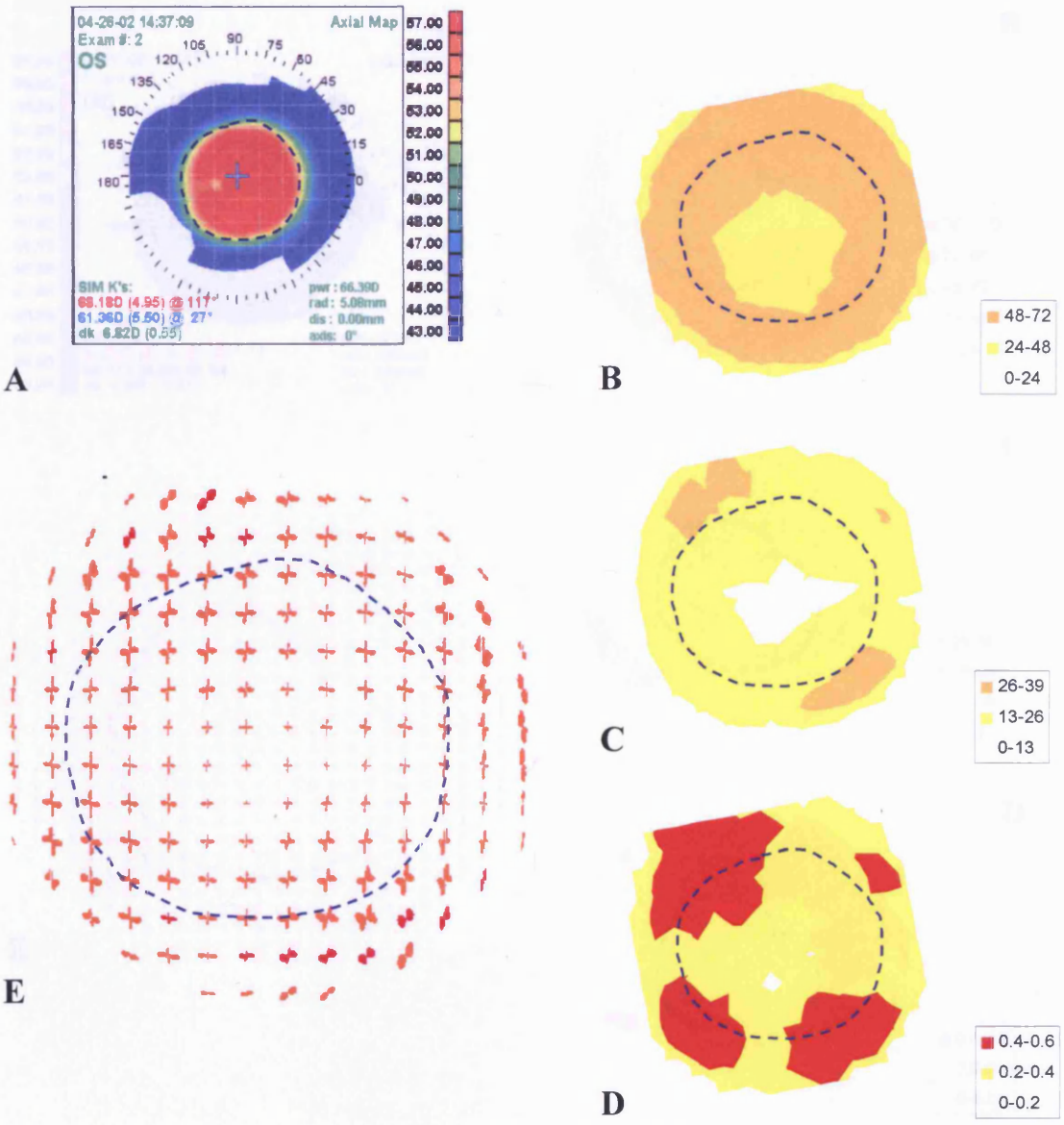

Figure 5.9. Map of corneal dioptric power for a keratoconus left eye (A) accompanied by maps showing the distribution of total collagen mass (B),aligned collagen mass (C), the index of orientation (D) and the preferred orientation of collagen (E) at 0.5mm intervals across a 6.5mm button taken from the same cornea. Due to variations in the amount of aligned collagen across the sample the polar plots have been scaled down by factors of 1.5 and 1 and coloured red and orange respectively. The region of highest dioptric power (as determined by videokeratography) is highlighted by a blue dashed line. (Sample K2 – tissue fixed in 2.5% formalin).

As with sample K1, total and aligned collagen mass are lower than normal in the apical region of sample K2. In contrast to the normal cornea, the index of orientation in sample K2 (which has a round cone), increases almost equally in all four quadrants of the peripheral cornea. The preferred orientation of collagen in this case is altered in both the apical and para-apical regions of the button.

K3 (7.5mm button from a right keratoconus cornea)

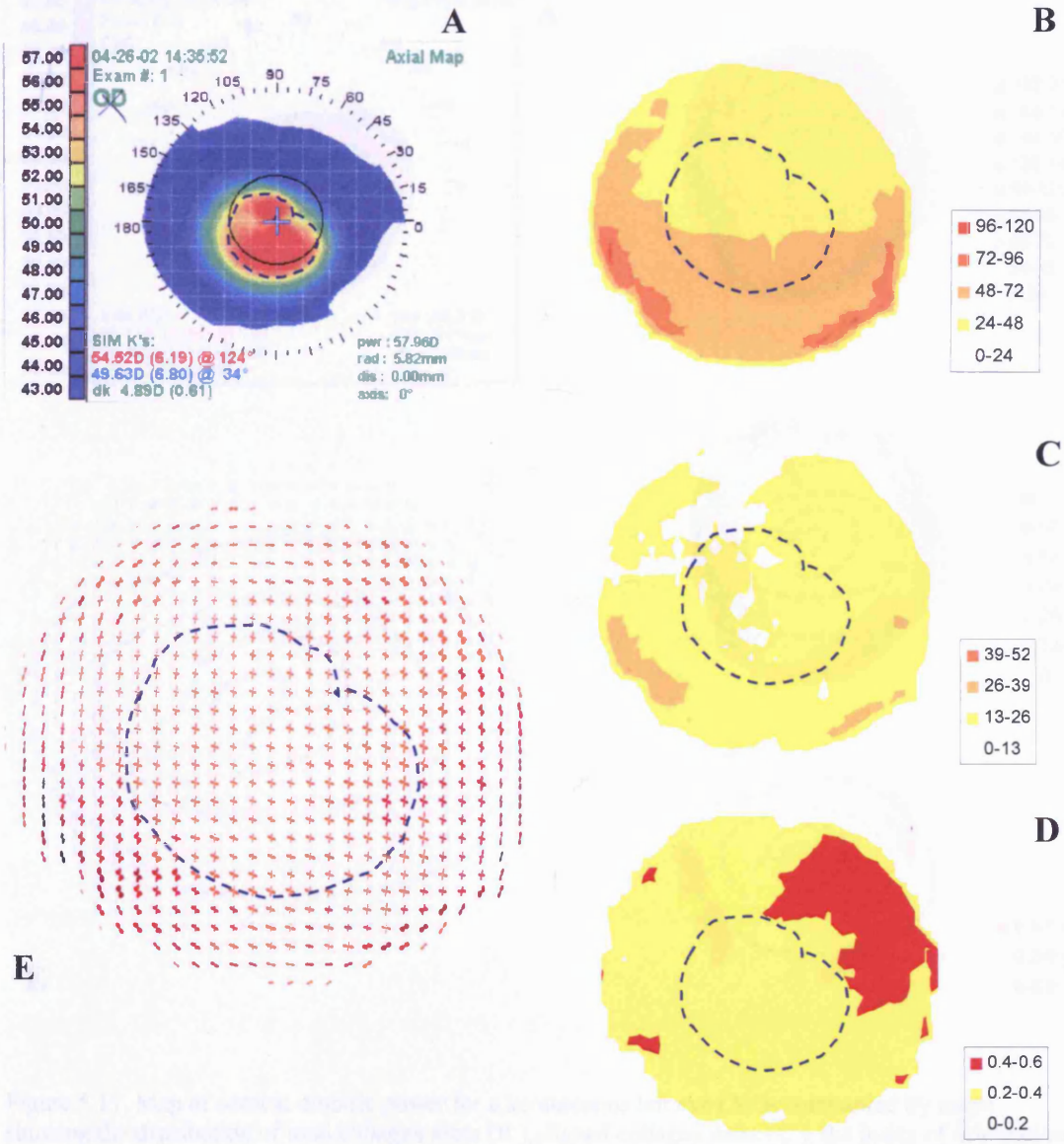

Figure 5.10. Map of corneal dioptric power for a keratoconus right eye (A) accompanied by maps showing the distribution of total collagen mass (B),aligned collagen mass (C), the index of orientation (D) and the preferred orientation of collagen (E) at 0.25mm intervals across a 7.5mm button taken from the same cornea. Due to variations in the amount of aligned collagen across the sample the polar plots (E) have been scaled down by factors of 3, 2, 1.5 and 1 and coloured black, brown, red and orange respectively. The region of highest dioptric power (as determined by videokeratography) is highlighted by a blue dashed line. (Sample K3 – tissue fixed in 2.5% formalin).

K4 (7.5mm button from a left keratoconus cornea)

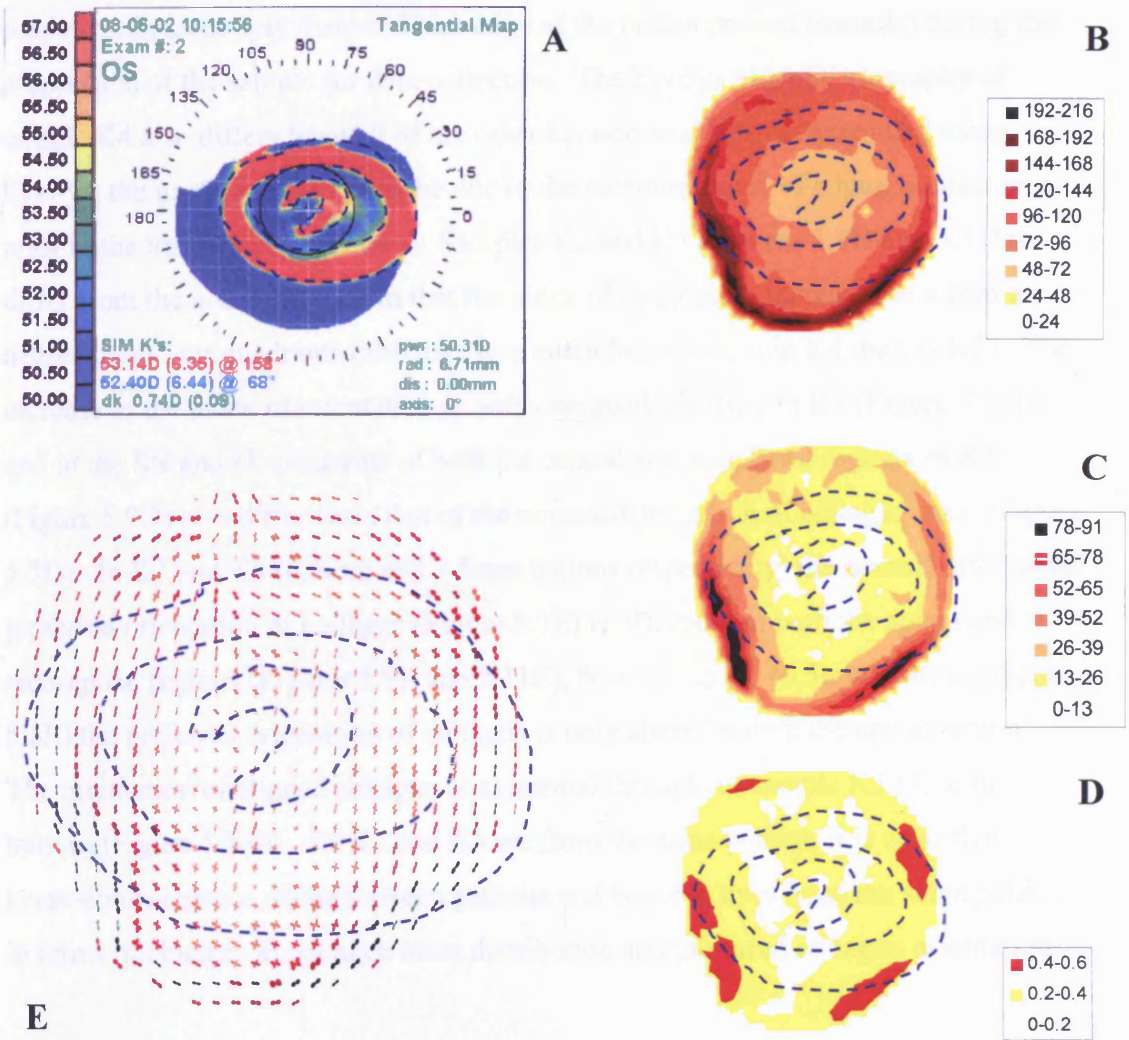

Figure 5.11. Map of corneal dioptric power for a keratoconus left eye (A) accompanied by maps showing the distribution of total collagen mass (B),aligned collagen mass (C), the index of orientation (D) and the preferred orientation of collagen (E) at 0.25mm intervals across a 7.25mm button taken from the same cornea. Due to variations in the amount of aligned collagen across the sample the polar plots (E) have been scaled down by factors of 7, 4, 2.5, 1.5 and 1 and coloured green, black, brown, red and orange respectively. The region of highest dioptric power (as determined by videokeratography) is highlighted by a blue dashed line. (Sample K4 – tissue fixed in 2.5% formalin).

Assuming that the effect of fixative on x-ray scattering is the same between samples and across individual samples, it is clear that there is an abnormal distribution of collagen mass in keratoconus buttons K1 to K4 (Figures 5.8 to 5.11). Both the total and the aligned collagen mass are lower than normal in the apical region of corneas K1, K2 and K3; however in K4 the total collagen mass was much higher than normal. The unusual shape of K4, as seen by the outline of the contour maps (Figure 5.11) and

the remarkably high total collagen mass at the edges of the button, indicate that its shape was in some way distorted (the edge of the button pushed inwards) during the preparation of the sample for data collection. The EyeSys videokeratography of sample K4 also differs from all of the other keratoconus buttons examined using EyeSys; the unusual pattern may be due to the recent removal of a hard contact lens prior to the image being recorded. Samples K2 and K4 (Figures 5.9D and 5.11D) differ from the normal cornea in that the index of orientation increases to a similar degree in all four quadrants (although to a much lesser extent in K4 than in K2). The increase in the index of orientation in only one quadrant (SN) in K3 (Figure 5.10D) and in the SN and IT quadrants of both the central and peripheral regions of K1 (Figure 5.9D) also differ from that of the normal distribution of collagen mass (Figure 5.7D). In K2 and K4 (6.5mm and 7.5mm buttons respectively) the normal orthogonal preferred orientation of collagen (Figure 5.7E) is disrupted in both the apical and para-apical regions (Figures 5.9E and 5.11E), however in K1 (6.5mm button) (Figure 5.8E) the preferred orientation of collagen is only altered within the apical region. The orientation of aligned collagen is as normal throughout sample K3 (7.5mm button) (Figure 5.10E). As K2 and K3 are from the same patient, it is clear that keratoconus corneas differ between patients and between eyes from the same patient in terms of changes in collagen mass distribution and preferred collagen orientation.

Figures 5.12-5.16, show similar data obtained by XRD and either Orbscan videokeratography (K5, 6, 7 and 9) or Visioptic Alcon Eye Map (K8) for three right (K5, K6 and K7) and two left (K8 and K9) keratoconus corneal buttons. An attempt has been made where possible to outline and superimpose the region of highest dioptric power onto the contour maps of collagen mass distribution and the polar plot maps of preferred collagen orientation.

In each of the 9 unscarred keratoconus corneal buttons (K1-9) there was a reduction in the aligned collagen mass at the apex of the cone and with the exception of one (K3), a swirling effect of the residual aligned collagen was seen around the apex. The swirling of aligned collagen around the apex of the cone was most prominent in buttons K5-7 (Figures 5.12E, 5.13E, 5.14E and 5.15E). The swirling effect seen in button K7 is magnified in Figure 5.14F.

K5 (7.5mm button from a right keratoconus cornea)

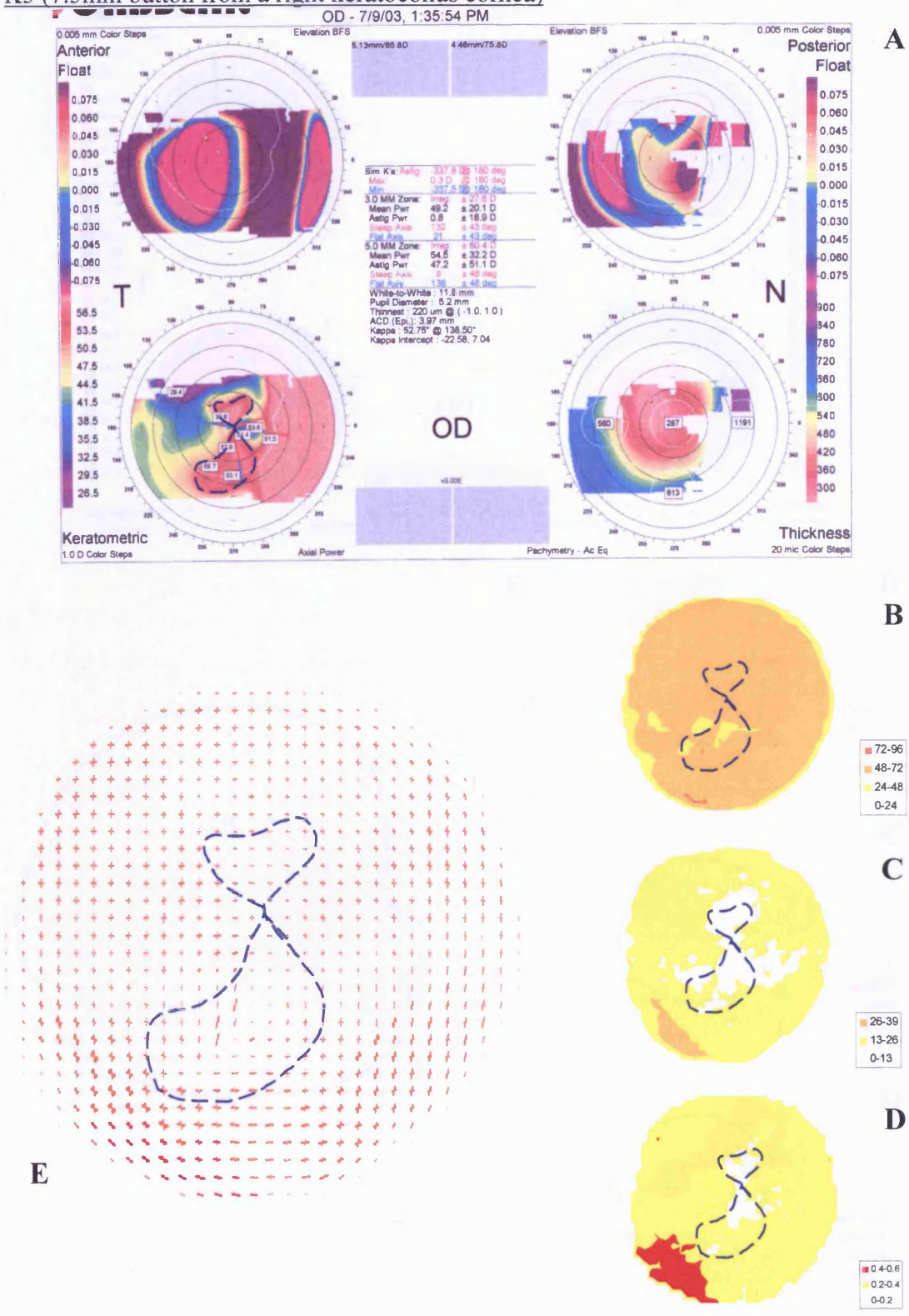

Figure 5.12. Map of corneal dioptric power for a keratoconus right eye (A) accompanied by maps showing the distribution of total collagen mass (B),aligned collagen mass (C), the index of orientation (D) and the preferred orientation of collagen (E) at 0.25mm intervals across a 7. 5mm button taken from the same cornea. Due to variations in the amount of aligned collagen across the sample the polar plots have been scaled down by factors of 2, 1.5 and 1 and coloured brown, red and orange respectively. The region highest dioptric power is highlighted by a blue dashed line. (Sample K5 – tissue frozen at -80°C).

K6 (7.5mm button from a right keratoconus cornea)

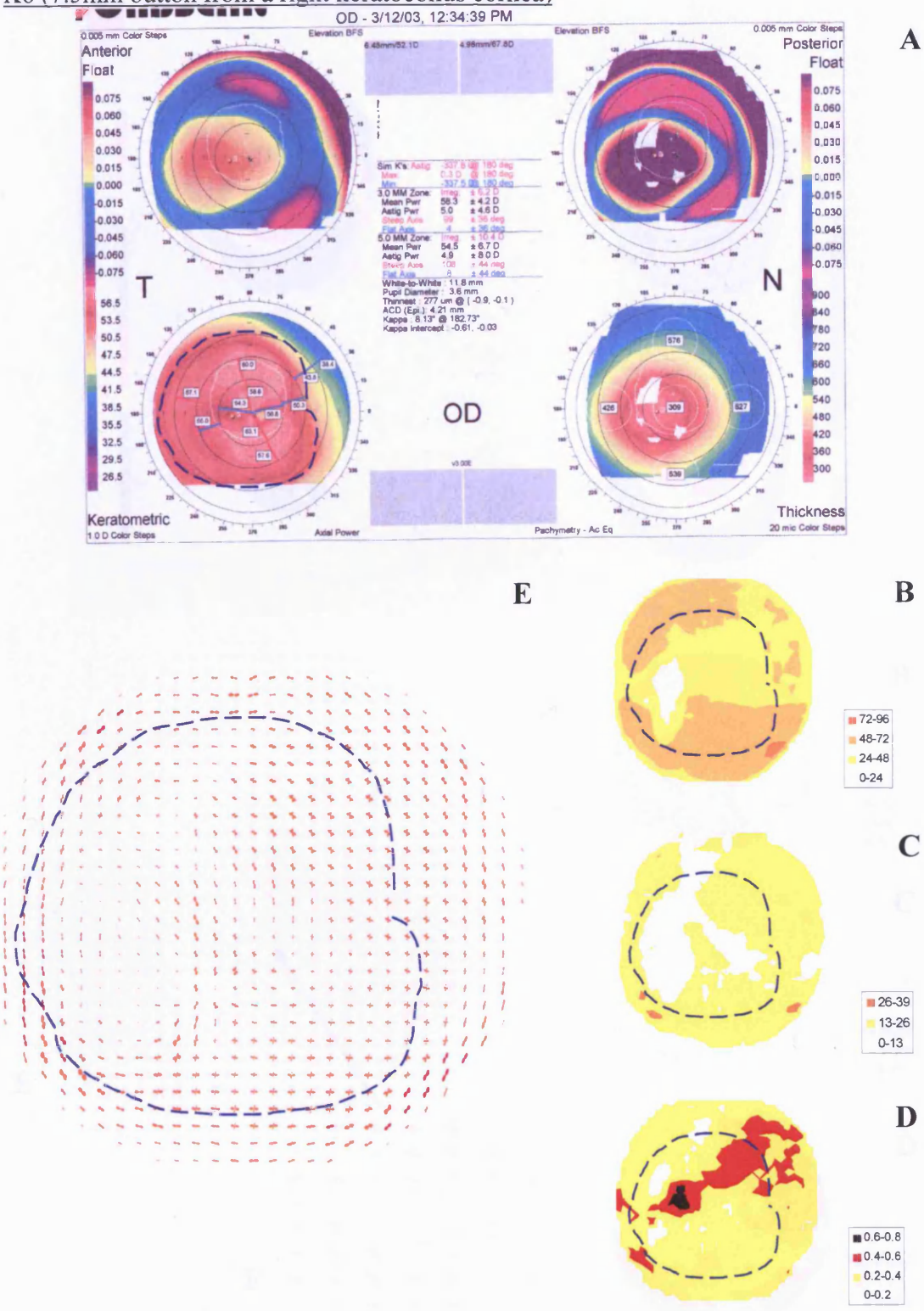

Figure 5.13. Map of corneal dioptric power for a keratoconus right eye (A) accompanied by maps showing the distribution of total collagen mass (B),aligned collagen mass (C), the index of orientation (D) and the preferred orientation of collagen (E) at 0.25mm intervals across a 7. 5mm button taken from a nasally decentred position in the same cornea. Due to variations in the amount of aligned collagen across the sample the polar plots have been scaled down by factors of 1.5 and 1 and coloured red and orange respectively. The region of highest dioptric power is highlighted by a blue dashed line. (Sample K6 – tissue frozen at -80°C).

K7 (8.0mm button from a right keratoconus cornea)

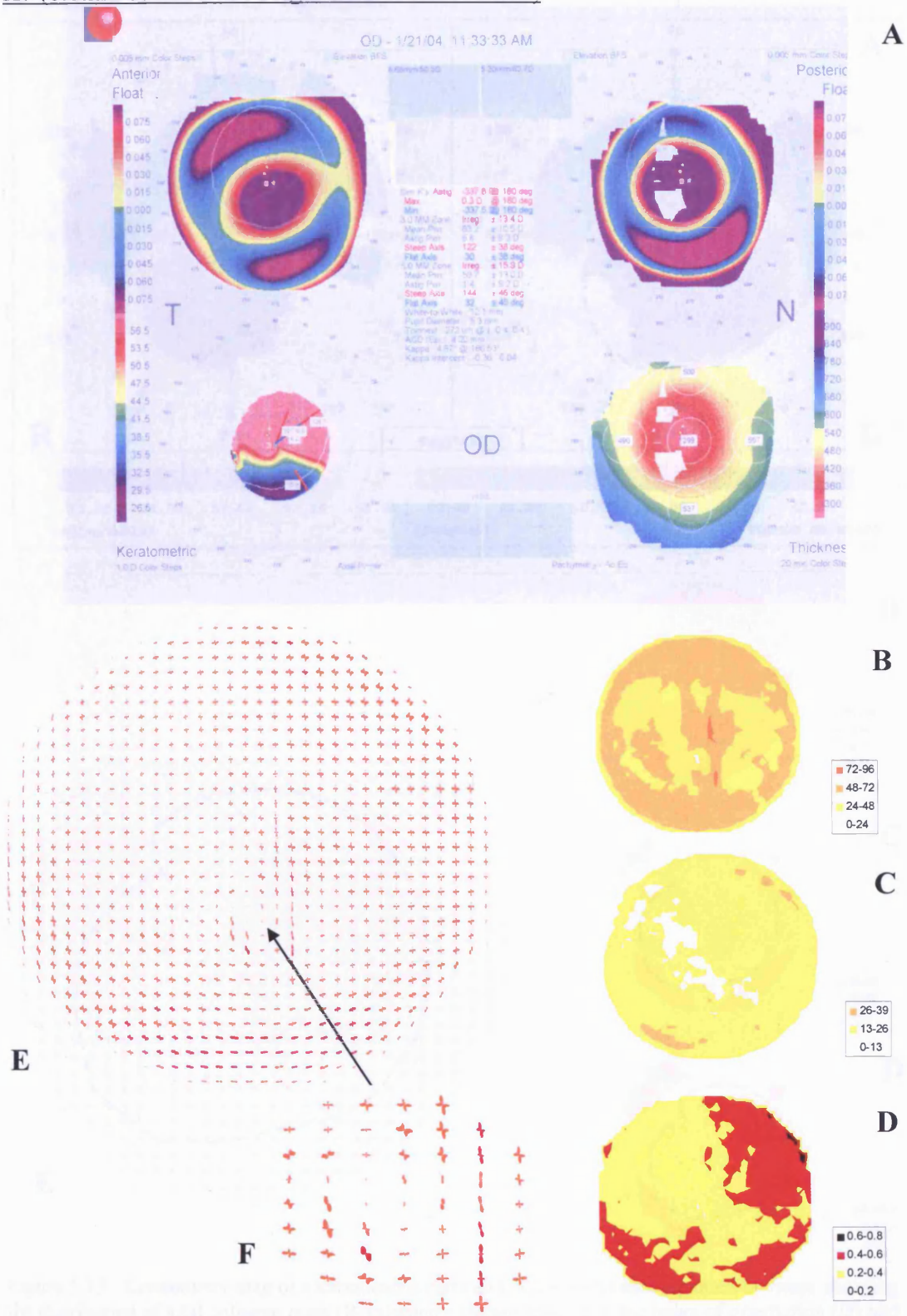

Figure 5.14. Map of corneal dioptric power for a keratoconus right eye (A) accompanied by maps showing the distribution of total collagen mass (B),aligned collagen mass (C), the index of orientation (D) and the preferred orientation of collagen (E) at 0.25mm intervals across a 8.0mm button taken from a nasally decentred position in the same cornea. Due to variations in the amount of aligned collagen across the sample the polar plots have been scaled down by factors of 1.5 and 1 and coloured red and orange respectively. The apical region of the button has been magnified (F) to show the preferred orientation of collagen more clearly. (Sample K7 – tissue frozen at -80°C).

K8 (7.5mm button from a left keratoconus cornea)

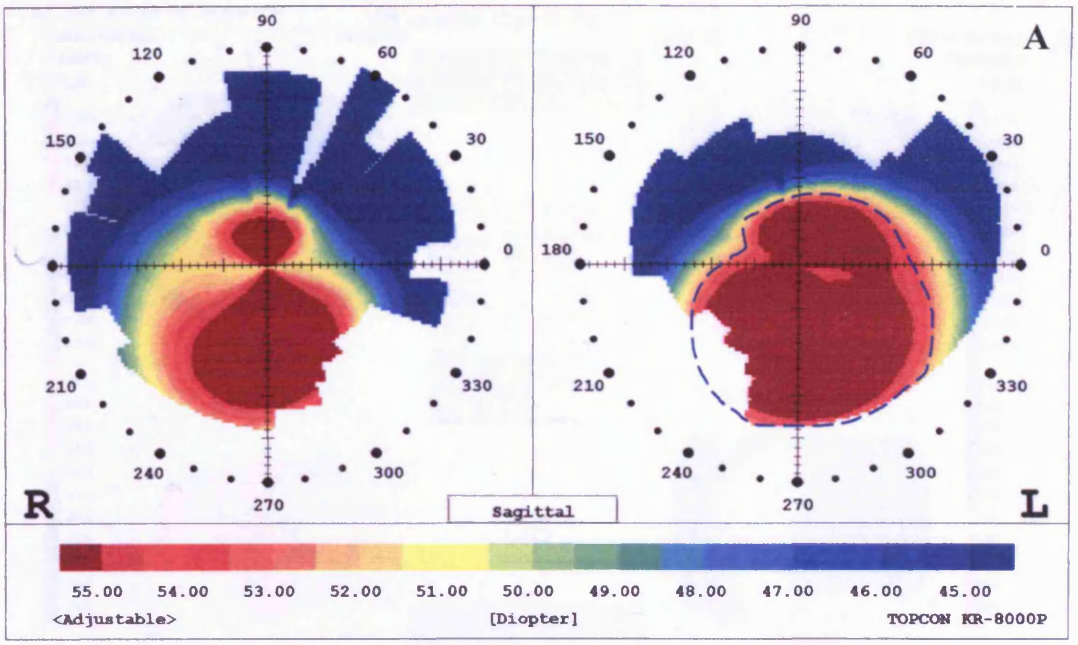

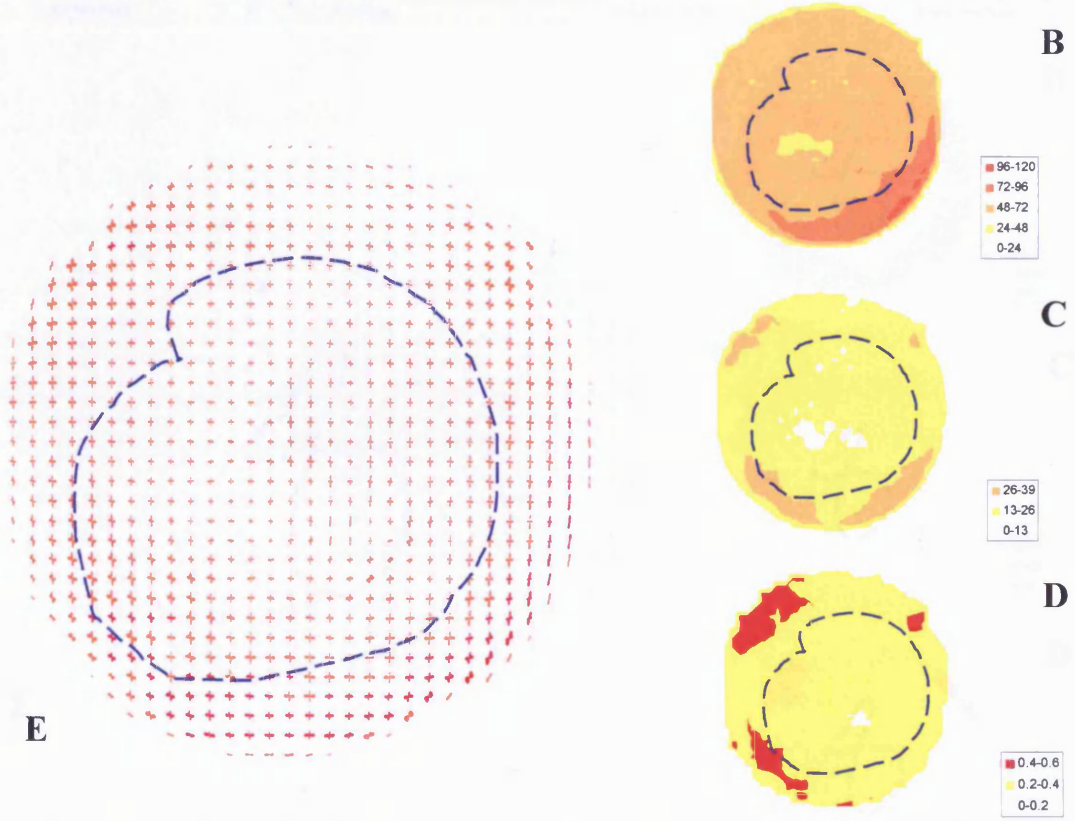

Figure 5.15. Keratometry map of a keratoconus right and left eye (A) accompanied by maps showing the distribution of total collagen mass (B),aligned collagen mass (C), the index of orientation (D) and the preferred orientation of collagen (E) at 0.25mm intervals across a 7. 5mm button taken from the same left cornea. Due to variations in the amount of aligned collagen across the sample the polar plots have been scaled down by factors of 1.5 and 1 and coloured red and orange respectively. The region of highest dioptric power is highlighted by a blue dashed line. (Sample K8 – tissue frozen at -80°C).

K9 (8.0mm button from a left keratoconus cornea (history of corneal hydrops)

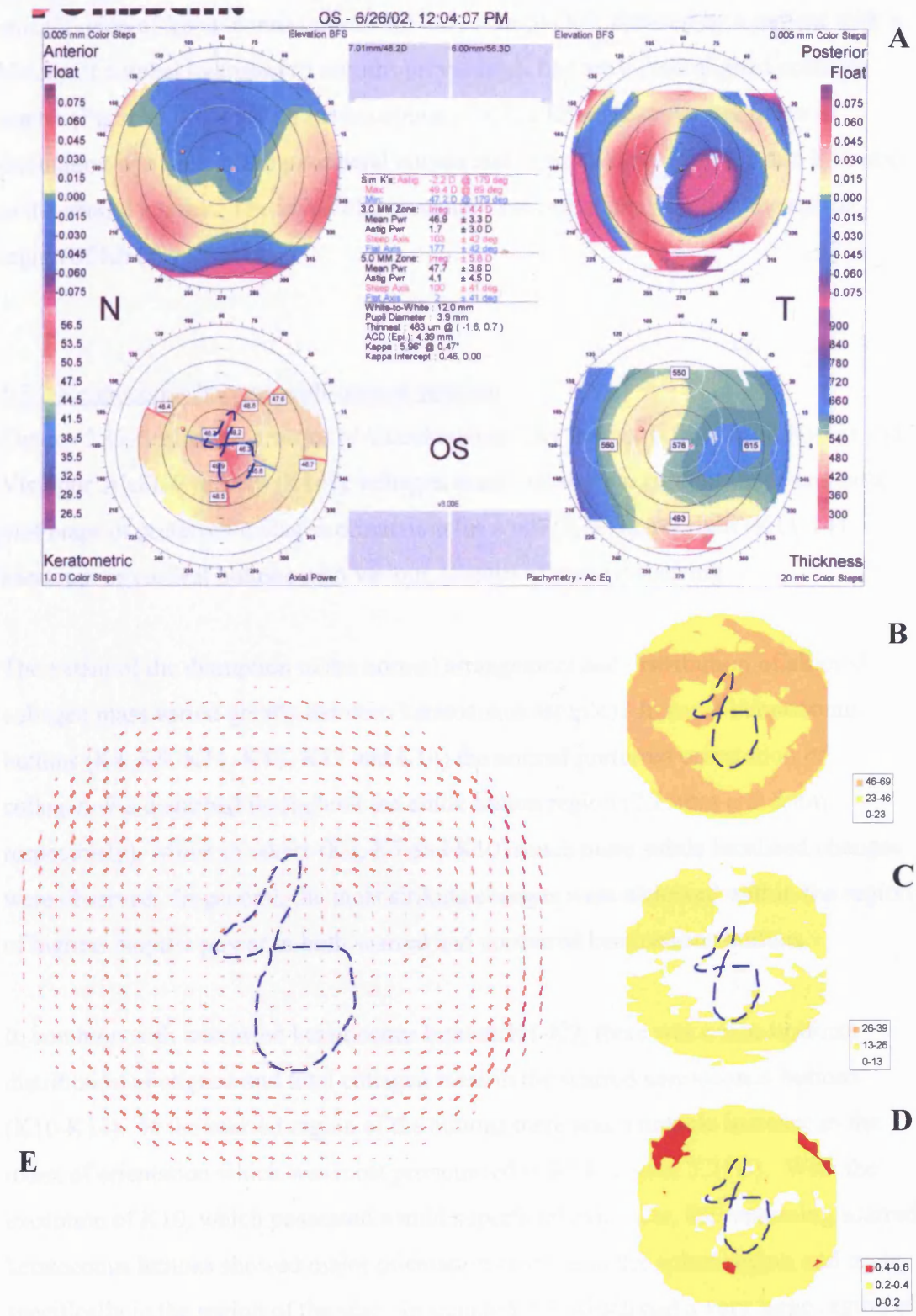

Figure 5.16. Keratometry map of a keratoconus left eye (A) accompanied by maps showing the distribution of total collagen mass (B),aligned collagen mass (C), the index of orientation (D) and the preferred orientation of collagen (E) at 0.25mm intervals across a 8.0mm button taken from the same left cornea. Due to variations in the amount of aligned collagen across the sample the polar plots have been scaled down by factors of 1.5 and 1 and coloured red and orange respectively. The region of highest dioptric power is highlighted by a blue dashed line. (Sample K9 – tissue frozen at -80°C).

As with K1-K3, the total and aligned collagen scatter is lower than normal in the apical region of keratoconus buttons K5-K9. Sample K9, donated by a patient with a history of corneal hydrops (15 months previously), had very little aligned collagen scatter (Figure 5.16C). With the exception of K7, a lower than normal index of orientation was seen in the peripheral cornea and in some cases (K5, K8 and K9) also in the central cornea. The index of orientation was remarkably high in the apical region of K6 (Figure 5.13D).

5.5.2 Keratoconus buttons with corneal scarring

Figures 5.17-5.21 show a series of videokeratography images (Orbscan (K10-13) and Visioptic Alcon Eye Map (K14)), collagen mass distribution contour maps and polar plot maps of preferred collagen orientation for a left (K10) and 4 right (K11-14) keratoconus corneal buttons with various degrees of corneal scarring.

The extent of the disruption to the normal arrangement and distribution of aligned collagen mass varied greatly between keratoconus samples. In some keratoconus buttons (K4, K9, K11, K12, K13 and K14) the normal preferred orientation of collagen was disturbed throughout the entire button region (7.25mm and 8mm respectively), whilst in others (K3, K7 and K10) much more subtle localised changes were observed. In general, the most striking changes were observed within the region of highest dioptric power in both scarred and unscarred keratoconus buttons.

In common with unscarred keratoconus buttons K1-K9, there was a non-uniform distribution of aligned and total collagen mass in the scarred keratoconus buttons (K10-K14). In the scarred region of the buttons there was a notable increase in the index of orientation which was most pronounced in K14 (Figure 5.21D). With the exception of K10, which possessed a mild superficial axial scar, the remaining scarred keratoconus buttons showed major orientation changes in the apical region and more specifically in the region of the scar. In sample K13, which had a very large region of high dioptric power (Figure 5.20A), encompassing the whole 8.5mm button, severe orientation changes were seen throughout the entire button (Figure 5.20E). In the unscarred buttons a swirling of preferentially aligned collagen around the region of least aligned collagen mass was frequently observed; however in 3/5 of the scarred

keratoconus buttons (K11-K13) there was often more than one region of reduced aligned collagen mass around which the remaining aligned collagen was preferentially orientated (Figures 5.18-5.20).

A further interesting point to note is that the normal increase in the index of orientation to between 40 and 60% collagen alignment in the four quadrants of the peripheral cornea (especially in the SN and IT quadrants) is severely disrupted in 8/9 unscarred buttons (with the exception being K7) and in 2 out of 5 scarred buttons (K11 and K13). In 2 of the unscarred corneas (K1 and K2) the increase in the index of orientation normally seen to occur at a distance of 7mm from the centre of the cornea, occurred well within the 6.5mm button region (Figures 5.8D and 5.9D). In sample K1, which had an inferior-temporally located oval cone, the increase in collagen alignment occurred very close to the centre of the button (on either side of the short axis of the apical region) in both the SN and IT quadrants. In sample K2 which had a large round cone, the increase in the index of orientation occurred close to the centre of the button (at the edge of the apical region) in all four quadrants to an equal extent. In 6 of the unscarred buttons (K3, K4, K5, K6, K8 and K9) and 2 of the scarred buttons (K11 and 13) the index of orientation was lower than normal in the four quadrants of the peripheral cornea and lacked symmetry between the SN and IT quadrants. In each of the scarred buttons there was a small region surrounding the scar where the index of orientation was higher than normal. In this region, which occurs at roughly right angles to the steepest axis of the cornea, the swirling effect of preferentially aligned collagen around each area of low aligned collagen mass merge together to follow the same course, thereby increasing the index of orientation.

K10 (7.5mm button from a right keratoconus cornea with a slight superficial axial scar)

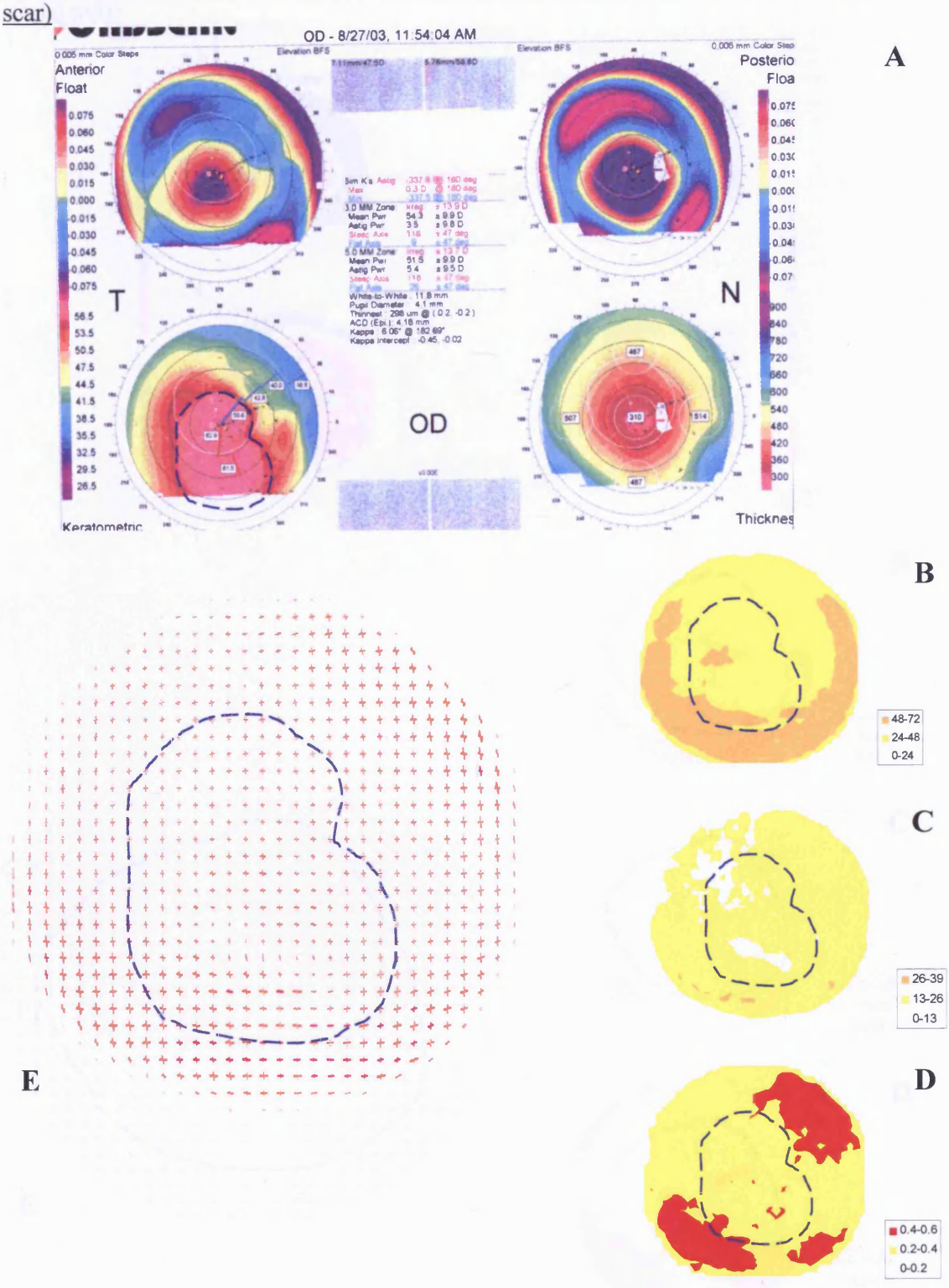

Figure 5.17. Keratometry map of a keratoconus right eye with a mild superficial axial corneal scar (A) accompanied by maps showing the distribution of total collagen mass (B), aligned collagen mass (C), the index of orientation (D) and the preferred orientation of collagen (E) at 0.25mm intervals across an 8.0mm button taken from the same right cornea. Due to variations in the amount of aligned collagen across the sample the polar plots have been scaled down by factors of 1.5 and 1 and coloured red and orange respectively. The region of highest dioptric power is highlighted by a blue dashed line. (Sample K10 – tissue frozen at -80°C).

K11 (8.0mm button from a left keratoconus cornea with a superficial scar above visual axis)

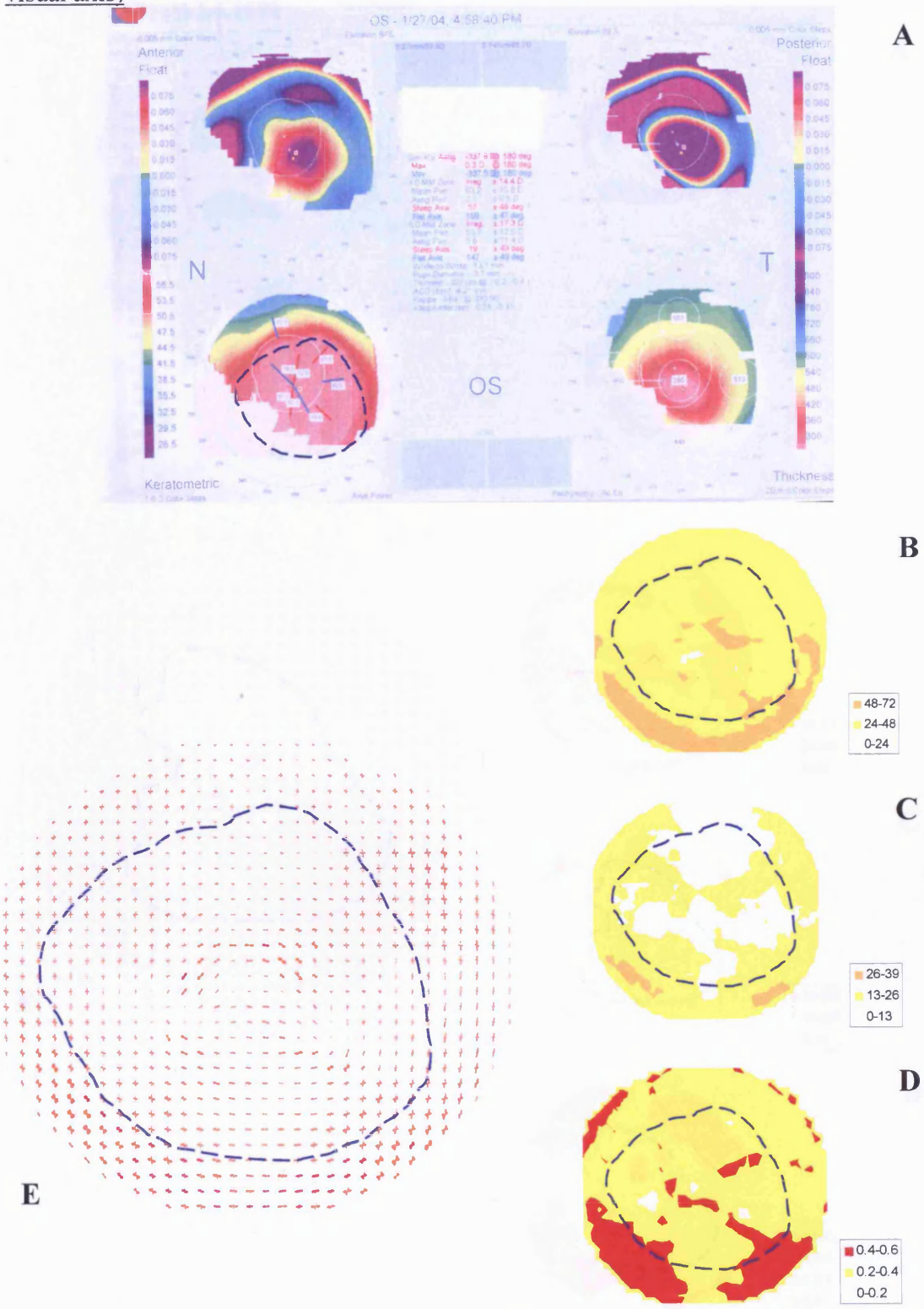

Figure 5.18. Keratometry map of a keratoconus left eye with a slight superficial scar above the visual axis (A) accompanied by maps showing the distribution of total collagen mass (B), aligned collagen mass (C), the index of orientation (D) and the preferred orientation of collagen (E) at 0.25mm intervals across a 8.0mm button taken from the same left cornea. Due to variations in the amount of aligned collagen across the sample the polar plots have been scaled down by factors of 1.5 and 1 and coloured red and orange respectively. The region of highest dioptric power is highlighted by a blue dashed line. (Sample K11 – tissue frozen at -80°C).

K12 (8.0mm button from a right cornea with a slight axial superficial scar)

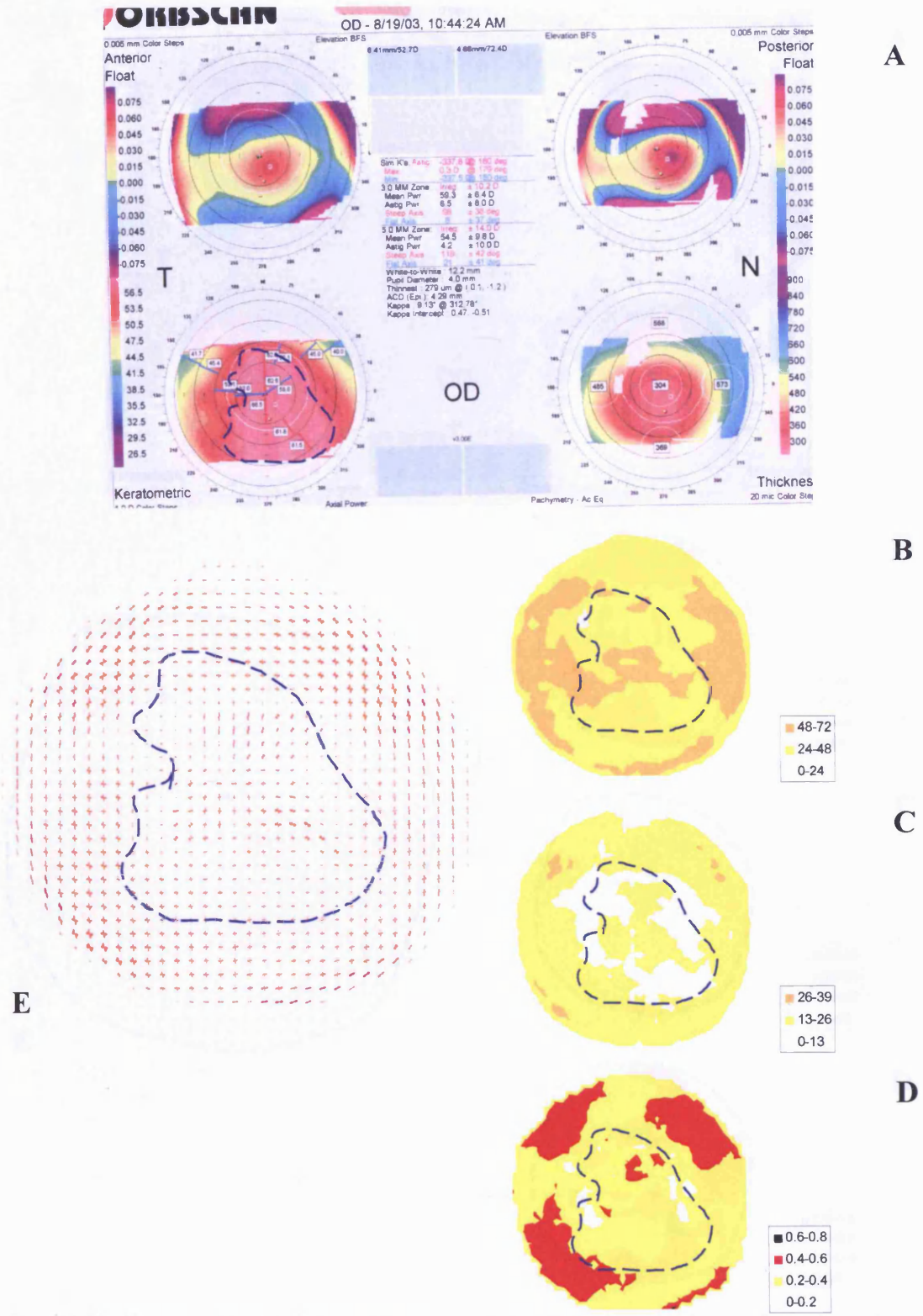

Figure 5.19. Keratometry map of a keratoconus right eye with a slight axial superficial corneal scar (A) accompanied by maps showing the distribution of total collagen mass (B), aligned collagen mass (C), the index of orientation (D) and the preferred orientation of collagen (E) at 0.25mm intervals across an 8.0mm button taken from the same right cornea. Due to variations in the amount of aligned collagen across the sample the polar plots have been scaled down by factors of 1.5 and 1 and coloured red and orange respectively. The region of highest dioptric power is highlighted by a blue dashed line. (Sample K12 – tissue frozen at -80°C).

K13 (8.5mm button from a severe right keratoconus cornea with minimal scarring)

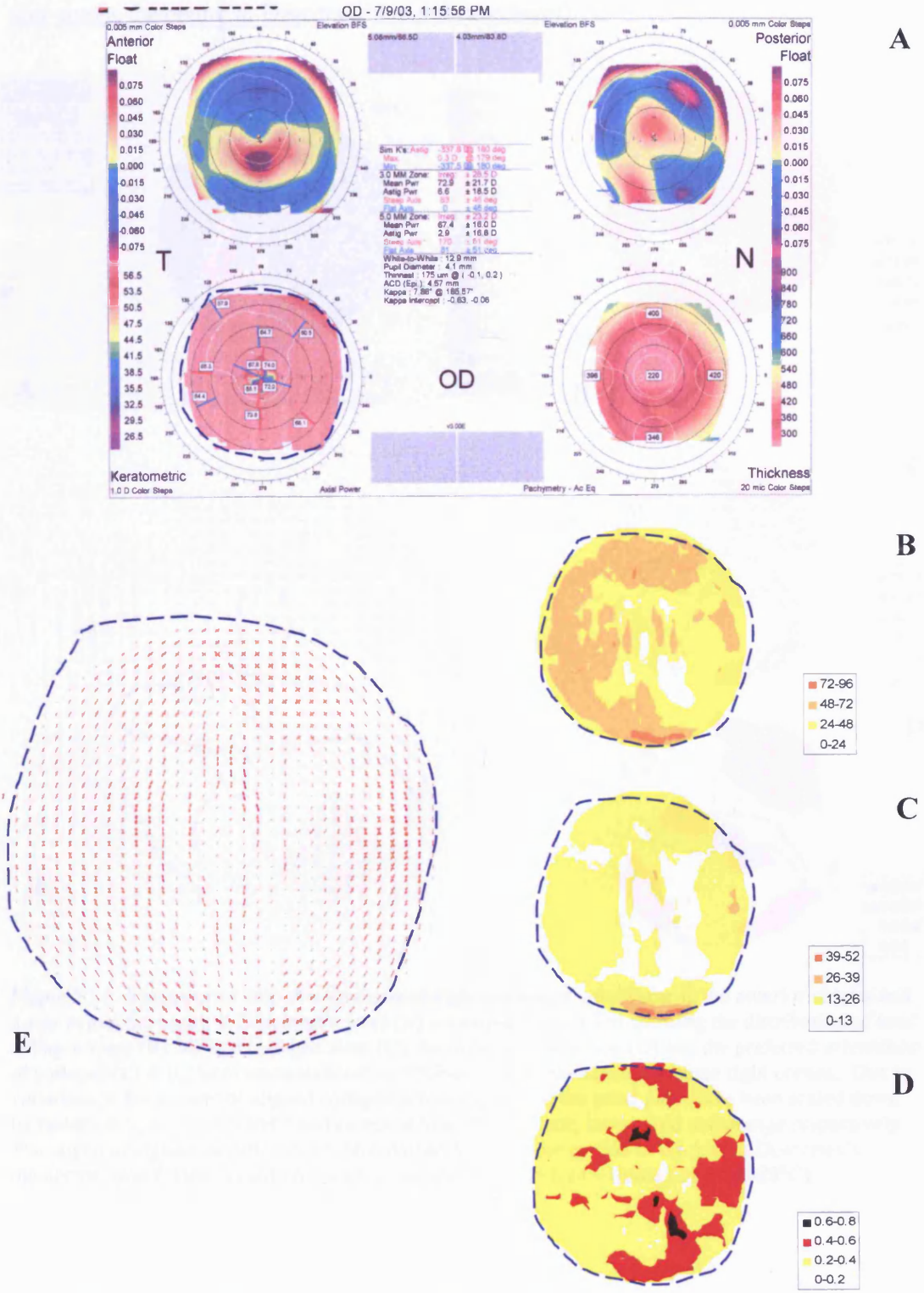

Figure 5.20. Keratometry map of a severe keratoconus right eye with minimal corneal scarring (A) accompanied by maps showing the distribution of total collagen mass (B), aligned collagen mass (C), the index of orientation (D) and the preferred orientation of collagen (E) at 0.25mm intervals across an 8.5mm button taken from the same right cornea. Due to variations in the amount of aligned collagen across the sample the polar plots (E) have been scaled down by factors of 3, 2, 1.5 and 1 and coloured black, brown, red and orange respectively. The region of highest dioptric power is highlighted by a blue dashed line. (Sample K13 – tissue frozen at -80°C).

K14 (right 7.75mm keratoconus button with splash scar in the anterior stroma and a scar across the centre at Descemet's membrane level)

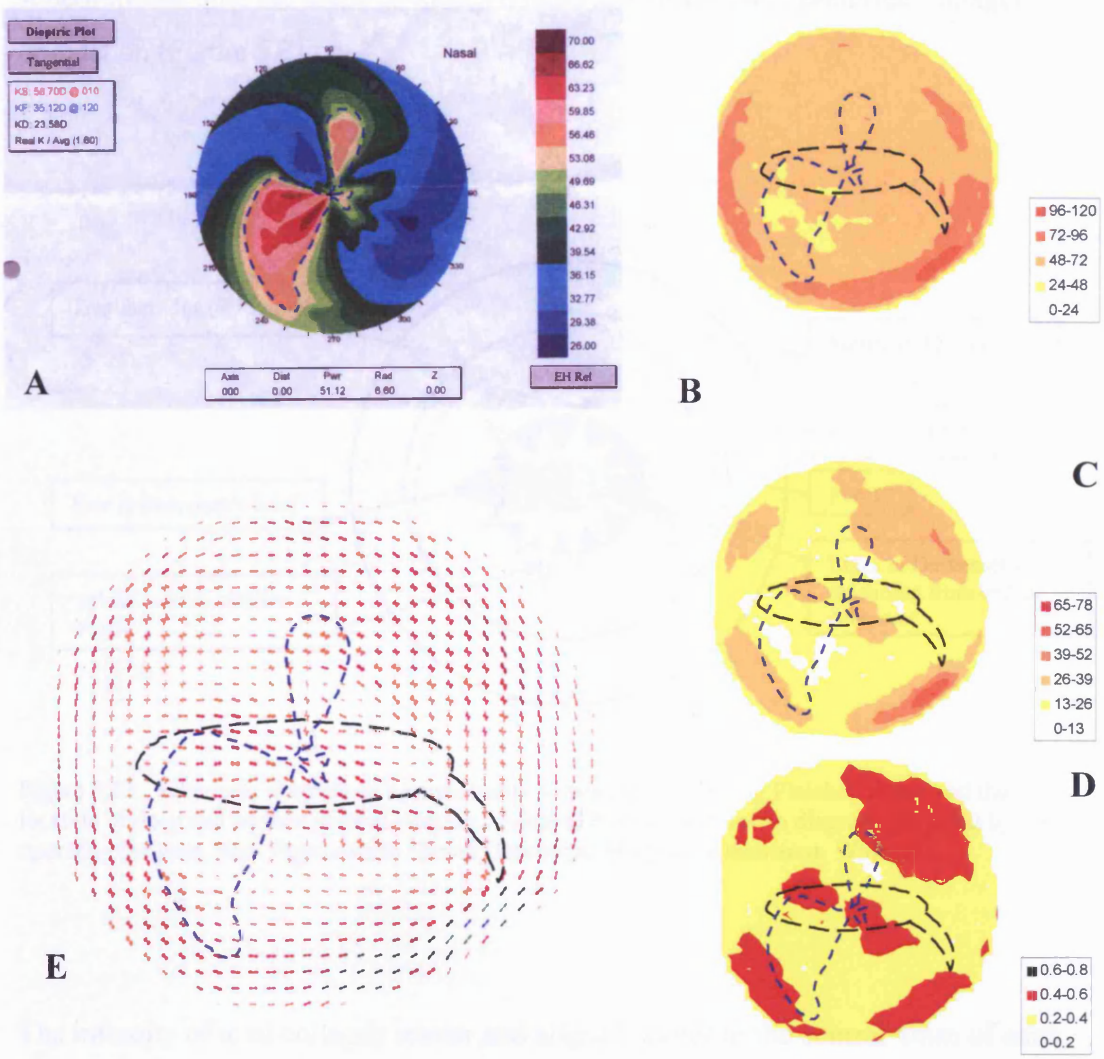

Figure 5.21. Keratometry map of a keratoconus right eye with a splash scar in the anterior stroma and a scar across the centre at Descemet's level (A) accompanied by maps showing the distribution of total collagen mass (B), aligned collagen mass (C), the index of orientation (D) and the preferred orientation of collagen (E) at 0.25mm intervals across a 7.75mm button taken from the same right cornea. Due to variations in the amount of aligned collagen across the sample the polar plots have been scaled down by factors of 5, 4, 3, 2, 1.5 and 1 and coloured blue, green, black, brown, red and orange respectively. The region of highest dioptric power (blue dashed line) and the outline of the scar at Descemet's membrane level (black dashed line) are highlighted. (Sample K14 – tissue frozen at -80°C).

Figure 5.22 schematically shows the location of the various scars in keratoconus button K14. An outline of the scar and lines in Descemet's membrane were superimposed onto the maps of collagen mass distribution and preferred collagen orientation (Figure 5.21).

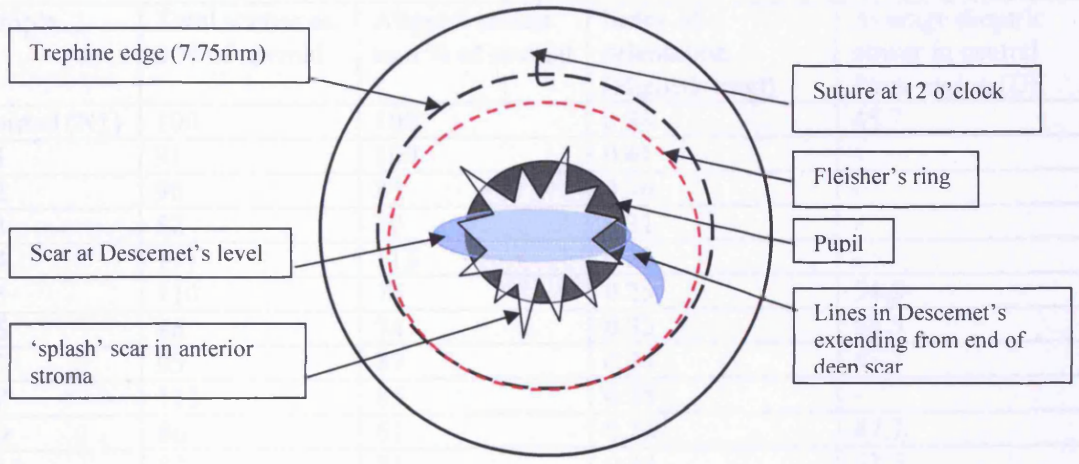

Figure 5.22. Schematic diagram of a keratoconus cornea (K14) showing Fleisher's ring and the location of deep and surface corneal scarring. Adapted from a hand drawn diagram provided by the operating surgeon, Nick Hawksworth (Royal Glamorgan Hospital, Llantrisant, Wales).

The intensity of total collagen scatter and aligned scatter in the central 4mm of each of the keratoconus corneal buttons (K1-14) was calculated and shown in Table 8 as a percentage of the scatter from the same sized region of a normal right cornea (sample N1). Due to variations between samples in terms of the step size used for data collection (0.4mm intervals for the normal cornea and 0.5 or 0.25mm intervals for the keratoconus corneal buttons), it was necessary for comparison purposes to scale the intensity values to account for this. The scatter intensity is scaled up by a factor of 4 for buttons mapped at a 0.5mm resolution, by 2.56 for a 0.4mm resolution and by 1 for a 0.25mm resolution. The index of orientation in the central 4mm of each button and the average dioptric power in the central 5mm of the cornea (where available) are also shown in Table 8. One must be cautious however when drawing conclusions from the results, as it must be remembered that a large variation in scatter intensities was found to exist between the three normal corneas (N1, N2 and N3) presented in

Section 5.3.1. The total collagen scatter in the central 4mm region of samples N2 and N3 was 83% and 152% respectively of the scatter in the same region of N1. Likewise, with respect to N1, the aligned scatter ranged from 74% in N3 to 132% N2 in the central 4mm region. The normal variation in the scatter intensities between the three corneas was however likely exaggerated by the presence of a fold in sample N2.

Sample	Total scatter as a % of normal	Aligned scatter as a % of normal	Index of orientation (aligned: total)	Average dioptric power in central 5mm region (D)
Normal (N1)	100	100	0.38	45.7
K1	91	100	0.41	-
K2	90	89	0.36	-
K3	82	70	0.31	-
K4	171	113	0.23	-
K5	110	75	0.25	54.5
K6	86	74	0.33	54.5
K7	95	87	0.34	53.7
K8	113	85	0.28	-
K9	86	61	0.26	47.7
K10	87	81	0.34	51.5
K11	80	69	0.32	56.7
K12	87	70	0.29	54.5
K13	76	69	0.34	67.4
K14	108	111	0.35	-

Table 8. Calculated values of the total and aligned collagen scatter in the central 4mm region (as a percentage of the scatter from the same region in a normal cornea) and the index of orientation in the same region of the normal and 14 keratoconus corneas. Where data was available, the average dioptric power in the central 5mm of the cornea has also been shown.

In the majority of the scarred and the unscarred keratoconus buttons (4/5 and 6/9 respectively) a lower than normal total collagen mass was observed in the central 4mm; this was to be expected as stromal thinning is characteristic of the disease. On average the aligned collagen mass was lower in the central 4mm of the scarred keratoconus corneal buttons (80% of the normal aligned collagen mass) than in the unscarred buttons (87% of normal aligned collagen mass). In the central 4mm region the index of orientation was on average 5% lower than normal in the scarred keratoconus buttons (ranging from -3% to -9%) and 7% lower than normal in the unscarred buttons (ranging from -15% to +3%).

Figure 5.23 shows the relationship between corneal dioptric power and total collagen mass, aligned collagen mass and the index of orientation in the central 4mm of 8 keratoconus corneal buttons (K5, K7, K9-K13) and 1 normal cornea (N1).

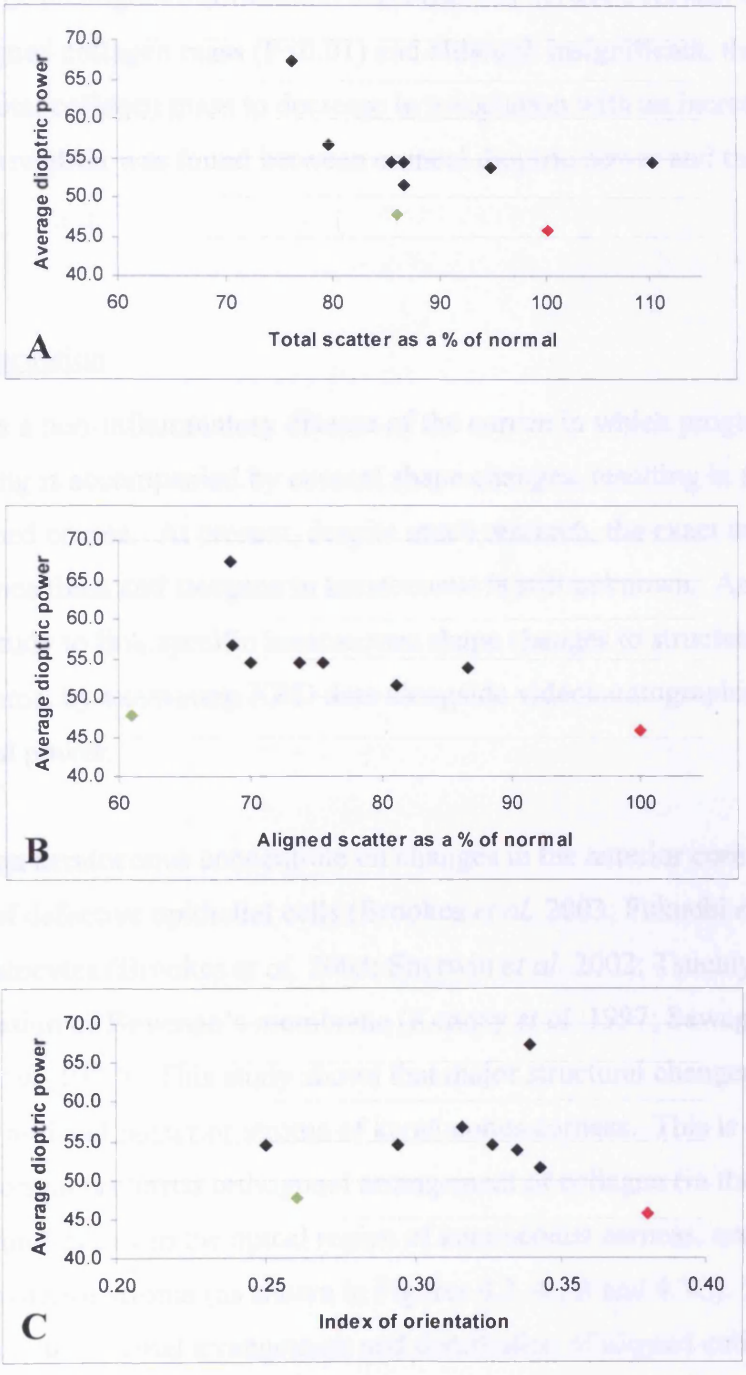

Figure 5.23 Graphs showing the relationship between the average dioptric power in the central 5mm of the cornea and the total collagen scatter (A), aligned collagen scatter (B) and the index of orientation (C) in the central 4mm^2 of 7 keratoconus corneas with no history of hydrops (black diamonds), 1 keratoconus cornea with a history of hydrops (green diamond) and 1 normal cornea (red diamond). All scatter values are shown as a percentage of the scatter from a normal cornea.

A statistical analysis (Pearson's r correlation) was performed to examine the relationship between collagen mass and dioptric power in the central region of the keratoconus corneas (Appendix 2.1). Data from sample K9 was omitted from the analysis due to the fact that it was the only cornea with a history of corneal hydrops. A highly significant negative correlation was observed between corneal dioptric power and aligned collagen mass ($P<0.01$) and although insignificant, there was a tendency for total collagen mass to decrease in association with an increase in dioptric power. No correlation was found between corneal dioptric power and the index of orientation.

5.6 Part B: Discussion

Keratoconus is a non-inflammatory disease of the cornea in which progressive stromal thinning is accompanied by corneal shape changes, resulting in the formation of a cone-shaped cornea. At present, despite much research, the exact mechanism by which the cornea thins and steepens in keratoconus is still unknown. An attempt was made in this study to link specific keratoconus shape changes to structural alterations within the stroma, by examining XRD data alongside videokeratographic images of surface corneal power.

Most studies on keratoconus concentrate on changes in the anterior cornea, such as the presence of defective epithelial cells (Brookes *et al.* 2003; Fukuchi *et al.* 1994), abnormal keratocytes (Brookes *et al.* 2003; Sherwin *et al.* 2002; Tsuchiya *et al.* 1986) and the fibrillation of Bowman's membrane (Kenney *et al.* 1997; Sawaguchi *et al.* 1998; Tuori *et al.* 1997). This study shows that major structural changes are also present in the mid and posterior stroma of keratoconus corneas. This is evident by the fact that the normal preferred orthogonal arrangement of collagen (in the SI and NT directions), which is lost in the apical region of keratoconus corneas, occurs mostly in the mid and posterior stroma (as shown in Figures 4.2, 4.3B and 4.3C). The extent of the disruption to the normal arrangement and distribution of aligned collagen mass varied greatly between keratoconus buttons, with some showing changes solely within the apical region (defined in this study as the region of highest dioptric power) (eg. Figure 5.15) and others exhibiting changes throughout both the apical and para-apical regions (eg. Figure 5.13). This finding is in agreement with previous XRD and

electron microscopical studies of keratoconus corneas (Daxer and Fratzl 1997; Krachmer *et al.* 1984; Meek *et al.* 2005b; Radner *et al.* 1998b; Sawaguchi *et al.* 1998). The abnormal preferred orientation of collagen in keratoconus corneas may reduce the ability of the cornea to resist the stress exerted by the extraocular muscles and also its ability to maintain a normal curvature.

In order to understand the mechanisms by which these changes in collagen orientation and mass distribution might occur in keratoconus corneas, it is necessary to first consider how the shape of the normal cornea is maintained. The insertion of some anterior lamellae into Bowman's membrane (Bron 2001; Muller *et al.* 2001) and the interlacing and bifurcating of lamellae in the anterior stroma (and to a lesser degree in the mid and posterior stroma) (Radner and Mallinger 2002; Radner *et al.* 1998a) are all believed to play a vital role in maintaining the shape and biomechanical stability of the cornea. The structure is further stabilised by the interaction between collagen fibrils and other matrix proteins, such as proteoglycans (Meek *et al.* 1986; Scott and Haigh 1985a), dermatopontin (Nieduszynski *et al.* 2004) and collagen types VI (Hirano *et al.* 1989; Myint *et al.* 1996) and XII (Cheng *et al.* 2003). In addition to these factors, the interlacing of lamellae and the bifurcation and fusion between individual lamellae (Radner and Mallinger 2002; Radner *et al.* 1998a) also help to maintain lamellae in a 'fixed' position relative to each other. It has also recently been suggested that the increase in the proportion of aligned collagen in the four quadrants of the peripheral cornea (Figures 5.1 G and H), which is likely due to additional collagen entering and leaving the peripheral region without going through the prepupillary cornea, may also play a role in maintaining correct cornea curvature (Aghamohamadzadeh *et al.* 2004). Bearing in mind the requirements for the maintenance of corneal stability and shape, it is interesting to note reports on the subject of keratoconus of localised fibrillation (adjacent to the apex of the cone) in Bowman's layer (Kenney *et al.* 1997), a reduction in the number of collagen lamellae (Takahashi *et al.* 1990) and also in the amount by which they interlace (Radner *et al.* 1998b). Based on calculations of ocular rigidity in normal and keratoconus eyes, Edmund (1988a) concluded that the elastic properties of collagen fibres and corneal matrix are altered in keratoconus corneas suggesting a reduction in inter-lamellar adhesion and a decreased resistance to sliding. In the present study a loss of collagen mass, a redistribution of the remaining collagen and gross changes in collagen

orientation were seen in most of the keratoconus buttons. The results provide compelling evidence that the corneal shape change associated with keratoconus coincides with a release of lamellae from their normal 'fixed' position, thus enabling them to slide past one another with greater ease.

Enzymatic digestion of collagen is thought to be at play in keratoconus corneas and may help to explain the process by which lamellae are released from their positions relative to each other. Abnormal keratocytes that are dissociated from their usual interconnected system and have higher than normal levels of Cathepsin B and G (Brookes *et al.* 2003; Sherwin *et al.* 2002) and four times as many interleukin-1 receptors than normal have been found in keratoconus corneas (Kim *et al.* 1999). One theory is that these abnormal keratocytes, which are present in the deep stroma and in localised regions of Bowman's layer (in close proximity to nerve cells), are either activated by nerve cells in response to excessive eye rubbing or undergo imperfect apoptosis (both of which are triggered by interleukin-1). Irrespective of the cause, the resultant release of Cathepsin B and G from the abnormal keratocytes may be responsible for the localised damage to Bowman's membrane and the degradation or modification of proteoglycans and type VI collagen in keratoconus corneas (Brookes *et al.* 2003). There is further electron microscopy evidence to suggest that Type I collagen also undergoes some enzymatic degradation within the apical region and that within the same region there is a reduction in the amount of lamellar interlacing (Radner *et al.* 1998b). Some authors believe, based on the up-regulation of enzymes in keratoconus corneas, that the development of keratoconus is primarily caused by an enzymatic degradation of corneal tissue (Kenney and Brown 2003; Sawaguchi *et al.* 1989; Stachs *et al.* 2004). An alternative theory is that the stromal thinning associated with the disease is not due to a loss of collagen mass but due to a redistribution of collagen mass, possibly to a location outside the button region (Polack 1976). In support of this, calculations of cross-sectional area in normal and keratoconus corneas revealed no difference between the two (Edmund 1988b). The two theories of keratoconus progression are not mutually exclusive, since enzymatic degradation could allow slippage between collagen fibrils.

The results presented in this study indicate that stromal thinning in keratoconus corneas is caused by a combined loss of collagen with the central 6-8mm button

region and a redistribution of the remaining collagen. By means of a localised enzymatic degradation and/or a modification of stromal components, collagen lamellae that pass through the apical region (where enzymatic digestion is most apparent) may be released from their normal fixed position relative to each other and therefore be free to slide over one another. In this way a certain amount of 'slack' may be created along some lamellae that previously had many bifurcations and followed an indirect course across the cornea, so enabling them to follow an alternate route. In this way, the effective length of the lamellae would increase and their tension decrease, thereby facilitating the tissue deformation associated with the disease. Further possibilities may be that 'slack' is created in the posterior stroma by the release of lamellae from their peripheral location at the limbus or by an unravelling of fibrils from the limbus. In the anterior stoma additional 'slack' may be created by the disinsertion of lamellae from Bowman's membrane (Meek *et al.* 2005b – Appendix 9). A mechanism such as described here is consistent with the fact that Vogt's of Striae can be made to disappear by applying pressure to the globe, thus indicating that in keratoconus corneas some of the posterior lamellae are not under tension (Bron 1988). A situation can easily be envisaged whereby the weakened apical region, in which at least some of the lamellae have been released from their tension, may be pushed outwards by intraocular pressure so causing the cornea to become cone shaped. As the cornea is forced outwards, some of the lamellae previously located within the apical region may be forced to follow an alternate course around the protrusion (shown schematically in Figure 5.24); this would be facilitated by the 'slack' created in the lamellae. This suggested mechanism provides a possible explanation for the observed redistribution of collagen mass and the swirling effect of aligned collagen around the apex of the cone and around regions of reduced aligned collagen mass (eg. Figure 5.14F). The swirling effect of 'surface' collagen fibrils around the apex of the cone has been previously shown by scanning electron microscopy (Figure 5.25) (Radner *et al.* 1998b).

Normal cornea (N1)

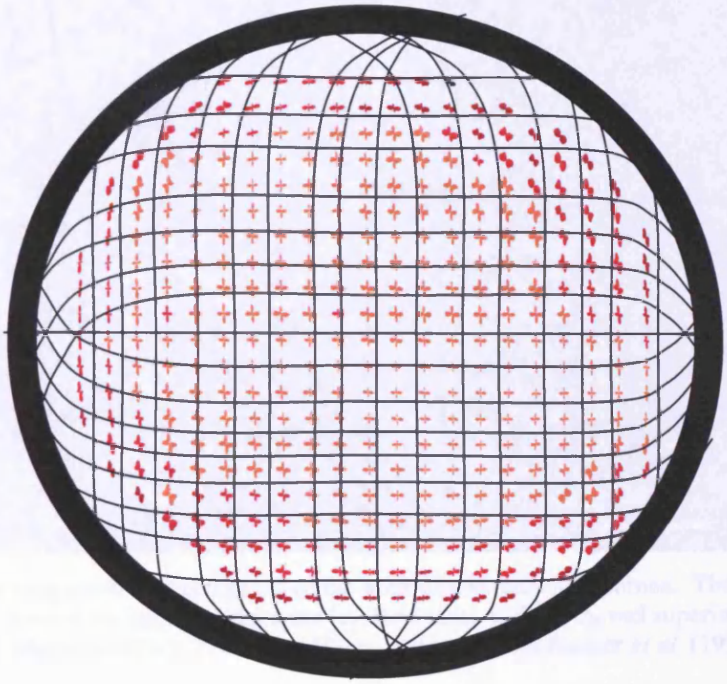

Keratoconus cornea (K7)

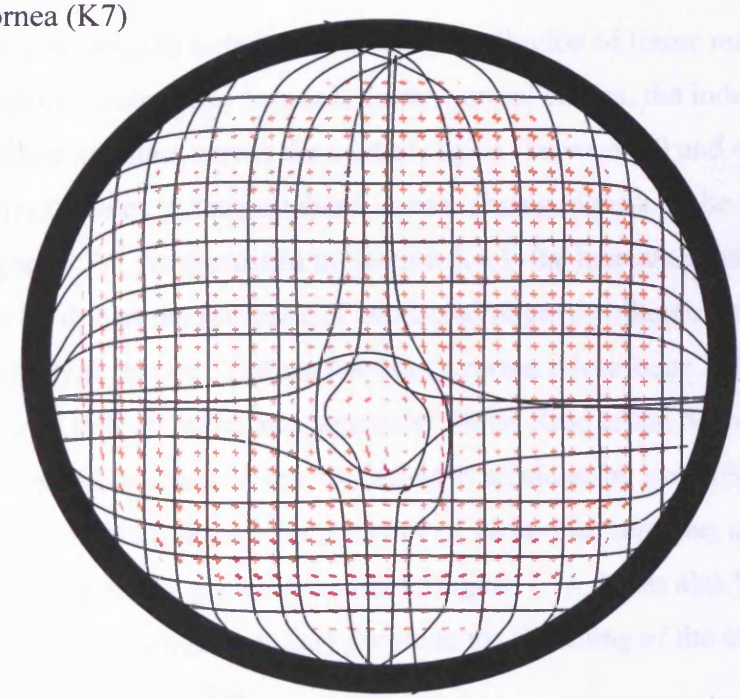

Figure 5.24. A schematic diagram of the preferred orientation of collagen fibrils in a normal (N1) and keratoconus cornea (K7).

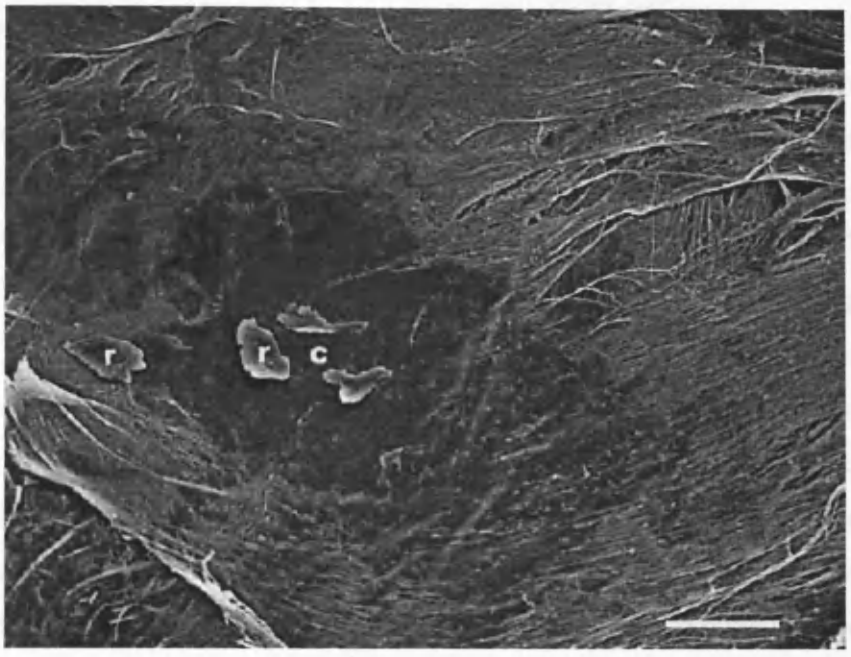

Figure 5.25. A scanning electron micrograph of the apex of a keratoconus cornea. The collagen fibrils run approximately around the centre of the apex (c). Remnants of the removed superimposed lamellae are highlighted (r). Magnification x 270, bar = 50μm. Adapted from Radner *et al.* (1998b).

A further interesting point to note is the unusual distribution of tissue mass in the peripheral region of keratoconus corneas. In the normal cornea, the index of orientation which is constant across the central region (between 20 and 40% collagen alignment) nearly doubles in the peripheral cornea (being highest in the SN and IT quadrants) (Figure 5.7). As discussed in Section 5.4.1, the increased index of orientation may be due to the presence of additional aligned collagen lamellae which traverse the peripheral cornea. The results from a recent microfocus XRD study showed an increase in both radial and tangential fibrils close to the limbus (Meek and Boote 2004). The authors believe that this effect is achieved by a combined bending of lamellae prior to the limbus and the presence of additional lamellae, anchored in the sclera which traverse the peripheral cornea (Figure 1.7). It has also been suggested that such an arrangement may facilitate the flattening of the cornea near its periphery (Meek and Boote 2004).

If the increase in the index of orientation in the four quadrants of the peripheral cornea plays a role in maintaining the correct curvature of the cornea, then one would expect the arrangement of collagen in this region of keratoconus corneas to be altered.

This proved to be true in 8/9 unscarred keratoconus buttons (eg. Figure 5.12) and in 2/5 of the scarred buttons (eg. Figure 5.20). Sample K2 which had a large, round, centrally located cone showed an equal increase in the index of orientation in all four of the quadrants, possible due to the fact that a round cone exerts a similar in stress in all directions. In the case of K1 which had a smaller, oval, inferior-temporally located cone, the increase in the index of orientation was more pronounced than normal in the SN and IT quadrants suggesting an increase in stress in these areas. In the majority of keratoconus corneas examined there appeared to be a loose relationship between the preferred orientation, the distribution of collagen mass and the shape of the cone (as determined by the outline of the region of highest dioptric power). As the region of highest dioptric power was used to estimate the shape of the cone in each case, differences in accuracy between different videokeratography systems may be partially to blame for the lack of consistency between samples in terms of the relationship between structural changes and corneal shape. It is unclear from this study whether the shape of the cone is determined by the nature of the structural changes or whether the shape of the cone is predetermined and causes the structural changes to occur.

In the majority of the scarred and unscarred keratoconus buttons (4/5 and 6/9 respectively) a lower than normal total collagen mass was observed in the central 4mm region of the cornea (Table 8). This was to be expected as stromal thinning is characteristic of the disease. Although the central 4mm region was studied in each cornea for comparison purposes, the overall loss of collagen in some of the keratoconus samples is likely to be underestimated due to the fact that the apical region is not always in the centre of the button. It must also be remembered that only a small number of normal corneas were examined in this study (due to the large amount of synchrotron x-ray beam time required to produce a single map) and that a large variation in collagen mass was observed between individual corneas. The apparent variation between normal corneas was likely exaggerated by the presence of folds.

In the 10 keratoconus buttons that showed a decrease in collagen mass in the central 4mm region, the mass also appeared to be lower throughout the remainder of the button. One must be cautious however, when concluding that a loss of tissue mass from a keratoconus corneal button of between 6-8mm is representative of the entire

cornea as the possibility remains that tissue may be redistributed from the apical region to an alternate location outside the button region by means of a translation or a realignment of collagen lamellae. Although insignificant, there was a tendency for total collagen mass to decrease as dioptric power increased (Figure 5.23A). A highly significant negative correlation was however observed between aligned collagen mass and dioptric power in keratoconus corneas (Figure 5.23B).

Cornea K9 was an anomaly in terms of the relationship between collagen mass and dioptric power; this may be due to the fact that it had a history of corneal hydrops (15 months previously). Although clinical information regarding the presence or absence of residual oedema after hydrops was unavailable, high pachymetry readings were recorded for sample K9 (Figure 5.16), indicating that the cornea was thicker than normal; however the total collagen scattering was lower than that of the normal cornea (by 14%). Although the results indicate that the increased thickness was not due to an increase in collagen mass but due to the cornea being swollen, one must be cautious when interpreting the data from such a sample, as the intensity of x-ray scatter is only proportional to the mass of the cornea if it is not very swollen or very dry. Although a recent XRD investigation of corneas left to swell freely for one hour in distilled water revealed no significant changes in the preferred orientation of collagen or the distribution of total and aligned collagen mass (Meek *et al.* 2005a), it is unknown what effects prolonged corneal swelling *in vivo* (with the presence of intraocular pressure) has on collagen orientation and mass distribution.

It seems likely that in keratoconus corneas the abnormalities in preferred collagen orientation are related to changes in the directions of stress within the cornea and these changes are themselves associated with the precise shape of the individual cornea. Variations between keratoconus corneas in terms of the shape, size and position of the cone may be responsible for the differences seen between samples in terms of the amount of lamellar disruption and re-alignment. However, in this study it was not possible the form a direct link between the size and shape of the cone and the extent and manner of the structural changes observed within the cornea. It must be acknowledged, that irrespective of the original cause of thinning in keratoconus the structural changes observed in this study and by others, would further accelerate the

progression of the disease as the biomechanical stability of the cornea is compromised.

Unfortunately it is also impossible to deduce at what stage in the progression of the disease these stromal changes occur due to the fact that a clinical grading system of keratoconus severity (other than general observations of the presence or absence of corneal scarring) was not employed in this study. In addition, very little is known about the sequence of events that lead to the structural changes associated with advanced keratoconus due to the fact that keratoconus corneas only become available for research after the need for penetrating keratoplasty.

A further problem associated with this study is that the videokeratography images of keratoconus corneal buttons were performed *in vivo*, however the XRD data was recorded for the same corneal buttons after their removal from the eye ball and therefore without the influence of intraocular pressure. As previous XRD studies have found no change in the preferred orientation of collagen and the distribution of tissue mass between corneas examined with or without a scleral rim, it has been assumed for the purposes of this study that the same is true of keratoconus corneal buttons. There is however a clear need for the construction of a sample holder in which the natural shape of the cornea can be maintained during XRD data collection.

5.7 General conclusions from Parts A and B

This study has confirmed many previous findings about the preferred orientation and distribution of collagen mass in the cornea; however, for the first time a right/left eye symmetry of aligned collagen mass distribution has been reported. The observed symmetry between right and left corneas may have important surgical implications and warrants further investigation.

This study has also shown that in keratoconus corneal buttons a change in preferred collagen orientation is accompanied by changes in collagen mass distribution. Total collagen mass in the central 4mm of the majority of the keratoconus buttons examined was lower than normal, thereby indicating a loss of collagen mass. However, outside this region, an abnormal distribution of collagen mass was observed, providing

evidence to support a redistribution of collagen mass in keratoconus corneas. The abnormal orientation and distribution of collagen mass in keratoconus corneas is indicative of a process of lamella slippage, which is possibly facilitated by some local enzymatic breakdown of collagen and extra-fibrillar material. In the majority of cases the index of orientation in the peripheral region of the keratoconus corneas also differed from that of the normal cornea, indicating that the normal reinforcement of collagen in the four quadrants of the normal cornea plays a role in maintaining the shape and stability of the cornea.

Irrespective of the original cause of stromal thinning in keratoconus, the altered organisation of collagen in the corneal stroma of affected corneas probably accelerates the progression of the disease.

5.8 Future Study

- In order to assess the relationship between preferred collagen orientation and corneal shape it would be interesting to study the amount of collagen fibrils lying in the SI and NT directions in a range of normal corneas with known levels of astigmatism.

- It is necessary to construct a sample holder in which the *in vivo* shape of the excised cornea may be maintained. A suggested design would be an airtight holder into which the cornea may be clamped in place with silicon oil filling a chamber behind it to maintain its curvature.

- To test the benefits of maintaining correct corneal orientation and right/left eye symmetry between donor and recipient in corneal transplant surgery, a series of clinical trials would be needed. In addition to this, it would be of interest to examine the effects of incisions at various angles with respect to the preferred orientation of collagen within the cornea.

- A high-angle XRD investigation of changes in keratoconus corneal structure at different tissue depths may shed more light on the mechanism by which the disease progresses.

- A low-angle XRD study of collagen interfibrillar spacing and fibril diameter across keratoconus corneas would also be of interest and may further aid understanding of the disease.

Chapter 6. A study of corneal ultrastructure in normal mice and in mice with a murine specific keratopathy

6.1 Introduction

Our understanding of corneal dystrophies can often be enhanced by the use of animal models. However, apart from one case report of keratoconus in the rhesus monkey (Peiffer *et al.* 1987), the disease has not been found to occur in any other non-human mammal, thereby slowing the progress of keratoconus research. In this study, the corneal ultrastructure of an inbred line of spontaneous mutant mice (named SKC mice), in which the adult males (and females to a much lesser extent) develop a cone shaped cornea (Tachibana *et al.* 2002), was examined in order to assess their use as a research model for the human disease keratoconus. Purchased BALB/c mice corneas were used as a control in the study due to the genetic origins of the SKC mice being part BALB/c.

The inbred line of SKC mice was formed using a male mutant mouse with cone shaped corneas as a progenitor, followed by repeated sib-mating (more than 20 times). The corneas of SKC mice resemble human keratoconus not only in phenotypic appearance but also in the expression of a transcription factor (c-fos) and in the apoptosis of keratocytes (Tachibana *et al.* 2002). Corneal changes in the SKC mice, which are androgen dependent and usually begin at approximately 3 months of age, start with a clouding of the cornea followed by a gradual bulging outwards. Male SKC mice frequently exhibit a thin central cornea, which histopathalogical examination has revealed to be the result of a reduction in stromal thickness; although in some cases the corneas appeared thick due to oedema (Tachibana *et al.* 2002). Figure 6.1A shows the macroscopic appearance of normal and SKC mice eyes and Figure 6.1B shows scanning electron microscopy images of corneas taken from an adult male SKC mouse and an adult male BALB/c mouse. Figures 6.1A and B are shown merely as examples of the two strains of mice and do not relate to specific corneas used in this study, for which no such pictures were recorded.

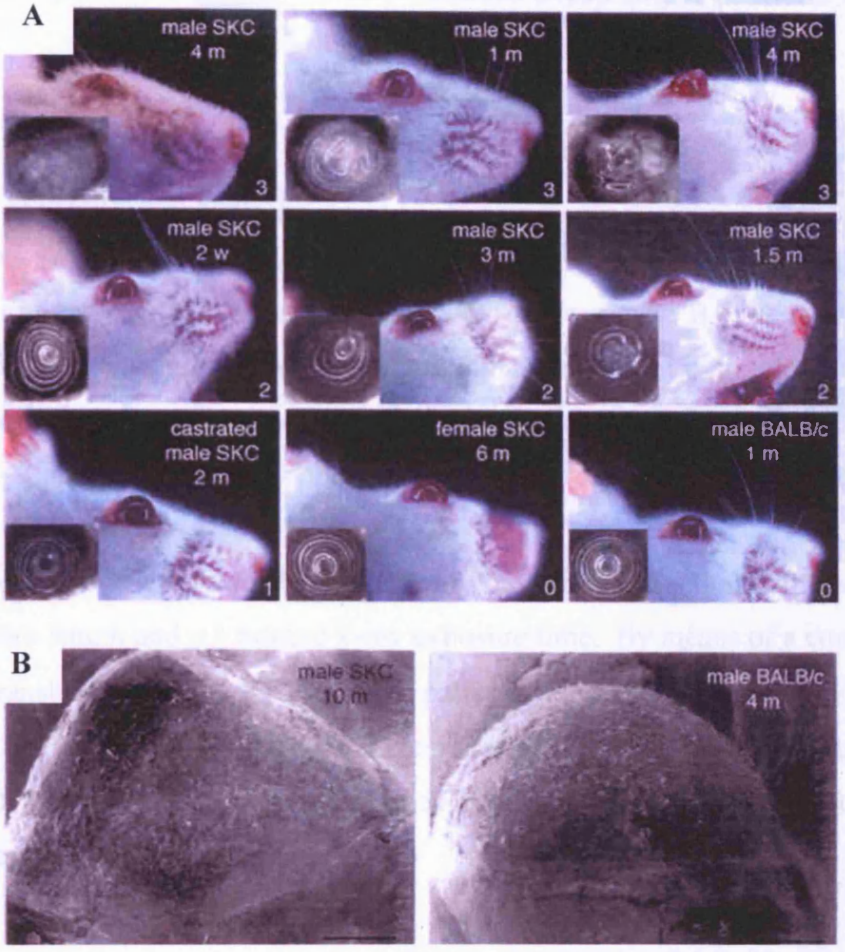

Figure 6.1. Examples of the macroscopic and keratoscopic (inset) appearance of male and female SKC mouse corneas aged between 1 and 6 months (A) and the scanning electron microscopic appearance of a 10 month old male SKC mouse cornea and a 4 month old male BALB/c mouse corneas. Reproduced from Tachibana *et al.* (2002).

6.2 Materials and methods

6.2.1 Sample preparation

The corneas from 3-month old SKC mice (8 male mice showing a keratoconus-like phenotype and 8 female mice) and from eight control BALB/c mice (4 male and 4 female) were developed and supplied by the Department of Ophthalmology at Kyoto Perfectural University of Medicine (Kyoto, Japan) (Tachibana *et al.* 2002). Unfortunately the corneas were not tagged to show their *in vivo* orientation and measurements relating to the severity of the corneal changes in individuals were not available. The corneas were transported frozen in dry ice and immediately transferred

to –80°C storage on arrival. The corneas remained frozen until required for data collection.

6.2.2 Data collection and analysis

In the manner described in Section 2.4.2, a low-angle XRD pattern was obtained from the centre of 6 male SKC corneas, 6 female SKC corneas and 6 BALB/c corneas (3 male and 3 female), using a camera of length 6.25m, a beam of dimensions 0.5x1.0mm and an exposure time of 2 minutes. The data was analysed as described in Section 2.4.3, to produce values for collagen centre-to-centre IFS and fibril diameter.

High-angle XRD images were also collected as described in Section 2.5.1 using a 20cm camera length and a 3 minute x-ray exposure time. By means of a computer operated translation stage, x-ray scattering patterns were recorded at 200μm intervals across the cornea and limbus (along the central axis) of 1 male BALB/c mouse (named A), 1 female BALB/c mouse (named B), 2 female SKC mice (named c and d) and 2 male SKC mice (named e and f).

The data was analysed predominantly as described in Section 2.5.2. However, in this study, due to missing ion chamber readings (which are normally used for data normalisation (Step 1)), it was necessary for the data to be normalised against the XRD pattern from the Mylar window of the sample holder (Figure 6.2).

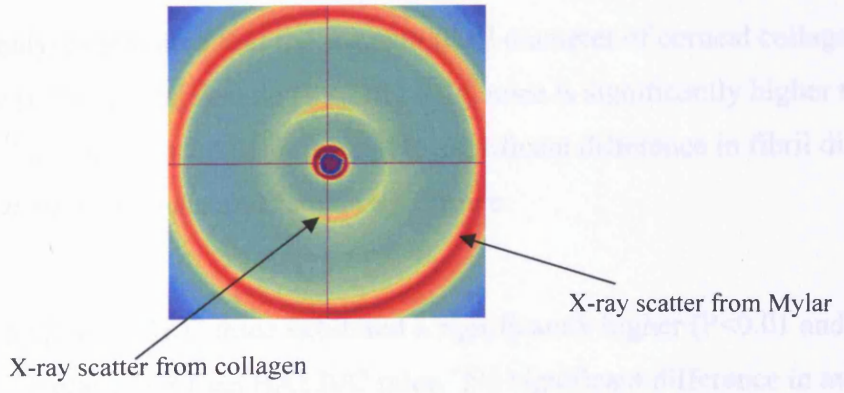

Figure 6.2. A high-angle x-ray pattern from the limbal region of a BALB/c mouse cornea showing the scatter of x-rays from corneal collagen and the Mylar window of the sample holder.

6.2.3 Statistical analysis

Statistical analyses of differences in IFS and fibril diameter between groups was performed using ANOVA (Appendix 3.1). Where ANOVA revealed a significant difference between groups of $p<0.01$, then a post hoc Tukey test was performed to pinpoint between which groups the significance difference exists (Appendix 3.2).

6.3 Results

6.3.1 Interfibrillar spacing and fibril diameter

The average fibril diameter and IFS of 3-month old BALB/c and SKC mice are shown in Table 9. Due to the lack of a gender effect on IFS and fibril diameter in normal BALB/c mice ($P>0.05$), male and female BALB/c mice were grouped for the purpose of this study to act as a control for the SKC mice. The volume fraction of fibrils (VFF) in the stroma was calculated for each group using Equation 7 in Section 3.3.1.

	Fibril diameter (nm) +/- S.E.	Interfibrillar Spacing (nm) +/- S.E.	Volume fraction of fibrils (VFF) +/- S.E.
Normal BALB/c (n = 6)	35.5 [a] +/- 0.3	48.0 [d] +/-1.0	0.38 [g] +/- 0.01
Male SKC (n = 6)	36.9 [b] +/- 0.2	61.8 [e] +/- 3.8	0.25 [h] +/- 0.03
Female SKC (n = 6)	37.0 [c] +/- 0.2	56.8 [f] +/- 1.0	0.29 [i] +/- 0.01

Statistical significance: [ab] ($p<0.01$), [ac] ($p<0.01$), [de] ($p<0.01$), [df] ($p<0.05$), [gh] ($p<0.01$), [gi] ($p<0.05$)

Table 9. Summary of corneal ultrastructure in control BALB/c and SKC mice.

Statistical analyses revealed that the average fibril diameter of corneal collagen fibrils in both male ($P<0.01$) and female ($P<0.01$) SKC mice is significantly higher than the average fibril diameter in BALB/c mice. No significant difference in fibril diameter was observed between male and female SKC mice.

Both male and female SKC mice exhibited a significantly higher ($P<0.01$ and $P<0.05$ respectively) average IFS than BALB/C mice. No significant difference in average IFS was observed between male and female SKC mice, however, the variation in IFS

between corneas (as indicated by the standard error), was far higher in the male SKC group than in any other. The VFF was significantly lower in the BALB/c mice than both the male and female SKC mice ($P<0.01$ and $P<0.05$ respectively), with the male SKC mice showing a three times greater variation in VFF within their group compared to the female SKC mice and the BALB/c mice. There was no significant difference between the male and female SKC mice in terms of VFF.

The average fibril diameter (35.5nm) and the average centre-to-centre IFS for 3-month old BALB/c mice (48.0nm, which corresponds to an interfibrillar Bragg spacing of 42.8nm) are comparable to those previously reported for 6-month old normal mice corneas (Quantock *et al.* 2001).

6.3.2 Index of orientation

To show the changes in the amount of collagen alignment from limbus to limbus, the index of orientation was plotted against distance from the centre of the cornea (Figure 6.3 A-C). The rapid increase in the index of orientation at the limbus (on both sides) of the cornea in the BALB/c mice is consistent with the presence of an annulus of aligned collagen surrounding the normal mouse cornea. Statistical analyses revealed that in 3 out of 4 of the SKC mice studied, (the exception being one male SKC mouse (mouse e)), this arrangement is significantly altered ($P<0.01$).

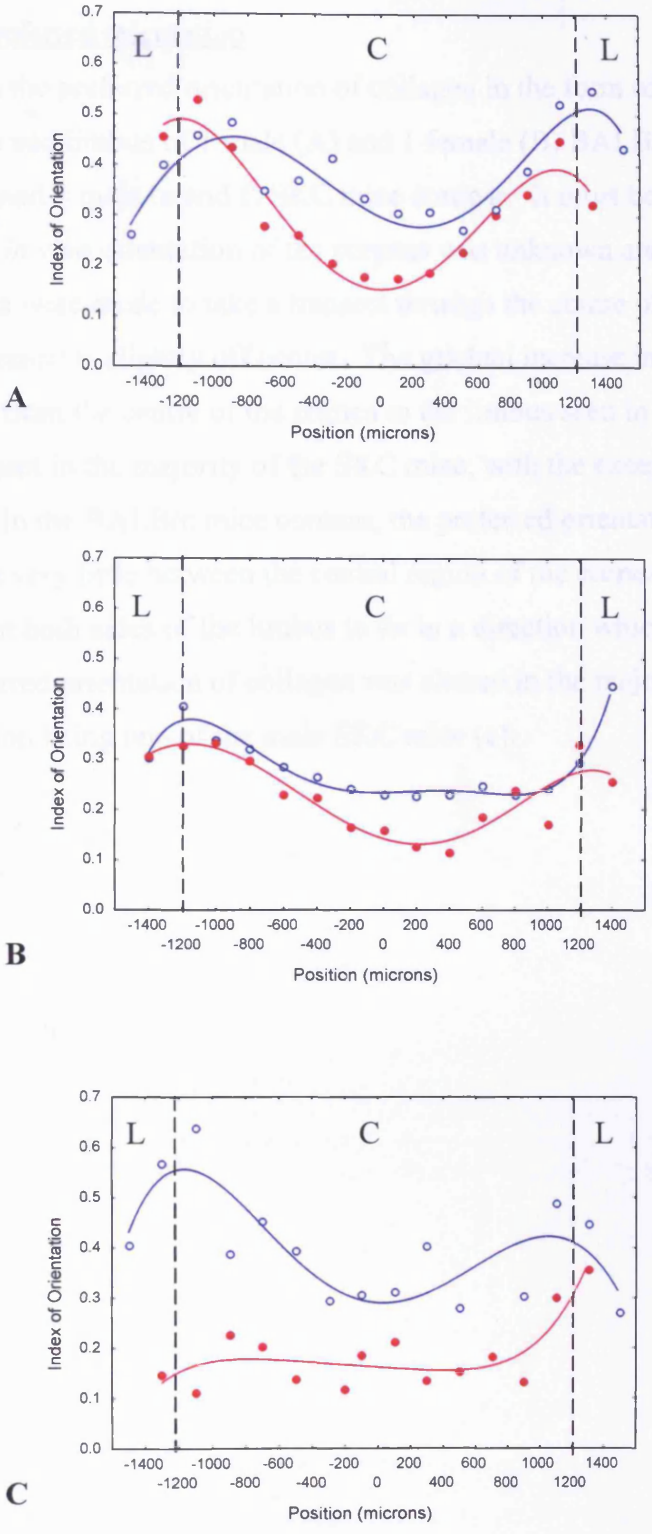

Figure 6.3. Index of orientation across the cornea and limbus of :
(A) 3-month old male (.) and a female (o) BALB/C mouse.
(B) Two 3-month old female SKC mice (mouse c (.) and mouse d (o))
(C) Two 3-month old male SKC mice (mouse e (o) and mouse f (.)).
The approximate position of the cornea (C) and limbus (L) is shown by a black dashed line.

6.3.3 Collagen preferred orientation

Figure 6.4 shows the preferred orientation of collagen in the form of polar plots, across the cornea and limbus of 1 male (A) and 1 female (B) BALB/c mice and 2 female (c and d) and 2 male (e and f) SKC mice corneas. It must be remembered however that the *in vivo* orientation of the corneas was unknown and also that although attempts were made to take a transect through the centre of each cornea, it is likely that the transect is slightly off centre. The gradual increase in the amount of aligned collagen from the centre of the cornea to the limbus seen in the BALB/c mice appears to be absent in the majority of the SKC mice, with the exception of one male SKC mouse (f). In the BALB/c mice corneas, the preferred orientation of the aligned collagen changes very little between the central region of the cornea and the limbus, but does appear at both sides of the limbus to lie in a direction which surrounds the cornea; the preferred orientation of collagen was altered in the majority of the SKC mice, the exception being one of the male SKC mice (e).

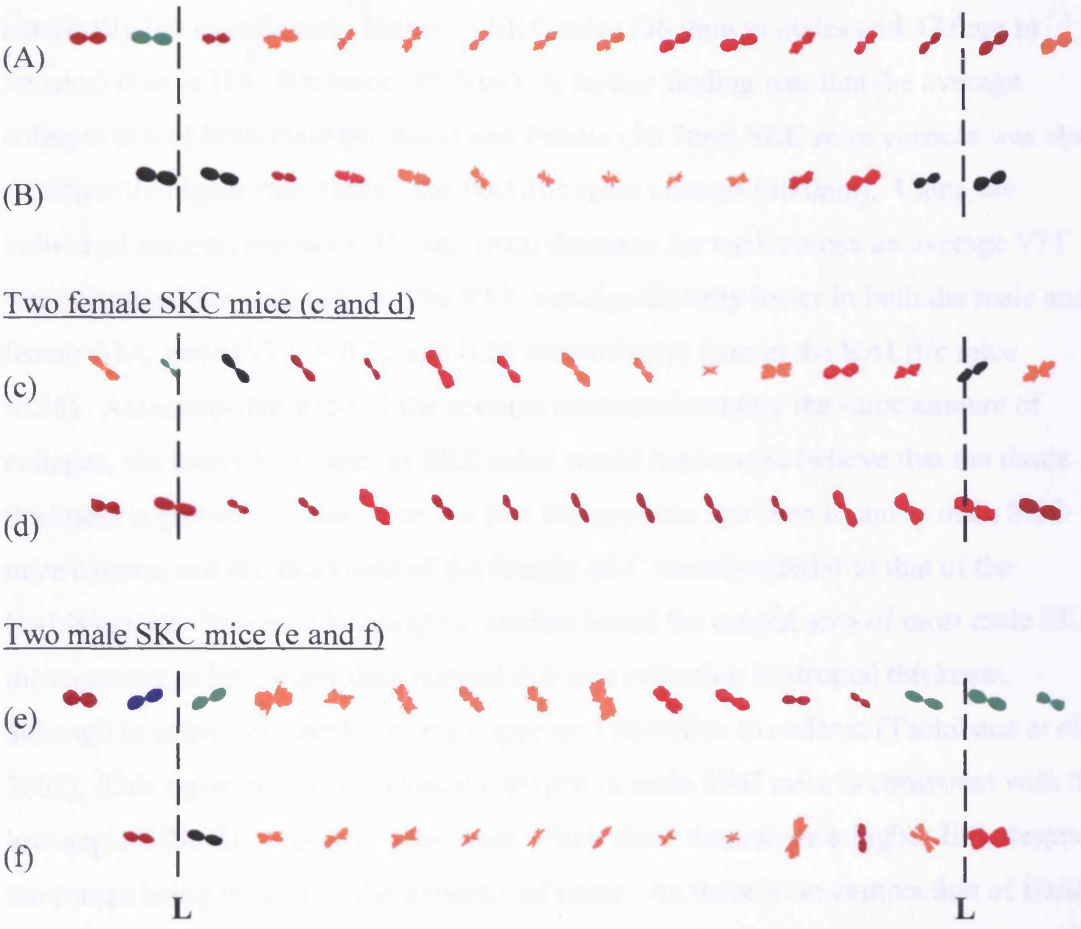

Figure 6.4. Polar plots of collagen preferred orientation across the cornea and limbus of 1 male (A) and 1 female (B) BALB/c mice and 2 female (mouse c and mouse d) and 2 male (mouse e and mouse f) SKC mice corneas. The position of the limbus (L) is highlighted by a black dashed line. The polar plots have been scaled according to scattering intensity, blue polar plots have been scaled down by a factor of 10, green by 8, black by 4, brown by 3, red by 1.5 and orange plots by a factor of 1.

6.4 Discussion

The fine structure of the corneas from an inbred line of mutant mice (SKC), in which the adult males (and very occasionally the females) develop a cone shaped cornea (Tachibana *et al.* 2002), was studied to assess their use as a research model for the human disease keratoconus. The structure of the SKC mice (a strain derived from BALB/c) corneas, as determined by XRD, was compared to that of normal BALB/c mice.

Analysis of the XRD patterns revealed the average collagen fibril diameter to be marginally but significantly higher in SKC mice (36.9nm in males and 37.0nm in females) than in BALB/c mice (35.5nm). A further finding was that the average collagen IFS of both male (61.8nm) and female (56.7nm) SKC mice corneas was also significantly higher than that of the BALB/c mice corneas (48.0nm). Using the individual measurements of IFS and fibril diameter for each cornea an average VFF was calculated for each group. The VFF was significantly lower in both the male and female SKC mice (VFF = 0.25 and 0.29 respectively) than in the BALB/c mice (0.38). Assuming that each of the corneas contained roughly the same amount of collagen, the lower VFF seen in SKC mice would lead one to believe that the tissue thickness is greater in these mice. In fact the opposite has been found in male SKC mice corneas and the thickness of the female SKC mice is similar to that of the BALB/c mice. Previous histological studies found the central area of most male SKC mice corneas to be thinner than normal due to a reduction in stromal thickness, although in some circumstances they appeared thick due to oedema (Tachibana *et al.* 2002). This reported loss of stromal collagen in male SKC mice is consistent with the low-angle XRD findings presented here which show there to be a higher IFS, despite the cornea being thinner in the majority of cases. As there is no compaction of fibrils the corneal thinning must therefore be the result of a loss of fibrillar collagen mass in the central area of male SKC mice corneas. In the case of any oedematous male SKC corneas, one would also expect the IFS to be higher than normal due to the presence of additional water between fibrils forcing them apart. It is also likely therefore that the cloudiness observed in some of the affected SKC corneas (Tachibana *et al.* 2002) may be attributed to a breakdown of the fibrillar array, in the form of an increase in both IFS and fibril diameter. The highly sensitive relationship between IFS and hydration provides a further explanation for the high variability of IFS values (ranging from 52.4nm to 79.3nm) and calculated VFF values (ranging from 0.15 to 0.35) seen within the group of male SKC corneas, as the severity of individual cases may have ranged from slightly affected to severely affected in terms of corneal clarity and shape changes. Unfortunately measurements of the severity of corneal changes for the individuals studied in this investigation were unavailable. As VFF is positively correlated with tissue tensile strength, it is not surprising that the male SKC mice had

the lowest VFF. The progression of the keratopathy is likely enhanced by the weakening of the tissue.

Female SKC mice which rarely show changes in corneal shape or clarity, did not differ significantly from male SKC mice in terms of IFS, fibril diameter or VFF, although a non-significant trend was apparent for SKC females to have a lower IFS and a higher VFF than their male counterparts. The IFS of female SKC mice was however significantly higher than that of the BALB/c mice and the VFF was significantly lower. In contrast to male SKC mice, histopathological examination revealed no difference in corneal thickness between female SKC mice and BALB/c mice (Tachibana *et al.* 2002) and so the increase in IFS and decrease in VFF may not be attributed to a loss of collagen. It is likely therefore that the difference between the female SKC mice and the BALB/c mice is due solely to differences in corneal hydration. As corneal clouding was not a reported feature of the SKC females used in this study, the difference in hydration is less likely to be due to an increased corneal hydration in the SKC females but is more likely due to some dehydration of the BALB/c mice corneas. As all of the samples were prepared in the same manner, differences between the two strains in terms of the rate of tissue dehydration may be responsible, caused for example by differences in proteoglycan composition. The levels of the various proteoglycans in BALB/c and SKC mice has not been investigated to date. An alternative explanation is that if the female SKC mice corneas were of a slightly higher hydration than the BALB/c mice and that the resulting structural alterations caused by the higher water content (increased IFS and fibril diameter), were not sufficient to significantly affect corneal transparency.

This study has highlighted the difficulties involved in examining the structure of mice corneas by means of low-angle XRD. During the preparation of the mice corneas for XRD, the potential for tissue dehydration is high due to their small size. Any variation in the time taken to dissect individual corneas, prior to them being wrapped in clingfilm and frozen, may affect the amount of surface evaporation that occurs from each cornea during the preparation process. As IFS is highly sensitive to tissue hydration, the potential error associated with the technique for determining the precise *in vivo* structure of mice corneas must be considered when examining the results. In

the present study the hydration of samples was not measured and so the results must be treated with some caution. A further problem lies in the size of the low-angle beam in relation to the size of the mouse cornea (1mm width beam and a 2.5-3mm cornea). The study detailed in Chapter 3, showed that in both the human and monkey cornea there is a sharp increase in both fibril diameter and IFS at the limbus; if this is also assumed to occur in the mouse cornea, then any error associated with the positioning of the cornea in the desired location to ensure that the beam passes through its centre, may also result in a large variation in IFS and fibril diameter between samples.

Bearing in mind the potential for some non- *in vivo* variation between samples as a result of the technique itself, this study has revealed that differences exist between the structure of affected SKC mice corneas and that of human keratoconus corneas. Previous XRD studies have shown there to be no difference between normal and keratoconus corneas in terms of IFS and fibril diameter (Daxer and Fratzl 1997; Fullwood *et al.* 1992). In human corneas the absence of any fibril compaction proves that the corneal thinning associated with keratoconus must be due to a loss of stromal collagen mass; in affected SKC mice the increase in IFS also suggests that the central corneal thinning must be due to a loss of stromal collagen, however it is clear from the results that differences exist in the mechanism by which the two keratopathies develop and progress.

All high angle XRD patterns taken across the corneas and limbus of BALB/c showed two lobes of increased x-ray scatter intensity, thus indicating that in the mouse cornea there is an abundance of aligned collagen lying in a uni-axial preferred direction. Unfortunately the corneas were not orientated so it was not possible to determine the direction in which the majority of collagen fibrils lie in the normal mouse cornea. The unidirectional preferred orientation of collagen fibrils seen in the mouse cornea also exists in the bovine cornea (Chapter 4) and the marmoset cornea (Boote *et al.* 2004 – Appendix 7). It does however differ from that of the human, in which XRD patterns from the central cornea show four lobes of increased scattering intensity (Figure 2.5).

In the normal mouse cornea the proportion of preferentially aligned collagen fibrils (as indicated by the index of orientation) increases smoothly from the centre of the cornea (where 20 % of the total collagen is preferentially aligned) to the limbus, at which point a maximal value of approximately 45% collagen alignment is reached. The polar plots show that in the BALB/c mice corneas there is a gradual change in preferred collagen orientation from the cornea to the limbus and on both sides of the limbus the collagen appears to be preferentially orientated in a direction surrounding the cornea. Major differences in the index of orientation at comparable distances from the centre of the cornea were observed between BALB/C and 3 out of 4 of the SKC mice (with the exception being one of the male SKC mice (e)). The disruption to the normal fibril arrangement was most obvious in one of the male SKC mice (mouse f) which showed no evidence of an increase in the index of orientation at the limbus, although the preferred orientation of collagen across the cornea and limbus did not appear to differ greatly from that of the BALB/c mice. Despite the increased likelihood for male SKC mice corneas to develop a cone shaped cornea, the fibril arrangement was altered in both male and female SKC corneas (Quantock *et al.* 2003 - Appendix 10).

It is tempting to speculate that the changes in preferred orientation and the increase in collagen alignment at the limbus of BALB/c mice may be due to the presence of a circum-corneal annulus of collagen such as is seen in the human cornea; it is however not possible to prove this without a producing a polar plot map of preferred collagen orientation for the whole cornea and limbus. In the human cornea it has been suggested that the presence of this annulus at the point where the cornea meets the less curved sclera, may be an integral component in maintaining corneal biomechanical stability and curvature (Meek and Newton 1999; Newton and Meek 1998a, b). As hypothesised in Chapter 5 and elsewhere (Meek *et al.* 2005b – Appendix 9), corneal shape changes in keratoconus may at least in part be caused by an unravelling of collagen fibrils from the limbus. It follows therefore that if a circum-corneal annulus of collagen does exist in the normal mouse cornea, then a disruption to such an arrangement may lead to corneal shape changes. Unfortunately the difficulties in obtaining keratoconus specimens complete with limbus have made

this theory impossible to test, further highlighting the need for an animal model of keratoconus.

In contrast to the generally accepted equal incidence of keratoconus in the male and female human population (Kennedy *et al.* 1986; Olivares Jimenez *et al.* 1997), there is an increased likelihood for male SKC mice to develop a misshapen cornea than for female SKC mice and the development of the condition has been shown to be androgen dependent (Tachibana *et al.* 2002). This XRD study has shown that the structural parameters are altered to a similar extent in both the male and female SKC mice. Due to the lack of information regarding the severity to which each cornea was affected it is impossible to draw definitive conclusions regarding the relationship between corneal shape, fibril arrangement and limbal integrity (in terms of index of orientation) in SKC mice eyes, although a disruption in fibrillar arrangement does appear to be a common factor in SKC mice. It is possible that the female SKC mice used in the study of fibril orientation were sub-clinically affected (showing no overt signs of a misshapen cornea) which might help to explain the slight disruption to fibrillar arrangement.

6.5 Conclusion

A detailed examination of SKC mice corneas, a strain in which the males (and very rarely the females) develop a cone shaped cornea, was performed in order to assess their suitability as an animal model for the human disease keratoconus. The initial report of the SKC strain highlighted many similarities with keratoconus in humans but also mentioned distinctions such as the fact that SKC mouse corneas often show cloudiness and the likelihood that inflammatory changes may be at play in the corneas of SKC mice (Tachibana *et al.* 2002).

The results revealed that structural parameters were disrupted to a similar extent in male and female SKC mice corneas despite the fact that none of the female SKC mice used in this study showed any evidence of corneal clouding or shape changes. The lack of structural differences between the male and female SKC mice examined in this study suggest that the presence of larger and more widely spaced corneal collagen

fibrils in the SKC mice population does not predispose the development of a cone shaped cornea.

This study has provided the first evidence of a possible circum-corneal annulus of collagen at the limbus of the normal mouse cornea, the existence of which, if confirmed, would enable the mouse to be used as a model for future studies examining the importance of the collagen annulus in terms of corneal strength and stability.

In 3 out of 4 SKC mice studied abnormalities in the extent of collagen alignment were seen across the cornea and most prominently at the limbus, where a circumferential annulus of aligned collagen is thought to be present in the normal mouse cornea. The fact that the arrangement appeared equally disturbed in both male and female SKC mice is somewhat confusing since females rarely develop a misshapen cornea. It is therefore impossible without further investigation to establish a causal relationship between corneal shape and the integrity of the circum-corneal annulus.

The distinctions between SKC mice and human keratoconus in terms of inflammatory changes and androgen dependency combined with the findings in this present study indicate that the SKC strain of mice is not a suitable animal model for the study of human keratoconus. It is more likely that the SKC strain of mice exhibit a murine specific keratopathy that differs from that of human keratoconus.

6.6 Future study

- In order to assess the similarities in structural organisation between the mouse and human cornea and to establish the existence of a circum-corneal annulus of collagen in the mouse, it would be useful to perform a detailed scan of the mouse cornea and limbus using high-angle XRD.

Chapter 7: General Discussion

Using both high and low-angle x-ray diffraction (XRD), the aims of this thesis were to study the stromal ultrastructure of the normal human cornea; in particular to examine collagen interfibrillar spacing (IFS) and fibril diameter across the cornea (Chapter 3), collagen preferred orientation throughout its thickness (Chapter 4) and the similarities in preferred orientation and distribution of collagen mass between left and right corneas (Chapter 5). The stromal arrangement of the marmoset monkey and bovine cornea (both of which are used frequently as animal models for ocular research), were also examined and compared to that of the human cornea (Chapters 3 and 4 respectively). In Chapter 5, quantitative high-angle XRD derived information about the arrangement and distribution of collagen mass in normal and keratoconus corneas was examined alongside videokeratographic images of the same corneas. Attempts were made to form a link between the structural changes in the stroma of the affected corneas and the specific corneal shape changes associated with the disease. Suggestions were also made about a possible mechanism to explain the process by which keratoconus corneas progressively thin and steepen. As keratoconus research is hampered by the lack of an animal model, this thesis set about examining the stromal ultrastructure of mice with a murine specific keratopathy (SKC) that manifests (predominantly in the males of the population) as a cone shaped cornea (Chapter 6). By comparing the stromal ultrastructure of the SKC mice to that of normal (BALB/c) mice an assessment was made regarding the suitability of the SKC mouse as an animal model for human keratoconus.

In Chapter 5A, high-angle XRD was used to map the preferred orientation of collagen and the distribution of tissue mass in both left and right human corneas. Although only a small number of samples were examined, due to the large amount of synchrotron x-ray beam time required to produce a single map and the limited availability of normal human corneas of known orientation, a symmetry was revealed between left and right corneas in terms of the distribution of aligned collagen mass. An increase in the index of orientation was observed in all four quadrants of the peripheral cornea but in particular in the superior-nasal and inferior-temporal quadrants. The increase in the index of orientation in the four quadrants is thought to

be caused by additional aligned collagen lamellae which traverse the peripheral cornea. The additional aligned collagen present in the oblique regions of the peripheral cornea may be involved in the flattening of the cornea prior to the limbus and the structural symmetry between left and right corneas may help to explain the topographical mirror symmetry seen in fellow corneas (Dingeldein and Klyce 1989; Smolek et al. 2002). The disruption to the normal collagen arrangement in keratoconus corneal buttons, which have a characteristic cone shaped appearance, supports this idea (Figures 5.8 – 5.21). By examining a range of normal human corneas, the results were shown to be highly reproducible (Figures 5.1, 5.5, A1.1). The reproducibility of the results are such, that it is now possible to recognise a left cornea from a right cornea solely by examining the maps of collagen mass distribution and identifying the quadrants with the highest index of orientation.

Despite the obvious strengths of the technique it is however not entirely without problems. The most obvious of these are the potential for specimen damage caused by the high-intensity of the beam, the use of corneal buttons and the fact that the sample is not maintained under intraocular pressure during data collection. Although the extent of specimen damage as a result of XRD has not been investigated thoroughly, a preliminary study was performed using different exposure times (between 35 and 180 seconds) to obtain high-angle XRD patterns across the central, thinnest region of the cornea. Once normalised against the ion chamber readings (which represent the intensity of the beam) and the exposure time, the results revealed no difference in either the intensity of x-rays scattered from the collagen or in the directions in which they were scattered. Although the results of the study indicate that there was no loss of collagen mass from the cornea after being exposed to an intense beam of x-rays for up to 180 seconds, the lowest exposure time needed to obtain good quality data was used in each study in order to minimise the risk of specimen damage.

Due to the availability of samples and the design of the sample holder, either corneal buttons or corneas with scleral rims were used in each study. Although the corneal collagen fibrils are released from their tension once they are excised from the globe, the fact that the lamellae then form waves within the plane of the cornea means that

XRD derived maps of preferred collagen orientation and mass distribution are unlikely to be affected, since the results are a 2-D projection of the cornea. In support of this, previous studies within this laboratory have shown that preferred collagen orientation and mass distribution, when examined by XRD, is the same in the central 8mm of a normal human cornea with 2mm scleral rim as it is in an 8mm corneal button excised from a normal human cornea (Abahussin, personal communication, 2005). However, because the effects of relieving tension on lamellae are not fully understood, it is necessary for future experiments to design a sample holder in which the cornea can be examined under intraocular pressure.

This thesis has produced many interesting findings about the structure of the primate cornea. In the human cornea, collagen fibrils are more closely packed in the prepupillary region than in the periphery (Table 2). This may provide an optimisation of both corneal strength (which is enhanced by a closer packing of fibrils) and corneal transparency (which is optimised by the thinness of the tissue) in the main optical region of the cornea. Within the central 7mm of the cornea the distribution of collagen mass is fairly uniform and the fibrils are preferentially aligned in the superior-inferior and nasal-temporal directions (Figures 5.2, 5.3, A1.2). The preferred orthogonal orientation of collagen, which is seen throughout the thickness of the human cornea (although predominantly in the posterior stroma) (Figure 4.2) and in the mid to posterior stroma of the bovine cornea (Figure 4.3), may provide greater stress resistance in the line of action of the rectus muscles.

In both the human and the marmoset monkey, there is a sharp increase in IFS and fibril diameter at the limbus (Figure 3.1, 3.3, 3.4, 3.5); this has been shown to coincide with a major increase in aligned collagen mass and a change in the preferred orientation of collagen to form a circum-corneal annulus (Figure 5.1, 5.2, 5.3, A1.1, A1.2). All of these factors provide additional strength which help to maintain the shape of the cornea at the point where is meets the less curved sclera.

In the disease keratoconus, the strength and stability of the cornea is compromised by the progressive thinning and weakening of the tissue, which leads to the formation of a cone shaped cornea. Due to the lack of early stage keratoconus samples and of an

animal model to study the disease, the precise mechanism by which the disease progresses and the sequence of events that lead to the characteristic shape changes associated with the disease are currently unknown. The SKC mouse strain held great promise as a potential animal model for the disease, as the corneas of the males have a similar phenotypic appearance to the corneas of human keratoconus patients. Unfortunately however, structural differences between the corneas of SKC mice and human keratoconus patients and the lack of any major differences in the arrangement of collagen in the corneas of male and female SKC mice, despite phenotypic differences in the shape of their corneas (Figure 6.3), proved the SKC strain to be an unsuitable model. The study did however have certain design problems, such as the fact that the orientation of the samples was unknown and that details of the clinical phenotype of individual corneas (e.g. the presence or absence of oedema) were not available, although it is unlikely that these factors influenced the conclusions of the study.

To learn more about the mechanism by which keratoconus progresses, an attempt was made to form a link between the structural changes in the stroma of affected corneas and the specific corneal shape changes associated with the disease. High-angle XRD revealed that the arrangement and distribution of collagen mass was disturbed, at least to some extent, in the majority of the keratoconus buttons examined. In some cases structural alterations were observed only within the region of highest dioptric power (apical region) (e.g. Figure 5.14), whilst in other keratoconus buttons changes were evident throughout the entire button region (e.g. Figure 5.16). Although in some cases a relationship was seen between the size and shape of the cone and the extent of the structural alterations in the stroma, there appeared to be a large variation between individual corneas. Finding a relationship between the two was further complicated in this study by the use of three different videokeratography systems to record corneal topography and the absence of a clinical grading scheme of keratoconus severity (other than general observations of the presence or absence of corneal scarring).

A strong negative correlation was found to exist between corneal dioptric power and aligned collagen mass in the central cornea (Figure 5.23B), suggesting that changes in

the arrangement of lamellae in the posterior stroma become more manifest as the disease progresses. The results of the study indicated a loss of total collagen mass in the central 4mm of most keratoconus corneas, although there was also evidence to suggest a redistribution of tissue mass within the button region. The results support a theoretical mechanism of corneal thinning and ectasia in keratoconus corneas, in which a combination of inter-lamella and inter-fibrillar slippage, facilitated by a localised enzymatic break down of the extra-fibrillar matrix and some type I collagen digestion, result in a redistribution of tissue mass.

Although the present investigation could not shed any light on the primary cause of stromal thinning in keratoconus or the precise sequence of events that occur during its progression, the altered organisation of collagen which has been highlighted in this study would likely accelerate the progression of the disease irrespective of its origins.

Appendix 1. Collagen preferred orientation and mass distribution in a normal right cornea with scleral rim (N3)

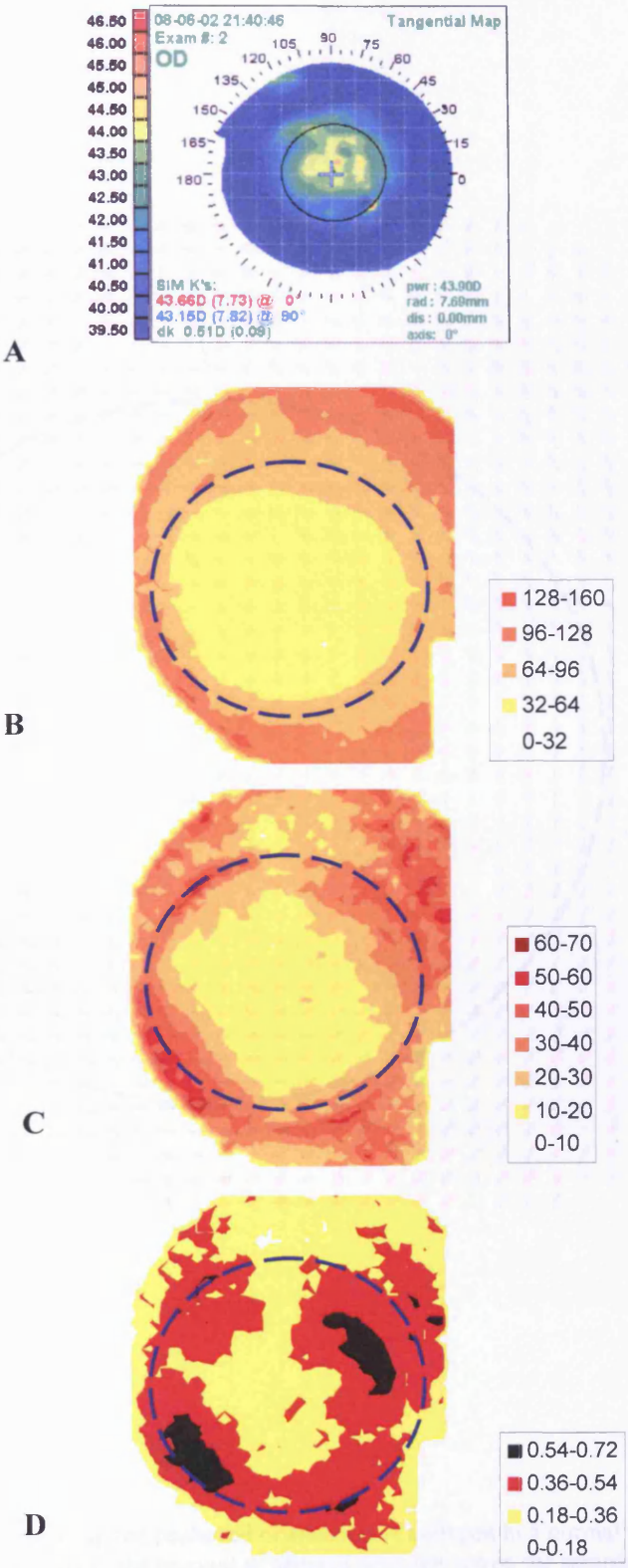

Figure A1.1. Maps showing the corneal dioptric power of a normal right eye (A) and the distribution of total collagen mass (B), aligned collagen mass (C) and the index of orientation (D) in the cornea and scleral rim of the same eye.

Right (N3)

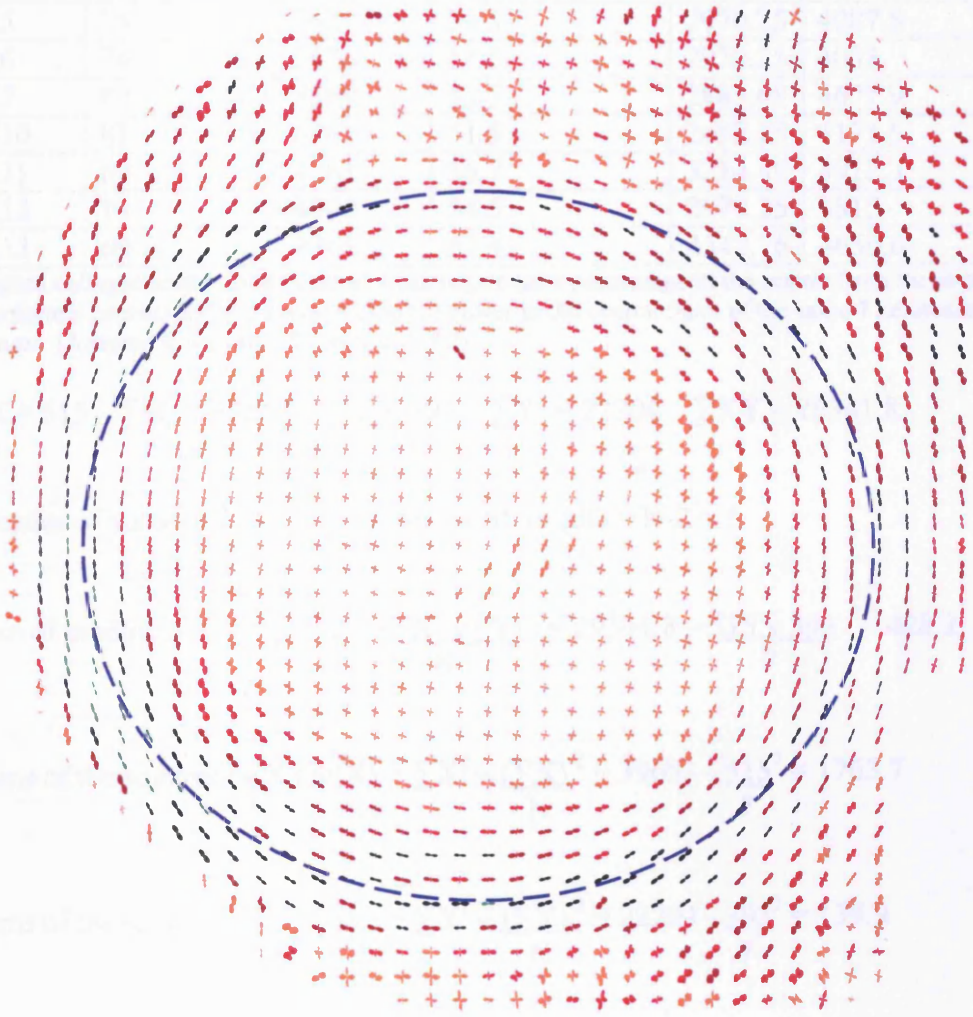

Figure A1.2. Polar plot map showing the preferred orientation of collagen in a normal right cornea with scleral rim. Due to variations in the amount of aligned collagen across the sample, the polar plots (E) have been scaled down by factors of 4.5,4, 3, 2 and 1.5 and colour coded using the colours blue, green, black, brown, red and orange respectively. The position of an average human limbus is highlighted by a blue dashed line.

Appendix 2. A statistical analysis of the relationship between corneal dioptric power and aligned collagen scatter in keratoconus corneas

A2.1. Pearson r correlation coefficient

Sample	Aligned scatter as a % of normal (X)	X^2	Average dioptric power in central 5mm region (Y)	Y^2	XY
K5	75	5625	54.5	2970.25	4087.5
K6	74	5476	54.5	2970.25	4033
K7	87	7569	53.7	2883.69	4671.9
K10	81	6561	51.5	2652.25	4171.5
K11	69	4761	56.7	3214.89	3912.3
K12	70	4900	54.5	2970.25	3815
K13	69	4761	67.4	4542.76	4650.6

Aligned collagen scatter in the central 4mm region (as a percentage of the scatter from the same region of a normal cornea) and the average dioptric power in the central 5mm of the same 7 keratoconus corneas. (Adapted from Table 8, Section 5.5.2).

$\sum X = 515 \quad \sum X^2 = 39653 \quad \sum Y = 393 \quad \sum Y^2 = 22204 \quad \sum XY = 29341.8$

Number of values (N) = 7 Degrees freedom (df) = N-2 = 5

$$\text{Sum of products (SP)} = \sum XY - \frac{(\sum X)(\sum Y)}{N} = 29341.8 - \frac{515 \times 393}{7} = 428.2$$

$$\text{Sums of the squares of X (SSX)} = \sum X^2 - \frac{(\sum X)^2}{N} = 39653 - \frac{515^2}{7} = 1763.7$$

$$\text{Sums of the squares of Y (SSY)} = \sum Y^2 - \frac{(\sum Y)^2}{N} = 22204 - \frac{393^2}{7} = 139.9$$

$$\text{Pearson r correlation coefficient (r)} = \frac{SP}{\sqrt{(SSX \times SSY)}} = \frac{428.2}{\sqrt{(1763.7 \times 139.9)}} = 0.86$$

Published r value for a one-tailed test at P = 0.01 (5df) = 0.8329

Inference:

There is a highly significant positive correlation ($P<0.01$) between corneal dioptric power and aligned collagen scatter in keratoconus corneas.

Appendix 3. A statistical analysis of collagen interfibrillar spacing in BALB/c and SKC mice corneas

A3.1. Single Factor ANOVA

	BALB/c	Female SKC	Male SKC
	51.4	55.6	63.1
	46.3	60.4	79.3
	47.8	59.0	57.8
	46.3	55.6	52.4
	50.5	54.4	59.0
	45.5	55.6	59.0
Mean	48.0	56.8	61.8
Total (T)	287.7	340.5	370.6

Average collagen interfibrillar spacing in 3-month old BALB/c and SKC mice corneas (adapted from Table 9, Section 6.3.1).

Sum of scores ($\sum x$) = 287.7+340.5+370.6 = 998.8

Square of the sum of scores $(\sum x)^2 = 998.8^2 = 997601.44$

Sum of squared scores $\sum x^2 = 56515.98$

Number of groups (k) = 3

Number of values per group (n) = 6

Total number of values (N) = 18

Degrees freedom (df):

Df total = N-1 = 17

Df between groups = k-1 =2

Df error = df total – df between groups = 17-2 = 15

Sum of squares (SS):

$$\text{SS total} = \sum x^2 - \frac{(\sum x)^2}{N} = 56515.98 - \frac{997601.44}{18} = 1093.68$$

$$\text{SS between groups} = \frac{\sum T^2}{n} - \frac{(\sum x)^2}{N} = \frac{82771.29+137344.36+115940.25}{6} - \frac{997601.41}{18}$$

$$= 56009.32-55422.3 = 587.02$$

SS error = SS total – SS between groups = 1093.68 – 587.02 = 506.66

Mean square (MS):

$$\text{MS between groups} = \frac{\text{SS between groups}}{\text{Df between groups}} = \frac{587.02}{2} = 293.5$$

$$\text{MS error} = \frac{\text{SS error}}{\text{Df error}} = \frac{506.66}{15} = 33.78$$

$$\text{F Ratio} = \frac{\text{MS between groups}}{\text{MS error}} = \frac{293.5}{33.78} = 8.6$$

Published F value at: P = 0.05 (2/15df) = 3.68, P = 0.01 (2/15df) = 6.36

Inference:

There is a highly significant difference (P<0.01) in IFS between groups. To find out where this significant difference lays a post hoc Tukey test was performed.

A3.2. Post hoc Tukey test:

Values and symbols are carried forward from the previous ANOVA analysis (A2.1)

	BALB/c	Female SKC	Male SKC
Mean IFS	48.0	56.8	61.8

Difference between means:

	Female SKC	Male SKC
BALB/c	-8.8	-13.8
Female SKC		-5.1

Df error = 15 MS error = 33.78 k = 3 n = 6

Published q value at P = 0.05 for k = 3 and 15df = 3.67, P = 0.01 = 4.84

Honestly Significant Difference (HSD) at $p = 0.05 = q \sqrt{\frac{MS\ error}{n}}$

$$= 3.67 \times \sqrt{\frac{33.78}{6}} = 8.7$$

$$HSD \text{ at } p = 0.01 = 4.84 \times \sqrt{\frac{33.78}{n}} = 11.48$$

Inference:

Both male and female SKC mice corneas have a significantly higher IFS than BALB/c mice ($P<0.01$ and $P<0.05$ respectively).

There is no significant difference in IFS between male and female SKC mice.

Collagen Fibrils Appear More Closely Packed in the Prepupillary Cornea: Optical and Biomechanical Implications

Craig Boote, Sally Dennis, Richard H. Newton, Hina Puri, and Keith M. Meek

Purpose. The size and organization of stromal collagen fibrils influence the biomechanical and optical properties of the cornea and hence its function. How fibrillar structure varies with position across the cornea has not been fully characterized. The present study was designed to quantify the collagen fibril spacing and diameter across the normal human cornea and to relate this to the properties of the tissue.

Methods. Small-angle x-ray diffraction was used to map in detail the variation in fibril spacing and fibril diameter along orthogonal medial-lateral and inferior-superior meridians of five normal human corneoscleral discs.

Results. Mean fibril diameters remained constant across all corneas up to the limbus, whereupon a sharp increase was observed. However, mean fibril spacing across the central 4 × 3 mm (prepupillary) cornea measured 5% to 7% lower than in the peripheral cornea.

Conclusions. Collagen fibrils in the prepupillary cornea appear to be more closely packed than in the peripheral cornea. Anisotropy in fibril packing across the cornea has potential implications for the transparency and refractive index of the tissue. Biomechanically, it is possible that the higher packing density of stress-bearing collagen fibrils in the prepupillary cornea is necessary for maintaining corneal strength, and hence curvature, in a region of reduced tissue thickness. By inference, these results could have important implications for the development of corneal models for refractive surgery. (*Invest Ophthalmol Vis Sci.* 2003;44:2941-2948) DOI: 10.1167/iovs.03-0131

By virtue of its remarkable mechanical strength and transparency, the human cornea serves both as a protective barrier and as the main refractive component of the eye. Conventionally, the central third of the cornea is considered the optical zone[1] and provides the bulk of the cornea's refractive function, constituting approximately 70% of the total focusing of the eye. The near-spherical optical zone forms the foveal image through the pupil and is thus often referred to as the prepupillary cornea, whereas the remaining peripheral cornea is less curved and serves mainly as a refractive surface for peripheral vision. The cornea merges with the sclera at the narrow annular limbus. The surface zones of the cornea are shown schematically in Figure 1.

Corneal function is governed largely by the structure of the stromal extracellular matrix, the bulk of which in human cornea comprises collagen fibrils arranged in approximately 200 parallel lamellae.[2] Fibrils within a lamella are parallel to each other and to the corneal surface, but run at angles in relation to fibrils in adjacent lamellae. This collagen network is responsible for the cornea's mechanical strength. When a force is applied to the cornea, the restoring force in the stretched fibrils balances the applied force, and the fibrils confer tensile reinforcement on the tissue. The diameter of collagen fibrils, their orientation in relation to the applied force, and the collagen content of the tissue all determine how effectively the fibrils can reinforce the tissue and hence determine its tensile strength.[3,4] Tissue strength is paramount to the refractive function of the cornea because of the need for the cornea to maintain correct surface curvature under intraocular pressure. Fibril organization in the stroma is also crucial to corneal transparency. Current theory requires a measure of fibrillar order for corneal light transmission,[5] and the uniformity of fibril diameters and their packing are thought to be instrumental in the establishment of a transparent cornea.[2,5]

X-ray diffraction is a technique that involves passing an intense beam of x-rays through an intact isolated cornea and recording the intensity of the scattered x-rays on a detector placed behind the specimen. Each lamella in the corneal stroma gives rise to small-angle equatorial diffraction due to interference between x-rays scattered from its constituent axially aligned fibrils (Fig. 2). This is because, over a short range, fibrils tend to be of a fairly uniform diameter and regularly spaced in the lateral direction. From the diffraction pattern, we can determine several key features of the cornea's internal structure, including the mean separation of fibrils and their average diameter (see Fig. 2). A comprehensive treatment of the technique can be found in a recent review.[6]

Fibril spacing and diameter in the central cornea have been measured in a number of species, both by small-angle x-ray diffraction[7] and electron microscopy.[8,9,10] However, there are only a very limited number of reports in the literature characterizing variations in fibrillar structure as a function of position across the cornea, despite the potential clinical importance of this knowledge. Notably, Borcherding et al.[11] measured semiquantitatively the variation in fibril diameter and spacing across the human cornea from electron micrographs, reporting that both parameters remained constant with increasing radial position, before increasing rapidly at the limbus. However, measurements from electron microscopy have tended to show considerable variation among studies,[8-11] which has been attributed largely to tissue shrinkage during specimen preparation.[12,13] By this token, structural parameters are more readily obtained from scattering experiments, which require no chemical fixing or dehydration of specimens and can thus be performed under conditions more comparable with those encountered in vivo. Furthermore, x-ray data are highly illustrative

From the Department of Optometry and Vision Sciences, Cardiff University, Cardiff, Wales, United Kingdom.

Supported by Wellcome Trust Grant WT055710 and Medical Research Council Grant G0001033.

Submitted for publication February 6, 2003; revised March 6, 2003; accepted March 9, 2003.

Disclosure: **C. Boote**, None; **S. Dennis**, None; **R.H. Newton**, None; **H. Puri**, None; **K.M. Meek**, None

The publication costs of this article were defrayed in part by page charge payment. This article must therefore be marked "*advertisement*" in accordance with 18 U.S.C. §1734 solely to indicate this fact.

Corresponding author: Craig Boote, Department of Optometry and Vision Sciences, Cardiff University, Redwood Building, Cardiff, Wales CF10 3NB, UK; bootec@cf.ac.uk.

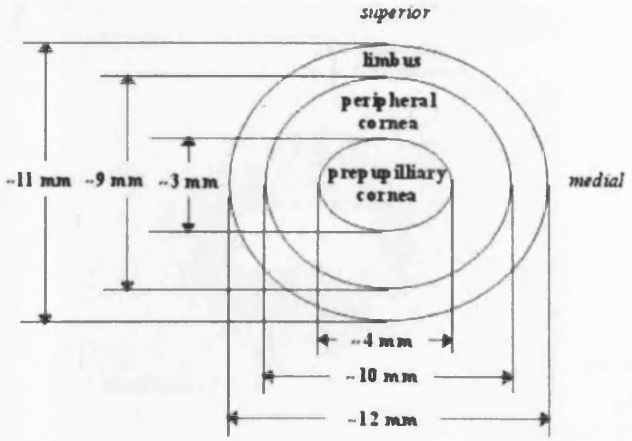

FIGURE 1. Conventional designation of surface zones in human cornea (anterior corneal face shown).

because they represent an average measurement of the volume of tissue through which the x-ray beam passes, sampling every fibril in the path of the x-rays throughout the entire corneal thickness. Recently, Daxer et al.[14] used x-ray diffraction techniques to study the spatial variation in human corneal fibril diameters and reported no significant differences within a central 7-mm region. In the present study, we built on this work by quantifying in detail the variation in fibril diameters and, moreover, fibril spacings across the human cornea, by using small-angle x-ray diffraction, and we related the findings to the tissue's properties.

MATERIALS AND METHODS

Specimens

Five time-expired, whole, excised human corneas, each having 3 mm of scleral rim attached, were obtained from the UK Corneal Transplant Service Eye Bank (Bristol, UK). Corneal epithelial and endothelial cell layers were removed before examination with x-rays. Tissue hydration of the specimens (expressed as mass of water/mass of dry cornea) ranged from 2.0 to 4.0. The tenets of the Declaration of Helsinki were observed throughout.

Data Collection

Small-angle x-ray diffraction patterns were collected on Station 2.1 at the UK Synchrotron Source at Daresbury, using a 9-m-long camera equipped with a multiwire gas detector. The x-ray beam had a wavelength of 0.154 nm and a cross section at the specimen measuring 0.5 mm vertically and 2 mm horizontally. Specimens were placed in airtight Perspex (Databank, UK) chambers with Mylar (DuPont-Teijin, UK) windows to minimize tissue dehydration. Incident x-rays were passed through the anterior corneal face parallel to the optical axis. Diffraction patterns were recorded at 0.4- to 1.0-mm intervals along the orthogonal inferior–superior and medial–lateral corneal meridians, using a stepper motor system to translate the specimen in the vertical direction, the sample being rotated through 90° between transects. Exposure time per data point was 3 minutes.

Data Processing

Figure 3 shows a typical x-ray diffraction pattern from the center of one of our specimens. X-ray intensity profiles were measured along a vertical transect through the center of each pattern, as shown in the figure, because this was the direction in which the x-ray beam was most finely focused. A typical resultant profile is shown in Figure 4a. Data processing then proceeded in 4 steps:

1. A square-power law background curve was fitted to and subtracted from the experimental data (Fig. 4a). This removed scattering from stromal matrix components other than fibrillar collagen.
2. Assuming cylindrical collagen fibrils, small-angle equatorial x-ray diffraction from a corneal lamella can be approximated as the fibril transform (i.e., scattering from a single fibril), multiplied by the interference function (deriving from the ordered arrangement of the cylinders).[15,16] A theoretical fibril transform was fitted to the experimental data by varying two parameters:

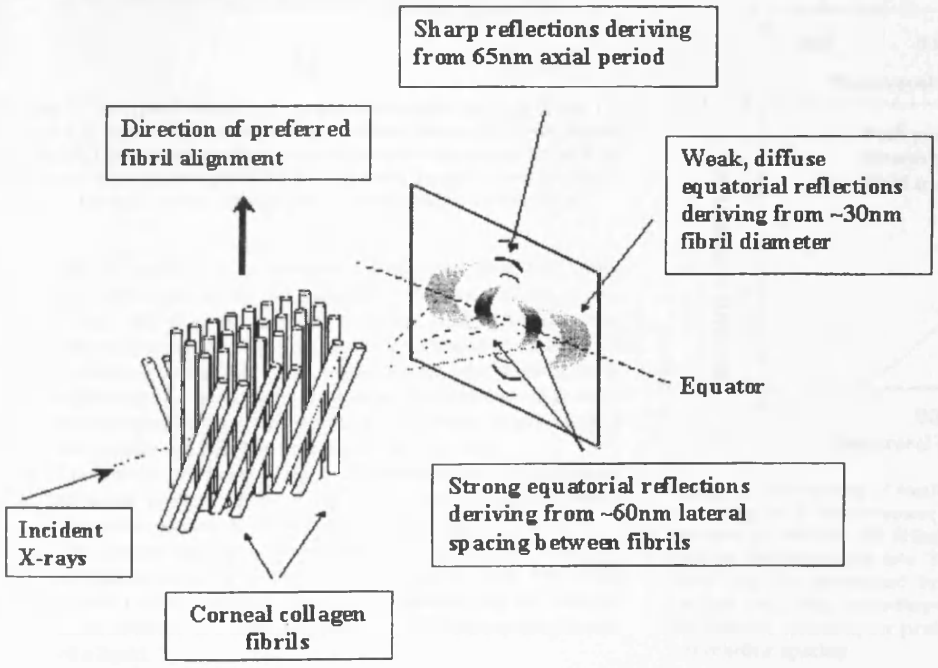

FIGURE 2. Small-angle x-ray diffraction from corneal collagen fibrils.

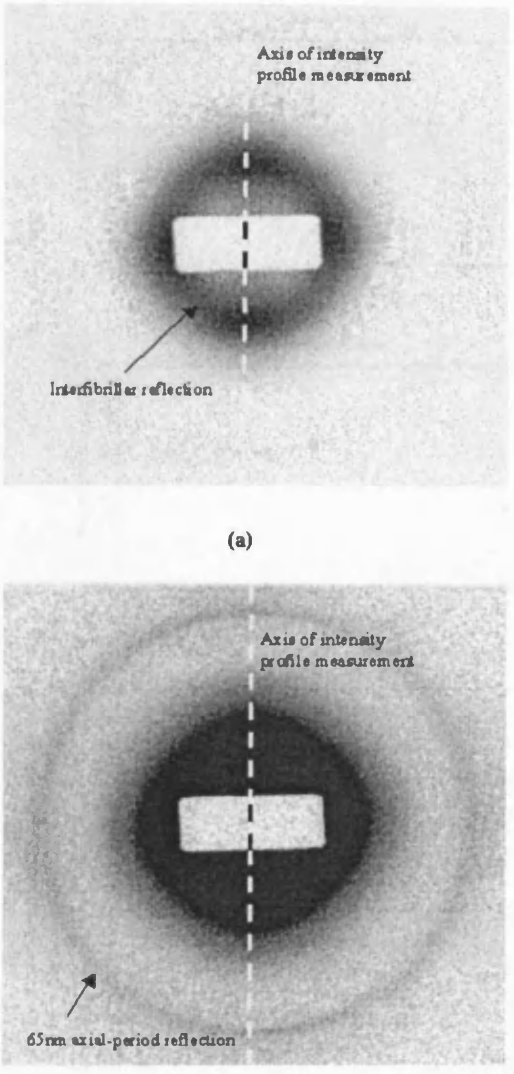

FIGURE 3. A typical small-angle x-ray diffraction pattern from the center of human cornea. The pattern is shown at two different display thresholds to highlight (**a**) the equatorial interfibrillar reflection and (**b**) the meridional axial period reflection. Intensity profiles were measured along a vertical transect through the pattern center, as indicated.

the fibril radius and an arbitrary scaling factor (Fig. 4b). Fitting was performed on the first subsidiary maximum of the experimental data (Fig. 4b), because this peak derives entirely from the fibril transform, with no significant contribution from the interference function.[16] The experimental data were then divided point-for-point by the calculated fibril transform to leave the interference function, whose peak position is governed by the average interfibrillar Bragg spacing (Fig. 4c).

3. The interfibrillar Bragg spacing and fibril radius were calibrated from the position of the 67-nm meridional reflection from a diffraction pattern of hydrated rat tail tendon.
4. The average center-to-center interfibrillar spacing (t) was calculated from the interfibrillar Bragg spacing (p) with $t = 1.12p$, where 1.12 is a packing factor that assumes that the arrangement of fibrils in a lamella approximates the short-range order of a liquid.[16]

RESULTS

Fibril diameters along superior–inferior and medial–lateral meridians of five human corneas are shown in Figure 5. The results show that the fibril diameter remained constant from the corneal center up to the limbus in all five corneas, with diameters typically measuring 32 to 34 nm. This is consistent with previous work[11,14]. In agreement with the Borcherding study,[11] fibril diameter rose sharply across the limbus, increasing by up to approximately 75%. There was no evidence of any dependency of these results on tissue hydration, an observation that is consistent with the findings of Daxer et al.[14]

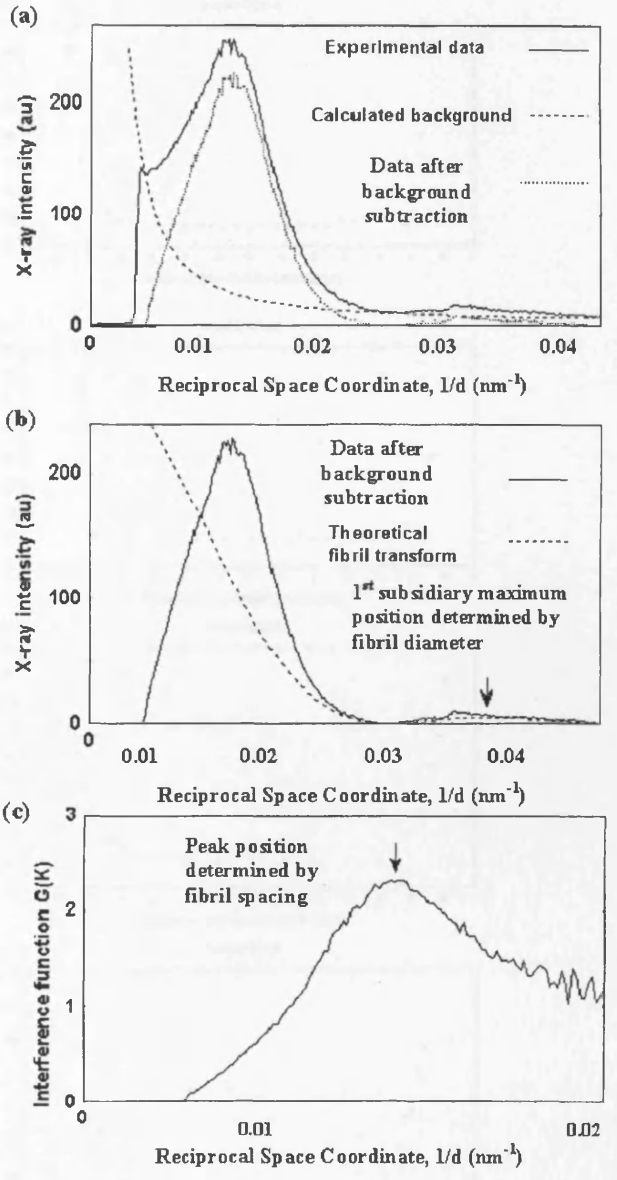

FIGURE 4. Processing of small-angle corneal diffraction data, showing (**a**) fitting of a square-power law background to the experimental intensity profile and (**b**) fitting of a theoretical fibril transform to the background-subtracted data. The position of the first subsidiary maximum peak is determined by the fibril diameter. (**c**) Dividing the experimental data point-for-point by the fibril transform yields the interference function, the peak position of which is determined by the interfibrillar spacing.

Appendix 4

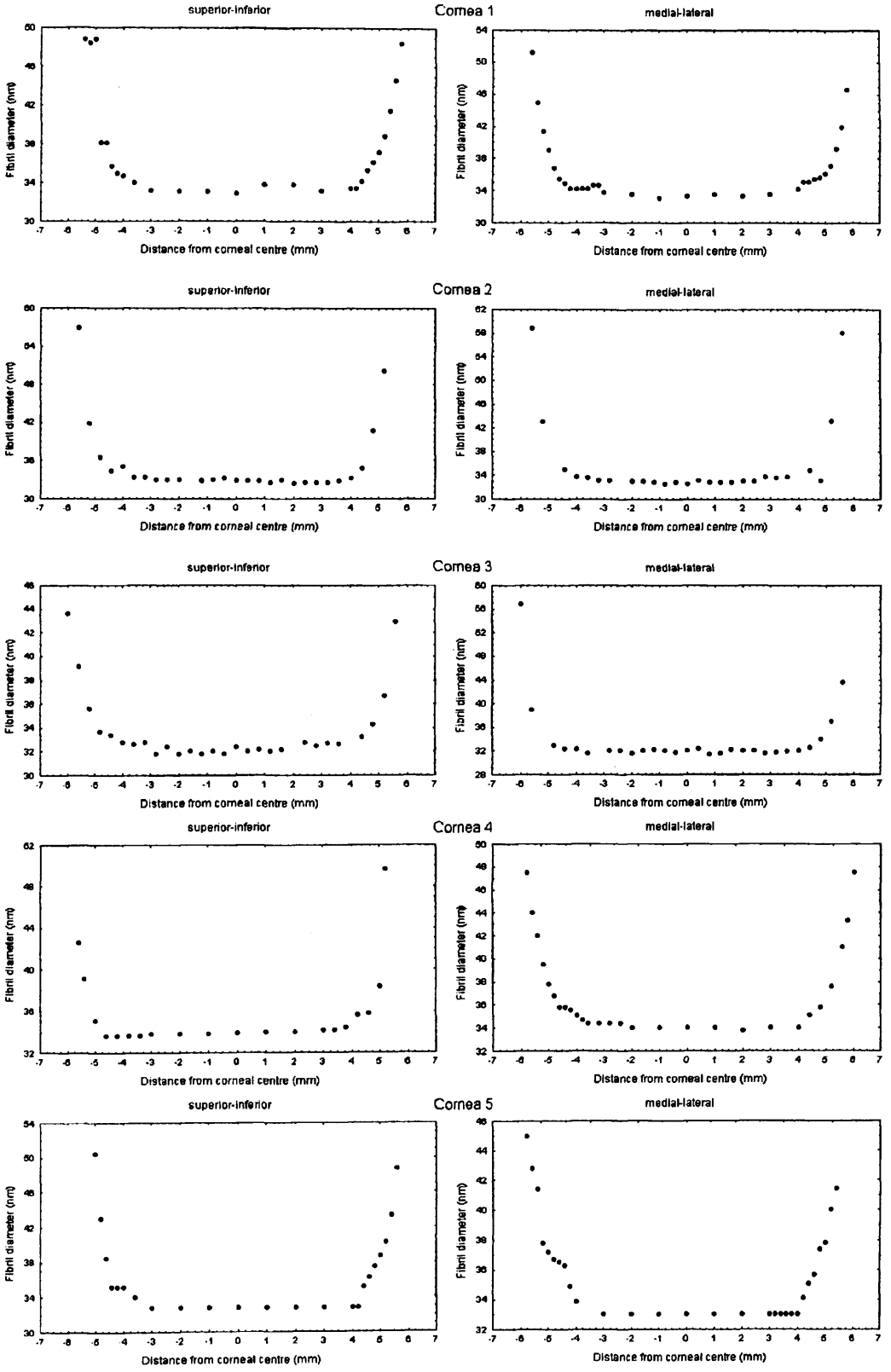

FIGURE 5. Fibril diameters across orthogonal superior–inferior and medial–lateral meridians of five normal human corneas.

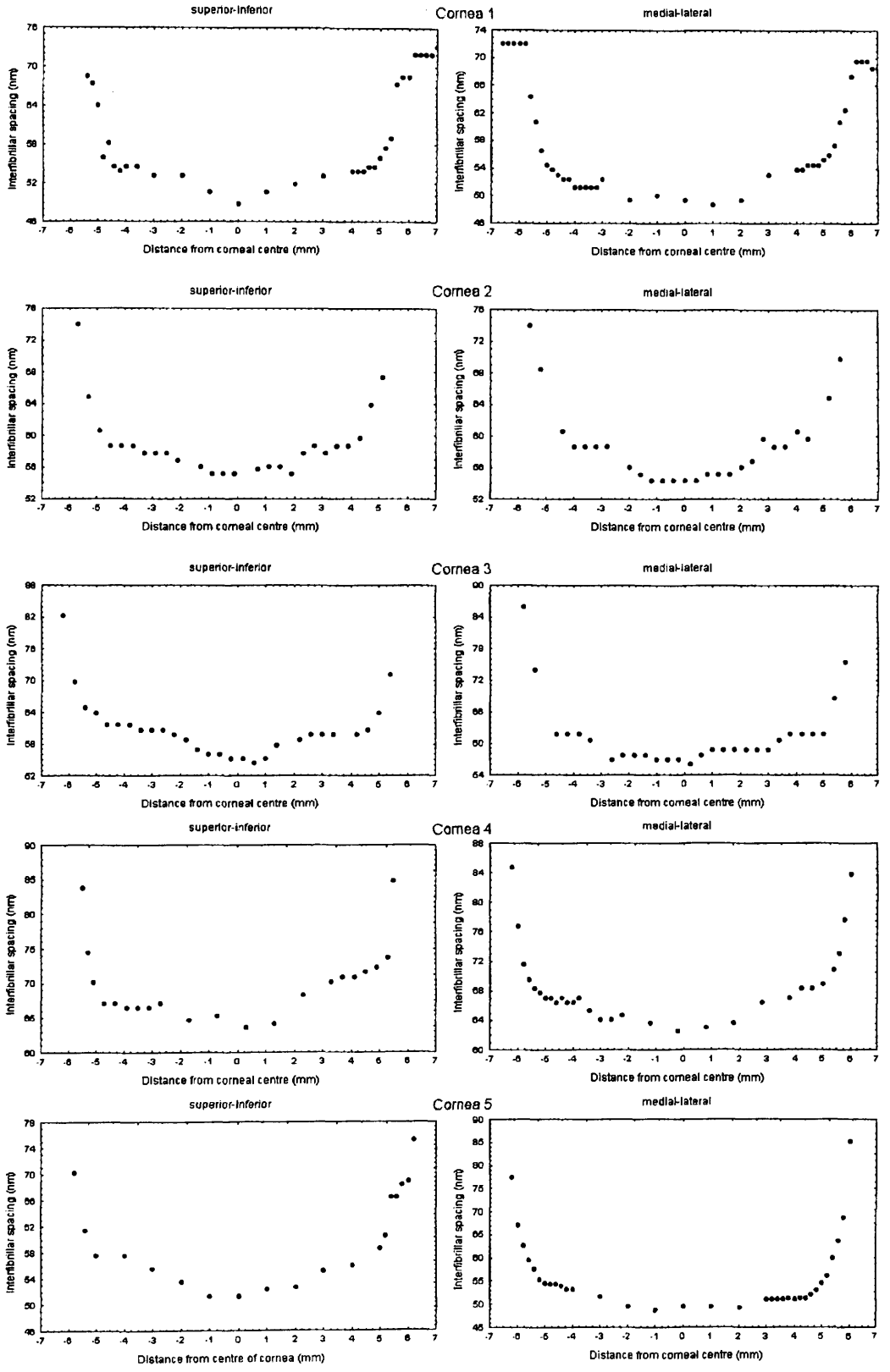

FIGURE 6. Center-to-center interfibrillar spacing across orthogonal superior-inferior and medial-lateral meridians of five normal human corneas.

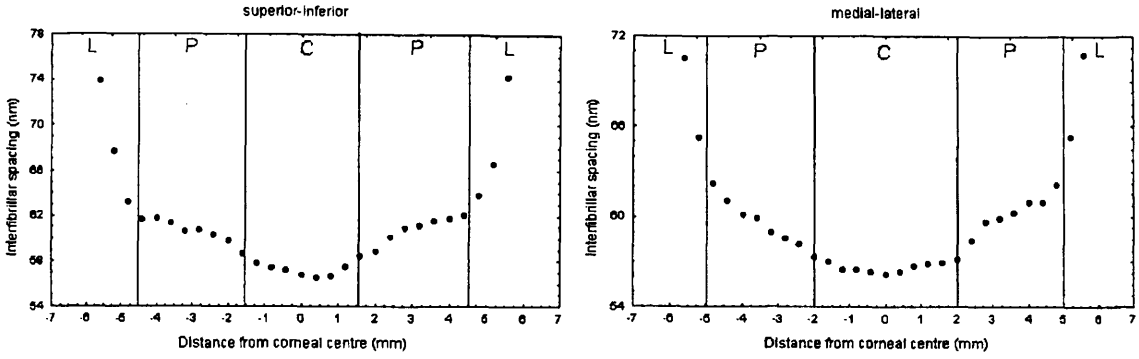

FIGURE 7. Center-to-center interfibrillar spacing, averaged over five corneas and normalized to physiological hydration. Central (prepupillary), peripheral, and limbal corneal surface zones are denoted by C, P, and L, respectively.

Figure 6 shows the equivalent data for the center-to-center interfibrillar spacing. In all five specimens the average fibril spacing was clearly reduced near the corneal center compared with the more peripheral regions, a result that contrasts with previous measurements from electron microscopy.[11] Across the limbus, fibril spacing rapidly increased by approximately 25% to 40%, an observation that is consistent with previous findings.[11]

Figure 7 shows interfibrillar spacing averaged over the five corneas and normalized to physiological hydration, onto which corneal surface zone boundaries have been superimposed. The mean fibril spacing within the prepupillary and peripheral corneal zones may be compared by inspection of the data in Table 1. Prepupillary fibril spacing measured 5% to 7% lower than in the peripheral cornea. A two-tailed Student's *t*-test revealed this difference to be statistically significant ($P \ll 0.01$) for all five specimens (Table 1). In contrast, reference to Table 2 shows that no significant difference was found in the fibril diameter measurements between the two corneal zones ($P \geq 0.01$). In addition, fibril spacing for the five individual corneas (normalized to physiological hydration) were grouped and analyzed using a two-tailed *t*-test. This again disclosed a significant difference between the two corneal zones ($P = 1.1 \times 10^{-14}$).

The variation in fibril spacing across the cornea appears to be qualitatively unaffected by tissue hydration. Reference to Table 1 shows that the differences in hydration (H) between specimens affected the fibril spacing in all corneal zones uniformly. The data correlate well with data in previous x-ray diffraction studies of stromal hydration.[17]

DISCUSSION

Our results disclose that fibril packing is nonuniform over the corneal surface and point to a more compact fibril matrix in the prepupillary cornea. Mean center-to-center interfibrillar separation measured 5% to 7% lower in the prepupillary cornea compared with the peripheral, a result that proved significant after statistical testing (Table 1). Considering the distinct functionality of the prepupillary and peripheral cornea and the well-established link between corneal function and fibril organization, it would be surprising if our results held no functional significance. In seeking an explanation for the results, it is instructive to consider the potential influence of fibril compaction on three corneal properties crucial to its function: transparency, refractive index, and mechanical strength.

The two most well-established models for describing the dependency of corneal transparency on fibril ultrastructure are those of Hart and Farrell[18] and Freund et al.[19] Although these models make considerable assumptions and simplifications in describing the structure of the stroma, they have been useful for assessing the importance of structural parameters on light-scattering in the cornea. It is implicit in both models that increased packing density of collagen fibrils predicts a reduction in tissue transparency.[18,19] Thus, the presence of more closely packed fibrils centrally seems detrimental to the refractive function of the most optically important corneal region. However, care should be taken in interpreting the results of transparency models, because the parameters included in the models are often mutually dependent.[18,19] Moreover, corneal

TABLE 1. Comparison of Interfibrillar Spacing in the Prepupilliary and Peripheral Zones of Five Human Corneas

Cornea	Hydration	Corneal Zone	Mean Interfibrillar Spacing (nm)	*P* (=)
1	2.0	Prepupilliary	49.7 ± 1.2	2.7×10^{-9}
		Peripheral	53.4 ± 2.3	
2	2.7	Prepupilliary	55.2 ± 0.6	1.9×10^{-13}
		Peripheral	58.5 ± 1.5	
3	2.9	Prepupilliary	56.7 ± 1.4	7.4×10^{-10}
		Peripheral	60.5 ± 2.2	
4	4.0	Prepupilliary	63.7 ± 0.9	6.7×10^{-5}
		Peripheral	67.0 ± 1.9	
5	2.0	Prepupilliary	50.0 ± 1.2	3.0×10^{-4}
		Peripheral	53.2 ± 1.8	

Data are means ± SD. The statistical significance level of the difference between the zones is shown.

TABLE 2. Comparison of Fibril Diameter in the Prepupilliary and Peripheral Zones of Five Human Corneas

Cornea	Hydration	Corneal Zone	Mean Fibril Diameter (nm)	*P* (=)
1	2.0	Prepupilliary	33.4 ± 0.6	0.01
		Peripheral	34.3 ± 1.2	
2	2.7	Prepupilliary	33.0 ± 0.3	0.01
		Peripheral	33.5 ± 1.1	
3	2.9	Prepupilliary	32.0 ± 0.4	0.01
		Peripheral	32.4 ± 0.8	
4	4.0	Prepupilliary	34.0 ± 0.1	0.06
		Peripheral	34.6 ± 0.9	
5	2.0	Prepupilliary	33.0 ± 0.1	0.05
		Peripheral	33.9 ± 1.3	

Data are means ± SD. The statistical significance level of the difference between the zones is also shown.

Appendix 4

thickness is at least 20% lower in the center of the cornea than at the periphery.[20,21] In terms of transparency, a thinner prepupillary cornea tends to compensate for a higher fibril packing density.

The issue of the cornea's refractive index is clearer. Bearing in mind that fibril diameters remain constant across the cornea (Fig. 5), we deduce that smaller center-to-center fibril spaces result in a higher collagen fibril volume fraction. Given that stromal collagen fibrils have a higher refractive index than the intervening material,[22] it follows that closer packing of fibrils predicts a higher refractive index, and hence dioptric power, in the tissue. In view of our findings, there is clearly room for more detailed study into the variation of refractive index and transparency as a function of position in the cornea.

What of the potential impact of our results on the biomechanics of the cornea? The cornea is reinforced by collagen fibrils, as described earlier. These fibrils are strongest axially, and directions of preferred fibril orientation thus associate with directions of heightened tissue strength. Fibril diameters are also biomechanically important, because they determine the fibrils critical length,[3] (l_c) given by

$$l_c = d\sigma_f/2\tau \quad (1)$$

where d is the fibril diameter, σ_f is the fibril's tensile strength and τ is the shear stress exerted on the fibril by the ground substance (we define ground substance as being stromal matrix elements other than fibrillar collagen). The critical length is the minimum fibril length required for effective tissue reinforcement.[3] As long as this condition is met, the tensile strength of the tissue (σ_t) is determined by the volume fraction of collagen present (β)

$$\sigma_t = \beta\sigma_f + (1 - \beta)\,\sigma_g \quad (2)$$

where σ_f and σ_g are the tensile strengths of the fibrils and ground substance, respectively.[3,23] It is our hypothesis that the higher packing density of collagen fibrils we have observed in the prepupillary cornea is necessary to maintain tissue strength, bearing in mind that the cornea is thinner centrally.[20,21] Inspection of equation 2 reveals that, for $\sigma_f > \sigma_g$, increasing the volume fraction of collagen produces a proportional increase in the mechanical strength of the tissue. Hence, we expect reduced prepupillary fibril spacing and thus increased collagen volume fraction to result in a stronger central cornea. Such a mechanism could help to preserve dioptric stability in the cornea by helping to maintain surface curvature in the presence of variations in tissue thickness. Of course, we are assuming that corneal collagen fibrils are at least as long as their critical length. Although the exact length of collagen fibrils in the cornea is unknown, Maurice[24] observed that corneal lamellae appear to run uninterrupted from limbus to limbus. Furthermore, electron microscopy has indicated that the critical length condition is met by most of the stress-bearing collagen fibrils in other connective tissues.[25]

We can currently only speculate as to the mechanisms that could be driving the changes in fibril spacing across the cornea. However, one possibility is that it may be related to variations in hydration across the tissue. Fibril spacing in the cornea is known to be highly sensitive to the tissue's water content. Reference to previous x-ray scattering work on corneal stroma reveals that, at the hydration levels encountered in our work, water is exclusively deposited into or removed from the interfibrillar spaces, rather than within the fibrils themselves.[17,26] Under these conditions, therefore, even subtle variations in tissue hydration could be expected to produce changes in the spacing of the fibrils, without affecting their diameter. How tissue hydration varies across the cornea is currently unknown, and clearly there is a need for detailed investigation of this question.

Information about the tissue strength of the cornea as a function of position and the parameters that influence it have obvious clinical relevance. Current models used in the simulation of refractive surgery make complex assumptions regarding the ultrastructure of the corneal stroma,[27,28] because there is a general lack of detailed structural information. Recently, scattering methods have been used in attempts to characterize tissue structure. Newton and Meek[29,30] determined the variation in collagen fibril orientation across the cornea and reported a gradual alteration in the preferred fibril orientation, from orthogonal at the corneal center to circumferential at the limbus. Such anisotropy in the cornea could explain why surgical incisions at some positions in the cornea are more likely to induce astigmatism than at others.[31] There appears to be no obvious correlation between our data and the variation of fibril orientations across the cornea. Nevertheless, our contention is that anisotropy in fibril packing across the cornea may well have similarly important clinical implications because of the influence of collagen packing density on tissue strength and hence corneal curvature.

We have presented herein the first evidence that fibrils are more closely packed in the optical zone of human cornea and argue that this could have important implications for the properties, and hence the function, of the cornea. So far, we have collected detailed structural data covering the medial-lateral and inferior-superior corneal meridians. We propose to compose a map of structural parameters over the entire corneal surface at similarly high resolution in the future. It is possible that detailed mapping of structural parameters across the corneal surface may be highly beneficial in the development of corneal models to optimize refractive surgery.

Acknowledgments

The authors thank Val Smith of the UK Corneal Transplant Service Eye Bank (Bristol, UK) and Gunter Grossmann and the staff of the Council for the Central Laboratory of the Research Councils Synchrotron Radiation Source (Daresbury, UK).

References

1. Waring GO. Making sense of keratospeak II: proposed conventional terminology for corneal topography. *Refract Corn Surg.* 1989;5:362-367.
2. Maurice DM. The structure and transparency of the corneal stroma. *J Physiol.* 1957;136:263-286.
3. Hukins DWL, Aspden RM. Composition and properties of connective tissues. *Trends Biochem Sci.* 1985;10:260-264.
4. Jeronimidis G, Vincent JFV. Composite materials. In: Hukins DWL ed. *Connective Tissue Matrix.* Macmillan; 1984:187-210.
5. Farrell RA. Corneal transparency. In: Albert DM, Jacobiec SA, eds. *Principles and Practice of Ophthalmology.* Philadelphia: Saunders; 1994.
6. Meek KM, Quantock AJ. The use of X-ray scattering techniques to determine corneal ultrastructure. *Prog Retinal Eye Res.* 2001;20:95-137.
7. Meek KM, Leonard DW. Ultrastructure of the corneal stroma: a comparative study. *Biophys J.* 1993;64:273-280.
8. Freund DE, McCally RL, Farrell RA, Cristol SM, L'Hernault NL, Edelhauser HF. Ultrastructure in anterior and posterior stroma of

Appendix 4

perfused human and rabbit corneas: relation to transparency. *Invest Ophthalmol Vis Sci.* 1995;36:1508-1523.

9. Kanai A, Kaufman HE. Electron microscopic studies of corneal stroma: ageing changes of collagen fibres. *Ann Ophthalmol.* 1973; 5:285-292.
10. Craig AS, Parry DAD. Collagen fibrils of the vertebrate corneal stroma. *J Ultra Mol Struct Res.* 1981;74:232-239.
11. Borcherding MS, Blacik LJ, Sittig RA, Bizzell JW, Breen M, Weinstein HG. Proteoglycans and collagen fibre organisation in human corneoscleral tissue. *Exp Eye Res.* 1975;21:59-70.
12. Fullwood NJ, Meek KM. A synchrotron X-ray study of the changes occurring in the corneal stroma during processing for electron-microscopy. *J Microsc.* 1993;169:53-60.
13. Craig AS, Robertson JG, Parry DAD. Preservation of corneal collagen fibril structure using low-temperature procedures for electron microscopy. *J Ultra Mol Struct Res.* 1986;96:172-175.
14. Daxer A, Misof K, Grabner B, Ettl A, Fratzl P. Collagen fibrils in the human corneal stroma: structure and ageing. *Invest Ophthalmol Vis Sci.* 1998;39:644-648.
15. Oster G, Riley DP. Scattering from cylindrically symmetric systems. *Acta Crystallogr.* 1952;5:272-276.
16. Worthington CR, Inouye H. X-ray diffraction study of the cornea. *Int J Biol Macromol.* 1985;7:2-8.
17. Meek KM, Fullwood NJ, Cooke PH, et al. Synchrotron X-ray diffraction studies of the cornea, with implications for stromal hydration. *Biophys J.* 1991;60:467-474.
18. Hart RW, Farrell RA. Light scattering in the cornea. *J Opt Soc Am.* 1969;59:766-774.
19. Freund DE, McCally RL, Farrell RA. Direct summation of fields for light scattering by fibrils with applications to normal corneas. *Appl Opt.* 1986;25:2739-2746.
20. Martola EL, Baum JL. Central and peripheral corneal thickness. *Arch Ophthalmol.* 1968;79:28-30.
21. Edmund C. Determination of the corneal thickness profile by optical pachometry. *Acta Ophthalmol.* 1987;65:147-152.
22. Leonard DW, Meek KM. Estimation of the refractive indices of collagen fibrils and ground substance of the corneal stroma using data from X-ray diffraction. *Biophys J.* 1997;72:1382-1387.
23. Krenchel H. *Fibre Reinforcement.* Copenhagen, Denmark: Akademisk Forlag; 1964.
24. Maurice DM. The cornea and sclera. In: Davson H, ed. *The Eye.* New York: Academic Press; 1969:489-599.
25. Muir H, Bullough P, Maroudas A. The distribution of collagen in human articular cartilage with some of its physiological implications. *J Bone Surg Ser B.* 1970;52:554-563.
26. Fratzl P, Daxer A. Structural transformation of collagen fibrils in corneal stroma during drying: an X-ray scattering study. *Biophys J.* 1993;64:1210-1214.
27. Hanna KD, Jouve FE, Waring GO, Ciarlet PG. Computer simulation of arcuate keratotomy for astigmatism. *Refract Corneal Surg.* 1992;8:152-163.
28. Moreira H, Campos M, Sawush MR, McDonnell JM, Sand B, McDonald PJ. Holmium laser thermokeratoplasty. *Ophthalmology.* 1993;100:752-761.
29. Newton RH, Meek KM. The integration of the corneal and limbal fibrils in the human eye. *Biophys J.* 1998;75:2508-2512.
30. Newton RH, Meek KM. Circumcorneal annulus of collagen fibrils in the human limbus. *Invest Ophthalmol Vis Sci.* 1998;39:1125-1134.
31. Meek KM, Newton RH. Organisation of collagen fibrils in the corneal stroma in relation to mechanical properties and surgical practice. *J Refract Surg.* 1999;15:695-699.

Eye (2003) 17, 927–936

www.nature.com/eye

Transparency, swelling and scarring in the corneal stroma

KM Meek[1], DW Leonard[2], CJ Connon[1], S Dennis[1] and S Khan[1]

Abstract

Purpose **This paper briefly reviews current explanations for corneal transparency and uses a well-developed model to try to explain the increased light scattering either accompanying corneal swelling or following phototherapeutic keratectomy (PTK).**
Methods **The direct summation of fields (DSF) method was used to compute light transmission as a function of wavelength. The method requires input of a number of structural parameters. Some of these were obtained from electron micrographs and others were calculated from X-ray diffraction data.**
Results **By swelling sections of stroma cut from different depths in the tissue, we have shown that fluid entering the cornea causes more swelling in the posterior lamellae than in the anterior lamellae. Furthermore, posterior lamellae can reach a higher final hydration than anterior lamellae. Collagen-free regions ('lakes') exist in corneas swollen *in vitro* and in Fuch's dystrophy corneas, many of which may be caused by the death of cells. The DSF method shows that local fibril disordering, increased refractive index mismatch, and increased corneal thickness together can account for a 20% increase in light scattering in a Fuch's dystrophy cornea at $H = 5.8$ compared to the normal cornea. Additional scattering is probably caused by 'lakes'. The DSF method applied to PTK rabbit stroma with high levels of haze suggests that the newly deposited collagen is not the cause of the increased light scattering.**
Conclusions **Fluid is not uniformly distributed within the corneal stroma when the cornea swells. Increased hydration of posterior lamellae may be because of known differences in the glycosaminoglycans between the anterior and posterior stroma. Lamellar interweave in the anterior stroma probably limits the extent to which the constituent lamellae can swell. The DSF method can be used to account for increased light scattering in oedematous corneas but cannot account for haze following PTK.**

Eye (2003) **17**, 927–936. doi:10.1038/sj.eye.6700574

Keywords: corneal transparency; stroma; swelling; oedema; phototherapeutic keratectomy

Introduction

One of the most remarkable properties of the cornea is its ability to transmit almost all the incident light in the visible part of the spectrum. The reasons for corneal transparency have occupied scientists for many decades and despite considerable advances in our understanding, to date there is still no universally accepted explanation. Even more perplexing are the causes of increased light scattering in the cornea during wound healing or in some pathological situations.

In this paper, we briefly review some of the theories put forward to explain corneal transparency and use the most well tested of these to try to model the light scattering expected from oedematous corneas and from corneas following phototherapeutic keratectomy (PTK).

Corneal transparency

Any system where the attenuation of light is only caused by scattering (in other words there are no other losses such as might be due, for example, to absorption) can be described by

$$F_t = \exp(-\alpha_s t) \quad (1)$$

where F_t is the percentage of the incident light transmitted without scattering, α_s is the scattering attenuation coefficient, and t is the

[1]Cardiff Institute of Tissue Engineering and Repair and Department of Optometry and Vision Sciences Cardiff University Cardiff, UK

[2]The Open University Oxford Research Unit Oxford, UK

Correspondence:
KM Meek
Cardiff Institute of Tissue Engineering and Repair and Department of Optometry and Vision Sciences Cardiff University Redwood Building, Cardiff CF10 3NB, UK
Tel: +442920 876317
Fax: +442920 874859
E-mail: Meekkm@cf.ac.uk

Received: 28 February 2003
Accepted in revised form: 28 February 2003

This work was funded by the Wellcome Trust and is currently funded by the Medical Research Council

thickness in the direction of the light path. In the case of a corneal lamella consisting of parallel collagen fibrils, the scattering attenuation coefficient can be written as the product $\rho\sigma$, where ρ is the number of fibrils per unit area in a cross-section (often called the bulk fibril number density or simply the number density) and σ is the scattering cross-section. Over the years there have been many models put forward to explain transparency; the difference between these models essentially depends on the mathematical formulation of the scattering cross-section term. Here we describe the most important of these models. All must consider the structure of the cornea, that is, the size and shape of the stromal constituents and their refractive indices since each of these factors influences the amount of light scattered by the structure. In particular, the refractive index of the collagen fibrils, the refractive index of the extrafibrillar material, and the ratio of these two refractive indices, all play a major role in determining the extent of light scattered by the stroma.

The simplest model[1] proposes that all corneal components have a *uniform* refractive index (which is equivalent to a zero value for the scattering cross-section). This essentially means that light cannot distinguish between fibrils and the material between them, hence it can propagate directly through the tissue unscattered. This model is generally rejected, partly because it fails to explain two important properties of the cornea, birefringence and transparency loss when the structure is distorted. Also, recent X-ray diffraction data have unambiguously confirmed earlier evidence for a difference in the refractive indices of the collagen fibrils and of the extrafibrillar material.[2]

Most modern models are based on the lattice theory put forward by Maurice.[3] By approximating the collagen fibril to perfect, infinitely long cylinders, an estimate of the scattering from an individual fibril can be calculated. The refractive index difference between the fibrils and interfibrillar matrix means that each fibril scatters a small amount of light. However, if the fibrils are packed in a lattice arrangement, correlation in their relative positions leads to destructive interference of light scattered away from the forward direction, all the light energy going into the constructive interference in the forward direction. However, both electron microscopy and X-ray diffraction do not show the presence of this regular packing of collagen fibrils.[4,5]

Table 1 shows these two models alongside the other main models, which are all based on Maurice's early work. Hart and Farrell[4] showed that only short-range order in the positions of the collagen fibrils is necessary for the required destructive interference of scattered photons. Results from X-ray diffraction showed that the type of short-range order in the packing seen in electron micrographs is indeed what is found in the tissue.[5] Feuk[6] developed a long-range order model based on small, random displacements of the fibrils from ideal lattice sites. Twersky,[7] assuming that the fibrils were arranged as in a two-dimensional fluid, expressed the distribution explicitly in terms of the volume fraction occupied by the fibrils. Benedek[8] considered the problem from the point of view of fluctuations in the fibril number density. These concepts were explored quantitatively by Vaezy and Clark,[9] who examined fluctuations in the spatial arrangement of the collagen fibrils using Fourier methods. Recently, Ameen *et al*[10] used photonic band structure methods to explain light transmission through corneal lattices. Space is too limited to go into these models in greater detail, so, for a fuller account, the reader is directed to reviews by Farrell and McCally[11] and Freegard.[12] A more generalised mathematical review of transparency in biological tissues is by Tuchin.[13]

Table 1 Models to explain corneal transparency

Perfect crystal lattice	Maurice (1957)[3]
Uniform refractive index	Smith (1969)[1]
Short-range order	Hart and Farrell (1969)[4]
Average area/fibril=correlation area	Benedek (1971)[8]
Perturbed lattice	Feuk (1971)[6]
Hard-core fibrils with PG coating	Twersky (1975)[7]

By way of a summary, it has been pointed out by Farrell and McCally[11] that all currently viable transparency theories agree with three points:

1. each fibril is an ineffective scatterer;
2. despite this, the large number of fibrils requires that destructive interference of scattered light must occur; and
3. the cornea is thin.

Direct summation of fields method

In 1986, Freund *et al*[14] published a method to compute light scattering from the cornea, following on from the theoretical principles previously advanced by Hart and Farrell.[4] The technique can be used to predict transmission by an arbitrary short-range order distribution of different-sized fibrils. A full account of the approach, called the direct summation of fields (DSF) method, is found in the original papers.[14,15] It is a statistical technique in which the scattering from each individual fibril is computed, then the effects of interference are included and summed for the whole tissue using a method called ensemble averaging. It is worth mentioning at this stage that, in this method, transmission is computed as a function of wavelength, ignoring the lamellar structure of the stroma and also the

presence of stromal cells. With these assumptions in mind, however, the DSF method has been tested and found to give reliable results in a number of situations.[16–18]

In order to use DSF to compute the expected light transmission, it is necessary to measure a number of structural and physical properties of the stroma. The refractive index of the hydrated collagen fibrils, the refractive index of the interfibrillar matrix, and the ratio of these have previously been obtained using X-ray diffraction measurements in a number of different species.[2] The relative positions of the individual fibrils, and the diameter of each fibril, are obtained from electron micrographs. There is a problem in using measurements from electron microscopy in that it has been shown that a number of microscope preparation protocols result in considerable shrinkage of fibril diameters and, particularly, interfibril spacings.[19] To overcome this problem, we have used X-ray diffraction (a technique where corneas can be examined without the need for any processing[20]) to measure the mean values of these parameters in the same tissue as used for microscopy, and then scaled the data from electron micrographs so as to compensate for this shrinkage. Table 2 gives the values for several of these parameters for human corneas. The corneas were obtained from the Eye Bank in culture medium, and were dehydrated to close to physiological hydration using polyethylene glycol.[21] It should be noted that the value for the fibril number density is lower than previously reported, partly owing to the scaling procedure.

Fibril diameters and spacings were measured by image analysis of selected electron micrographs where collagen fibrils were sectioned in cross-section. The positions and diameters of collagen fibrils in a human cornea were obtained after image analysis of these micrographs and scaled using X-ray data from the same samples as described above. By taking the corneal thickness as 0.52 mm and combining these data with the refractive index data in Table 2, the DSF method was used to predict the transmission as a function of wavelength. As expected (Figure 1), transmission was predicted to exceed 90% throughout most of the visible spectrum.

In their original paper[4] and later[16,15,11] Farrell and co-workers made only limited reference to how changes in

Table 2 Data from normal human cornea (relevant parameters were used in the direct summation of fields method to predict light transmission (Figure 1))

Average fibril diameter	30.8 ± 0.8 nm
Refractive index of fibrils	1.411 ± 0.001
Refractive index of extrafibrillar matrix	1.365 ± 0.003
Refractive index ratio	1.033 ± 0.002
Number density	$292 \pm 70\ \mu m^2$

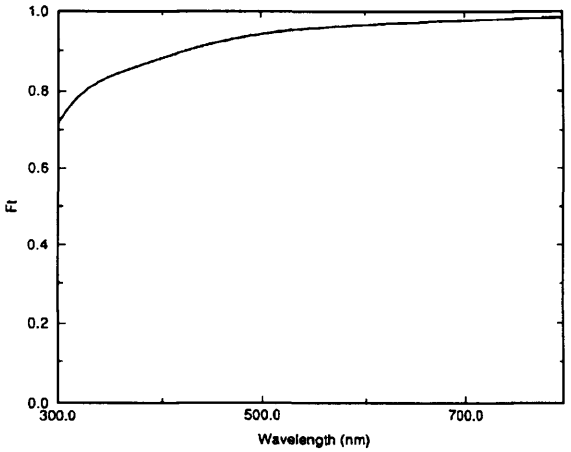

Figure 1 The summation of scattered fields method was used to predict transmission (F_t) as a function of wavelength in the human cornea. Data on corneal fibril positions and sizes were obtained from electron micrographs and were scaled to account for shrinkage during specimen preparation. Other data were taken from Table 2.

the individual parameters might affect transparency in abnormal conditions. It is of interest to examine the theoretical effects of changing each of these parameters, keeping the rest constant, so as to gauge to which parameters light transmission is most sensitive. It should be remembered that here we are testing a single model for transparency, which has certain implicit assumptions about the tissue. Note also that this is a theoretical situation; in practice, many of the parameters are related, and a change in one is often accompanied by a change in one or more of the others. With these caveats, Figure 2a shows that increasing the fibril radius to 20 nm reduces transmission, particularly in the blue end of the spectrum, whereas reducing the radius has the opposite effect. So why not have small collagen fibrils in humans, as is found in fish? The answer is probably down to tissue mechanics — larger fibrils mean a stronger cornea.

The independent effect of the fibril number density on light scattering is difficult to assess, as altering the fibril number density by increasing the separation of the fibrils simultaneously changes the effects of interference. However, we find that keeping the relative positions of the fibrils constant but moving the fibrils apart (Figure 2b) leads to less scattering (greater transmission). An important point to realise, however, is that, contrary to what is often asserted, increased interfibril spacings (for example, when the cornea swells) are not *per se* responsible for the increased light scattering that accompanies oedema.

From Equation (1) it is clear that light scattering will increase with increased corneal thickness (assuming the increased thickness is because of extra tissue mass rather

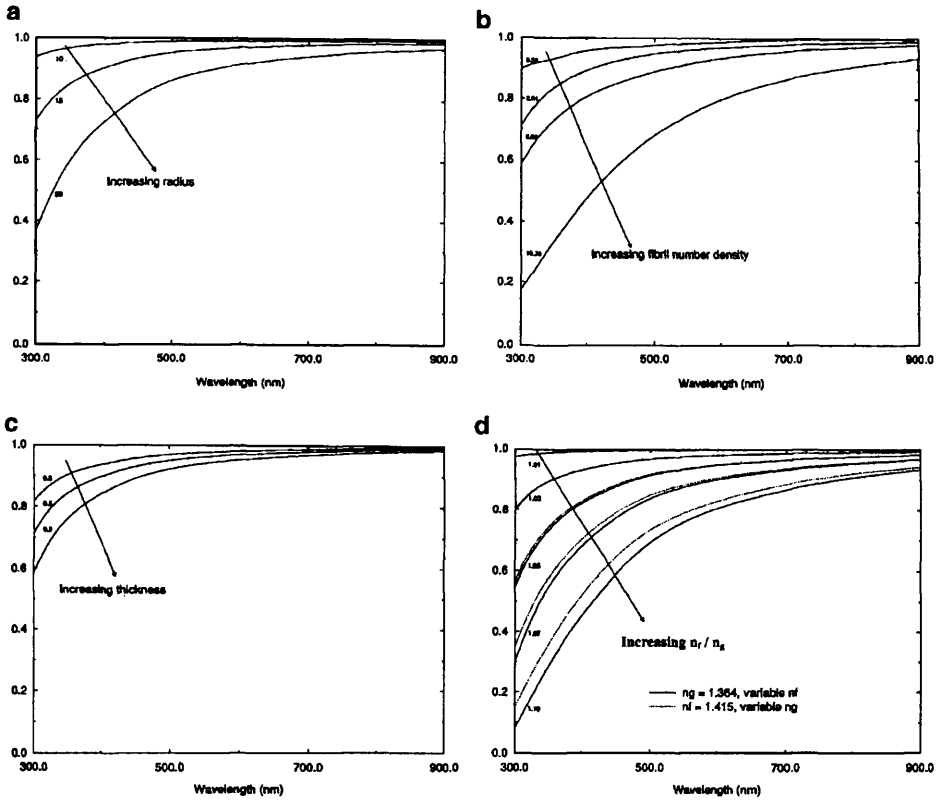

Figure 2 Theoretical effects of varying individual parameters as predicted by the summation of scattered fields model. The predicted transmission of light (F_t) is plotted against wavelength. The number by each curve represents the values of the parameters being varied, in units of nm (a), $\mu m^{-2} \times 10^{-2}$ (b), and mm (c).

than oedema). However, Figure 2c shows that this effect is relatively small, the corneal thickness could almost double without seriously increasing scattering. This presumably accounts for why, for example, a bovine cornea has similar transparency to a thinner human cornea.

Light transmission through the cornea is very sensitive to an increased mismatch in the refractive indices of the collagen and the extrafibrillar matrix. Theoretically, there are two ways of varying their ratio, either keep the refractive index of the fibrils constant and vary that of the matrix, or *vice versa*. Both have a similar effect (Figure 2d). If the ratio is one, there is total transmission throughout the spectrum. This is the uniform refractive index condition. As we increase the ratio, transmission reduces, once again, particularly at the blue end of the spectrum.

In conclusion, the DSF method can be used to demonstrate that light scattering in the cornea will increase if:

1. order in the spatial arrangement of the fibrils is destroyed;
2. fibril diameters increase;
3. fibril number density increases;
4. there is an increased refractive index imbalance between the hydrated fibrils and the extrafibrillar matrix;
5. corneal thickness increases.

So far, we have imagined the cornea as a structure made only of collagen fibrils and extrafibrillar matrix. Of course, there are a large number of keratocytes in the stroma, which gradually reduce in density from the anterior to the posterior stroma.[22,23] Maurice[3] believed that there were insufficient of these to contribute significantly to scattering. Besides, they are relatively thin in the direction of the light path through the cornea. More recently, Jester *et al*[24] have suggested that these cells contain special proteins called corneal crystallins, which produce a uniform refractive index in the cells and may match the refractive index of the cytoplasm to that of the surrounding matrix. This, together with the dimensions of the cells, renders them weak scatterers (except for their nuclei, which are readily visible in the confocal microscope). However, if keratocytes change their shape

or spill their contents, a different situation ensues, and they are capable of becoming very efficient scatterers.[25,26]

Cornea oedema

An understanding of structure and transparency changes when the cornea swells is dependent on our knowledge of where imbibed water is situated, both at the level of the tissue as a whole and within the lamellae themselves.

In many animals, the anterior stroma is less ordered,[15] less hydrated,[27–29] has a higher keratocyte density,[22,23] has a lower keratan sulphate (KS) to chondroitin/dermatan sulphate (DS) ratio,[28] and is less easily swollen[29–31] than the posterior stroma. We have examined four frozen human corneas (two at physiological hydration and two swollen in culture medium). These were sectioned at 100 μm intervals from the anterior to posterior using a Mikrom sliding microtome. All sections were weighed and then placed in dH_2O. At fixed intervals, each section was reweighed and then returned to the dH_2O to continue swelling until a constant weight was reached. The hydration of each section was calculated for both the physiological and the swollen corneas. The results (Figure 3) confirm results from other species[27–29] and show that hydration increases with tissue depth in both the physiological and the swollen human corneas. This may be related to the gradual increase in the KS/DS ratio with depth, since KS is known to show greater water absorption than DS.[32,33] However, as Bron[34] has pointed out it is possible that there is a differential loss of proteoglycans between anterior and posterior stroma as the cornea swells and this, if it happens, would affect the swelling at different stromal depths.

The corneal sections were immersed in distilled water until they essentially stopped swelling. The final hydrations achieved were plotted as a function of tissue depth (Figure 4). We found that the maximum achievable hydration increases as a function of depth. This means that the posterior stroma is capable of swelling much more than the anterior. It is likely that anterior swelling is limited by lamellar interweaving and insertions into Bowman's layer, a phenomenon that may have considerable importance in maintaining the correct shape of the cornea.[31,34]

Information on the distribution of imbibed water *within* the lamellae has been obtained using X-ray diffraction methods. When the denuded cornea swells, there is a linear relation between the fibril separation *squared* and the hydration.[35] Interfibrillar centre-to-centre spacings were determined for bovine corneas as a function of hydration using X-ray diffraction, and the results are shown in Figure 5 (line a). By extrapolating this line to $H = 0$, it is possible to plot a theoretical graph of the expected interfibril spacing on the assumption that all the water entering the stroma has gone towards separating the constituent fibrils.[5,21] This theoretical plot is shown in Figure 5 (line b). The shading around the theoretical plot is the uncertainty owing to the uncertainty in determining the spacing at $H = 0$ from the experimental data. The interesting point is that at a given hydration, the interfibril spacing is lower than it should be considering the amount of water in the stroma. This must mean that some of the water is not between fibrils, and thus must be in fibril-free regions. Some of these regions are probably places occupied by cells that have died post mortem. If we assume that keratocytes occupy

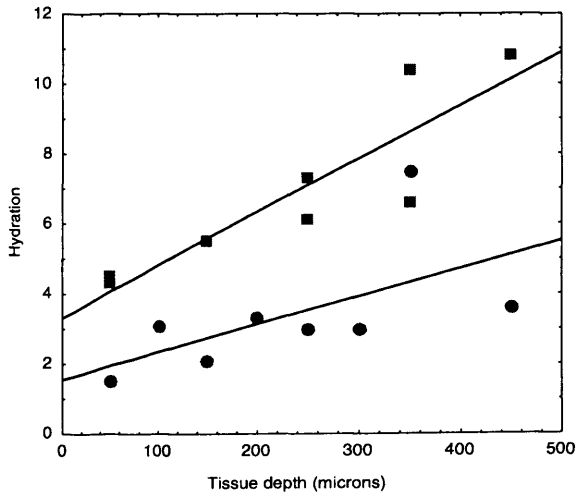

Figure 3 Hydration plotted as a function of stromal depth in the normal and swollen human cornea. (Circles) data from two corneas at about $H = 3$; (squares) data from two corneas at about $H = 7$.

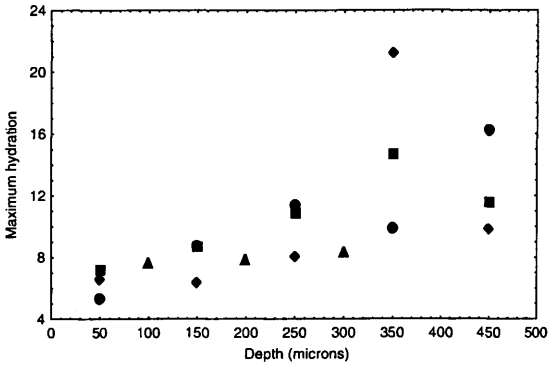

Figure 4 The final hydration achieved in four human corneas plotted as a function of stromal depth. (Circles) 72-year-old male subject; (squares) 82-year-old female subject; (diamonds) 91-year-old male subject; (triangles) 79-year-old male subject.

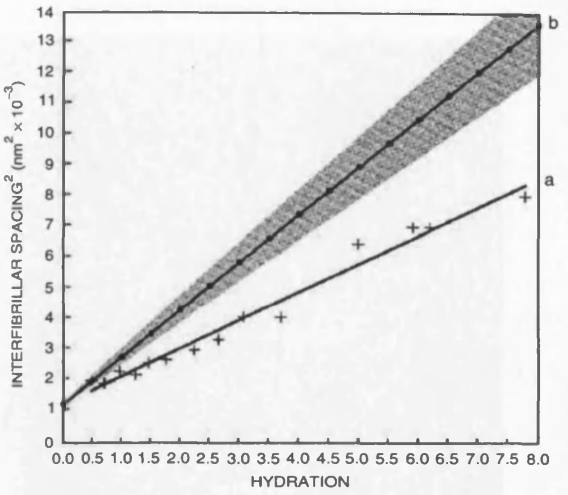

Figure 5 Graph (a) shows the variation of the centre-to-centre collagen fibril spacing (squared) plotted as a function of tissue hydration. The data were obtained using low-angle synchrotron X-ray diffraction. Graph (b) is the theoretical centre-to-centre fibril spacing on the assumption that all the fluid entering the stroma is distributed evenly between the collagen fibrils. The shaded area represents the uncertainty in line (b) owing to the uncertainty in determining the intersect of line (a) at $H=0$. Reproduced from Meek *et al*[21] with permission.

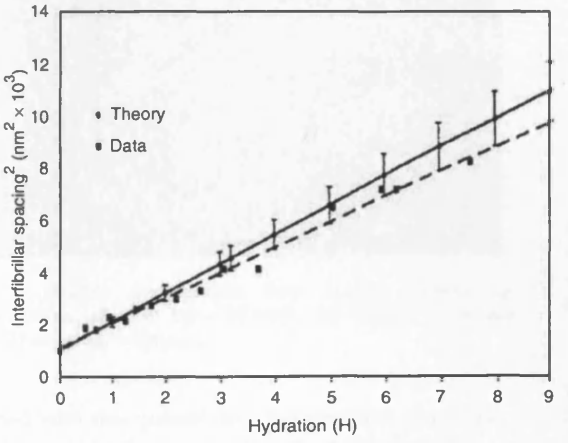

Figure 6 The lower line shows the data from line (a) in Figure 5. The upper line shows the theoretical centre-to-centre collagen fibril spacing on the assumption that 15% of the fluid entering the stroma goes into fibril-free regions ('lakes'). Reproduced from Huang and Meek[36] with permission.

15% of the stromal volume, we can take this into account in the theoretical calculation, and the match between theory and experiment becomes much better (Figure 6).

So it appears that fibril-free regions ('lakes') form in swollen corneas, and that when cells die, the spaces previously occupied by them might themselves become 'lakes' that could contribute to an increase in light scattering.

Light scattering in oedematous corneas

A full survey of the literature probing the causes of scattering when the cornea swells is beyond the scope of this article. From a theoretical standpoint, 'lakes' would add a term to the total scattering cross-section that would vary as B/λ^2.[37,38] By measuring transmission as corneas swelled, Farrell *et al* were able to compute the scattering cross-section and demonstrated that it has a $1/\lambda^2$ dependence, as predicted by the presence of 'lakes'.[35] Lakes are not seen in the normal human cornea, but they are present in bullous keratopathy and Fuch's dystrophy corneas.[39] Some fibril-free regions appear to be because of matrix disorder (Figure 7), while others might reflect the presence of dead cells. The question is, to what extent does the intralamellar disordering lead to light scattering?

In principle, the summation of scattered fields approach could again be used to compute the theoretical effects of disordering and/or lakes. The required structural information (fibril positions, diameters, number density) can be obtained from electron micrographs scaled according to the X-ray diffraction measurements as described previously. However, as the cornea swells, the extra water will change the refractive indices of the interfibrillar matrix and also, possibly, of the collagen fibrils themselves. However, we know from previous studies[21] that collagen fibrils do not swell appreciably above physiological hydration, so their refractive index is independent of tissue hydration and stays constant at 1.416. As water or electrolyte enters the interfibrillar matrix, it dilutes it and the refractive index falls. The amount by which it falls can be estimated by measuring the change in the refractive index of the stroma as a function of tissue thickness or hydration (Figure 8) and then applying Gladstone and Dales's law of refractive indices to the system.[2] Since the imbibed fluid does not enter the fibrils themselves,[21] this fall in the refractive index as the stroma swells leads to an increase in the ratio of the refractive index of the fibrils to that of the interfibrillar matrix and to a corresponding increase in light scattering. We found that between physiological hydration and $H=3.8$, there was a 0.15% reduction in the refractive index of the matrix and a corresponding 0.1% increase in the ratio of the refractive indices of the fibrils and the matrix (S Khan, S Dennis, and K Meek, unpublished results). Between physiological hydration and $H=5.8$, these percentages were 0.59% and 0.58%, respectively.

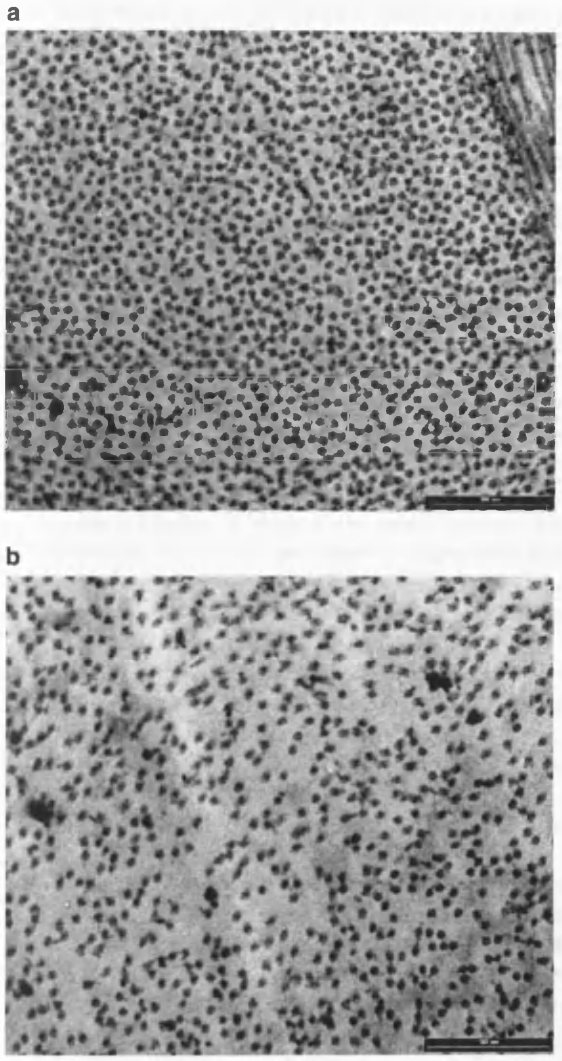

Figure 7 Electron micrographs from human corneas: (a) normal cornea ($H = 3.8$; bar = 500 nm). (b) Fuch's dystrophy cornea ($H = 5.8$; bar = 500 nm).

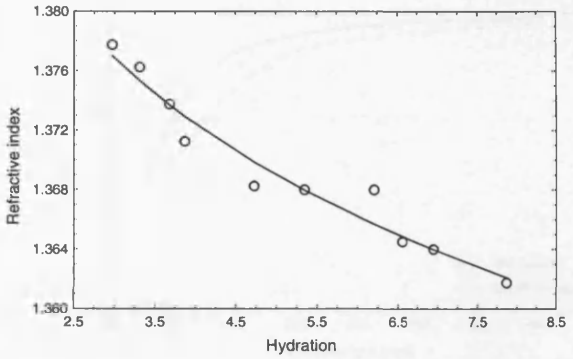

Figure 8 Refractive index of the human cornea plotted as a function of tissue hydration. The hydration of the stroma was altered by dialysing the denuded stroma against phosphate buffer pH 7.1[36] to which different amounts of the osmotic agent polyethylene glycol were added.[21] The continuous line is a least-squares best fit to the data points.

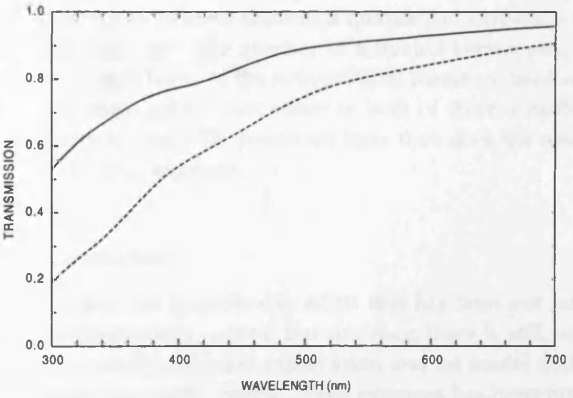

Figure 9 The Summation of Scattered Fields method was used to predict transmission as a function of wavelength in the swollen human corneas. (Continuous line) normal; (broken line) Fuch's dystrophy.

Armed with this quantitative information, it is now possible to apply the summation of scattered fields method to Fuch's dystrophy corneas. The result is shown in Figure 9. It can be appreciated that the intralamellar disruption in the spatial arrangement of fibrils, the increased mismatch in the refractive indices, and the increased thickness of the stroma together lead to the overall reduction in light transmission.

Phototherapeutic keratectomy

It is well known that haze develops following laser ablation to the anterior stroma. The definition of haze is difficult because of the different methods used to measure it, and even less certain is the origin of the haze.[40] Various authors have ascribed the observed haze to irregularities in the epithelium,[41,42] to subepithelial deposits,[43] to the presence of vacuoles,[44] to the deposition of poorly organised collagen,[45,46] or to the presence of activated keratocytes.[25,26] However, none of these suggestions have been experimentally or theoretically shown to account for increased light scattering. We have used PTK in rabbits to predict the percentage transmission of visible light through the newly deposited collagen using the DSF method and hence to see if this collagen could account for the observed haze. All experimental procedures were carried out in accordance with the ARVO Resolution on the Use of animals in Ophthalmic and Vision Research.

PTK took place at St Thomas' Hospital London using an Omnimed excimer laser (Summit Technology, Boston, MA, USA) with a wavelength of 193 nm. The pulse energy resulted in a radiant exposure of 180 mJ/cm^2 at a pulse frequency of 10 Hz. The beam shape was circular with a fixed diameter of 6.0 mm. Wounds were allowed to heal for up to 19 months. We used an objective measurement for corneal haze developed by Lohmann *et al*[47] in which haze was determined using a slit-lamp-mounted charged-coupled device (CCD) system. The results of the haze measurements are shown in Figure 10 and confirm that both a transitory haze (which peaks after a month) and a more persistent or late developing haze (which remains for many months) occur. The question we address here is to what extent the persistent haze can be ascribed to the nature of the newly deposited collagen.

After 8 months of healing, the rabbit corneas had laid down a layer of newly deposited collagen that had almost compensated for the amount removed (approximately 100 μm). Apart from the most superficial layer, most of this collagen had formed a lamellar structure, although the order in the fibril packing was visibly poor. Micrographs were taken at different depths and typical ones were used in the DSF method to predict light transmission. In this case, however, we had no information about refractive indices in the new matrix, so we made the assumption that these were normal.

Figure 11 shows that despite the fact that the fibril diameters and organisation had not returned to normal, only a very small drop in light transmission is predicted. This is probably due, in large part, to the fact that the newly deposited layer extended to only about 100 μm. The thinness of this collagenous layer, therefore, counteracts the increased scattering caused by the poor organisation of the new collagen. It appears, therefore,

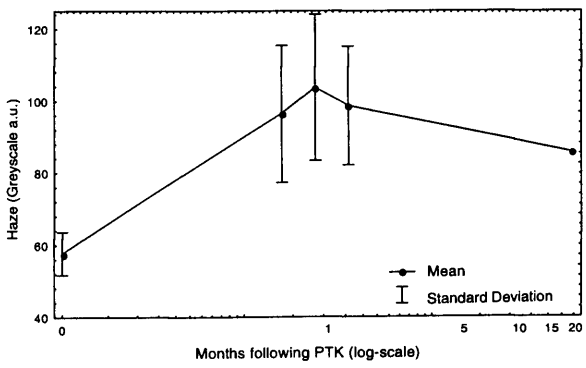

Figure 10 Development of haze as a function of time during wound healing in rabbit corneas. Reproduced from Connon *et al*[48] with permission.

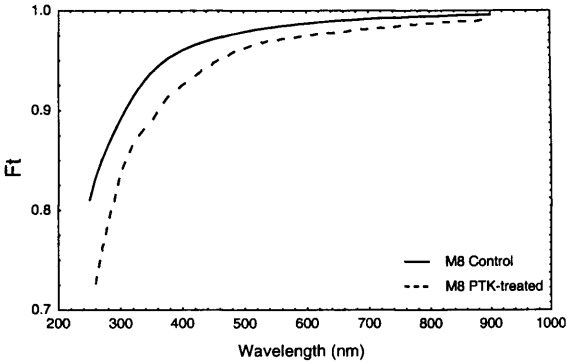

Figure 11 The Summation of Scattered Fields method was used to predict transmission as a function of wavelength in a rabbit cornea 8 months after PTK and in its control cornea. Reproduced from Connon *et al*[48] with permission.

that newly deposited collagen is not the cause of persistent haze following PTK. Electron microscopy of our rabbit corneas showed a qualitative correlation between haze, the number of activated keratocytes, and the smoothness of the subepithelial basement lamina. We therefore believe that either or both of these contribute more to post-PTK persistent haze than does the newly deposited collagen.

Conclusions

Despite the considerable effort that has been put into understanding corneal transparency, there is still no universally accepted explanation and no model that has been thoroughly tested. Some progress has been made, particularly with respect to our understanding of what factors govern corneal fibril size[49,50] and organisation, including the roles of the ambient ions[51] and of proteoglycans. The recent availability of gene-targeted mice with null mutations for selected proteoglycans[52–54] now makes it possible to correlate the structural effect of selected deletions with tissue transparency. For example, it is interesting that lumican-null mice have cloudy corneas,[52] decorin-null mice have clear corneas,[53] and keratocan-null mice have mostly clear corneas.[54] These and similar tissues open the possibility to greatly increase our understanding of the causes of light scattering from abnormal corneas in the near future.

Acknowledgements

We thank Professor John Marshall and Anne Patmore for carrying out the PTK and making the haze measurements shown in Figure 10. We also thank Mr Nick Hawksworth for supplying postoperative

Appendix 5

pathological corneas, Dr Val Smith for supplying normal human corneas from the Bristol Eye Bank, and Dr S Akhtar for assistance with electron microscopy. We are grateful to the staff at the SRS Daresbury laboratory for their ongoing help with the data collection.

References

1 Smith JW. The transparency of the corneal stroma. *Vis Res* 1969; **9**: 393–396.
2 Leonard DW, Meek KM. Refractive indices of the collagen fibrils and extrafibrillar material in the corneal stroma. *Biophys J* 1997; **72**: 1382–1387.
3 Maurice DM. The structure and transparency of the corneal stroma. *J Physiol* 1957; **136**: 263–286.
4 Hart RW, Farrell RA. Light scattering in the cornea. *J Opt Soc Am* 1969; **59**: 766–774.
5 Sayers Z, Koch MHJ, Whitburn SB, Meek KM, Elliott GF, Harmsen A. Synchrotron X-ray diffraction study of the corneal stroma. *J Mol Biol* 1982; **160**: 593–607.
6 Feuk T. On the transparency of the stroma in the mammalian cornea. *IEEE Trans Biomed Eng* 1970; **BME17**: 1866–1890.
7 Twersky V. Transparency of pair-correlated, random distributions of small scatterers, with applications to the cornea. *J Opt Soc Am* 1975; **65**: 524–530.
8 Benedek GB. Theory and transparency of the eye. *Appl Opt* 1971; **10**: 459–473.
9 Vaezy S, Clark JI. Quantitative analysis of the microstructure of the human cornea and sclera using 2-D Fourier methods. *J Microsc* 1994; **175**: 93–99.
10 Ameen DB, Bishop MF, McMullen T. A lattice model for computing the transmissivity of the cornea and sclera. *Biophys J* 1998; **75**: 2520–2531.
11 Farrell RA, McCally RL. Corneal transparency. In: Albert DM, Jakobiec FA (eds). *Principles and Practice of Ophthalmology*. WB Saunders: Philadelphia, PA, 2000, pp 629–643.
12 Freegard TJ. The physical basis of transparency of the normal cornea. *Eye* 1997; **11**: 465–471.
13 Tuchin VV. Light scattering study of tissues. *Phys Usp* 1997; **40**: 495–515.
14 Freund DE, McCally RL, Farrell RA. Direct summation of fields for light scattering by fibrils with applications to normal corneas. *Appl Opt* 1986; **25**: 2739–2746.
15 Freund DE, McCally RL, Farrell RA, Cristol SM, L'Hernault NL, Edelhauser HF. Ultrastructure in anterior and posterior stroma of perfused human and rabbit corneas: relation to transparency. *Invest Ophthalmol Vis Sci* 1995; **36**: 1508–1523.
16 Freund DE, McCally RL, Farrell RA. Light scattering tests of structure in normal and swollen rabbit corneas. *Johns Hopkins APL Tech Dig* 1991; **12**: 137–143.
17 Leonard DW. The ultrastructure of the corneal stroma and its implications for transparency. PhD thesis, The Open University, Milton Keynes, UK, 1996.
18 Rawe IM, Leonard DW, Meek KM, Zabel RW. X-ray diffraction and transmission electron microscopy of Morquio Syndrome Type A cornea: a structural analysis. *Cornea* 1997; **16**: 369–376.
19 Fullwood NJ, Meek KM. A synchrotron X-ray study of the changes occurring in the corneal stroma during processing for electron microscopy. *J Microsc* 1993; **169**: 53–60.
20 Meek KM, Quantock AJ. The use of X-ray scattering techniques to determine corneal ultrastructure. *Prog Ret Eye Res* 2001; **20**: 95–137.
21 Meek KM, Fullwood NJ, Cooke PH, Elliott GF, Maurice DM, Quantock AJ *et al*. Synchrotron X-ray diffraction studies of the cornea with implications for stromal hydration. *Biophys J* 1991; **60**: 467–474.
22 Patel S, McLaren J, Hodge D, Bourne W. Normal human keratocyte density and corneal thickness measurement by using confocal microscopy *in vivo*. *Invest Ophthalmol Vis Sci* 2001; **42**: 333–339.
23 Moller-Pedersen T, Ehlers N. A three-dimensional study of the human corneal keratocyte density. *Curr Eye Res* 1995; **14**: 459–464.
24 Jester JV, Moller-Pedersen T, Huang J, Sax CM, Kays WT, Cavangh HD *et al*. The cellular basis of corneal transparency: evidence for 'corneal crystallins'. *J Cell Sci* 1999; **112**: 613–622.
25 Moller-Pedersen T, Cavanagh HD, Petroll WM, Jester JV. Stromal wound healing explains refractive instability and haze development after photorefractive keratectomy: a 1-year confocal microscopic study. *Ophthalmology* 2000; **107**: 1235–1245.
26 Moller-Pedersen T. The cellular basis of corneal transparency and haze development (Abstract). *Ophthalmic Res* 2002; **34**: 4.
27 Turss R, Friend J, Reim M, Dohlman CH. Glucose concentration and hydration of the corneal stroma. *Ophthalmic Res* 1971; **2**: 253–260.
28 Castoro JA, Bettelheim AA, Bettelheim FA. Water gradients across bovine cornea. *Invest Ophthalmol Vis Sci* 1988; **29**: 963–968.
29 Lee D, Wilson G. Non-uniform swelling properties of the corneal stroma. *Curr Eye Res* 1981; **1**: 457–461.
30 Kikkawa Y, Hirayama K. Uneven swelling of the corneal stroma. *Invest Ophthalmol* 1970; **9**: 735–741.
31 Müller L, Pels E, Vrensen GFJM. The specific architecture of the anterior stroma accounts for maintenance of corneal curvature. *Br J Ophthalmol* 2001; **85**: 437–443.
32 Plessy B, Bettelheim FA. Water vapor sorption of keratan sulfate. *Mol Cell Biochem* 1975; **6**: 85–91.
33 Bettelheim FA, Plessy B: The hydration of proteoglycans of bovine cornea. *Biochim Biophys Acta* 1975; **381**: 203–214.
34 Bron AJ. The architecture of the corneal stroma. *Br J Ophthalmol* 2001; **85**: 379–383.
35 Goodfellow JM, Elliott GF, Woolgar AE. X-ray diffraction studies of the corneal stroma. *J Mol Biol* 1978; **119**: 237–252.
36 Huang Y, Meek KM. Swelling studies on the cornea and sclera: the effects of pH and ionic strength. *Biophys J* 1999; **77**: 1655–1665.
37 Farrell RA, McCally RL, Tatham PER. Wavelength dependencies of light scattering in normal and cold swollen rabbit corneas and their structural implications. *J Physiol (London)* 1973; **233**: 589–612.
38 Farrell RA, McCally RL. On corneal transparency and its loss with swelling. *J Opt Soc Am* 1976; **66**: 342.
39 Quantock AJ, Meek KM, Brittain P, Ridgway AE, Thonar EJ. Alteration of the stromal architecture and depletion of keratan sulphate proteoglycans in oedematous human corneas: histological, immunochemical and X-ray diffraction evidence. *Tissue Cell* 1991; **23**: 593–606.

Appendix 5

40 Corbett MC, Marshall J. Corneal haze after photorefractive keratectomy, a review of etiological mechanisms and treatment options. *Lasers Light* 1996; **7**: 173–196.
41 Tuft SJ, Marshall J, Rothery S. Stromal remodelling following photorefractive keratectomy. *Lasers Ophthalmol* 1987; **1**: 177–183.
42 Marshall J, Trokel S, Rothery S, Krueger RR. Long term healing of the central cornea after photorefractive keratectomy using an excimer laser. *Ophthalmology* 1988; **95**: 1411–1421.
43 Hanna KD, Pouliquen Y, Waring GO, Savoldelli M, Cotter J, Morton K *et al*. Corneal stromal wound healing after 193 nm excimer laser ablation. *Arch Ophthalmol* 1989; **107**: 895–901.
44 Rawe IM, Zabel RW, Tuft SJ, Chen V, Meek KM. A morphological study of rabbit corneas after laser keratectomy. *Eye* 1992; **6**: 637–642.
45 Fantes FE, Hanna KD, Waring III GO, Pouliquen Y, Thompson KP, Savoldelli M. Wound healing after excimer laser keratomileusis in monkeys. *Arch Ophthalmol* 1990; **108**: 665–675.
46 Wu WCS, Stark WJ, Green WR. Corneal wound healing after 193 excimer laser keratectomy. *Arch Ophthalmol* 1991; **109**: 1426–1432.
47 Lohmann CP, Fitzke F, O'Brart D, Muir MK, Timberlake G, Marshall J. Corneal light scattering and visual performance in myopic individuals with spectacles, contact lenses, or excimer laser photorefractive keratectomy. *Am J Ophthalmol* 1993; **155**: 444–453.
48 Connon CJ, Marshall J, Patmore AL, Brahma A, Meek KM. Persistent haze and disorganisation of anterior stromal collagen appear unrelated following phototherapeutic keratectomy (PTK). *J Refract Surg* 2003; **19**: 1–11.
49 Adachi E, Hayashi T. *In vitro* formation of hybrid fibrils of type V collagen and type I collagen. Limited growth of type I collagen into thick fibrils by type V collagen. *Connect Tissue Res* 1986; **14**: 257–266.
50 Birk DE. Type V collagen: heterotypic type I/V collagen interactions in the regulation of fibril assembly. *Micron* 2001; **32**: 223–237.
51 Kostyuk O, Nalovina O, Mubard T, Reginio JW, Meek KM, Quantock AJ *et al*. Transparency of the bovine corneal stroma at physiological hydration and its dependence on concentration of the ambient anion. *J Physiol* 2002; **243**(2): 633–642.
52 Chakravarti S, Petroll WM, Hassell JR, Jester JV, Lass JH, Paul J *et al*. Corneal opacity in lumican-null mice: defects in collagen fibril structure and packing in the posterior stroma. *Invest Ophthalmol Vis Sci* 2000; **41**: 3365–3373.
53 Danielson KG, Baribault H, Holmes DF, Graham H, Kadler KE, Iozzo RV. Targeted disruption of decorin leads to abnormal collagen fibril morphology and skin fragility. *J Cell Biol* 1997; **136**: 729–743.
54 Saika S, Shiraishi A, Liu CY, Funderburgh JL, Kao CW, Converse RL *et al*. Role of lumican in the corneal epithelium during wound healing. *J Biol Chem* 2000; **275**: 2607–2612.

Biophysical Journal Volume 85 October 2003 2205–2212

Changes in the Refractive Index of the Stroma and Its Extrafibrillar Matrix When the Cornea Swells

Keith M. Meek, Sally Dennis, and Shukria Khan
Structural Biophysics Group, Department of Optometry and Vision Sciences, Cardiff University, Cardiff, United Kingdom

ABSTRACT The transparency of the corneal stroma is critically dependent on the hydration of the tissue; if the cornea swells, light scattering increases. Although this scattering has been ascribed to the disruption caused to the arrangement of the collagen fibrils, theory predicts that light scattering could increase if there is an increased mismatch in the refractive indices of the collagen fibrils and the material between them. The purpose of this article is to use Gladstone and Dale's law of mixtures to calculate volume fractions for a number of different constituents in the stroma, and use these to show how the refractive indices of the stroma and its constituent extrafibrillar material would be expected to change as more solvent enters the tissue. Our calculations predict that solvent entering the extrafibrillar space causes a reduction in its refractive index, and hence a reduction in the overall refractive index of the bovine stroma according to the equation $n'_s = 1.335 + 0.04/(0.22 + 0.24\,H')$, where n'_s is the refractive index and H' is the hydration of the swollen stroma. This expression is in reasonable agreement with our experimental measurements of refractive index versus hydration in bovine corneas. When the hydration of the stroma increases from $H = 3.2$ to $H = 8.0$, we predict that the ratio of the refractive index of the collagen fibrils to that of the material between them increases from 1.041 to 1.052. This change would be expected to make only a small contribution to the large increase in light scattering observed when the cornea swells to $H = 8$.

INTRODUCTION

The cornea is the major refracting lens in the eye, responsible for some two-thirds of the eye's total dioptic power. Measurements of corneal refractive index have been made by a number of researchers in a variety of animal species, and most authors report values very close to 1.375 (Maurice, 1957; Farrell and McCally, 2000; Sivak, 1988).

The cornea not only refracts most of the incident light, but it also transmits >95% of this light. Corneal transparency has been the subject of much study over the years (Maurice, 1957; Hart and Farrell, 1969; Smith, 1969; Feuk, 1970; Benedek, 1971; Twersky, 1975; Worthington, 1984; Freund et al., 1986, 1995). It is now generally accepted that transparency depends on the destructive interference of light scattered away from the forward direction and that this, in turn, requires a certain amount of short-range ordering of collagen fibril positions (Hart and Farrell, 1969; Farrell and McCally, 2000). In Farrell's model, the scattering cross section per unit length for an isolated fibril, σ, may be expressed as (Farrell and McCally, 2000):

$$\sigma = \frac{k^3(n_f + n_e)^2}{8n_e^4}\left\{1 + \frac{2}{(m^2+1)^2}\right\} \times \frac{R_0^2\rho_s^2}{\rho^2}\left\{\frac{(1-f_f^s)M_c - f_f^s M_g}{(1-f_f^s)}\right\}^2, \quad (1)$$

where k is the modulus of the scattering vector, $m = n_f/n_e$, ρ_s is the mass density of the stroma, ρ is the number of fibril axes per unit area in a cross-section cut, R_0 is the refractive increment (the change in refractive index with solute concentration), f_f^s is the volume fraction occupied by the hydrated fibrils in the stroma, and M_c and M_g are the mass fractions of dry collagen in the fibrils and biomolecules in the extrafibrillar matrix, respectively. From this equation it is clear that the scattering cross section depends on n_f, n_e, and hence m, i.e., the refractive indices of the hydrated collagen fibrils, of the extrafibrillar matrix, and their ratio.

Apart from the uniform refractive index model (Smith, 1969), all other explanations of corneal transparency assume that there is a significant difference in the values of n_f and n_e. Unfortunately, the two components (collagen fibrils and extrafibrillar matrix) cannot easily be isolated and examined in their physiological state, so it is not possible to obtain direct measurements of their refractive indices accurately (Maurice, 1957). Instead, their values must be estimated from known physical and chemical properties of the stroma and its constituents. Maurice (1957) found the refractive index of dry collagen, n_c, to be 1.55, and went on to calculate n_f as 1.47 and n_e as 1.345. In a later article, these values were refined to $n_f = 1.51$ and $n_e = 1.345$ (Maurice, 1969).

Worthington (1984) used Gladstone and Dale's law of mixtures together with known values of the relative weights and densities of the corneal components to calculate the refractive indices. This was later refined by Leonard and Meek (1997) to give values of $n_f = 1.416$ and $n_e = 1.356$ for bovine corneal stroma. These were close to the values for human corneas reported by Freund and co-workers (Freund et al., 1995; $n_f = 1.407$ and $n_e = 1.352$). However, all the methods mentioned above rely on assumptions, many of which are now known to be incorrect. With measurements of volume fractions computed directly from x-ray diffraction

Submitted January 20, 2003, and accepted for publication July 7, 2003.

Address reprint requests to Keith M. Meek, Redwood Bldg., King Edward VII Ave., Cathays Park, Cardiff University, Cardiff CF10 3NB, UK. Tel.: 44-292-087-6317; E-mail: meekkm@cf.ac.uk.

0006-3495/03/10/2205/08 $2.00

Appendix 6

data, Leonard and Meek (1997) used Gladstone and Dale's law to calculate the refractive indices for four species. They also reported average values from 40 species of $n_f = 1.416$ and $n_e = 1.359$. Very little difference in refractive indices was found between the species studied.

There is much uncertainty as to the mechanism by which light scattering increases as the cornea swells. Several changes occur in the tissue, some of which probably affect scattering more than others. For example, the hydrations of the various components are altered to differing degrees and their refractive indices change accordingly. The fibrils move further apart so that the phase difference between the various scattered waves is altered, changing scattering cross sections (Farrell and McCally, 2000). The number density and volume fraction of the fibrils both decrease. Freund et al. (1986) have produced a robust method for calculating corneal transmission from normal and swollen corneas, and have tested the method on slightly swollen corneas (up to 25%; Freund et al., 1991). However, to precisely relate changes in structure to changes in transparency as the cornea swells, it is necessary to know how the extra water is distributed (inside/outside fibrils, within "lakes"; Meek et al., 1991; Huang and Meek, 1999), how the collagen fibril arrangement changes (Freund et al., 1991; Meek and Quantock, 2001), and how the refractive indices change. The purpose of the present article is to address this last issue. Only when we know how the refractive indices change as fluid enters the stroma can we model how this affects light scattering (Benedek, 1989).

In this article we develop a simplified theoretical model of the corneal stroma consisting of hydrated, pseudo-hexagonally packed collagen fibrils embedded in a homogeneous, hydrated matrix. First, we apply Gladstone and Dale's law of refractive indices to calculate the volume fraction occupied by solvent in the physiological stroma. Along the way, we calculate values for a number of important structural parameters in the cornea. In the second part of the article, we apply the same law to determine a relationship between the refractive index of the whole stroma, and later the refractive index of the extrafibrillar matrix, as a function of tissue hydration. In the final part of the article, we compare the results of the theoretical variation of stromal refractive index versus hydration, with experimentally measured values.

Gladstone and Dale's law of mixtures applied to stroma at physiological hydration

According to Gladstone and Dale's law, the refractive index of a composite may be expressed as the partial sum of the refractive indices of its components n_1, $n_2, \ldots n_N$, each weighted by the volume fraction occupied by that component, $f_1, f_2, \ldots f_N$ (Maurice, 1957; Worthington, 1984):

$$n_{tot} = n_1 f_1 + n_2 f_2 + \cdots + n_N f_N. \quad (2)$$

Gladstone and Dale's law allows us to calculate a number of different volume fractions and refractive indices. Applying this law to the corneal stroma, and substituting known values for the refractive index of the bovine cornea, the refractive index of dry collagen and the refractive index of salt solution (solvent) (Table 2), the following expressions can be derived (the derivation of these equations is given in detail in Leonard and Meek, 1997, their Eqs. 9 and 10; however, the equations have been slightly modified from those in Leonard and Meek, 1997, by replacing the refractive index of water, 1.333, by the refractive index of salt solution, 1.335):

$$n_f = 1.335 + 0.212 f_c^f \quad (3)$$

$$n_e = 1.335 + \frac{0.042 - 0.212 f_c^s}{1 - f_f^s}, \quad (4)$$

where f_c^s and f_f^s are the volume fractions of dry fibrillar material in the stroma and hydrated fibrils in the stroma, and f_c^f is the volume fraction of collagen molecules in a fibril (see Table 1). The volume fractions f_c^s and f_f^s are related by:

$$f_c^f = f_c^s / f_f^s. \quad (5)$$

The value of f_c^f can be found by considering a unit cell along the length of a collagen fibril (Katz and Li, 1973),

$$f_c^f = \rho M_c / 5 D p_m^2 N_A \sin\gamma, \quad (6)$$

where ρ is the partial specific volume of collagen, M_c is the molecular weight of collagen, D is the collagen axial periodicity, p_m is the center-to-center lateral spacing of

TABLE 1 Definitions and values for various volume fractions when the stroma is at physiological hydration

Symbol	Meaning	Value
f_c^f	Volume fraction of collagen molecules in a hydrated fibril	0.37*
f_c^s	Volume fraction of dry fibrillar material in the stroma	0.12*
f_p^s	Volume fraction of dry extrafibrillar material in the stroma	0.10*
f_f^s	Volume fraction of hydrated fibrillar material in the stroma	0.32*
f_e^s	Volume fraction of hydrated extrafibrillar material in the stroma	0.68*
f_{iw}^s	Volume fraction of intrafibrillar solvent in the stroma	0.20
f_{ew}^s	Volume fraction of extrafibrillar solvent in the stroma	0.58
f_w^f	Volume fraction of solvent in a fibril	0.63
$f_p'^e$	Volume fraction of dry extrafibrillar material in the swollen extrafibrillar matrix	Function of tissue hydration
$f_p'^s$	Volume fraction of dry extrafibrillar material in the swollen stroma	Function of tissue hydration
$f_e'^s$	Volume fraction of hydrated extrafibrillar material in the swollen stroma	Function of tissue hydration

*Leonard and Meek (1997).

Appendix 6

TABLE 2 Definitions and values for refractive indices when the stroma is at physiological hydration

Symbol	Meaning	Value
n_s	Refractive index of stroma at physiological hydration	1.375*
n_f	Refractive index of hydrated fibrils	1.413
n_e	Refractive index of hydrated extrafibrillar matrix	1.359
n_c	Refractive index of dry collagen	1.547†
n_p	Refractive index of dry extrafibrillar material	1.485
n_w	Refractive index of solvent (salt solution)	1.335‡

*Sivak (1988).
†Maurice (1957, 1969).
‡Farrell and McCally (2000).

collagen molecules within a fibril, γ is the packing angle of the collagen molecules, and N_A is Avogadro's number. Substituting known values of these parameters and the value of p_m obtained from wide-angle x-ray diffraction, Leonard and Meek (1997) obtained the value $f_c^f = 0.37$.

Leonard and Meek (1997) considered the stroma to consist of "unit cells" representing the average volume occupied by each fibril (thus neglecting the contribution of keratocytes to the stromal volume). With this model, they estimated the volume fraction per unit length of fibrils in the stroma, f_f^s, from the interfibrillar center-to-center Bragg spacing, p_i, and the fibril diameter, a, both of which can be measured from low-angle x-ray diffraction patterns from the cornea (Gyi et al., 1988; Meek and Leonard, 1993), using

$$f_f^s = \pi a^2/(4 \times 1.12 p_i^2). \quad (7)$$

The factor 1.12 relates the Bragg spacing from a liquidlike arrangement of fibrils (Worthington and Inouye, 1985) to the equivalent mean center-to-center spacing of the fibrils in a pseudo-hexagonal lattice. For bovine cornea at physiological hydration they calculated a value of $f_f^s = 0.32 \pm 0.08$. Although the uncertainty was rather large, the mean value was close to the average value of the fibril volume fraction from 40 species ($f_f^s = 0.28 \pm 0.03$). Using the calculated values of f_c^f, f_c^s, and f_f^s specific for cow (Table 1), we can substitute into Eqs. 3 and 4 to obtain $n_f = 1.413$ and $n_e = 1.359$.

By compartmentalizing the hydrated stroma into hydrated collagen fibrils, dry extrafibrillar matrix, and extrafibrillar solvent, we can, for completeness, calculate the volume fractions of fibrillar and nonfibrillar fluid, although for the purposes of later arguments, separation into fibrillar and nonfibrillar compartments is not really necessary. Gladstone and Dale's law may be written as

$$n_s = n_f f_f^s + n_p f_p^s + n_w f_{ew}^s, \quad (8)$$

where the meaning of the symbols is defined in Tables 1 and 2.

We also know that

$$f_f^s + f_p^s + f_{ew}^s = 1, \quad (9)$$

from which we can use known values of f_f^s and f_p^s to calculate $f_{ew}^s = 0.58 \pm 0.08$. The estimated uncertainty is based on the precision of the value for f_f^s.

We therefore know values of all the terms in Eq. 8 except n_p, which can thus be determined, giving the value $n_p = 1.485$. The uncertainties in the values of f_f^s and f_{ew}^s imply that this figure has a precision of better than 4%.

The next step is to consider the compartmentalization of the solvent and the collagen within each fibril. Using the fact that $f_c^f + f_w^f = 1$, we see that $f_w^f = 0.63$. This value is written in Table 1.

Finally, we can calculate the volume fraction of intrafibrillar solvent in the stroma (f_{iw}^s) by using the fact that $f_{iw}^s = f_w^f \times f_f^s$. This value, $f_{iw}^s = 0.20$, is also presented in Table 1.

Gladstone and Dale's law applied to swollen corneas

Dependence of stromal refractive index on tissue hydration

Since the volume fractions of intrafibrillar and extrafibrillar solvent in the stroma are 0.20 and 0.58 respectively (Table 1), the total volume fraction of solvent in the stroma, f_w^s, is 0.78. If the cornea swells such that the volume of solvent increases by a factor P to $(1 + P) \times$ its initial value, then to a good approximation its hydration (weight of water/dry weight) also increases by a factor P (since the mass of the additional ions introduced is negligible compared with the mass of the stroma).

In this section, we will use the convention that primed notation refers to the values of parameters in the swollen cornea. Thus using V to represent the initial volume of the stroma, V_w for the initial volume of solvent in the stroma and V' for the new (swollen) volume of the stroma, we can write

$$V' = V + PV_w. \quad (10)$$

Hence,

$$V'/V = 1 + Pf_w^s, \quad (11)$$

where V_w/V is the volume fraction of the total solvent content of the stroma, f_w^s.

With the value for f_w^s given above, we get

$$V'/V = 1 + 0.78P. \quad (12)$$

It has been shown previously that, above physiological hydration, swelling of corneal collagen fibrils is negligible (Meek et al., 1991). If the additional solvent therefore does not go into the fibrils, the refractive index of the fibrils remains unchanged but the extra solvent in the extrafibrillar space will cause a reduction in the value of n_e. Furthermore, because the volume of the stroma is now greater, the various stromal volume fractions will change. The purpose of this section is to determine what changes occur in the volume fractions and the refractive indices, and hence to derive an

Appendix 6

expression for the expected change in the refractive index of the stroma as the tissue swells.

Equation 12 states that when the stroma swells, its volume increases by the factor 0.78 P. The volume fractions can be defined in terms of the new volume of the fibrils, V'_f, and the new volume of the swollen stroma as follows:

$$f'^s_f = V'_f/V'. \tag{13}$$

Since we assume the fibrils do not swell (Meek et al., 1991), the new volume of the fibrils, V'_f, is the same as the original volume of the fibrils, V_f, and substituting from Eq. 12,

$$f'^s_f = V_f/\{(1 + 0.78P)V\} = f^s_f/(1 + 0.78P), \tag{14}$$

where we have used the definition $f^s_f = V_f/V$. Similarly, since the volume occupied by dry extrafibrillar material, V_p, does not change, the new volume fraction of the dry extrafibrillar material in the stroma, f'^s_p, can be defined as

$$f'^s_p = V_p/V' = V_p/\{(1 + 0.78P)V\} = f^s_p/(1 + 0.78P). \tag{15}$$

Finally, since $f'^s_{ew} = 1 - (f'^s_f + f'^s_p)$, we get

$$f'^s_{ew} = 1 - \{(f^s_f + f^s_p)/(1 + 0.78P)\}. \tag{16}$$

With these new volume fractions, we can apply Gladstone and Dale's law to the swollen stroma:

$$n'_s = f'^s_f n_f + f'^s_p n_p + f'^s_{ew} n_w \tag{17}$$

or

$$n'_s = n_w + \{f^s_f n_f + f^s_p n_p - (f^s_f + f^s_p)n_w\}/(1 + 0.78P)\}. \tag{18}$$

This can be simplified by substituting the values from Tables 1 and 2:

$$\begin{aligned} n'_s &= 1.335 + (0.32 \times 1.413 + 0.10 \times 1.485 \times \\ &\quad (0.32 + 0.10) \times 1.335)/(1 + 0.78P) \\ &= 1.335 + 0.04/(1 + 0.78P). \end{aligned} \tag{19}$$

This equation shows how the refractive index of the stroma should vary as a function of the fractional increase in solvent above physiological hydration (P). To reexpress this in terms of the physiological value of the tissue hydration (H_{phys}) and the hydration of the swollen cornea (H'), we use the fact that:

$$H' = (1 + P)H_{phys} \tag{20}$$

or

$$P = (H'/H_{phys}) - 1.$$

Using the known value $H_{phys} = 3.2$ and substituting into Eq. 19 gives:

$$n'_s = 1.335 + 0.04/(0.22 + 0.24H'). \tag{21}$$

This relationship is plotted in Fig. 1. It should be noted that the model predicts that the refractive index of the swollen stroma depends on knowledge of only two parameters in the physiological stroma, the refractive index (obtained by setting $P = 0$ in Eq. 19), and the total volume fraction of the solvent (the value 0.78 in Eq. 19). The value for n_s used in the present work was taken from Leonard and Meek (1997), where no uncertainty was quoted. However, other measurements, including those from the present work, suggest this figure is accurate to $>\pm 0.2\%$. Our value for the volume fraction of solvent in the stroma was derived using some values for which the uncertainty was also not quoted. The only other determination we have seen for this quantity comes from Worthington (1984) who quotes 0.819 (again without a precision estimate), which differs from our value by 5%. Using these uncertainties, we have estimated the precision with which our theoretical relationship (Eq. 21) is known, and these confidence limits are included in Fig. 1.

Dependence of n_e and m on tissue hydration

As can be seen from Eq. 1, the important refractive indices, as far as transparency of the cornea is concerned, are those of the collagen fibrils (n_f) and the extrafibrillar matrix (n_e) as well as their ratio (m). It is now possible to calculate how these vary as solvent enters the stroma. On the assumption that the fibrils themselves do not swell (Meek et al., 1991), n_f will remain unchanged (i.e., $n'_f = n_f$). To calculate the dependence of n'_e on P, we start by applying Gladstone and Dale's law to the extrafibrillar matrix,

$$n'_e = n_w + f'^e_p(n_p - n_w), \tag{22}$$

where f'^e_p is the volume fraction of dry proteoglycans, etc., in the swollen extrafibrillar matrix.

But $f'^e_p = f'^s_p / f'^s_e$ where volume fractions are defined in Table 1, and from Eq. 15 and the known value of f^s_p,

$$f'^s_p = \frac{f^s_p}{1 + 0.78P} = \frac{0.10}{1 + 0.78P}. \tag{23}$$

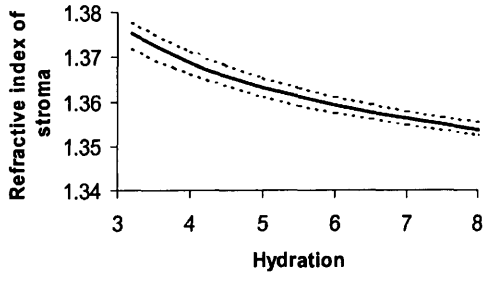

FIGURE 1 Refractive index of stroma as a function of tissue hydration calculated using Gladstone and Dale's law. Dotted lines indicate confidence limits of the solid curve.

Appendix 6

Also, since $f'^{s}_{e} + f'^{s}_{f} = 1$, we substitute for f'^{s}_{f} using Eq. 14 and write

$$f'^{s}_{e} = 1 - \{f^{s}_{f}/(1 + 0.78P) = 1 - 0.32/(1 + 0.78P), \quad (24)$$

using the known value of f^{s}_{f}.

We can thus use Eqs. 23 and 24 to determine f'^{e}_{p}:

$$f'^{e}_{p} = \frac{0.10}{0.68 + 0.78P}. \quad (25)$$

We can now substitute Eq. 25 into Eq. 22, insert known values from Table 1, and get the following:

$$n'_{e} = 1.335 + 0.015/(0.68 + 0.78P). \quad (26)$$

As before, this can be expressed in terms of H':

$$n'_{e} = 1.335 + 0.015/(0.244H' - 0.1). \quad (27)$$

This relationship is plotted in Fig. 2. The confidence limits represent the effects of the uncertainties in the values of n_p, f^{s}_{f}, and $(f^{s}_{iw} + f^{s}_{ew})$.

Finally, the ratio m' can be expressed as:

$$m' = n'_{f}/n'_{e} = 1.413/\{1.335 + 0.015/(0.244H' - 0.1)\}. \quad (28)$$

This relationship is plotted in Fig. 3.

Measurement of corneal refractive index

To test the relationship derived in Eq. 21 (Fig. 1), the refractive indices of swollen bovine corneas were measured as a function of tissue hydration.

Samples

Fresh bovine eyeballs were obtained from the abattoir and the corneal discs were excised from the eyes within 3 h of death. The endothelium and epithelium were removed by scraping with a scalpel and the epithelium side tagged using cotton. The corneas were wrapped in clingfilm and left at 4°C until needed.

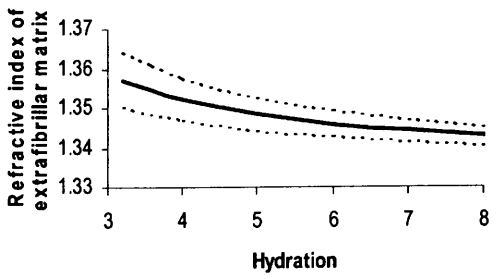

FIGURE 2 Refractive index of extrafibrillar matrix as a function of tissue hydration calculated using Gladstone and Dale's law. Dotted lines indicate confidence limits due to uncertainties in experimental data.

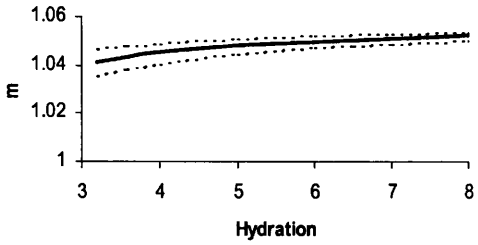

FIGURE 3 Refractive index ratio, m, as a function of tissue hydration, calculated using Gladstone and Dale's law. Dotted lines indicate confidence limits due to uncertainties in experimental data. The value $m = 1$ corresponds to the situation where the refractive indices of the collagen fibrils and the extrafibrillar matrix are equal. This was found not to be the case for either the physiological or the swollen stroma.

Tissue equilibrium

The individual corneas were placed in 14-kDa cutoff dialysis tubing, which was carefully smoothed to ensure no air bubbles were trapped inside. Each piece of dialysis tubing was clamped at both ends and then placed into an equilibration solution containing a fixed concentration of polyethylene glycol. Buffer equilibrium solutions of Na_2HPO_4/NaH_2PO_4 at pH 7.1 were used and NaCl was added as required to reach a final ionic strength (μm) of 0.03 as previously described by Huang and Meek (1999). Concentrations of 0, 0.5, 0.75, 1.0, 1.5, 2.0, 2.5, 2.7, 3.0, and 3.5% polyethylene glycol (20 kDa, BDH Ltd., Warwickshire, England) were used to adjust the hydration of the tissues (Meek et al., 1991). The refractive index of the swollen tissue was then measured as described below. The corneas were reweighed to allow an average hydration during the course of the experiment to be calculated. They were then placed in an oven at 60°C until a constant dry weight was obtained.

Tissue hydration (H) was calculated using the following equation:

$$H = \frac{Average\ Wet\ Weight - Dry\ Weight}{Dry\ Weight}$$

Refractometry

A bench-top Abbe 60 Series Refractometer (Bellingham and Stanley Ltd., Tunbridge Wells, England) was used for the experiment. This was calibrated using a silica test plate of known refractive index, supplied with the instrument, and the calibration was checked using a series of sugar solutions of known refractive index. The instrument was standardized before each experiment by adjusting the illumination to give a clear black/white boundary from distilled water. Transmitted illumination was from a bench lamp and reflected illumination from an in-built LED light source to observe the critical angle. This resulted in one side of the field of view from each cornea appearing black and the other white. All measurements were made at room temperature.

The cornea was placed on the refractometer stage tag-side-(anterior stroma)-up and the refractive index measured by adjusting the LED light source until a good borderline quality was observed. The cornea was then placed posterior-side-up and the refractive index was measured in the same way.

The average refractive index measurements from anterior and posterior stroma as a function of tissue hydration are shown in Fig. 4 *a*, and the predicted relationship (Eq. 21) is superimposed for comparison. A Pearson linear correlation analysis (Fig. 4 *b*) yielded a significant positive correlation of 0.78 ($p < 0.01$) between the experimental points and their corresponding theoretical values.

DISCUSSION

Leonard and Meek (1997) used their versions of Eqs. 3 and 4 to calculate the values $n_f = 1.413$ and $n_e = 1.357$. Corneal keratocytes are thought to occupy ~10% of the stromal volume (Kaye, 1969) and this was neglected in Leonard and Meek's calculations based on their x-ray diffraction data. However, if we assume the refractive index of the cells matches that of the extrafibrillar space, we can reapply Gladstone and Dale's law, taking into account the volume occupied by the keratocytes. If 10% of the stromal volume is not available to the fibrils, the fibrillar volume fraction is reduced from 0.32 to 0.29 and the volume fraction of the extrafibrillar material is increased from 0.68 to 0.71. From Eqs. 3 and 4, the effect of these changes is to leave the value of n_f unaltered, but to reduce the calculated value of n_e to 1.358. This represents <0.1% change in the value of the refractive index when the presence of cells is taken into account. For this reason it was decided to neglect the effects of keratocytes in the present work.

The refractive index of a polymer solution (such as the extrafibrillar matrix of the corneal stroma), n_e, can be expressed in terms of the specific refractive increment of the constituent proteins (R_o) and on their concentration (c):

$$n_e = n_w + R_o c. \quad (29)$$

For the cornea at physiological hydration, Eq. 25 gives the value $f_p^e = 0.147$ (setting $P = 0$). The density of the extrafibrillar material when dry is 1.06 gm/ml (Leonard and Meek, 1997), so its concentration is 1.06×0.147, which equals 0.156 gm/ml. The value of R_o for most proteins is ~0.18 ml/gm (Farrell and McCally, 2000). Substituting for these values, Eq. 29 gives $n_e = 1.362$ (taking the values of all parameters to three decimal places in the calculations). Within the precision of the volume fractions quoted in Table 1, we regard this to be in reasonable agreement with the value of $n_e = 1.359$ calculated in the present work.

We have shown both from a theoretical standpoint and experimentally how the average refractive index of the corneal stroma is reduced as the tissue swells. The agreement between experiment and theory, though showing a significant correlation, is clearly not exact (Fig. 4). Inspection of the distribution of data points in Fig. 4 *a* suggests that there is a shallower slope in the experimental data compared to the experimental curve. It is well-known that the anterior stroma swells very little in vitro (Müller et al., 2001), so its refractive index will not change much as the cornea as a whole swells. Conversely, most of the swelling takes place below these anterior layers, so changes in tissue hydration should primarily be reflected in changes in the refractive index of the posterior lamellae (Patel et al., 2000). This being the case, it is interesting to plot the swelling data for the anterior and the posterior stroma separately (Fig. 5). Despite the scatter in the experimental data points, it is evident that the theoretical expression fits the posterior swelling data (Fig. 5 *a*) better than the anterior data (Fig. 5 *b*), as expected.

Some caution is needed when applying the results to corneas swollen in vivo. For example, bulbous keratopathy, a condition where the stroma swells after surgical intervention, is known to be accompanied by changes in the composition of the extrafibrillar matrix (Quantock et al., 1991) which, in turn, may be expected to alter the refractive index in a way not predicted by the current analysis. However, the contribution of the nonaqueous fraction of the extrafibrillar matrix to the refractive index is relatively small (the matrix is very hydrated and becomes more so as the

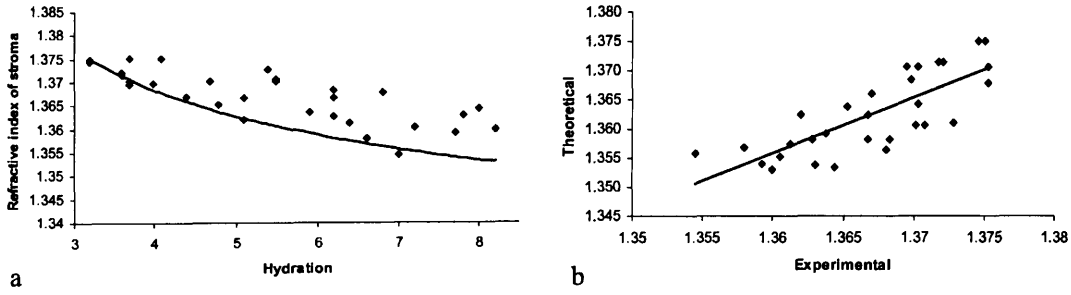

FIGURE 4 (*a*) Experimental values of the refractive index of bovine stroma (each point represents the average of anterior and posterior measurements from a given cornea) compared with the theoretical variation predicted by Eq. 21 (*continuous line*). (*b*) Linear regression of experimental and theoretical data in Fig. 4 *a* indicates a correlation coefficient of 0.78.

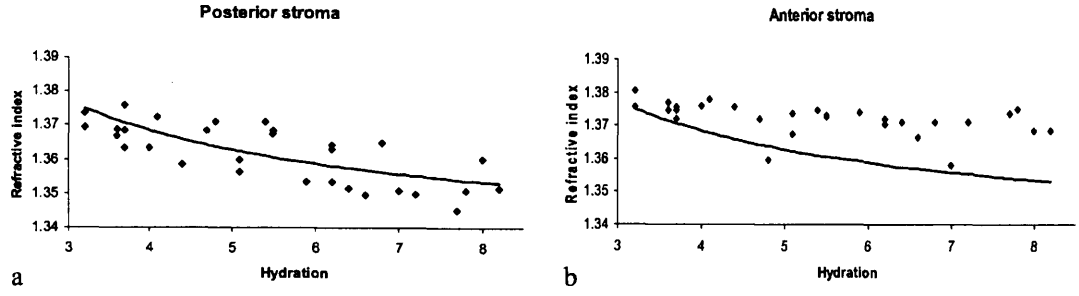

FIGURE 5 Refractive index measured at the posterior stroma (*a*) and anterior stroma (*b*). In each case, the continuous line is the theoretical prediction (Eq. 21).

tissue swells) and it will thus make only a small contribution to the refractive index.

In this article we have derived a simple expression that relates the refractive index of the corneal stroma to the increase in the volume fraction of solvent as the tissue swells (Eq. 19). From this it can be seen that only two parameters are required to specify the new refractive index, the refractive index of the stroma at physiological hydration and the volume fraction of solvent in the physiological stroma. We have calculated our value for the latter (78%) from the volume fractions of a number of other constituents, and it is in good agreement with the value of 77.2% estimated from the chemical composition of the stroma (Leonard and Meek, 1997). The change in refractive index with corneal swelling was previously studied by Fatt and Harris (1973), who produced a formula relating corneal refractive index to corneal thickness. However, their equation is asymptotic to $n_s = 1.342$, whereas, at very large hydrations, the refractive index of the stroma must approach that of the solvent, as does our Eq. 19.

In the bovine cornea, the refractive index is different on the epithelial and endothelial sides, as previously reported for human and porcine corneas (Patel et al., 1995; Watanabe and Uozato, 2001). This refractive gradient was shown by Patel and co-workers to have no practical importance in terms of the power of the normal cornea and may simply arise from the differential hydration between the anterior and posterior cornea (Castoro et al., 1988).

Changes in the refractive index of the extrafibrillar matrix as the cornea swells would be expected to affect light scattering. According to Eq. 1, an increase in m, the ratio of the refractive indices of the fibrils and the matrix, would cause scattering to increase, and it is possible that this contributes to the increased light scattering observed in swollen corneas. The actual effect of such a change is difficult to assess because the swelling will be accompanied by changes in other parameters on which transmission depends, such as order in the packing of the fibrils and their number density. However, if we consider the effects of changes in refractive index alone, assuming these other parameters remain constant, the transparency model of Freund et al. (1986) predicts that the change in refractive indices between $H = 3.2$ and $H = 8$ reported here would cause an ~5% increase in light scattering (Leonard, 1996; Meek et al., 2003), considerably less than the increase actually observed. It appears, therefore, that changes in refractive index of the extrafibrillar material make only a small contribution to the observed increase in light scattering when the cornea swells.

We thank Dr. Andrew Quantock for valuable advice and discussions.

This work was funded by a program grant from the Medical Research Council (G0001033) and a refurbishment grant from the Royal Society/ Wolfson Foundation.

REFERENCES

Benedek, G. B. 1971. Theory and transparency of the eye. *Applied Optics.* 10:459–473.

Benedek, G. B. 1989. The molecular basis for corneal transparency. *In* Proceedings of the Corneal Biophysics Workshop. Corneal Biomechanics and Wound Healing. L. A. McNicol, and E. Strahlman, editors. National Eye Institute, Bethesda, MD. 1–15.

Castoro, J. A., A. A. Bettelheim, and F. A. Bettelheim. 1988. Water gradients across bovine cornea. *Invest. Ophthalmol. Vis. Sci.* 29:963–968.

Farrell, R. A., and R. L. McCally. 2000. Corneal transparency. *In* Principles and Practice of Ophthalmology. D. M. Albert and F. A. Jakobiec, editors. W. B. Saunders: Philadelphia, PA. 629–643.

Fatt, I., and M. G. Harris. 1973. Refractive index of the cornea as a function of its thickness. *Am. J. Optom. Physiol. Opt.* 50:383–386.

Feuk, T. 1970. On the transparency of the stroma in the mammalian cornea. *IEEE Trans. Biomed. Eng. BME.* 17:1866–1890.

Freund, D. E., R. L. McCally, and R. A. Farrell. 1986. Direct summation of fields for light scattering by fibrils with applications to normal corneas. *Appl. Optics.* 25:2739–2746.

Freund, D. E., R. L. McCally, R. A. Farrell, S. M. Cristol, N. L. L'Hernault, and H. F. Edelhauser. 1995. Ultrastructure in anterior and posterior stroma of perfused human and rabbit corneas: relation to transparency. *Invest. Ophthalmol. Vis. Sci.* 36:1508–1523.

Freund, D. E., R. L. McCally, and R. A. Farrell. 1991. Light scattering tests of structure in normal and swollen rabbit corneas. *Johns Hopkins APL Tech. Digest.* 12:137–143.

Gyi, T. J., K. M. Meek, and G. F. Elliott. 1988. The interfibrillar spacings of collagen fibrils in the corneal stroma: a species study. *Int. J. Biol. Macromol.* 10:265–269.

Appendix 6

Hart, R. W., and R. A. Farrell. 1969. Light scattering in the cornea. *J. Opt. Soc. Am.* 59:766–774.

Huang, Y., and K. M. Meek. 1999. Swelling studies on the cornea and sclera: the effects of pH and ionic strength. *Biophys. J.* 77:1655–1665.

Katz, E. P., and S. T. Li. 1973. The intermolecular space of reconstituted collagen fibrils. *J. Mol. Biol.* 73:351–369.

Kaye, G. I. 1969. Stereologic measurements of cell volume fraction of rabbit corneal stroma. *Arch. Ophthalmol.* 82:792–794.

Leonard, D. W. 1996. The ultrastructure of the corneal stroma and its implications for transparency. Ph.D. Thesis. The Open University, Milton Keynes, UK.

Leonard, D. W., and K. M. Meek. 1997. Refractive indices of the collagen fibrils and extrafibrillar material of the corneal stroma. *Biophys. J.* 72: 1382–1387.

Maurice, D. M. 1969. The cornea and sclera. *In* The Eye. H. Davson, editor. Academic Press, New York. 489–599.

Maurice, D. M. 1957. The structure and transparency of the corneal stroma. *J. Physiol.* 136:263–286.

Meek, K. M., and A. J. Quantock. 2001. The use of x-ray scattering techniques to determine corneal ultrastructure. *Prog. Ret. Eye Res.* 20:95–137.

Meek, K. M., and D. W. Leonard. 1993. Ultrastructure of the corneal stroma: a comparative study. *Biophys. J.* 64:273–280.

Meek, K. M., N. J. Fullwood, P. H. Cooke, G. F. Elliott, D. M. Maurice, A. J. Quantock, and R. S. Wall. 1991. Synchrotron x-ray diffraction studies of the cornea with implications for stromal hydration. *Biophys. J.* 60: 467–474.

Meek, K. M., D. W. Leonard, C. J. Connon, S. Dennis, and S. Khan. 2003. Transparency, swelling and scarring in the corneal stroma. *Eye*. In press.

Müller, L. J., E. Pels, and G. F. J. M. Vrensen. 2001. The specific architecture of the anterior stroma accounts for maintenance of corneal curvature. *Br. J. Ophthalmol.* 85:437–443.

Patel, S., J. L. Alió, and J. J. Pérez-Santonja. 2000. A model to explain the difference between changes in refraction and central ocular surface power after laser in situ keratomileusis. *J. Refract. Surg.* 16:330–335.

Patel, S., J. Marshall, and F. W. Fitzke, III. 1995. Refractive index of the human corneal epithelium and stroma. *J. Refract. Surg.* 11:100–105.

Quantock, A. J., K. M. Meek, P. Brittain, A. E. A. Ridgway, and E. J.-M. A. Thonar. 1991. Alteration of the stromal architecture and depletion of keratin sulphate proteoglycans in oedematous human corneas: histological, immunochemical and x-ray diffraction evidence. *Tissue Cell.* 23:593–606.

Sivak, J. G. 1988. Corneal optics in aquatic animals: how they see above and below. *In* The Cornea: Transactions of the World Congress on the Cornea. H. D. Cavanagh, III, editor. Raven Press Ltd., New York. 181–186.

Smith, J. W. 1969. The transparency of the corneal stroma. *Vision Res.* 9:393–396.

Twersky, V. 1975. Transparency of pair-correlated, random distributions of small scatterers, with applications to the cornea. *J. Opt. Soc. Am.* 65:524–530.

Watanabe, C., and H. Uozato. 2001. Distribution of refractive index of the cornea. *Invest. Ophthalmol. Vis. Sci.* 42:S899.

Worthington, C. R. 1984. The structure of cornea. *Quart. Rev. Biophys.* 17:423–451.

Worthington, C. R., and H. Inouye. 1985. X-ray diffraction study of the cornea. *Int. J. Biol. Macromol.* 7:2–8.

Available online at www.sciencedirect.com
SCIENCE DIRECT®
Journal of Structural Biology 146 (2004) 359–367
Journal of Structural Biology
www.elsevier.com/locate/yjsbi

Spatial mapping of collagen fibril organisation in primate cornea—an X-ray diffraction investigation

Craig Boote,* Sally Dennis, and Keith Meek

Structural Biophysics Group, School of Optometry and Vision Sciences, Cardiff University, Wales, UK

Received 23 October 2003, and in revised form 15 December 2003

Abstract

New insights are presented into the collagenous structure of the primate cornea. Wide-angle X-ray diffraction was used to map the fibrillar arrangement and distribution of collagen over three common marmoset corneas. The maps provide a point of reference to help interpret data from pathological corneas or primate models of refractive surgery. The results herein disclose a circum-corneal annulus of highly aligned collagen, 0.5–1.5 mm wide, where the cornea and sclera fuse at the limbus; a feature similar to that observed in human tissue. As in humans, the annulus is not uniform, varying in width, fibril angular spread, and collagen density around its circumference. However, more centrally the marmoset cornea exhibits a preferred lamella orientation in which proportionally more fibrils are oriented along the superior–inferior corneal meridian. This observation is in striking contrast with the situation in human cornea, where there is an orthogonal arrangement of preferentially aligned fibrils. Investigation of a further 16 corneas confirmed that approximately 33% (±1%) ($n = 76$) of fibrils in the central marmoset cornea lie within a 45° sector of the superior–inferior meridian. Implications for the mechanical and optical properties of the cornea are discussed.

Keywords: Cornea; Collagen; Lamellar structure; X-ray fibre diffraction; Primate; Marmoset monkey; Biomechanical; Light polarisation; Birefringence

1. Introduction

The cornea performs an essential dual function in the mammalian visual system: protecting the contents of the eye whilst also serving as its principal refracting surface. Maintenance of correct corneal curvature, and hence normal refractive function, is contingent on the tissue's ability to withstand both external mechanical trauma and the intra-ocular pressure. This requisite mechanical toughness is provided by the collagenous architecture of the corneal stroma. The stroma constitutes the majority of the corneal thickness and exhibits a fine structure characterised by layers of stacked lamellae (Maurice, 1957). Each lamella is composed of regularly spaced collagen fibrils which run parallel to each other and the corneal surface, but subtend fairly large angles with fibrils in adjacent lamellae (Komai and Ushiki, 1991). Restoring forces in the stretched fibrils act to balance any applied force on the cornea and thereby confer tensile reinforcement on the tissue. It has been established that, for fibrils of a given diameter, the tensile strength of a collagenous connective tissue will be governed largely by: (1) the orientation of the fibrils with respect to the applied force, and (2) the volume fraction of collagen in the tissue (Hukins and Aspden, 1985; Jeronimidis and Vincent, 1984). Thus a direct role for collagen fibril organisation in promoting biomechanical stability, and hence corneal shape, appears likely. Given that corneal shape strongly influences refractive status, there is considerable interest in establishing how the direction and quantity of stromal fibrils vary over the corneal surface.

The orientation of corneal lamellae in the human eye has been the subject of investigation for some time. Kokott (1938) put forward evidence of a preferential lamellar direction in the central cornea in which proportionally more fibrils are oriented along the

*Corresponding author. Fax: +44-29-2087-4859.
E-mail address: bootec@cf.ac.uk (C. Boote).

1047-8477/$ - see front matter © 2004 Elsevier Inc. All rights reserved.
doi:10.1016/j.jsb.2003.12.009

Appendix 7

superior–inferior and medial–lateral meridians than in the oblique sectors. This was later confirmed and quantified by X-ray diffraction (Daxer and Fratzl, 1997; Meek et al., 1987). Later Newton and Meek (1998a,b) discovered that in more peripheral corneal regions this arrangement no longer predominates, and characterised a well-defined circumferential annulus of fibrils at the limbus. The clinical import of this is that the anisotropy in lamella orientation across the cornea could explain why incisions at some positions are more likely to produce post-operative astigmatism than at others (Meek and Newton, 1999). More recently the same authors have used X-ray diffraction to map fibril orientations over a complete human cornea (Newton and Meek, 2001). In the future the availability of such information could help to optimise models used in the simulation of refractive surgery, which currently rely on complex assumptions regarding corneal ultrastructure (Hanna et al., 1992; Moriera et al., 1993).

By comparison with human cornea, collagen organisation in the primate corneal stroma has been relatively poorly characterised. As early as 1966, it was noted that the fibrillary texture of monkey cornea closely resembled that of man (Ehlers, 1966). However, subsequent investigation of stromal collagen organisation to date has been limited to highly localised studies of the central cornea (Jacobsen et al., 1984; Ozanics et al., 1976, 1977) and the trabecular meshwork (Nishida and Mizutani, 1994). Collectively, the literature points to a lamellar arrangement and general morphology grossly similar to that seen in human cornea, while small-angle X-ray scattering (SAXS) patterns from the centre of macaque monkey corneas have disclosed collagen fibrils only marginally larger and more widely spaced than those observed in humans (Meek and Leonard, 1993). However, no literature exists documenting collagen organisation as a function of position in the primate cornea, despite the biomechanical importance of this information Clinically, factors impacting on the biomechanical stability of the monkey cornea are of considerable interest, particularly as the monkey is widely used as an animal model for human ocular diseases affecting corneal shape (Fortune et al., 2002; Ollivier et al., 2003; Peiffer et al., 1987), and in developing new techniques for refractive surgery (Melles et al., 1998; Petroll et al., 1992; Werblin, 1992). In this paper we have employed wide-angle X-ray scattering (WAXS) methods to gain new insight into the collagenous makeup of the corneal stroma of the common marmoset, and we compare the results with those obtained from humans. In particular, we were able to answer the fundamentally important questions of whether, as in humans: (1) there is any preferred direction of the lamellae in the central primate cornea, and (2) there is a circumferential annulus of fibrils at the limbus.

2. Materials and methods

2.1. Specimen preparation

Ten healthy common marmosets (*Callithrix jacchus*), aged between 7 months and $14\frac{1}{2}$ years, were sacrificed by intra-peritoneal injection of a lethal dose of barbiturate (Department of Physiology, Oxford University, UK). The 12 o'clock orientation of each eyeball was identified by a scleral suture and the eyes were removed intact within 2 h of death and immediately snap-frozen in liquid nitrogen cooled isopentane. They were then wrapped in aluminium foil and stored at −80 °C. Immediately prior to examination with X-rays each eye was thawed and the cornea excised using a scalpel, leaving at least 0.5 mm of scleral rim attached. The ARVO statement for the use of animals in ophthalmic research was adhered to at all times.

2.2. X-ray diffraction

WAXS patterns were collected on station 14.1 at the UK Synchrotron Radiation Source (Daresbury, UK), using a 15 cm long camera equipped with a Quantum 4R CCD detector (ADSC, Poway, CA). The X-ray beam had a wavelength of 0.1488 nm and a square cross-section at the specimen measuring 0.2×0.2 mm. During data collection the corneo-scleral discs were wrapped in clingfilm and placed in airtight Perspex (Databank, UK) chambers with Mylar (DuPont-Teijin, UK) windows to minimise tissue dehydration. Mylar produces a circular X-ray reflection at ~0.55 nm. On the detector this is situated well outside the ~1.6 nm corneal collagen reflection and, as such, may be ignored. X-rays were passed through the anterior corneal face parallel to the cornea's optical axis. A specimen translation stage (Newport, UK) interfaced with the X-ray camera shutter enabled the specimen to be moved between exposures in the vertical and horizontal directions within the plane of the cornea (positional error <0.001 mm). X-ray exposures were recorded at 0.5 mm (horizontal) × 0.5 mm (vertical) intervals over the entire surface of three corneo-scleral discs (1 pair of eyes from a $14\frac{1}{2}$ year old marmoset + 1 left eye from a 7-month-old animal). In addition a square 2×2 grid (0.25 mm interval) of four exposures, located within the central 2 mm corneal region, was recorded from the left and right eyes of the remaining eight animals. The X-ray exposure time per data point was 150 s.

2.3. Data analysis

WAXS patterns from corneal stroma feature a single X-ray reflection arising from interference between X-rays scattered by collagen molecules within the fibrils (see Meek and Quantock (2001) for a review). A WAXS pattern from the limbal region of one of our marmoset

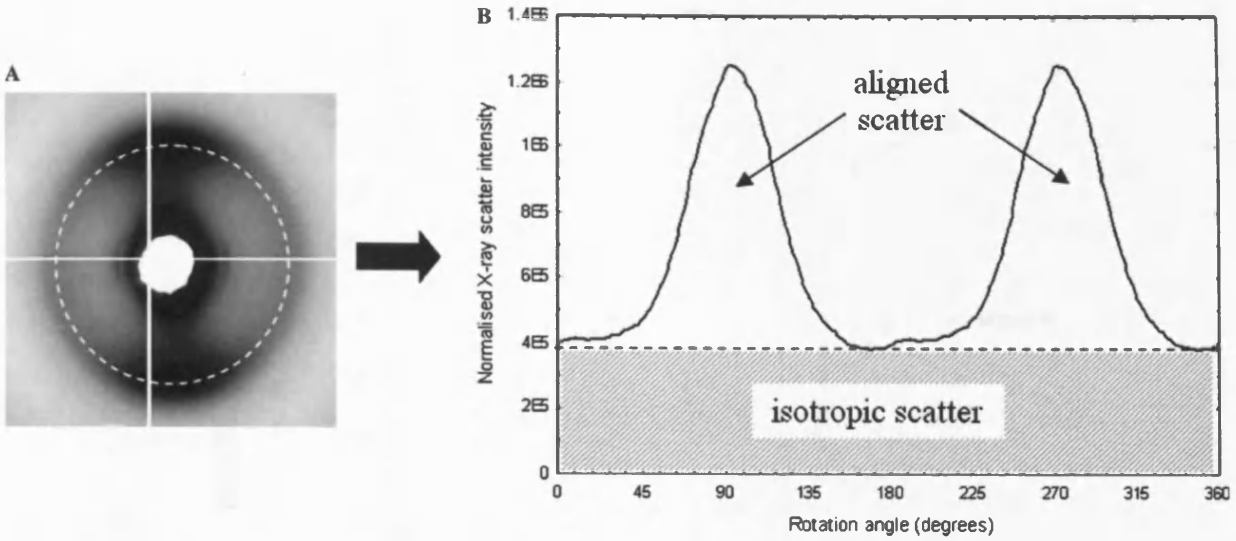

Fig. 1. Analysis of a typical WAXS pattern from primate cornea (A), to obtain the distribution of normalised X-ray scatter intensity around the intermolecular collagen reflection (B). The distribution may be divided into two components: (1) isotropic scatter from collagen fibrils distributed equally in all directions, and (2) scatter from preferentially aligned fibrils.

corneas is shown in Fig. 1A. As collagen molecules tend to lie along the fibril axis, we may approximate molecular alignment as fibrillar alignment. An isolated stromal lamella composed of fibrils all running in one direction would produce two sharp diffraction maxima located either side of a line corresponding to the fibril long axis. It follows that a stack of such lamellae with a completely isotropic radial distribution of fibrils would produce a circular X-ray reflection of uniform intensity around the circumference. Conversely, corneas possessing a preferred lamellae direction give rise to lobed X-ray reflections which, by definition, contain information about the fibril orientation within the plane of the cornea, averaged through the stromal depth.

For each WAXS pattern, the distribution of normalised X-ray scatter intensity around the collagen intermolecular reflection was obtained using Optimas 6.5 (MediaCybernetics, UK) image analysis software and Excel (Microsoft, UK) spreadsheets (see Fig. 1). This analysis procedure has been described in detail previously (Newton and Meek, 1998a). The X-ray scatter distribution was divided into two components: (1) isotropic scatter from collagen fibrils distributed equally in all directions, and (2) scatter from preferentially aligned fibrils (Fig. 1B). A similar approach has been used before to analyse X-ray diffraction data from human corneas (Daxer and Fratzl, 1997). The aligned scatter angular distribution was then converted into polar

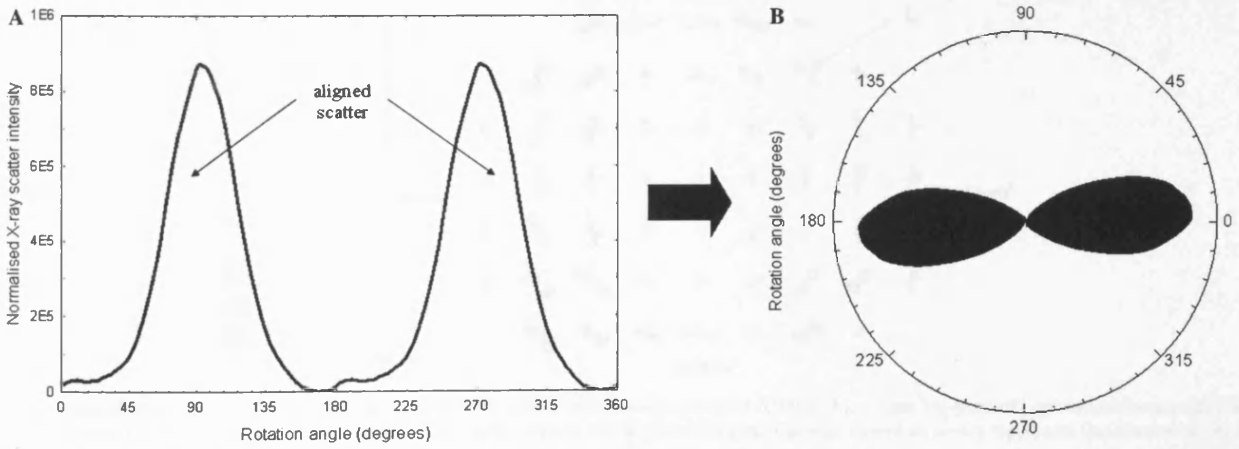

Fig. 2. Conversion of the X-ray scatter distribution from preferentially aligned fibrils (A), into polar coordinates. The radial extent of the polar plot (B) in any direction is proportional to the number of fibrils preferentially aligned in that direction. A 90° phase shift is introduced to account for the fact that collagen fibrils scatter X-rays in a plane normal to their long axis.

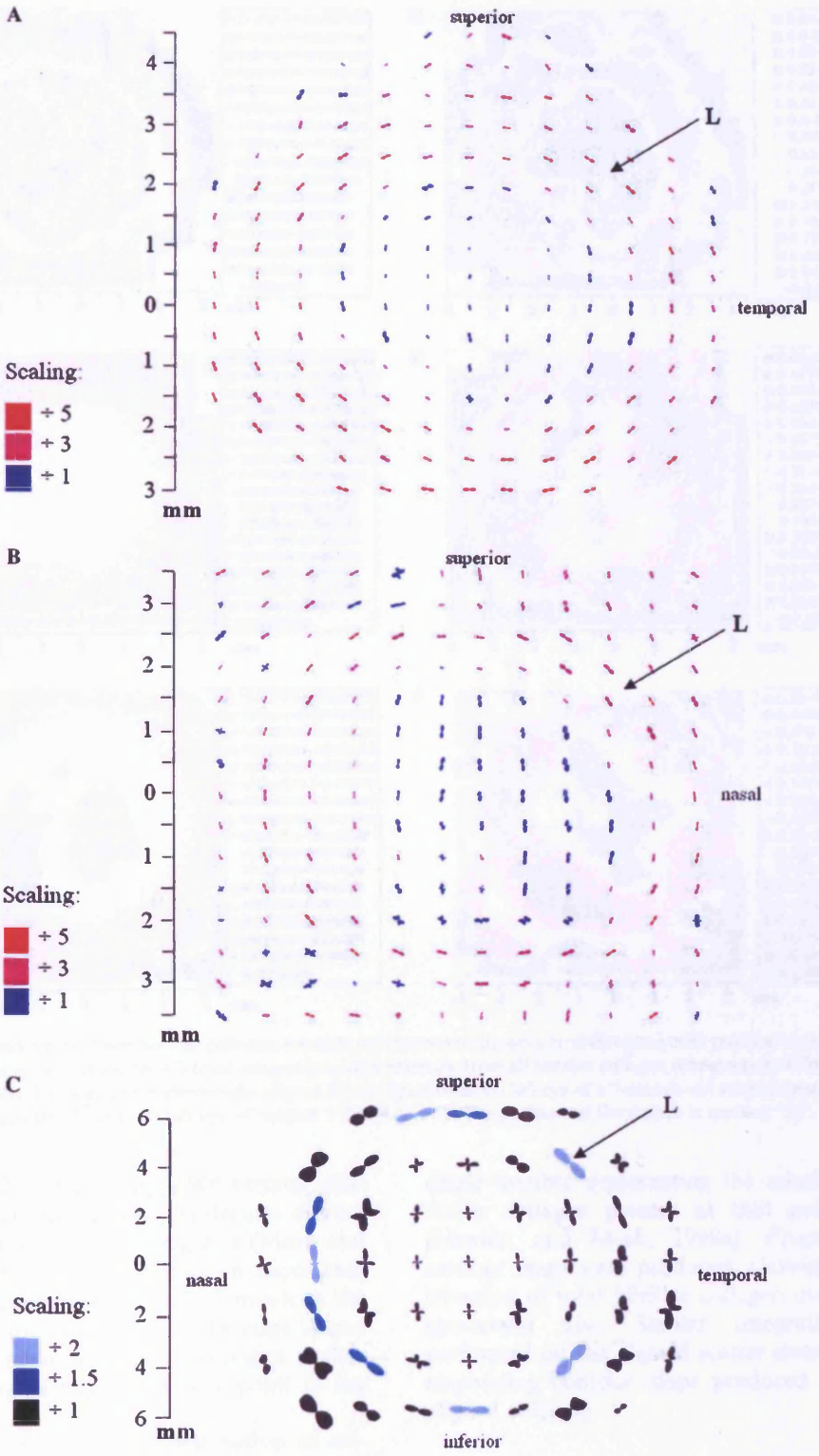

Fig. 3. Maps of preferred collagen fibril orientation across a left 7-month-old marmoset cornea (A), a right 14½-year-old marmoset cornea (B), and a human cornea (C). Each data point takes the form of a polar plot in which the radial extent of a plot from its centre represents the relative number of fibrils preferentially aligned in that direction, at that point in the tissue. The polar plots have been scaled within each map, as indicated in the keys. The position of the limbus is marked "L." Human map courtesy of Dr. Richard Newton and Professor Keith Meek.

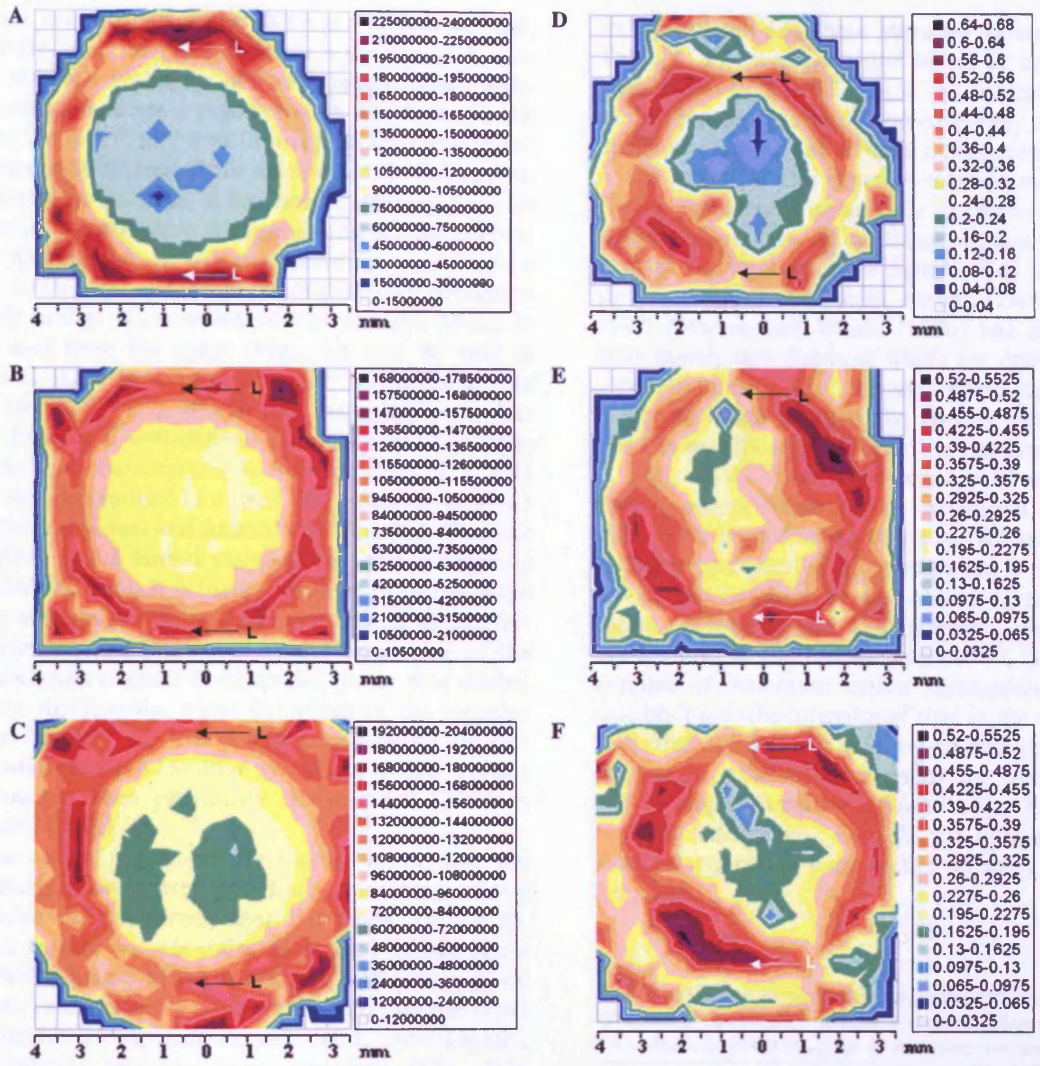

Fig. 4. Contour maps of X-ray scatter from fibrillar collagen across three marmoset corneo-scleral discs (superior position at top), sampled at 0.5 mm (horizontal) × 0.5 mm (vertical) resolution. (A–C) total integrated scatter intensity from all fibrillar collagen (irrespective of fibril orientation). (D–F) proportion of the total scatter that is due to preferentially aligned fibrils. Specimens: (1) left eye of a 7-month-old subject (maps A + D), (2) right eye from a $14\frac{1}{2}$ year subject (maps B + E), and (3) left eye of subject 2 (maps C + F). The position of the limbus is marked "L".

coordinates (see Fig. 2), introducing a 90° angular shift to account for the fact that collagen molecules diffract X-rays in a plane normal to their long axis (Meek and Quantock, 2001). Each sampling position on a specimen could now be represented by a polar plot, in which the distance from the centre of the plot to the edge in any direction gives the relative amount of collagen preferentially aligned in that direction, at that point in the tissue (Fig. 2).

In order to further quantify the distribution of collagen across the tissue, integrated X-ray scatter intensities were calculated for all sampling positions across the three corneo-scleral discs examined. From each diffraction pattern, a 360° integration of the total X-ray scatter intensity distribution (Fig. 1B) was computed to give a single number representing the relative amount of fibrillar collagen present at that point in the tissue (Newton and Meek, 1998a). From these numbers contour maps were produced, showing the spatial distribution of total fibrillar collagen over the whole corneo-scleral disc. Similar integrations were also performed on the aligned scatter distributions and corresponding contour maps produced for preferentially aligned collagen.

3. Results

Figs. 3A and B show maps of preferentially aligned fibrillar collagen across a left cornea from a 7-month-old

Appendix 7

marmoset and a right cornea from a $14\frac{1}{2}$ year animal, respectively. Sampling points form a square grid with 0.5 mm intervals vertically and horizontally. Each sampling position features a polar plot, in which the radial extent of the plot in any direction represents the number of preferentially aligned fibrils oriented in that direction. As indicated in the keys, it has been necessary to scale the plots in order to show the limbal and central corneal regions simultaneously. A corresponding map from a human cornea (at 2×2 mm resolution) is presented alongside in Fig. 3C, courtesy of Newton and Meek. It can be seen from the maps (Figs. 3A and B) that in marmosets there is a predominance of fibrils at the limbus (marked "L") which run tangentially to the cornea, forming a well-defined circum-corneal annulus much like that characterised in humans (Fig. 3C). This feature was also verified in a third marmoset cornea (left eye from the $14\frac{1}{2}$-year-old animal—not shown). The size of the plots at the limbus suggests that the collagen is highly oriented here. It is further evident from the maps that the annulus is non-uniform around its circumference. Fibril number (indicated by the magnitude of the polar plots) and angular fibril spread (polar plot shape) both vary significantly, while the width of the annulus measures between 0.5 and 1.5 mm, depending on circumferential position. Similar variation within human specimens has been previously documented (Newton and Meek, 1998a).

In the central region of the marmoset cornea, the maps clearly show a preferred fibril orientation along the superior–inferior corneal meridian (Figs. 3A and B). A similar feature was identified in a third cornea (data not shown). This result is particularly interesting, given that in the central human cornea there are two preferred fibril directions: superior–inferior and, additionally, the orthogonal temporal–nasal meridian (Fig. 3C). While some limited evidence of an orthogonal preponderance of fibrils was seen in the corneas of some of the marmosets we studied, in general the preferred lamellar orientation in the central marmoset cornea was found to be overwhelmingly along the superior–inferior direction. In order to quantify this further, we took four adjacent diffraction patterns from the centre of the three mapped corneas and four patterns (0.25 mm apart) from the centre of an additional 16 marmoset corneas and computed normalised X-ray scatter profiles around the intermolecular reflection, as described in Section 2.3. We then calculated the sum of the total scatter intensity within a 45° sector of the superior direction, and expressed this as a fraction of the total scatter intensity integrated through 180°, to give a measure of the proportion of fibrils oriented along (or within 22.5° either side of) the superior–inferior meridian. A similar analysis of the inferior direction would have yielded identical results, since corneal WAXS patterns are centrosymmetric. For each cornea the average of the four patterns was calculated and these averaged values are shown in Table 1. The average value of all 19 corneas was determined as 0.33 ($\pm$0.01) ($n = 76$), indicating that in the central marmoset cornea approximately one third of the fibrils throughout the stromal depth are oriented within a 45° sector of the superior–inferior meridian. For a cornea featuring a completely isotropic distribution of lamellae directions, we would expect this value to be one quarter. In light of these figures, it is interesting that similar analysis of human cornea (Daxer and Fratzl, 1997; Newton and Meek, 1998b) has shown that approximately two thirds of fibrils are oriented along the superior–inferior and temporal–nasal directions in humans, although whether the two directions are populated in exactly equal proportion remains unknown.

Figs. 4A–C show contour maps of total scatter intensity across three whole marmoset corneo-scleral discs. The maps disclose that total scatter from fibrillar collagen (irrespective of orientation) is fairly constant across the majority of the cornea (green/yellow contours). However near the periphery scatter increases rapidly and at the limbus (marked "L") forms a clear annulus of maximum scatter (orange/red contours) of roughly twice the intensity of that in the central cornea. With this in mind it is relevant to note that the number of stromal lamellae increases at the corneal periphery and we might therefore expect fibrillar X-ray scatter to increase accordingly. Outside the cornea some highly localised regions of even higher intensity are evident in the sclera.

Table 1
Ratio of integrated X-ray scatter from collagen fibrils oriented within a 45° sector of the superior–inferior corneal meridian (I_{si}) to total X-ray scatter from all fibrils (I_{tot}), for 19 marmoset corneas.

Subject	Age (years/months)	Left/right eye	Mean I_{si}/I_{tot} (SEM)
1	11/4	Left	0.47(0.02)
		Right	0.27(0.01)
2	1/5	Left	0.35(0.01)
		Right	0.32(0.01)
3	0/7	Left	0.40(0.02)
		Right	0.31(0.01)
4	0/7	Left	0.30(0.01)
		Right	0.34(0.01)
5	1/0	Left	0.32(0.01)
		Right	0.32(0.01)
6	0/7	Left	0.30(0.01)
		Right	0.36(0.01)
7	1/6	Left	0.32(0.01)
		Right	0.34(0.01)
8	1/0	Left	0.30(0.01)
		Right	0.37(0.02)
9	14/5	Left	0.32(0.01)
		Right	0.31(0.01)
10	0/7	Left	0.28(0.01)

Each number represents the mean and associated standard error calculated from four X-ray patterns recorded from the centre of each cornea.

Appendix 7

Figs. 4D–F feature contour maps displaying the proportion of the total scatter intensity that is due to preferentially aligned fibrillar collagen only. Blue/yellow contours in the central corneal region are indicative of relatively low proportions of aligned collagen, while further out the orange/red contours point to proportionally much greater alignment. An annulus of maximum aligned scatter can clearly be observed at the limbus (marked "L"). These data reconcile well with the maps of fibril orientation shown in Figs. 3A and B. The aligned scatter contour maps confirm that the degree of fibrillar alignment is significantly elevated at the limbus compared to more central corneal regions, while discontinuities in the contours around the annulus highlight the non-uniformity of the limbus. A further point of note is the shape of the contours. While the contours define a generally circular central corneal region in the maps of total scatter (Figs. 4A–C), the central cornea in the aligned scatter contour maps clearly appears more rhombic in shape (Figs. 4D–F). This is a consequence of the fact that the limbal annulus exhibits greater aligned scatter in the four oblique regions in-between the superior, inferior, temporal, and nasal positions, than at the four positions themselves. A similar feature has been recently characterised in human cornea (Aghamohammadzadeh et al., 2004), and points to elevated levels of fibrillar alignment in the oblique sectors of the peripheral cornea.

4. Discussion

Reference to Figs. 3A and B indicates that there is a preferred lamellar direction in the central marmoset cornea which is directed along the superior–inferior corneal meridian. This result is confirmed and quantified in Table 1, which shows that approximately 33% of fibrils are oriented within a 45° sector of the superior–inferior direction; significantly higher than the figure of 25% expected if the angular fibril distribution were completely homogeneous. In contrast, the central human cornea demonstrates an orthogonal preferred fibril orientation (Fig. 3C) directed superior–inferior and nasal–temporal. The fact that these two directions correspond to the direction of insertion of the four rectus oculo-motor muscles prompted some to suggest that preferentially aligned collagen exists in order to take up the mechanical forces of the eye muscles along the corneal trajectories (Daxer and Fratzl, 1997; Kokott, 1938). In light of the current study this situation appears unlikely in the marmoset. Under such a system it might be expected, from biomechanical considerations, that nasal–temporal fibrils would outnumber superior–inferior ones, given that the medial recti exert the greater force on the globe, and that horizontal eye movements are more frequent than vertical ones. In fact, as shown in Figs. 3A and B, we observed virtually no extra fibrils (above the isotropic "background" distribution) along the nasal–temporal direction in the central marmoset cornea. Of course our measurements cannot tell us at which depth in the stroma the preferred fibril alignment might be occurring. Meek et al. (1987) showed using SAXS methods that the orthogonal preferred fibril arrangement in human cornea is more prevalent in the posterior half of the stroma. It is likely that the preferred alignment we observe in marmosets is also more pronounced in the posterior stroma, particularly as Ozanics et al. (1977) reported that fibril directions in the central anterior stroma appeared fully isotropic throughout the gestation period of developing primate corneas.

The differences we have identified in the collagen organisation of the central marmoset cornea, compared to that of humans, may also impact on the optical properties of the tissue. The structure and organisation of stromal lamellae determine the cornea's birefringence properties and how it scatters polarised light at small angles (Bour, 1991; Maurice, 1957; Stanworth and Naylor, 1950). While a proportion of corneal birefringence arises intrinsically from within each individual collagen fibril, there is a second component which has its origins in the stack formed by the lamellae (Born and Wolf, 1980; Donahue et al., 1995). Thus, analysis of polarised light transmission by the cornea can yield information about stromal lamellar orientation. Results from such an experiment on rabbit and bovine corneas were reported to be consistent with a model where the stromal lamellae demonstrated preferred orientation along either one or two axes (McCally and Farrell, 1982). More recently, Weinreb and co-workers (2002) applied optical imaging techniques to macaque monkey eyes, yielding information on corneal polarisation in the primate. Interestingly, the most notable finding in this study was that the corneal polarisation magnitude in the monkey eyes varied considerably from that measured in humans. It is our hypothesis that the observations of Weinreb et al. have their origin in the difference between lamellar orientations in the human and primate corneal stroma indicated by the current study.

Towards the corneal periphery, the marmoset cornea displays more commonality with that of humans. An annulus of collagen fibrils circumscribing the cornea, much like that seen in human cornea, is clearly identifiable (Fig. 3). This is the first time the feature has been characterised unambiguously in non-human tissue, although evidence of an annulus has recently been found in mice and awaits confirmation (Quantock et al., 2003). It is likely that a significant proportion of the alignment we observe in the marmoset annulus is located in more posterior parts of the cornea and in particular the trabecular meshwork. Indeed, Nishida and Mizutani (1994) observed the primate trabecular meshwork using electron microscopy and concluded that in peripheral

Appendix 7

regions of the corneo-scleral sheet most collagen bundles appear to run parallel to the circumference of the limbus.

We suspect the annulus to be important in maintaining the shape of the marmoset cornea, occurring as it does at the limbus, where the differing curvatures of the cornea and sclera meet. An annulus of highly ordered fibrils would certainly help to withstand the increased circumferential tension at the limbus (Maurice, 1969), particularly as we have shown that the collagen is highly reinforced in this region (Fig. 4). Nevertheless, it is unlikely that the shape mediation of the marmoset cornea is borne solely by the limbal annulus, and we suspect that lamellar interplay in the anterior cornea may also contribute. A proportion of the anterior lamellae of the primate corneal stroma insert into the adjacent Bowman's layer (Jacobsen et al., 1984), a feature which has been suggested to help preserve the curvature of the anterior cornea (Bron, 2001). Furthermore, interweaving of anterior stromal lamellae may also help to promote biomechanical stability, as has been supposed in humans (Bron, 2001; Müller et al., 2001), although the extent of lamellar interweave in primates is yet to be determined.

Some aspects of the primate eye have been well characterised. For instance, investigation of the visual optics (Troilo et al., 1993) and retinal characteristics (Coletta et al., 2001; Troilo et al., 1993) of the marmoset eye have shown that it in these respects it is well approximated as a scaled-down version of the human eye. However, considering the widespread use of monkeys in vision research, there has been surprisingly little study done on the structure of primate cornea. Hitherto, it has been assumed that the corneal structure of monkeys mirrors closely that of humans. However, the current study indicates this view to be ill-founded, and points to significant differences between the two in terms of the collagenous architecture of the central cornea, with implications for corneal mechanics and optics. The results presented herein should lessen the reliance on such assumptions, and could be used to aid the interpretation of experimental data from, for example, refractive surgery simulations using monkeys. In addition, they provide a normal control for the analysis of pathological data from primate models of corneal dystrophies, where the stroma displays structural abnormality.

Acknowledgments

The authors thank Mike Macdonald, Rob Kehoe, and Steve Buffy of the Daresbury SRS, Warrington, UK for help with data collection. All marmoset corneas used in this study were provided by Dr. Stuart Judge (Department of Physiology, Oxford University, UK), whom the authors gratefully acknowledge for tissue harvesting and useful discussions. This work was funded by MRC Grant No. G0001033.

References

Aghamohammadzadeh, M., Newton, R.M., Meek, K.M., 2004. X-ray scattering used to map the preferred collagen orientation in the human cornea and limbus structure. In press.

Born, M., Wolf, E., 1980. Principles of Optics, sixth ed. Pergamon Press, New York.

Bour, L., 1991. Polarized light and the eye. In: Charman, W.N. (Ed.), Visual Optics and Instrumentation. CRC Press/Macmillan, New York, pp. 310–325.

Bron, A.J., 2001. The architecture of the corneal stroma. Br. J. Ophthalmol. 85, 379–383.

Coletta, N.J., Troilo, D., Marcos, S., 2001. Optical quality of the marmoset eye. Invest. Ophthalmol. Vis. Sci. 42, ARVO Abstract 877.

Daxer, A., Fratzl, P., 1997. Collagen fibril orientation in the human corneal stroma and its implications in keratoconus. Invest. Ophthalmol. Vis. Sci. 38, 121–129.

Donahue, D.J., Stoyanow, B.J., McCally, R.L., Farrell, R.A., 1995. Numerical modelling of the cornea's lamellar structure and birefringence properties. J. Opt. Soc. Am. A 12, 1425–1438.

Ehlers, N., 1966. The fibrillary texture and the hydration of the cornea. Acta Ophthalmol. 44, 620–630.

Fortune, B., Cull, G., Wang, L., Van Buskirk, E.M., Cioffi, G.A., 2002. Factors affecting the use of multifocal electroretinography to monitor function in a primate model of glaucoma. Doc. Ophthalmol. 105, 151–178.

Hanna, H.D., Jouve, F.E., Waring, G.O., Ciarlet, P.G., 1992. Computer simulation of arcuate keratotomy for astigmatism. Refract. Corneal Surg. 8, 152–163.

Hukins, D.W.L., Aspden, R.M., 1985. Composition and properties of connective tissues. Trends Biochem. Sci. 10, 260–264.

Jacobsen, I.E., Jensen, O.A., Prause, J.U., 1984. Structure and composition of Bowman's membrane. Study by frozen resin cracking. Acta Ophthalmol. 62, 39–53.

Jeronimidis, G., Vincent, J.F.V., 1984. Composite materials. In: Hukins, D.W.L. (Ed.), Connective Tissue Matrix, 1. Macmillan, England, pp. 187–210.

Kokott, W., 1938. Ubermechanisch-funktionelle strikturen des auges. Albrecht von Graefes. Arch. Ophthalmol. 138, 424–485.

Komai, Y., Ushiki, T., 1991. The three-dimensional organisation of collagen fibrils in the human cornea and sclera. Invest. Ophthalmol. Vis. Sci. 32, 2244–2258.

Maurice, D.M., 1957. The structure and transparency of the corneal stroma. J. Physiol. 136, 263–286.

Maurice, D.M., 1969. The cornea and sclera. In: Davson, H. (Ed.), The Eye. Academic Press, New York, pp. 489–599.

McCally, R.L., Farrell, R.A., 1982. Structural implications of small-angle light scattering from cornea. Exp. Eye Res. 34, 99–113.

Meek, K.M., Leonard, D.W., 1993. Ultrastructure of the corneal stroma: a comparative study. Biophys. J. 64, 273–280.

Meek, K.M., Newton, R.H., 1999. Organisation of collagen fibrils in the corneal stroma in relation to mechanical properties and surgical practice. J. Refract. Surg. 15, 695–699.

Meek, K.M., Quantock, A.J., 2001. The use of X-ray scattering techniques to determine corneal ultrastructure. Prog. Retin. Eye Res. 20, 95–137.

Meek, K.M., Blamires, T., Elliott, G.F., Gyi, T.J., Nave, C., 1987. The organisation of collagen fibrils in the human corneal stroma: a synchrotron X-ray diffraction study. Curr. Eye Res. 6, 841–846.

Melles, G.R., Eggink, F.A., Lander, F., Pels, E., Rietveld, F.J., Beekhuis, W.H., Binder, P.S., 1998. A surgical technique for posterior lamellar keratoplasty. Cornea 17, 618–626.

Appendix 7

Moriera, H., Campos, M., Sawush, M.R., McDonnell, J.M., Sand, B., McDonald, P.J., 1993. Holmium laser thermokeratoplasty. Ophthalmology 100, 752–761.

Muller, L.J., Pels, E., Vrensen, G.F.J.M., 2001. The specific architecture of the anterior stroma accounts for maintenance of corneal curvature. Br. J. Ophthalmol. 85, 437–443.

Newton, R.H., Meek, K.M., 1998a. Circum-corneal annulus of collagen fibrils in the human limbus. Invest. Ophthalmol. Vis. Sci. 39, 1125–1134.

Newton, R.H., Meek, K.M., 1998b. The integration of the corneal and limbal fibrils in the human eye. Biophys. J. 75, 2508–2512.

Newton, R.H., Meek, K.M., 2001. Mapping the orientations of the collagen fibrils in human cornea and sclera. Invest. Ophthalmol. Vis. Sci. 42, ARVO Abstract 1517.

Nishida, S., Mizutani, S., 1994. Collagen fibrils as skeletal frame in monkey trabecular meshwork. Jpn. J. Ophthalmol. 38, 30–37.

Ollivier, F.J., Brooks, D.E., Komaromy, A.M., Kallberg, M.E., Andrew, S.E., Sapp, H.L., Sherwood, M.B., Dawson, W.W., 2003. Corneal thickness and endothelial cell density measured by non-contact specular microscopy and pachymetry in Rhesus macaques (*Macaca mulatto*) with laser-induced ocular hypertension. Exp. Eye Res. 76, 671–677.

Ozanics, V., Rayborn, M., Sagun, D., 1976. Some aspects of corneal and scleral differentiation in the primate. Exp. Eye Res. 22, 305–327.

Ozanics, V., Rayborn, M., Sagun, D., 1977. Observations on the morphology of the developing primate cornea: epithelium, its innervation and anterior stroma. J. Morphol. 153, 263–298.

Peiffer Jr., R.L., Werblin, T.P., Patel, A.S., 1987. Keratoconus in a rhesus monkey. J. Med. Primatol. 16, 403–406.

Petroll, W.M., New, K., Sachdev, M., Cavanagh, H.D., Jester, J.V., 1992. Radial keratotomy III. Relationship between wound gape and corneal curvature in primate eyes. Invest. Ophthalmol. Vis. Sci. 33, 3283–3291.

Quantock, A.J., Dennis, S., Adachi, W., Kinoshita, S., Boote, C., Meek, K.M., Matsushima, Y., Tachibana, M., 2003. Annulus of collagen fibrils in mouse cornea and structural matrix alterations in a murine-specific keratopathy. Invest. Ophthalmol. Vis. Sci. 44, 1906–1911.

Stanworth, A., Naylor, E.J., 1950. The polarization optics of the isolated cornea. Br. J. Ophthalmol. 34, 201–211.

Troilo, D., Howland, H.C., Judge, S.J., 1993. Visual optics and retinal cone topography in the common marmoset (*Callithrix jacchus*). Vision Res. 33, 1301–1310.

Weinreb, R.N., Bowd, C., Zangwill, L.M., 2002. Scanning laser polarimetry in monkey eyes using variable corneal polarization compensation. J. Glaucoma 11, 378–384.

Werblin, T.P., 1992. Astigmatism after cataract extraction: 6-year follow up of 6.5- and 12-millimeter incisions. Refract. Corneal Surg. 8, 448–458.

Available online at www.sciencedirect.com
SCIENCE DIRECT®
Journal of Structural Biology 149 (2005) 1–6
Journal of Structural Biology
www.elsevier.com/locate/yjsbi

Lamellar orientation in human cornea in relation to mechanical properties

Craig Boote[a,*], Sally Dennis[a], Yifei Huang[b], Andrew J. Quantock[a], Keith M. Meek[a]

[a] *Structural Biophysics Group, School of Optometry and Vision Sciences, Cardiff University, Wales, UK*
[b] *The Ophthalmic Centre, Great Wall Hospital, Beijing, China*

Received 9 June 2004, and in revised form 24 August 2004
Available online 14 October 2004

Abstract

We have applied wide-angle X-ray scattering to the human cornea in order to quantify the relative number of stromal collagen fibrils directed along the two preferred corneal lamellar directions: superior–inferior and nasal–temporal. The data suggest that, on average, the two directions are populated in equal proportion at the corneal centre. Here, approximately one-third of the fibrils throughout the stromal depth tend to lie within a 45° sector of the superior–inferior meridian, and similarly for the nasal–temporal direction. However, in some eyes we have measured significant differences between the two preferential fibril populations, with some corneas exhibiting as much as 25% more collagen in one direction than the other. Based on these findings, a mechanical model of the normal cornea may be envisaged, whereby the fibril tension in the underlying "background" of isotropically arranged collagen helps to balance the intraocular pressure; while the extra preferentially aligned fibrils take up the additional tensile stress along the superior–inferior and nasal–temporal meridians exerted by the rectus muscles and the orbicularis. It is possible that, through a direct impact on the elastic modulus of the tissue, an imbalance of superior–inferior and nasal–temporal fibrils in some eyes might affect corneal shape.

Keywords: Corneal stroma; Collagen fibrils; X-ray scattering; Biomechanics

1. Introduction

The human corneal stroma exhibits a layered structure comprising over 200 lamellae through its central thickness (Maurice, 1957). Each lamella consists of uniformly narrow collagen fibrils embedded in a hydrated matrix rich in proteoglycans, glycoproteins, salts, and keratocytes. Fibrils within a given lamella run approximately parallel, but subtend large angles with those in adjacent lamellae (Komai and Ushiki, 1991). Collagen fibrils reinforce biological materials (Jeronimidis and Vincent, 1984; Hukins and Aspden, 1985) and, because they are strongest axially, knowledge of their orientations within a particular tissue may be used to model its mechanical performance (Hukins, 1984). In the cornea, the relationship between fibril orientation and tissue mechanics is of considerable interest, since the mechanical performance of the cornea helps determine the shape of the tear film and thereby refractive status.

In 1938, Kokott was the first to suggest that collagen fibrils in the deeper layers of the stroma in the central cornea are not isotropically arranged, but rather adopt a preferential orientation along the superior–inferior and nasal–temporal corneal meridians (see Fig. 1). X-ray scattering studies later confirmed this, and indicated that the preferred orientation is more prevalent in the posterior half of the stroma (Meek et al., 1987). Notably, some have proposed that this preferential fibril

* Corresponding author. Fax: +44 29 20874859.
E-mail address: bootec@cf.ac.uk (C. Boote).

1047-8477/$ - see front matter
doi:10.1016/j.jsb.2004.08.009

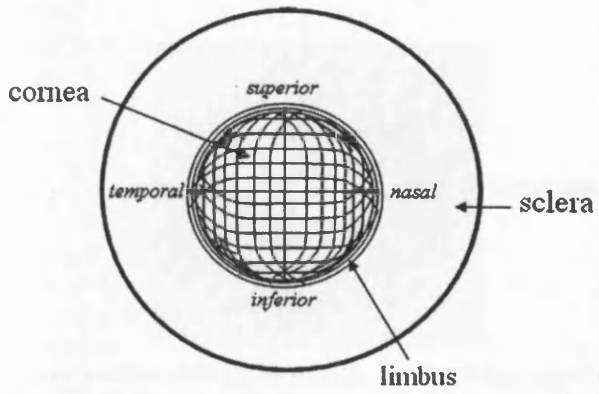

Fig. 1. Schematic showing the preferential orientation of collagen fibrils in the cornea of the human eye (right eye shown). The central cornea is characterized by a preponderance of fibrils arranged in the orthogonal superior–inferior and nasal–temporal directions. These fibrils are thought to bend at the periphery to coalesce with a circumferential annulus of fibrils where the cornea fuses with the sclera at the limbus.

orientation exists in order to take up the stress of the ocular rectus muscles along the corneal meridians (Daxer and Fratzl, 1997; Kokott, 1938). Whilst further quantitative analysis has indicated that, in total, around two-thirds of fibrils of the stroma tend to lie within 45° sectors of the superior–inferior and nasal–temporal directions (Daxer and Fratzl, 1997; Newton and Meek, 1998a), it has up to now remained unknown in what proportion each sector is populated. In order to resolve this question, we initiated a wide-angle X-ray scattering (WAXS) study.

2. Materials and methods

2.1. Specimens

Four time-expired healthy adult human corneas of various ages, obtained from the UK Corneal Transplant Service Eye Bank (Bristol, UK), were wrapped in cling film and stored frozen at −80 °C prior to the experiment. A further three corneas were obtained from the Ophthalmic Centre, Great Wall Hospital (Beijing, China), and stored in a 2.5% formalin solution. None of the donor corneas used had any previous history of refractive surgery. The 12 o'clock position of each cornea was identified with a limbal suture.

2.2. Data collection

WAXS experiments were performed on station 14.1 at the UK Synchrotron X-ray Source (Daresbury, UK), using an X-ray beam of wavelength 0.1488 nm which had a square 0.2 mm × 0.2 mm cross-section at the specimen. In order to minimise tissue dehydration during X-ray exposure, the corneas were placed in air-tight Perspex (Databank, UK) chambers with Mylar (Dupont-Teijin, UK) windows. X-rays were passed through the anterior corneal face parallel to the cornea's optical axis for 90 s per exposure, and the resulting WAXS patterns recorded on a Quantum 4R CCD detector (ADSC, Poway, CA) located 150 mm behind the specimen. A specimen translation stage (Newport, UK), interfaced with the X-ray camera shutter, allowed the specimen to be moved between exposures in the vertical and horizontal directions within the corneal plane. Nine diffraction patterns, from sampling positions forming a square 3 × 3 grid, were recorded from within the central 2 mm region of each of the seven corneas.

2.3. Data analysis

A typical WAXS pattern from one of the corneas is shown in Fig. 2A. It features a single reflection formed by interference between X-rays scattered by the regularly arranged collagen molecules lying near-axially within the stromal fibrils (Meek and Quantock, 2001). Each single stromal lamella will produce a pair of diffraction spots either side of a line representing the long axis of its constituent molecules/fibrils. It follows that corneal stroma featuring a completely homogeneous arrangement of lamellae would be expected to produce a circular X-ray reflection of uniform intensity around its circumference. However, as shown in Fig. 2A, diffraction patterns from the central human cornea generally exhibit four lobes of heightened intensity, arising from the orthogonal arrangement of preferentially aligned fibrils. By measuring the distribution of intensity around these peaks, we may quantify the extent of fibril alignment in the corneal stroma.

For each WAXS pattern, the normalised intensity profile (Fig. 2B) was obtained using Optimas 6.5 (MediaCybernetics, UK) image analysis software and Excel (Microsoft, UK) spreadsheets, a procedure which has been described in detail previously (Newton and Meek, 1998b). The intensity profile essentially gives the orientation distribution of the fibrils, once a 90° phase shift has been introduced to account for the fact that collagen molecules scatter X-rays in a plane perpendicular to their long axis. We then calculated the integral of the scatter intensity within a 45° sector of each of the superior and nasal directions, I_s and I_n in Fig. 2, and expressed these two values as fractions of the total scatter intensity summed through 180°. This gave a measure of the proportion of fibrils oriented along (or within 22.5° either side of) the two preferred corneal meridians, averaged throughout the stromal depth. Of course, since corneal WAXS patterns are by definition centro-symmetric, a similar analysis of the inferior and temporal directions would have yielded identical results.

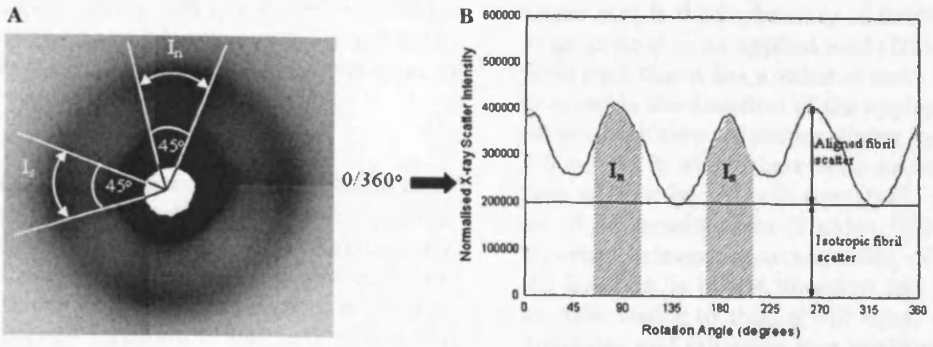

Fig. 2. Analysis of a WAXS pattern from the centre of human cornea (A), to produce the normalised X-ray scatter intensity distribution (B). The four intensity peaks arise from the orthogonal arrangement of preferentially aligned fibrils in the posterior stroma. A sector integration is used to calculate the scattered intensity, I_s and I_n, around 45° arcs of the superior and nasal intensity peaks. Expressing I_s and I_n as a fraction of the total scatter integrated through 180° then provides a measure of the proportion of fibrils oriented along (or within 22.5° either side of) the superior–inferior and nasal–temporal preferred directions.

3. Results

Table 1 shows the proportion of fibrils oriented within 45° sectors of the superior–inferior (R_{si}) and nasal–temporal (R_{nt}) meridians for our seven human corneas, as determined from the WAXS data. For each cornea, the difference between the two ratios was analysed statistically using a two-tailed Student's t test. In addition, the data for all seven corneas was grouped to find the average ratios and associated pooled P-value. Of the seven corneas we examined, on average, ~29% of fibrils throughout the stromal depth were oriented within 45° sectors of the superior–inferior and nasal–temporal meridians. The figure of 58% (± 2%) we obtain for the two preferred fibril populations combined compares well with previous X-ray studies (Daxer and Fratzl, 1997; Newton and Meek, 1998a). However, there is clearly considerable variation between specimens. For corneas 3, 4 and 6 we measured a statistically significant imbalance between the superior–inferior and nasal–temporal directions. In particular, cornea 3 appeared to have almost 25% more fibrillar collagen directed along the superior–inferior meridian compared to the nasal–temporal. In contrast, corneas 4 and 6 exhibited a significant imbalance in favour of the nasal–temporal direction.

4. Discussion

In biomechanical terms, it is instructive to consider the cornea as a linear elastic, bi-composite material in which the collagen fibrils provide the reinforcing structure and the interfibrillar material the ground substance. At low applied stress/strain it is also sometimes useful to include a correction factor to account for non-linear elastic behaviour of the cornea (Hjortdal, 1996), but we shall ignore this in our simplified model. The elastic modulus of the cornea in any particular direction, E_c, may then be expressed as:

$$E_c = E_f \beta \eta + E_g(1 - \beta), \quad (1)$$

where E_f and E_g are the elastic moduli of the fibrils and the ground substance, respectively, β is the volume fraction occupied by the fibrils, and η is the reinforcement efficiency factor which depends upon the orientation of the fibrils (Jeronimidis and Vincent, 1984; Hukins, 1984). However, because the elastic modulus of a colla-

Table 1
Proportion of collagen fibrils oriented within 45° sectors of the superior–inferior (R_{si}) and nasal–temporal (R_{nt}) directions for seven adult human corneas, as calculated from n WAXS patterns recorded from the central 2 mm corneal region

Cornea	Stored	R_{si} (SD)	R_{nt} (SD)	P	n
1	Frozen	0.29 (± 0.01)	0.28 (± 0.01)	0.10	9
2	Frozen	0.30 (± 0.01)	0.29 (± 0.01)	0.14	9
3	Frozen	0.31 (± 0.01)	0.25 (± 0.01)	8.41×10^{-8}	9
4	Frozen	0.27 (± 0.01)	0.30 (± 0.01)	4.81×10^{-9}	9
5	Fixed	0.30 (± 0.01)	0.28 (± 0.01)	0.07	9
6	Fixed	0.28 (± 0.01)	0.33 (± 0.01)	2.76×10^{-9}	9
7	Fixed	0.29 (± 0.01)	0.31 (± 0.01)	0.01	9
Pooled		0.29 (± 0.02)	0.29 (± 0.02)	0.82	63

The statistical significance of the difference between R_{si} and R_{nt} is represented by a P-value obtained using a two-tailed Student's t test.

gen fibril (0.5–1 Gpa) (Fung, 1981; Kato et al., 1989) is at least 10 000 times greater than that of the interfibrillar matrix (~40 kPa) (Hjortdal, 1996), the second term of Eq. (1) may be ignored, yielding:

$$E_c = E_f \beta \eta. \quad (2)$$

Hence, the main factors determining the elastic modulus along a particular corneal meridian are: (1) the fibril elastic modulus, (2) the fibril volume fraction, and (3) the fibril orientations with respect to that direction. Now, let us consider which of these factors is likely to vary from one corneal meridian to the next. Given that the fibril diameter does not change significantly over the cornea until the limbus is reached (Borcherding et al., 1975; Boote et al., 2003), and that the intermolecular collagen spacing within fibrils appears likewise constant (Boote, unpublished results), there is no reason to suppose that the elastic modulus of the fibrils will vary for different meridians. What of the volume fraction? Recent work has indicated that collagen fibrils are more tightly packed in the optical corneal zone compared to the periphery (Boote et al., 2003). However, the same study also indicated that the interfibrillar spacing falls off in a symmetric manner about the corneal centre. We might therefore reasonably expect the fibril volume fraction to be, on average, similar along different corneal meridians. Thus, the elastic modulus of the human cornea along its various meridians will be, to a first approximation, simply proportional to η (see Eq. (2)).

The reinforcement efficiency, η, is a quantitative measure of the ability of a pattern of collagen fibrils to reinforce a tissue in tension (Krenchel, 1964). For a laminated structure, in which the fibril directions are restricted to the lamellae planes, η has the form:

$$\eta = \int_0^{\pi} \frac{g(\phi)\cos^4\phi \, d\phi}{g(\phi)\, d\phi}, \quad (3)$$

where $g(\phi)$ is the probability of finding a fibril oriented at an angle ϕ to an applied load (Hukins, 1984). η is defined such that it has a value of unity if all the fibrils are oriented in the direction of the applied tension, but falls off to zero if they are perpendicular to this direction. For a laminate in which there is no preferred fibril orientation, η (from Eq. (3)) will equal 0.375 along every meridian in the lamella plane (Hukins, 1984). Conversely, for a perfect orthogonal arrangement of fibrils, where half the lamellae lie in one direction and half in a direction at right angles to this, η will equal 0.5 along the two directions and fall away to a minimum of 0.25 midway between the two (Hukins, 1984).

The situation in the human cornea appears to be somewhere in between the two aforementioned extremes. Table 1 indicates the two preferred corneal meridians are, on average, populated in equal proportion, while the X-ray scatter intensity distributions (e.g., Fig. 2B) indicate a Gaussian spread about these directions. We may qualitatively predict the mechanical performance of the ideal isotropic and orthogonal lamellar structures and of our human corneal model. We define E_{norm} to be the normalised elastic modulus, such that $E_{norm} = 1$ if all fibrils are aligned along the direction of interest and $E_{norm} = 0$ if they are perpendicular. Now, given E_f and β may be effectively treated as constants, E_{norm} simply takes the form of η (see Eq. (2)).

When we plot E_{norm} as a function of angle (see Fig. 3) the implication is that the normal human cornea will be equipped to withstand tensile stress more effectively along its superior–inferior and nasal–temporal trajectories than along the oblique directions. Moreover, the data in Fig. 3 implies that on average the elastic modulus will be similar along the two preferred trajectories. Such structural reinforcement might be necessary to balance the stress exerted by the ocular rectus muscles, as

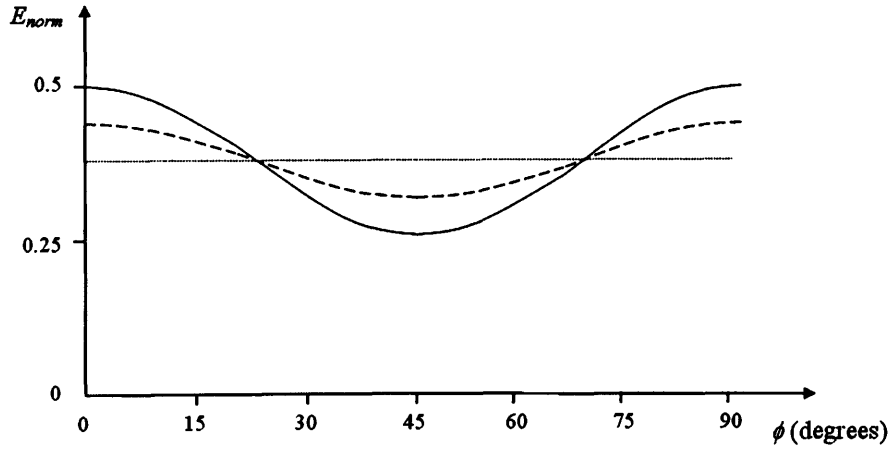

Fig. 3. Variation of normalised elastic modulus, E_{norm}, with angle, ϕ, for three theoretical collagenous lamellar structures: (1) A laminate in which the lamellae are arranged isotropically about ϕ (dotted line); (2) A laminate in which half the lamellae lie perfectly oriented at $\phi = 0°$ and the remaining half lie orthogonally at $\phi = 90°$ (continuous line); (3) An idealised human corneal stroma in which two identical Gaussian distributions of lamellae are spread about orthogonal preferred meridians at $\phi = 0°/90°$ (dashed line).

Appendix 8

has long been supposed (Daxer and Fratzl, 1997; Kokott, 1938); particularly in the horizontal direction. Indeed, Löpping and Weale (1965) noted that corneal curvature can be altered by prolonged action of the medial recti. Vertically, we may expect the action of the orbicularis, in moving the eyelids and squeezing the eyeball, to exert stress principally along the vertical corneal meridian. With-the-rule astigmatism is commonplace in neonates (Fischer, 1948), and has been attributed to the orbicularis squeezing the eye-ball during extended periods of crying (Marin-Amat, 1956). Moreover, Weale (1982) proposed that merely by inducing prolonged eyelid closure, the orbicularis might provide sufficient stress to produce a comparable reduction in the vertical corneal radius of curvature. We might then reasonably expect additional fibrils to be oriented along the superior–inferior meridian in order to help balance this. Thus, it may be that a balance of reinforcing fibrils along the superior–inferior and nasal–temporal meridians is a prerequisite if corneal shape is to be maintained under the combined action of muscles promoting eye movement and opening/closure.

In the cornea there is a significant proportion of corneal X-ray scatter which we may attribute to fibrils that are arranged isotropically (Fig. 2B). We expect this underlying "background" of isotropic fibrils to make an equal contribution to the absolute corneal elastic modulus along every meridian, without affecting the form of E_{norm} (Fig. 3). As such this arrangement appears ideal for setting up the isotropic tension in the cornea required to balance the intraocular pressure. Although the flexural stiffness of an isolated collagen fibril is negligible compared to its stiffness in tension (Jeronimidis and Vincent, 1984), any bending force which tends to stretch the fibril will enable it to take up at least some of the applied stress in tension and thereby confer mechanical reinforcement (Hukins, 1984). In the eye the intraocular pressure induces an outward force directed perpendicular to the stromal fibrils, causing them to bend and stretch. Furthermore, the lamellar structure of the cornea, together with its unusually narrow fibril diameter distribution (Borcherding et al., 1975), is designed to enable efficient collagen packing for enhanced reinforcement. Finally, it is worth noting some additional features of stromal collagen architecture which may further enhance the cornea's biomechanical stability. It is thought that the interweaving of lamellae and their insertion into the Bowman's layer both contribute to shape mediation of the anterior cornea (Bron, 2001; Müller et al., 2001); while the circumferential reinforcement of fibrils at the limbus (see Fig. 1) are thought to help withstand the increased tension in that region brought about by the differing curvatures of the cornea and sclera (Maurice, 1984).

It is reasoned that a specific arrangement of stromal collagen fibrils will be crucial in governing corneal shape and, since the cornea provides over 70% of the eye's dioptric power, in determining refractive status. Indeed, it is likely that some incidences of post-operative astigmatism might be due to incisions being made in corneal regions where fibril reinforcement is pivotal (Meek and Newton, 1999). The current data suggest that, centrally, the human cornea features, on average, equal numbers of reinforcing fibrils along its superior–inferior and nasal–temporal meridians (Table 1). However, some individual corneas show a considerable imbalance. We suspect that, through its effect on the corneal elastic modulus, this could impinge significantly on the relative superior–inferior and nasal–temporal radii of curvature, with implications for the cornea's refractive function.

Acknowledgments

The authors thank Val Smith of the UK Corneal Transplant Service Eye Bank (Bristol, UK) for provision of human corneas. The assistance of Dr. Mike MacDonald, Dr. Rob Kehoe, and Dr. Steve Buffy of the UK Synchrotron Radiation Source (Daresbury, UK) is also gratefully acknowledged. This work was funded by MRC Grant: G0001033.

References

Boote, C., Dennis, S., Newton, R.H., Puri, H., Meek, K.M., 2003. Collagen fibrils appear more closely packed in the prepupilliary cornea: optical and biomechanical implications. Invest. Ophthalmol. Vis. Sci. 44, 2941–2948.

Borcherding, M.S., Blacik, I.J., Sittig, R.A., Bizzell, J.A., Breen, M., Weinstein, H.G., 1975. Proteoglycans and collagen fibre organisation in human corneoscleral tissue. Exp. Eye Res. 21, 59–70.

Bron, A.J., 2001. The architecture of the corneal stroma. Br. J. Ophthalmol. 85, 379–383.

Daxer, A., Fratzl, P., 1997. Collagen fibril orientation in the human corneal stroma and its implications in keratoconus. Invest. Ophthalmol. Vis. Sci. 38, 121–129.

Fischer, F.P., 1948. Senescence of the eye. In: Sorsby, A. (Ed.), Modern Trends in Ophthalmology, vol. 2. Butterworth & Co, London.

Fung, Y.C., 1981. Biomechanics. Mechanical Properties of Living Tissues. Springer, New York.

Hjortdal, J.O., 1996. Regional elastic performance of the human cornea. J. Biomech. 29, 931–942.

Hukins, D.W.L., 1984. Collagen orientation. In: Hukins, D.W.L. (Ed.), Connective Tissue Matrix, vol. 5. Macmillan, London, pp. 212–240.

Hukins, D.W.L., Aspden, R.M., 1985. Composition and properties of connective tissues. Trends Biochem. Sci. 10, 260–264.

Jeronimidis, G., Vincent, J.F.V., 1984. Composite materials. In: Hukins, D.W.L. (Ed.), Connective Tissue Matrix, vol. 5. Macmillan, London, pp. 187–210.

Kato, Y.P., Christiansen, D.L., Hahn, R.A., Shieh, S.J., Goldstein, J.D., Silver, F.H., 1989. Mechanical properties of collagen fibres: a comparison of reconstituted and rat tail tendon fibres. Biomaterials 10, 38–42.

Kokott, W., 1938. Ubermechanisch-funktionelle strikturen des auges. Albrecht von Graefes Arch. Ophthalmol. 138, 424–485.

Appendix 8

Komai, Y., Ushiki, T., 1991. The three-dimensional organisation of collagen fibrils in the human cornea and sclera. Invest. Ophthalmol. Vis. Sci. 32, 2244–2258.

Krenchel, H., 1964. Fibre Reinforcement. Akademisk Forlag, Copenhagen.

Löpping, B., Weale, R.A., 1965. Changes in corneal curvature following ocular convergence. Vision Res. 5, 207–215.

Marin-Amat, M., 1956. Les variations physiologiques de la courbure de la corneépendant de vie. Leur importance et transcendance dans la refraction oculaire. Bull. Soc. Belge Ophthalmol. Mol. 113, 251–293.

Maurice, D.M., 1957. The structure and transparency of the corneal stroma. J. Physiol. 136, 263–286.

Maurice, D.M., 1984. The cornea and sclera. In: Davson, H. (Ed.), The Eye. Academic Press, Orlando.

Meek, K.M., Blamires, T., Elliott, G.F., Gyi, T.J., Nave, C., 1987. The organisation of collagen fibrils in the human corneal stroma: a synchrotron X-ray diffraction study. Curr. Eye Res. 6, 841–846.

Meek, K.M., Newton, R.H., 1999. Organisation of collagen fibrils in the corneal stroma in relation to mechanical properties and surgical practice. J. Refract. Surg. 15, 695–699.

Meek, K.M., Quantock, A.J., 2001. The use of X-ray scattering techniques to determine corneal ultrastructure. Prog. Retin. Eye Res. 20, 95–137.

Müller, L.J., Pels, E., Vrensen, G.F.J.M., 2001. The specific architecture of the anterior stroma accounts for maintenance of corneal curvature. Br. J. Ophthalmol. 85, 437–443.

Newton, R.H., Meek, K.M., 1998a. The integration of the corneal and limbal fibrils in the human eye. Biophys. J. 75, 2508–2512.

Newton, R.H., Meek, K.M., 1998b. Circum-corneal annulus of collagen fibrils in the human limbus. Invest. Ophthalmol. Vis. Sci. 39, 1125–1134.

Weale, R.A., 1982. A Biography of the Eye. Lewis & Co., London.

Changes in Collagen Orientation and Distribution in Keratoconus Corneas

Keith M. Meek,[1] *Stephen J. Tuft,*[2] *Yifei Huang,*[3] *Paulvinder S. Gill,*[1] *Sally Hayes,*[1] *Richard H. Newton,*[1] *and Anthony J. Bron*[4]

Purpose. To map the collagen orientation and relative distribution of collagen fibrillar mass in keratoconus corneal buttons.

Methods. Structural analysis was performed by obtaining synchrotron x-ray scattering patterns across the samples at 0.25-mm intervals. The patterns were analyzed to produce two-dimensional maps of the orientation of the lamellae and of the distribution of total and preferentially aligned lamellae.

Results. Compared with normal corneas, in keratoconus the gross organization of the stromal lamellae was dramatically changed, and the collagen fibrillar mass was unevenly distributed, particularly around the presumed apex of the cone.

Conclusions. The development of keratoconus involves a high degree of inter- and probably intralamellar displacement and slippage that leads to thinning of the central cornea and associated changes in corneal curvature. This slippage may be promoted by a loss of cohesive forces and mechanical failure in regions where lamellae bifurcate. (*Invest Ophthalmol Vis Sci.* 2005;46:1948-1956) DOI:10.1167/iovs.04-1253

The quality of image formation on the retina depends on the shape and transparency of the optical media, including the cornea, the main refractive component of the eye. Corneal shape and transparency are maintained by the ordered arrangement of its collagen fibrils, which lie parallel to each other and to the plane of the cornea.[1] In many animal corneas, these lamellae are not uniformly disposed[2]; and, in the human cornea, there is a preferred orientation in the inferior-superior and nasal-temporal directions,[3,4] mainly in the posterior stroma.[3] This preferred orientation occurs at the center of the cornea and is maintained to within 2 mm of the limbus, where a gradual change to a circular or tangential disposition occurs.[5,6] This may preserve the precise optics of the cornea by imparting stability at the limbus, a zone of abrupt curvature change between the sclera and cornea. Because the organization of corneal collagen is critical to the maintenance of the shape of the cornea, some modification is to be expected in disorders such as keratoconus, in which the shape is compromised.

Keratoconus is the commonest dystrophy of the cornea, with an incidence of approximately 50 to 230 per 100,000 of the population.[7,8] It is a frequent indication for keratoplasty in the United Kingdom (20% compared with 38% for endothelial failure[9]). Keratoconus is characterized by a progressive thinning and ectasia of the central cornea that causes myopia and irregular astigmatism. A rigid contact lens can restore useful vision in many patients, but in advanced disease a corneal graft may be necessary.

X-ray scattering (diffraction) is a powerful technique in which an intense beam of x-rays is passed through the tissue to produce a scattering pattern consisting of one or more reflections where constructive interference of the scattered beam occurs. The distribution of the scattered x-rays can then be used to determine quantitatively the gross orientation of all the collagen fibrils in the path of the x-ray beam—that is, in the full thickness of the tissue. Figure 1 shows how a beam of x-rays is scattered by an array of identical collagen fibrils with a distribution of angular orientations in the plane at right angles to the beam's direction. The scattered x-rays from fibrils oriented in a given direction produce a so-called equatorial reflection at right angles to the collagen fibril axes. The intensity of the reflection is proportional to the mass of fibrils oriented in that direction and falling in the path of the x-ray beam. Thus, if fibrils were arranged equally at all angles in the plane perpendicular to the x-ray beam, the reflection would be a ring of uniform intensity. If there were a distribution of fibrils around a single preferred orientation, the reflection would be two symmetrical arcs—the degree of arcing being quantitatively related to the angular spread in the fibril direction.

Using x-ray scattering, Daxer and Fratzl[4] demonstrated that in advanced keratoconus the angle between the preferred collagen orientations at the center of the cone were altered from 90° and 180° to 60° and 120°—evidence that the structural change in these corneas is related to large-scale changes in the directions of the collagen lamellae. Improvements in high-intensity synchrotron x-ray sources have resulted in faster data collection times and have now made it feasible to map in great detail the preferred directions of the collagen lamellae in corneal buttons, as well as the relative distribution of collagen fibril mass. We used these techniques to compare collagen orientation and the distribution of fibrillar mass in normal and keratoconus corneas.

Methods

Tissues

Two corneal buttons were obtained after penetrating keratoplasty for keratoconus and were marked for purposes of orientation. Neither patient had a history of acute corneal hydrops or other significant eye disease. Cornea A was a 7.75-mm button from a 49-year-old man with advanced keratoconus of the left eye, with an apical scar and irregular keratometry (<6.0 mm). The apex of the cone was displaced slightly inferiorly relative to the center of the cornea, but there was no

From the [1]School of Optometry and Vision Sciences, Cardiff University, Cardiff, United Kingdom; [2]Moorfields Eye Hospital, London, United Kingdom; the [3]Department of Ophthalmology, Great Wall Hospital of PLA, Beijing, Peoples Republic of China; and the [4]Nuffield Department of Ophthalmology, University of Oxford, Oxford, United Kingdom.

Supported by Grant 0055710 from The Wellcome Trust and Grant G0001033 from the Medical Research Council.

Submitted for publication October 25, 2004; revised January 14, 2005; accepted January 18, 2005.

Disclosure: **K.M. Meek**, None; **S.J. Tuft**, None; **Y. Huang**, None; **P.S. Gill**, None; **S. Hayes**, None; **R.H. Newton**, None; **A.J. Bron**, None

The publication costs of this article were defrayed in part by page charge payment. This article must therefore be marked "*advertisement*" in accordance with 18 U.S.C. §1734 solely to indicate this fact.

Corresponding author: Keith M. Meek, School of Optometry and Vision Sciences, Cardiff University, Redwood Building, King Edward VII Avenue, Cardiff CF10 3NB, UK; meekkm@cf.ac.uk.

Investigative Ophthalmology & Visual Science, June 2005, Vol. 46, No. 6

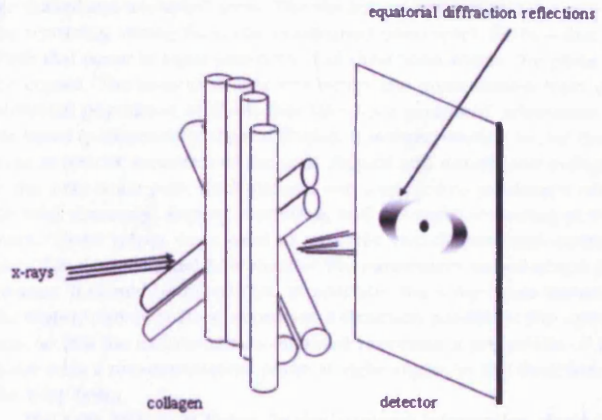

FIGURE 1. A beam of parallel x-rays scattered by an array of collagen fibrils with different orientations within a plane perpendicular to the direction of the incident x-ray beam. At small angles, as shown, the equatorial x-ray scattering arises from the distribution of collagen fibrils, and at wide angles it arises from the distribution of collagen molecules within the fibrils[9]; but, because the constituent collagen molecules are arranged approximately parallel to the fibril axis, for the present purposes, molecular orientation is a good approximation of fibril orientation.

peripheral thinning. Cornea B was a 7.5-mm button from a 28-year-old man who had a 13-year history of keratoconus. There was an apical cone with a small apical corneal scar. There was high astigmatism with right eye keratometry of 5.8 mm at 10° and <5.5 mm at 110° (normal, ~7.6 mm). Unfortunately, no videokeratography was available. A normal left human cornea with scleral rim attached was obtained from the CTS Eye Bank (Bristol, UK) and was equilibrated to physiological hydration, as described previously.[5] The central, 7.75-mm button was trephined for comparison with the pathologic corneal buttons. The keratoconus buttons and normal cornea used in the present study were treated similarly, by being tightly wrapped in clinging film to prevent evaporation and stored at −80°C until x-ray examination. All donors had given permission to use their tissues for research. Tissue procurement and use was in accordance with the Declaration of Helsinki and local regulations.

X-ray Data Collection

Each cornea was mounted in an air-tight Perspex cell, in which the humidity was maintained during the lengthy exposure to the x-ray beam (approximately 20 hours). Tissue hydration was measured before and after the experiment and was found to have decreased by <1%. Irradiation was performed at the synchrotron radiation source (SRS; Daresbury, UK). The specimens were examined at Station 7.2 by a beam with a 0.1-mm diameter cross section, a camera length of 12 cm, and an x-ray wavelength of 0.1488 nm. The specimen cell was mounted on a translation stage that could be moved both horizontally and vertically, either manually or by means of a stepper motor. With exposures of 30 seconds, scattering patterns were collected on an image plate detector (Mar Research, Hamburg, Germany) at each point across a 0.25 × 0.25-mm grid, to give nearly 800 x-ray patterns per specimen. Scattering from noncollagenous components of the tissue was subtracted, and the patterns were normalized to take account of fluctuations in x-ray beam intensity.[5]

Analysis of X-ray Data

Figure 2a shows a wide-angle x-ray pattern from a region of a keratoconus cornea where collagen fibrils were preferentially aligned mainly in one direction. The pattern consists of an x-ray reflection that takes the form of equatorial arcs, indicating in this case a spread of fibril axis orientations about the vertical direction. Starting at 0° at the left of the reflection, the intensity of the scattered x-rays was measured as a function of angle. The result is the intensity distribution shown in Figure 2b. This distribution contains three types of information about the fibril orientations. The total area under the graph (the total scattered intensity) is proportional to the total mass of fibrillar collagen in the path of the x-ray beam. This has two components, represented by

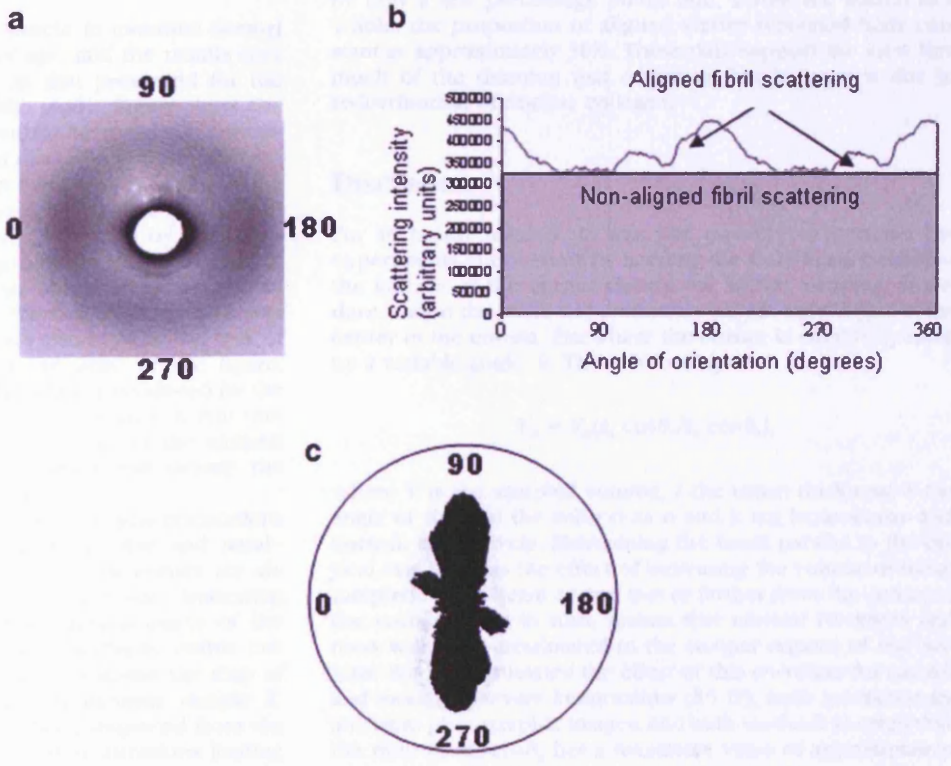

FIGURE 2. (a) Wide-angle x-ray pattern from near the cone of a keratoconus cornea. The *white spot* at the center is the shadow of a lead beam-stop used to suppress the intense unscattered x-ray beam. (**b**) Integrated intensity as a function of angle around the reflection. The scatter intensity can be divided into two components. Nonaligned scattering (*shaded area*) comes from a population of fibrils equally distributed in at all angles within the plane of the cornea. Aligned scattering (*clear area*) comes from a population of fibrils that have a preferential orientation within the plane of the cornea. After removal of the nonaligned component and the application of a 90° phase shift to account for the fact that x-ray equatorial reflections occur at right angles to the fibril or molecular axis, the data in (**b**) are plotted as a polar plot (**c**). Asymmetry in this plot shows the preferred orientation of the collagen averaged throughout the tissue thickness at the position through which the x-rays pass.

the shaded and unshaded areas. The shaded area represents the part of the scattering arising from the nonaligned (isotropic) fibrils—that is, fibrils that occur in equal numbers in all directions within the plane of the cornea. The unshaded area represents the contribution from the additional population of fibrils that take up a preferred orientation in the tissue (preferentially aligned fibrils). It is thus possible to use these areas as relative measures of the total aligned and nonaligned collagen in the x-ray beam path. Each pattern was analyzed to produce a value for total scattering, aligned scattering, and isotropic scattering at that point. These values were used to produce two-dimensional contour plots that demonstrated how each of the parameters varied across the corneas. It should be noted that, in practice, the x-ray beam traverses the slightly curved corneal buttons in a direction parallel to the optical axis, so that the measurements obtained represent a projection of the tissue onto a two-dimensional plane at right angles to the direction of the x-ray beam.

The x-ray pattern in Figure 2a also contains information about the distribution in the spread of the axes of the preferentially aligned fibrils. To represent this angular distribution of fibrils, the following procedure was performed. First, the nonaligned fibril scatter was removed (i.e., the shaded part of the graph in Fig. 2b was subtracted, leaving only the unshaded area). This left the distribution of x-ray intensity as a function of angle for only the preferentially aligned fibrils. This distribution was then converted into a polar (vector) plot (Fig. 2c), taking into account the fact that the x-ray intensity appears at right angles to the fibril axis.[10,11] The radial length of the polar plot at a given angle is directly proportional to the mass of collagen fibrils aligned at that angle. The overall size of the plot is therefore related to the total mass of aligned collagen, and the asymmetry gives an indication of the preferential direction(s) of this collagen. Thus, in this example, most preferentially aligned fibrils run vertically and none run horizontally. Polar plots were produced from the scattering patterns obtained from each point on the grid, and these plots were then assembled as a montage to show how the preferred collagen orientation varies across the normal and the keratoconus corneal buttons.

Results

We used the techniques described herein to examine normal corneas between 25 and 86 years of age, and the results (not shown) were essentially the same as that presented for the button chosen as the control for the study. Figure 3a is the collagen orientation map for this control button. Each constituent polar plot shows the preferred directions of the collagen fibrils at that point in the tissue. The control cornea shows the two preferred, orthogonal orientations of lamellae throughout most of the button. This arrangement is shown by the cross-shaped polar plots, indicating collagen preferentially aligned in the vertical and horizontal directions. The plots are smaller in the central part where the cornea is thinner, as there are fewer collagen fibrils in the path of the x-ray beam. Note the lack of an orthogonal arrangement toward the edge of the figure. Although the possibility of some edge effects produced by the trephining process cannot be excluded, it is known that outside the central 7 mm (i.e., toward the edge of the excised button), additional fibrils cross the cornea and swamp the contribution from the orthogonal lamellae.[12]

Figure 3b shows the map of preferred collagen orientations in keratoconus button A. The inferior-superior and nasal-temporal preferred orientations in the normal cornea are absent in the tissue, except at the temporal side, indicating rearrangement of lamellar orientations across much of the corneal button. The region of the cone is clearly visible just below the center of the montage. Figure 4 shows the map of preferred collagen orientation from keratoconus sample B. Again, many lamellae appear to have been displaced from the normal orthogonal arrangement into other directions leading to severe disruption of the collagen orientation throughout the button. In Figures 3b and 4, there is evidence that the lamellae tend to curve around or are tangential to the edge of the cone.

Contour plots of total and preferentially aligned collagen from the two keratoconus buttons and the normal button are presented in Figure 5. The normal cornea shows a fairly regular increase in collagen mass from the center outward (Fig. 5a). This reflects the increasing thickness as one moves outward from the central cornea (compounded by the slight curvature of the cornea). Figures 5b and 5c show the positions of the keratoconus cones, where the amount of collagen is greatly reduced. Figures 5d, 5e, and 5f show the distribution of preferentially aligned collagen in the three corneas. In the normal cornea, the preferentially aligned collagen did not follow the same distribution pattern as the total collagen and, in particular, preferentially aligned collagen increased at the edge of the button in the four quadrants, to form a diamond shape in the center. This pattern is characteristic of normal human corneas and is likely to be due to the presence of additional anchoring lamellae that traverse and hence contribute to the increased thickness of the peripheral cornea.[12] Nevertheless, the amount of preferentially aligned collagen is relatively uniform throughout the central (prepupillary) cornea. The preferentially aligned collagen in keratoconus (Figs. 5e, 5f), in contrast, showed much more variation than normal. The uniformity across the central cornea was lost, with regions of more highly aligned collagen intermixed with regions in which there was little aligned collagen. There appeared to be a gross distortion of the normal diamond-shaped distribution of peripherally oriented fibrils.

It would be of interest to compare the total and aligned scatter summed across each of the corneas. However, because scattering increases away from the central cornea and because of the unknown edge effects of the trephining process, it is safer to consider just the central parts of the buttons. Table 1 shows the relative scatter from the central 20 mm^2. It is striking that, despite the considerable thinning that occurred in part of the keratoconus corneas, the total scatter was reduced by only a few percentage points and, across the button as a whole, the proportion of aligned scatter remained fairly constant at approximately 30%. These data support the view that much of the thinning that occurs in keratoconus is due to redistribution of fibrillar collagen.

Discussion

For technical reasons, it was not possible to perform the experiments in this study by keeping the x-ray beam normal to the surface of the cornea during the whole mapping procedure, and so the beam and cornea are only at right angles at the center of the cornea. Elsewhere the cornea is effectively tilted by a variable angle, θ. The relationship is

$$V_k = V_n(t_k \cos\theta_n / t_n \cos\theta_k),$$

where V is the sampled volume, t the tissue thickness, θ the angle of tilt, and the subscripts n and k are keratoconus and normal, respectively. Maintaining the beam parallel to the optical axis thus has the effect of increasing the volume of tissue sampled by the beam as one moves farther from the center of the cornea. This, in turn, means that corneal thickness and mass will be overestimated in the steeper regions of the buttons. We have estimated the effect of this curvature for normal and moderate/severe keratoconus (55 D), both geometrically and from photographic images, and both methods showed that the ratio $\cos\theta_n/\cos\theta_k$ has a maximum value of approximately

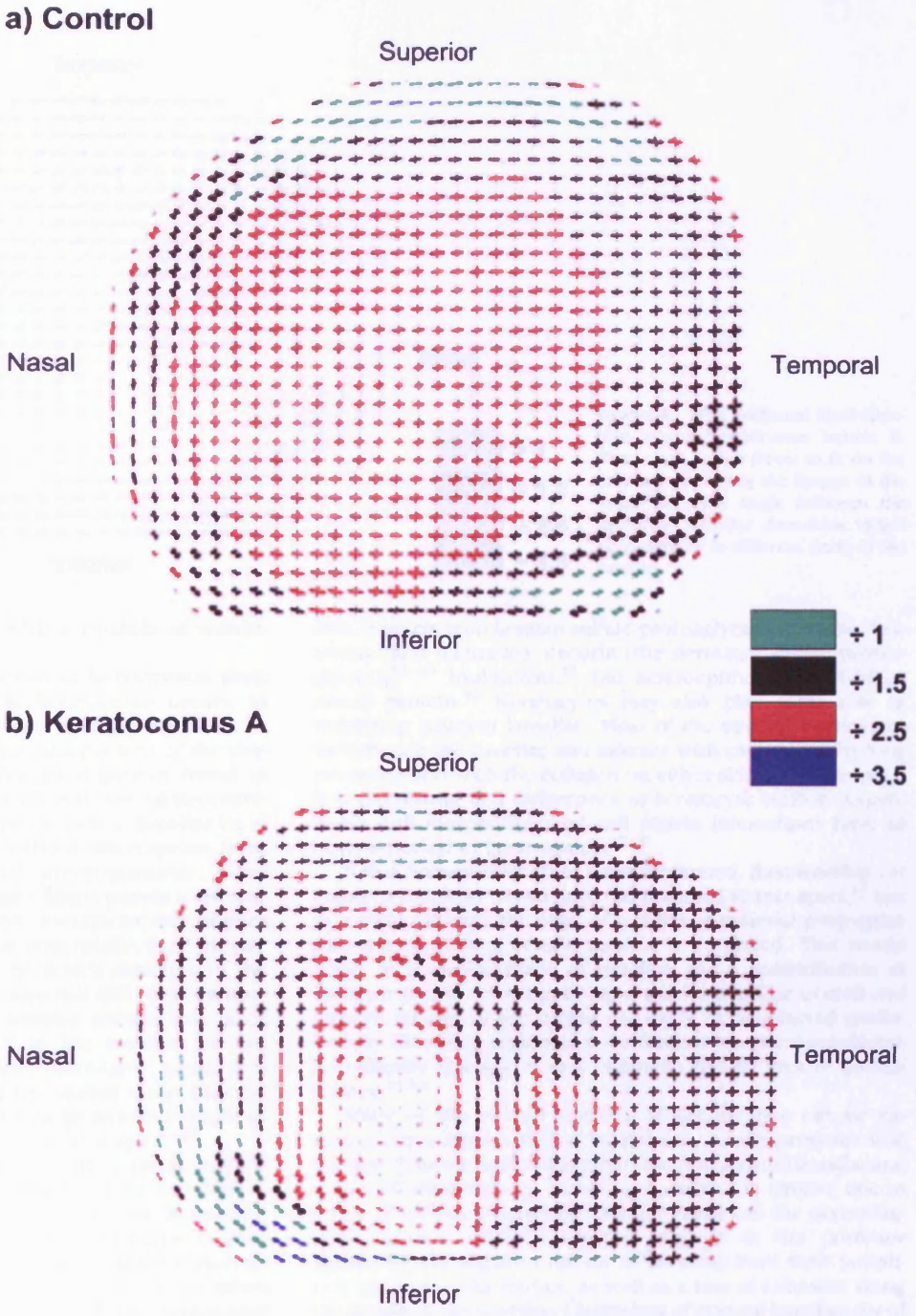

FIGURE 3. The preferred fibril direction across (**a**) the normal corneal button and (**b**) keratoconus button A. The scale of the individual polar plots was chosen so that the shape of those in the thinnest part of the cornea could just be discerned. As a consequence, plots in other regions were too large to fit in the montage and so were scaled down by the factors indicated by the color key. The *cross-shaped symbols* across most of the normal button indicate vertical and horizontal preferred orientations. In the keratoconus button, the region of greatest thinning was elongated vertically, and contained the least aligned collagen. There is also the suggestion that the cone was subdivided into two more circular regions. There were large, local variations in the sizes of the plots, probably arising from thinning and a focal increase in area (i.e., ectasia).

1.06, indicating an oversampling of the keratoconus button of ~6% at its steepest position.

Two chief mechanisms for the development of keratoconus have been put forward. One proposes that ectasia is closely associated with tissue degradation or reduced maintenance,[13] whereas the other suggests that it is due to slippage between collagen fibrils,[14] with no overall tissue loss. These concepts are not mutually exclusive, since enzymatic degradation could permit slippage between collagen fibrils.

The x-ray data presented herein, extend the findings of Daxer and Fratzl,[4] indicating a gross rearrangement of vertical and horizontal collagen lamellae in keratoconus. We have provided evidence that many of the posterior lamellae are displaced, particularly near the presumed apex of the cone and that changes can occur at least to the edge of the excised buttons. The total scattering contour maps in Figures 5a, 5b, and 5c show that, in keratoconus, there is a very uneven distribution of collagen, with no circular symmetry in the center of the cornea. Similarly, a distortion of the peripheral diamond-shaped pattern of anchoring lamellae, suggests a redistribution of preferentially aligned collagen at the periphery of the button (Figs. 5d, 5e, 5f). This change in fibril orientation is difficult to explain on the basis of tissue degradation alone, since collagen loss would be unlikely to give rise to a systematic realignment of fibrils. In our opinion, it is more readily explained in terms of collagen fibril

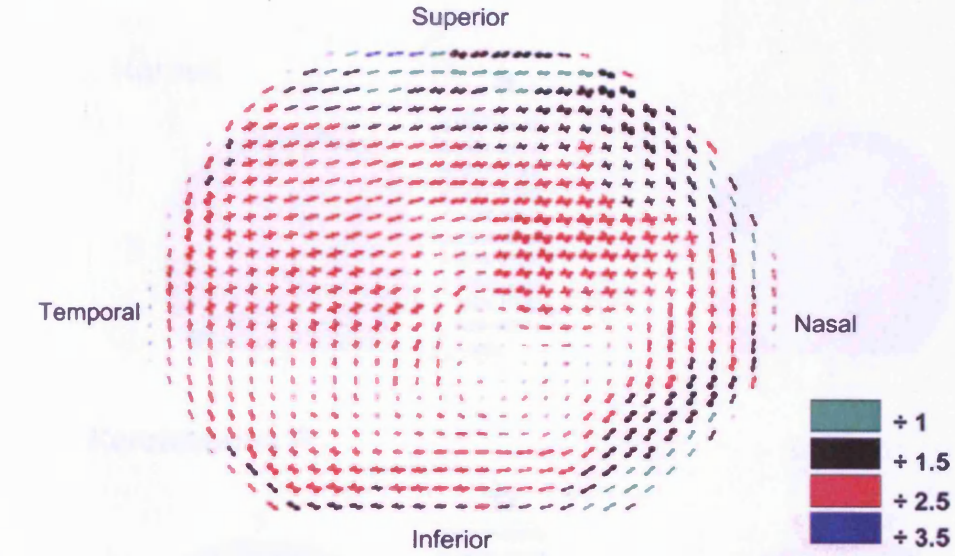

FIGURE 4. The preferred fibril direction across keratoconus button B. Plots were scaled down to fit on the montage, by using the factors in the color key. The angle between the preferred lamellar directions varied considerably in different parts of the sample.

slippage, perhaps in conjunction with a process of remodeling.

Any explanation for the mechanism of keratoconus must account for the altered profile of the keratoconus cornea, in the apparent absence of breaks in the collagen bundles. To understand how the ordered lamellar arrangement of the corneal stroma may give rise to the disrupted pattern found in keratoconus, it is necessary to review normal corneal structure. In the posterior two thirds of the human cornea, lamellae lie in the plane of the cornea and run without interruption from limbus to limbus with a limited anteroposterior interweave.[15–18] At the limbus, the collagen fibrils pursue a circular or pseudocircular course. The term pseudocircular implies that, although fibrils enter the limbus tangentially, their precise origins are unknown. Although the preferred direction of the posterior lamellae is in the inferior–superior and nasal–temporal directions, the lamellae of the anterior stroma have little preferred meridional arrangement.[3] In the anterior stroma, there is an extensive anteroposterior interweave, and a proportion of the lamellae that arise in the limbus insert into the region of Bowman's layer.[18–30] This arrangement is thought to be essential for the maintenance of corneal shape.[31,32]

The anterior lamellae often split in both a lateral and an anterior–posterior direction.[29,33,34] Studies from our laboratory[6,12] and elsewhere[29,34] indicate that many corneal lamellae do not course straight across the cornea from limbus to limbus, but rather follow a less direct route. Scanning electron microscopy of normal corneas revealed frequent instances when lamellae split into two narrower lamellae (Fig. 6a), which may subsequently fuse with lamellae running in a different direction.[29] The constituent collagen fibrils within these lamellae are therefore somewhat longer than they would have to be if they were to follow a more direct route. The points at which lamellae split[35] are potentially weak, and rely on interfibrillar forces to maintain cohesion (Fig. 6b). Surgical dissection of the corneal stroma is not resistance free, even posteriorly where there is less anteroposterior interweave, suggesting that there are other elements that bind the collagen lamellae together.[36] Part of this resistance is due to interactions between the collagen fibrils (e.g., type III and heteromeric type I and V collagens) and other matrix proteins, such as the proteoglycans,[37,38] dermatopontin,[39] and type VI collagen.[40] Type VI collagen acts as a bridge between type I collagen fibrils[41] and also interacts with keratan sulfate proteoglycans (lumican, keratocan, and mimecan), decorin (the dermatan sulfate proteoglycan),[42–44] hyaluronan,[45] and keratoepithelin, or TGFβ-induced protein.[46] Keratocytes may also play some role in stabilizing adjacent lamellae. Most of the stromal keratocytes lie between the lamellae and interact with each other via long processes and with the collagen on either side. In this respect, it is interesting that differences in keratocyte surface components, cell morphology and cell–matrix interactions have all been reported in keratoconus.[47,48]

If this "interfibrillar glue" were weakened, then lamellae (or collagen bundles) would have the potential to tear apart,[14] just as a nick, cut into the edge of a piece of material propagates into a tear when a certain tension is exceeded. This would result in a displacement of lamellae and a redistribution of collagen locally, as we have reported herein. The central and inferior regions of the cornea are likely to be affected preferentially (the main region of cone formation), since interlamellar cohesive strength is at a minimum in that area in normal cornea.[49,50]

Many of the clinical features of keratoconus can be explained by a biomechanical hypothesis, which proposes that corneal thinning and ectasia is the result of an interlamellar and an interfibrillar slippage of collagen within the stroma, due to a loss of cohesion between collagen fibrils and the noncollagenous matrix.[4,14,49–54] Lamellar slippage in the posterior stroma would require a release of lamellae from their peripheral location at the limbus, as well as a loss of cohesion along the length of the lamellae. Unraveling of corneal lamellae (or of individual fibrils) from the limbus, and/or throughout the cornea would account for the lateral rearrangement of lamellae. This unraveling would also increase the effective length of lamellae, thus releasing tension on the fibrils and allowing deformation. For the anterior lamellae, unraveling could imply, in addition, the disinsertion of lamellae from their anchoring sites in Bowman's layer.

Thinning is a presenting finding in keratoconus[54] and Edmund[52] demonstrated that, except in advanced keratoconus, the cross-sectional area of corneas in optical section did not differ from that of normal corneas. This implies that ectasia occurs by a redistribution of stromal mass, rather than by a loss from extensive tissue degradation. While Edmund found no direct evidence that lamellae are released from their limbal

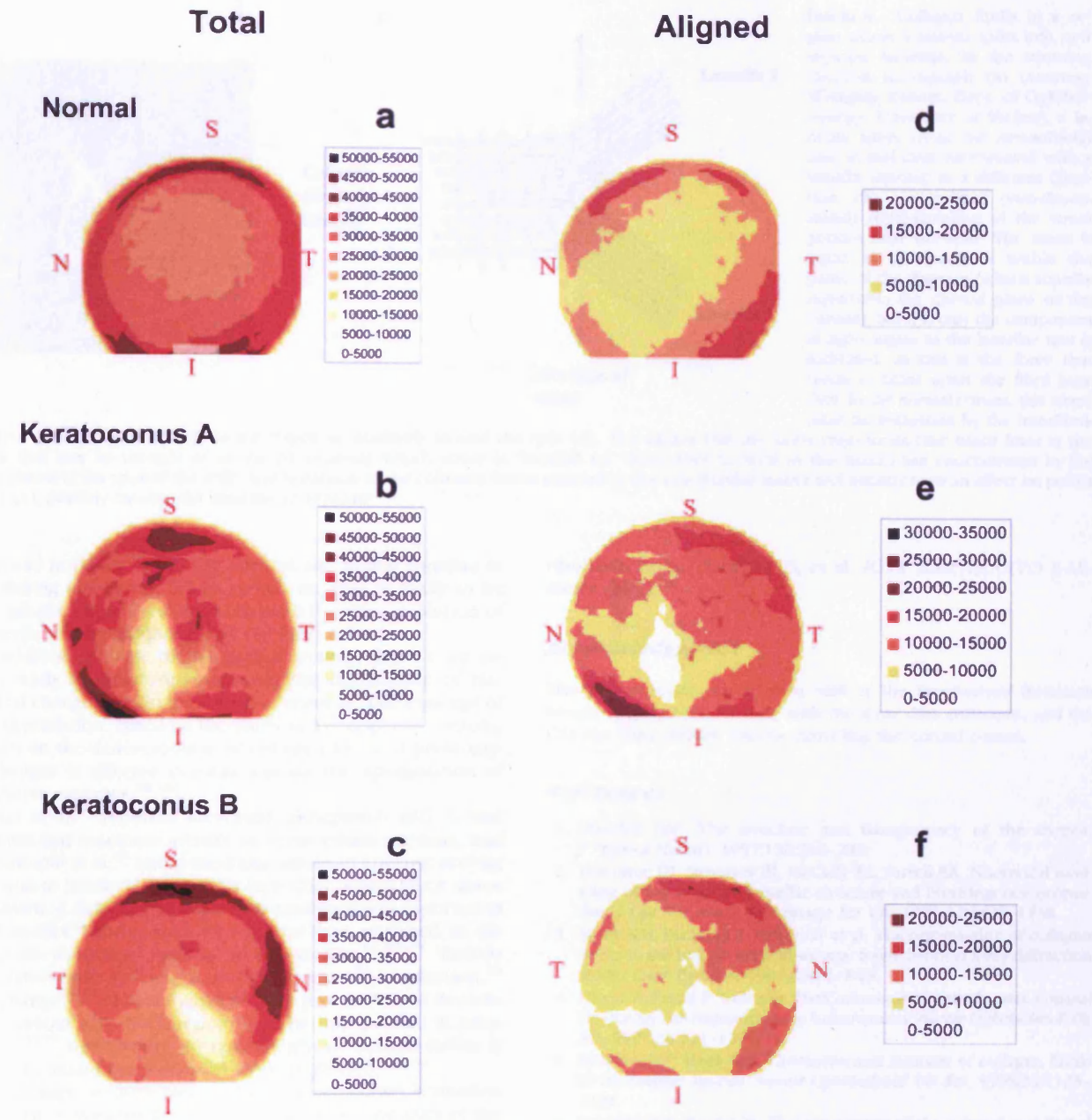

FIGURE 5. Scattering-intensity maps from the corneal buttons. (**a**), (**b**), and (**c**) are the total scatter (arbitrary units) and (**d**), (**e**), and (**f**) are the aligned scatter (same arbitrary units). The superior (S) inferior (I), nasal (N) and temporal (T) sides of each button are indicated.

location,[55] Owens and Watters[56] showed that thickness was reduced outside the cone. Measuring 4 mm from the center, they found a significant reduction of (5.8%) superiorly, (6.9%) superotemporally, (13.8%) inferotemporally, (9.4%) inferonasally, and (8.2%) nasally. There was a 7.6% reduction in thickness inferiorly, 5.6 mm from the corneal center.[56]

Processes that lead to a lengthening of stromal collagen lamellae without rupture must be assumed to occur physiologically in the developing eye with prenatal corneal growth. This could come about in different ways. Birk et al.[57] established that in chick tendon and cornea, collagen fibrils grow by a process of interstitial extension, due to fusion of fibril "segments" which increase in length over time (e.g., 10–30 μm in the 14-day-old tendon and >60 μm in the 18-day-old tendon).[57–59] For the cornea, it cannot be excluded too, that remodeling includes fibril end-lengthening and fibril slippage before cessation of growth. We hypothesize that one mechanism for keratoconus could be that the physiological events

TABLE 1. Relative X-Ray Scatter from the Central 20 mm^2 of the Corneal Buttons

Specimen	Total Scatter*	Aligned Scatter*	Ratio of Aligned to Total Scatter (%)
Normal	100	100	30
Keratoconus A	96	108	34
Keratoconus B	93	88	29

* Data are expressed as a percentage of normal.

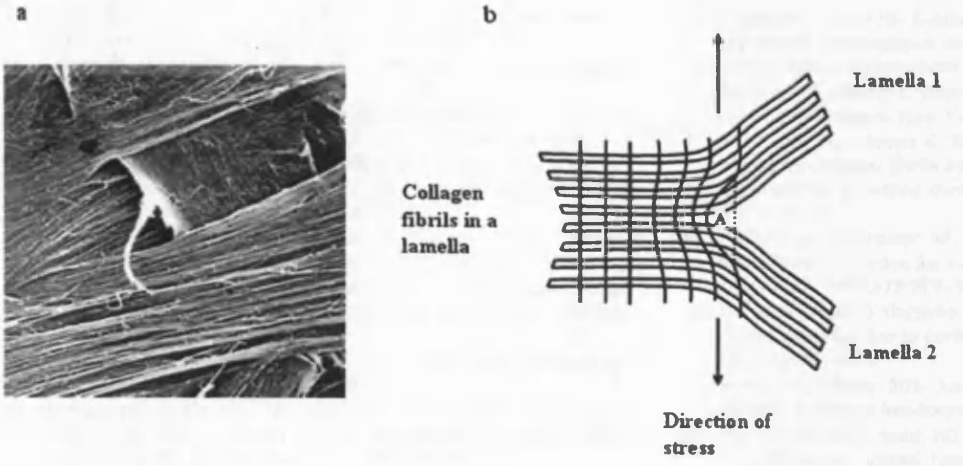

FIGURE 6. Collagen fibrils in a region where a lamella splits into two separate lamellae. In the scanning electron micrograph (**a**) (courtesy Wolfgang Radner, Dept. of Ophthalmology, University of Vienna), a lamella splits (near the *arrowhead*) and, in this case, interweaves with a lamella running in a different direction. (**b**) A simplified (two-dimensional) representation of the stress pattern near the split. The stress is equal in all directions within the plane of the diagram (which actually represents the curved plane of the cornea), but it is only the component at right angles to the lamellae that is indicated, as this is the force that tends to tease apart the fibril bundles. In the normal cornea, this stress must be withstood by the interfibrillar matrix. Strain is relieved only in the region immediately around the split (A). This means that the stress trajectories (the *black lines* in the diagram that may be thought of as the paths along which stress is "handed on" from fibril to fibril in the tissue) are concentrated in the neighborhood of the apex of the split. Any reduction in the cohesive forces exerted by the interfibrillar matrix will initially have an effect on points such as (A), possibly causing the lamellae to separate.

that would normally "lock" the corneal and limbal lamellae in place during childhood, fail to switch in. This is likely to be under genetic control and could explain the slow evolution of keratoconus from childhood and the early teens.

In addition to these biomechanical events, there is an extensive body of literature supporting the occurrence of biochemical changes within keratoconus corneas. The concept of tissue degradation, based on the study of keratoplasty buttons, depends on the demonstration of collagen loss and proteoglycan changes in affected corneas and on the upregulation of degradative enzymes.[60-63]

Zhou et al.[64] reported increased cathepsin-B and -G and gelatinase and caseinase activity in keratoconus corneas, and Sawagamuchi et al.[65] found focal alterations in enzyme activity in relation to breaks in Bowman's layer that would favor tissue breakdown. A defect in glycoprotein synthesis was reported in earlier studies[66] and numerous workers have reported an abnormal electron-dense material in the stroma.[35,67-73] Various investigators have variously found an increase,[73] a reduction,[74] or no change[61,75] in proteoglycans. The proteoglycans decorin and keratocan have been reported to be upregulated in keratoconus,[76,77] whereas the glycosaminoglycan keratan sulfate is reduced in amount and possibly downregulated.[78-80]

In summary, we have shown that in keratoconus, formation of the cone is associated with displacement of the axes of the collagen fibrils and distortion of the orthogonal matrix. This implies a degree of lamellar fluidity and slippage. We propose that the displacement and redistribution are primarily caused by an unraveling of lamellae, along their length and from their limbal anchors, and a teasing apart at points where lamellae bifurcate and from Bowman's layer. This alteration could result from the failure of a "locking mechanism" normally established in infancy and childhood, or from the effects of enzymatic digestion. We contend that in keratoconus, an as yet unidentified primary event,[13] which may be under genetic control, triggers a breakdown of the "glue" that stabilizes collagen fibrils and facilitates the process of lamellar or fibrillar slippage that we describe herein. This hypothesis has therapeutic implications, and it is relevant that attempts are being made to slow down the progression of keratoconus by enhancing stromal cross-linking. Some success has been claimed recently for a photosensitizing regimen in which cross-linking is enhanced by exposing the eye to UVA after the application of topical riboflavin drops (Sandner D, et al. *IOVS* 2002;43:ARVO E-Abstract 2887).[81]

Acknowledgments

The authors thank the support staff at the Synchrotron Radiation Source at Daresbury for help with the x-ray data collection, and the CTS Eye Bank (Bristol, UK) for providing the normal cornea.

References

1. Maurice DM. The structure and transparency of the cornea. *J Physiol (Lond)*. 1957;136:263-286.
2. Donohue DJ, Stoyanov BJ, McCally RL, Farrell RA. Numerical modeling of the cornea's lamellar structure and birefringence properties. *J Opt Soc Am A Opt Image Sci Vis*. 1995;12:1425-1438.
3. Meek KM, Blamires T, Elliott GF et al. The organisation of collagen fibrils in the human corneal stroma: a synchrotron x-ray diffraction study. *Curr Eye Res*. 1987;6:841-846.
4. Daxer A, Fratzl P. Collagen fibril orientation in the human corneal stroma and its implications in keratoconus. *Invest Ophthalmol Vis Sci*. 1997;38:121-129.
5. Newton RH, Meek KM. Circumcorneal annulus of collagen fibrils in the human limbus. *Invest Ophthalmol Vis Sci*. 1998;39:1125-1134.
6. Newton RH, Meek KM. The integration of the corneal and limbal fibrils in the human eye. *Biophys J*. 1998;75:2508-2512.
7. Krachmer JH, Feder RS, Belin MW. Keratoconus and related noninflammatory corneal thinning disorders. *Surv Ophthalmol*. 1984;28:293-322.
8. Rabinowitz YS. Keratoconus. *Surv Ophthalmol*. 1998;42:297-319.
9. Vail A, Gore SM, Bradley BA, et al. Corneal transplantation in the United Kingdom and Republic of Ireland. *Br J Ophthalmol*. 1993;77:650-656.
10. Meek KM, Quantock AJ. The use of x-ray scattering techniques to determine corneal ultrastructure. *Prog Ret Eye Res*. 2001;96-137.
11. Connon CJ, Meek KM. Organization of corneal collagen fibrils during the healing of trephined wounds in rabbits. *Wound Repair Regen*. 2003;11:71-78.
12. Aghamohammedzadeh KM, Newton RH, Meek KM. X-ray scattering used to map the preferred collagen orientation in human cornea and limbus. *Structure*. 2004;12:249-256.
13. Kenney MC, Brown DJ, Rajeev B. Everett Kinsey Lecture. The elusive causes of keratoconus: a working hypothesis. *CLAO J*. 2000;26:10-13.

Appendix 9

14. Polack F. Contribution of electron microscopy to the study of corneal pathology. *Surv Ophthalmol.* 1976;20:375-414.
15. Kokott W. Das Spaltlinienbild der Sklera. *Klin Monatsbl Augenheilkd.* 1934;92:117-185.
16. Kokott W. Über mechanisch-funktionelle Strukturen des Auges. *Albrecht von Graefes Arch Ophthalmol.* 1938;138:424-485.
17. Smelser GK, Oszanics V. New concepts in anatomy and histology of the cornea. In: King JH, McTigue JW, eds. *The Cornea World Congress.* London; Butterworth, 1965:1-20.
18. Maurice DM. The cornea and sclera. In: Davson H, ed. *The Eye.* 2nd ed. Vol. 1. New York: Academic Press, 1969:489-600.
19. Salzmann M. *The Anatomy and Histology of the Human Eyeball in the Normal State: Its Development and Senescence.* Chicago: University Chicago Press;1912.
20. Polack FM. Morphology of the cornea. I. Study with silver stains. *Am J Ophthalmol.* 1961;51:1051-1056.
21. McTigue JW. The human cornea: a light and electron microscopic study of the normal cornea and its alterations in various dystrophies. *Trans Am Ophthalmol Soc.* 1967;65:591-660.
22. Fine BS, Yanoff M. *Ocular Histology: A Text and Atlas.* 2nd ed. New York: Harper and Row; 1979.
23. Goldman JN, Benedek CH, Dohlman CH, et al. Light diffraction and scattering in swollen human corneas. *Invest Ophthalmol.* 1968;7:501-519.
24. Bron AJ, Tripathi RC. The anterior corneal mosaic. *Br J Physiol Opt.* 1970;25:8-13.
25. Hogan MJ, Alvarado JA, Weddell JE. *Histology of the Human Eye.* Philadelphia: WB Saunders; 1971.
26. Davson H. *The Eye.* New York: Academic Press; 1984. *Vegetative Physiology and Biochemistry*; Vol 1b.
27. Smolek MK, McCarey BE. Interlamellar adhesive strength in human eyebank corneas. *Invest Ophthalmol Vis Sci.* 1990;31:1087-1099.
28. Komai Y, Ushiki T. The three-dimensional organisation of collagen fibrils in the human cornea and sclera. *Invest Ophthalmol Vis Sci.* 1991;32:2244-2258.
29. Radner W, Zehetmayer M, Aufreiter R, et al. Interlacing and cross-angle distribution of collagen lamellae in the human cornea. *Cornea.* 1998;17:537-543.
30. Klyce SD, Beuerman RW. Structure and function of the cornea. In: Kaufman HE, Barron BA, McDonald MB, et al., eds. *The Cornea.* New York: Churchill Livingstone; 1989:3-28.
31. Müller LJ, Pels E, Vrensen GFJM. The specific architecture of the anterior stroma accounts for maintenance of corneal curvature. *Br J Ophthalmol.* 2001;85:437-443.
32. Bron AJ. The architecture of the corneal stroma. *Br J Ophthalmol.* 2001;85:379-383.
33. Radner W, Zehetmeyer M, Mallinger R, et al. Zur dreidimensionalen Anordnung der collagenen Lamellen im posterioren Stroma der menschlichen Hornhaut. *Spektr Augenheilkd.* 1993;7:77-80.
34. Radner W, Mallinger R. Interlacing of collagen lamellae in the midstroma of the human cornea. *Cornea.* 2002;21:598-601.
35. Pataa CL, Joyon L, Roucher F. Ultrastucture du keratocone. *Arch Ophtalmol (Paris).* 1970;80:403-418.
36. Maurice DM. Some puzzles in the microscopic structure of the stroma. *J Refract Surg.* 1996;12:677-683.
37. Meek KM, Elliott GF, Nave C. A synchrotron x-ray diffraction study of bovine cornea stained with cupromeronic blue. *Collagen Relat Res.* 1986;6:203-218.
38. Scott JE, Haigh M. Proteoglycan-Type I collagen fibril interactions in bone and non-calcifying tissues. *Biosci Rep.* 1985;5:71-81.
39. Nieduszynski IA, Brown GM, Ellis TS, et al. Dermatopontin interactions with keratan sulphate proteoglycans (abstract). Eighth Corneal Conference, Cardiff, Wales, UK 2004. *Ophthalmic Res.* 2004;36:285.
40. Hirano K, Kobayashi M, Kobayashi K, et al. Experimental formation of 100-nm periodic fibrils in the mouse corneal stroma and trabecular meshwork. *Invest Ophthalmol Vis Sci.* 1989;30:869-874.
41. Cho HI, Covington, HI, Cintron C. Immunolocalization of type VI collagen in developing and healing rabbit cornea. *Invest Ophthalmol Vis Sci.* 1990;31:1096-1102.
42. Takahashi T, Cho HI, Kublin CL, et al. Keratan sulfate and dermatan sulfate proteoglycan associate with type VI collagen in fetal rabbit cornea. *J Histochem.* 1993;41:1447-1457.
43. Bidanset DJ, Guidry C, Rosenberg LC, et al. Binding of the protein decorin to collagen type VI. *J Biol Chem.* 1992;267:5250-5256.
44. Nakamura M, Kimura S, Kobayashi M, et al. Type VI collagen bound to collagen fibrils by chondroitin/dermatan sulfate glycosaminoglycan in mouse corneal stroma. *Jpn J Ophthalmol.* 1997;41:71-76.
45. Kielty CM, Whittaker SP, Grant ME, et al. Type VI collagen microfibrils: evidence for a structural association with hyaluronan. *J Cell Biol.* 1992;118:979-990.
46. Rawe IM, Zhan Q, Burrows R, et al. Beta-Ig: molecular cloning and in situ hybridization in corneal tissues. *Invest Ophthalmol Vis Sci.* 1997;38:893-900.
47. Rock ME, Moore MN, Anderson JA, Binder PS. 3-D computer models of human keratocytes. *CLAO J.* 1995;21:57-60.
48. Yue BY, Baum JL, Smith BD. Identification of collagens synthesised by cultures of normal human corneal and keratoconus stromal cells. *Biochim Biophys Acta.* 1983;755:318-325.
49. Smolek MK. Interlamellar cohesive strength in the vertical meridian of human eye bank corneas. *Invest Ophthalmol Vis Sci.* 1993;34:2962-2969.
50. Smolek MK, Beekhuis WH. Collagen fibril orientation in the human corneal stroma and its implications in keratoconus. *Invest Ophthalmol Vis Sci.* 1997;38:1289-1290.
51. Bron AJ. Keratoconus: the Disease. *J Br Contact Lens Assoc.* 1984;7:56-62.
52. Edmund C. Corneal tissue mass in normal and keratoconic eyes in vivo estimation based on area of horizontal optical sections. *Acta Ophthalmol.* 1988;66:305-308.
53. Fullwood NJ, Tuft SJ, Malik NS, et al. Synchrotron x-ray diffraction studies of keratoconus corneal stroma. *Invest Ophthalmol Vis Sci.* 1992;33:1734-1741.
54. Kerr-Muir MG, Woodward EG, Leonard TJ. Corneal thickness, astigmatism, and atopy. *Br J Ophthalmol.* 1987;71:207-211.
55. Edmund C. The corneo-limbal ring in normal and keratoconic eyes. *Acta Ophthalmol.* 1988;66:376-380.
56. Owens H, Watters GA. An evaluation of the keratoconic cornea using computerised corneal mapping and ultrasonic measurements of corneal thickness. *Ophthalmic Physiol Opt.* 1996;16:115-123.
57. Birk DE, Nurminskaya MV, Zycband EI. Collagen fibrillogenesis in situ: fibril segments undergo post-depositional modification resulting in linear and lateral growth during matrix development. *Dev Dyn.* 1995;202:229-243.
58. Birk DE, Hahn RA, Linsenmyer CY, et al. Characterization of fibril segments from chicken embryo cornea, dermis and tendon. *Matrix Biol.* 1996;15:111-118.
59. Birk DE, Zycband EI, Woodruff S, et al. Collagen fibrillogenesis in situ: fibril segments become long fibrils as the developing tendon matures. *Dev Dyn.* 1997;208:291-298.
60. Kao WW, Vergnes JP, Ebert J, et al. Increased collagenase and gelatinase activities in keratoconus. *Biochem Biophys Res Commun.* 1982;107:929-936.
61. Rehany U, Lahav M, Shoshan S. Collagenolytic activity in keratoconus. *Ann Ophthalmol.* 1982;14:751-754.
62. Yue BYJT, Sugar J, Benveniste K. Heterogeneity in keratoconus: possible biochemical basis. *Proc Soc Exp Biol Med.* 1984;175:336-341.
63. Collier SA. Is the corneal degradation in keratoconus caused by matrix-metalloproteinases? *Clin Exp Ophthalmol.* 2001;29:339-334.
64. Zhou L, Sawaguchi S, Twining SS, et al. Expression of degradative enzymes and protease inhibitors in corneas with keratoconus. *Invest Ophthalmol Vis Sci.* 1998;39:1117-1124.
65. Sawagamuchi S, Twinning SS, Yue BY, et al. Alpha 2 macroglobulin levels in normal human and keratoconus corneas. *Invest Ophthalmol Vis Sci.* 1994;35:4008-4014.
66. Robert L, Schillinger G, Moczar M, et al. Etude biochimique du keratocone. II. *Arch Ophthalmol.* 1970;30:590-608.

67. Jakus MA. *Ocular Fine Structure. Selected Electron Micrographs.* London: JA Churchill Ltd.; 1964.
68. Teng CC. Electron microscopic study of the pathology of keratoconus: Part I. *Am J Ophthalmol.* 1963;55:18-47.
69. Gottinger W, Aubock L. Electron microscopic findings in keratoconus. *Klin Monatsbl Augenheilkd.* 1970;157:762-772.
70. Pouliquen Y, Faure JP, Limon S, et al. Extracellular deposits of corneal stroma in keratoconus: electron microscopic study [in French]. *Arch Ophtalmol Rev Gen Ophtalmol.* 1968;28:283-294.
71. Pouliquen Y, Graft B, DeKozak J, et al. Etude morphologique et biochimique du keratocone. I. Etude morphologique. *Arch Ophthalmology.* 1970;30:497-532.
72. Pouliquen Y, Graf B, Frouin MA, et al. Histological and ultrastructural interpretation of corneal lesions in keratoconus. *Ber Zusammenkunft Dtsch Ophthalmol Ges.* 1972;71:52-57.
73. Critchfield JW, Calandra AJ, Nesburn AB, et al. Keratoconus: I Biochemical studies. *Exp Eye Res.* 1988;46:953-963.
74. Buddecke E, Wollensak J. Acid mucopolysaccharide and glycoprotein in the human cornea in relation to age and keratoconus. *Albrecht von Graefes Arch Klin Exp Ophthalmol.* 1966;171:105-120.
75. Oxlund H, Simonsen AH. Biochemical studies of normal and keratoconus corneas. *Acta Ophthalmol.* 1985;63:666-669.
76. Funderburgh JL, Hevelone ND, Roth MR, et al. Decorin and biglycan of normal and pathologic human corneas. *Invest Ophthalmol Vis Sci.* 1998;39:1957-1964.
77. Wentz-Hunter K, Cheng EL, Ueda J, et al. Keratocan expression is increased in the stroma of keratoconus corneas. *Mol Med.* 2001; 7:470-477.
78. Funderburgh JL, Panjwani N, Conrad GW, et al. Altered keratan sulfate epitopes in keratoconus. *Invest Ophthalmol Vis Sci.* 1989; 30:2278-2281.
79. Funderburgh JL, Funderburgh ML, Rodrigues MM, et al. Altered keratan sulphate proteoglycan antigenicity in selected corneal disease. *Invest Ophthalmol Vis Sci.* 1990;31:419-428.
80. Wollensak J, Buddecke E. Biochemical studies on human corneal proteoglycans: a comparison of normal and keratoconic eyes. *Graefes Arch Clin Exp Ophthalmol.* 1990;228:517-523.
81. Wollensak G, Spoerl E, Seiler T. Riboflavin/ultraviolet-A-induced collagen crosslinking for the treatment of keratoconus. *Am J Ophthalmol.* 2003;135:620-627.

Annulus of Collagen Fibrils in Mouse Cornea and Structural Matrix Alterations in a Murine-Specific Keratopathy

Andrew J. Quantock,[1] Sally Dennis,[1] Wakako Adachi,[2] Shigeru Kinoshita,[2] Craig Boote,[1] Keith M. Meek,[1] Yoshibumi Matsushima,[3] and Masayoshi Tachibana[3]

Purpose. Mouse corneas were investigated to see whether a limbal annulus of corneal collagen exists as in humans. Mice with corneas predisposed to topographical changes (the SKC strain) were also examined, to establish the size and spacing of stromal collagen fibrils and the integrity of the annulus.

Methods. X-ray diffraction was used to measure collagen fibril spacing and diameter in normal (the BALB/c strain; four male, two female) and SKC (six male and six female) corneas and to identify the degree of preferred collagen orientation at 200-μm intervals across two BALB/c and four SKC corneas.

Results. The average collagen fibril diameter measured 35.5 nm in 3-month-old BALB/c corneas, and 36.9 nm and 37.0 nm, respectively, in corneas of age-matched male and female SKC mice. In male and female SKC corneas, average collagen interfibrillar Bragg spacing was significantly higher (64.5 and 59.9 nm, respectively) than in corneas of BALB/c mice (49.7 nm). Circumferentially aligned collagen, indicative of a limbal annulus of fibrillar collagen 2.2 mm in diameter, was identified in mouse cornea. On occasion, this was disturbed in the SKC phenotype.

Conclusions. Collagen fibrils are marginally larger in the corneas of SKC mice than in the corneas of BALB/c mice and are considerably more widely spaced. An annulus of fibrillar collagen probably exists near the limbus of the normal mouse cornea that may help promote biomechanical stability and maintain corneal shape. A loss of structural integrity in the annulus of some SKC mice may predispose the corneas to biomechanical instability and shape changes. (*Invest Ophthalmol Vis Sci.* 2003;44:1906-1911) DOI:10.1167/iovs.02-0884

The corneal stroma is a tough, transparent connective tissue composed of uniformly thin collagen fibrils, regularly spaced and stacked in a lamellar array.[1] It has a characteristic fine structure that is believed to be crucial if the cornea is to transmit and help focus light. This is because light transmission requires some sort of order in the lateral packing of the collagen fibrils.[2-4] Moreover, because corneal shape helps determine refractive status and given that collagen fibrils are stronger along their axes, a compelling argument can be made in support of a role for collagen fibrillar arrangement and orientation in the promotion of biomechanical stability and, as a consequence, the maintenance of corneal shape. With this in mind we note that within an individual lamella, collagen fibrils lie more or less parallel to one another in the plane of the cornea, whereas angles subtended between fibrils in adjacent lamellae tend to be fairly large.[1] It is perhaps relevant, then, that Daxer and Fratzl[5] have documented profound alterations in the fibrillar organization in the central 7-mm zone in human corneas with keratoconus and concluded that they may contribute to biomechanical instability and shape changes.

We suspect that collagen orientations in more peripheral regions may also be instrumental in maintaining the proper shape of the cornea, and a region of particular interest is the limbus—the corneoscleral junction—where tissues with different radii of curvatures meet and where the circumferential tension is at least twice as high as in neighboring regions.[6] Here, in humans at least, proportionally more collagen fibrils than elsewhere in the cornea run circumferentially, and in doing so form a circumcorneal annulus of fibrillar collagen that is believed to be important for proper corneal curvature.[7-9]

To discover whether an annulus of fibrillar collagen exists near the limbus of the mouse cornea as it does in humans, we initiated a series of x-ray-scattering experiments using synchrotron radiation (see Meek and Quantock[10] for a review). These included an investigation of structural changes in the corneas of SKC mice, a recently reported strain in which the males are prone to the development of misshapen corneas.[11] To this end, a series of x-ray fiber diffraction patterns from normal (the BALB/c strain) and SKC corneas were obtained and analyzed to determine collagen interfibrillar spacing and fibril diameter, as well as the spatial orientation of collagen molecules and fibrils in the plane of the cornea as a function of position across the cornea. Data are highly illustrative, because they represent an average throughout the whole region of the cornea through which the x-ray beam passes, and structural information of this type has usually been acquired from mouse corneas in studies of species differences[12,13] and transgenic defects.[14] The present work provides the first evidence of a circumcorneal annulus of fibrillar collagen near the limbus in the mouse cornea and indicates occasional alterations in the stromal ultrastructure in SKC mice.

Materials and Methods

Specimens

Twelve corneas were obtained from 3-month-old SKC mice (three male, three female), a strain derived from BALB/c, CF#1, and STS in

From the [1]Structural Biophysics Group, Department of Optometry and Vision Sciences, Cardiff University, Cardiff, Wales, United Kingdom; the [2]Department of Ophthalmology, Kyoto Prefectural University of Medicine, Kyoto, Japan; and the [3]Saitama Cancer Center, Saitama, Japan.

Supported by a Medical Research Council Programme grant, a Biotechnology and Biological Sciences Research Council Direct Access Beamtime award, and grants-in-aid from the Ministry of Education, Science, Sports, and Culture of Japan and the Japan Society for the Promotion of Science.

Submitted for publication August 29, 2002; revised November 14, 2002; accepted December 5, 2002.

Disclosure: **A.J. Quantock**, None; **S. Dennis**, None; **W. Adachi**, None; **S. Kinoshita**, None; **C. Boote**, None; **K.M. Meek**, None; **Y. Matsushima**, None; **M. Tachibana**, None

The publication costs of this article were defrayed in part by page charge payment. This article must therefore be marked "*advertisement*" in accordance with 18 U.S.C. §1734 solely to indicate this fact.

Corresponding author: Andrew J. Quantock, Biophysics Group, Department of Optometry and Vision Sciences, Cardiff University, Redwood Building, King Edward VII Ave., Cathays Park, Cardiff CF10 3NB, UK; quantockaj@cf.ac.uk.

Investigative Ophthalmology & Visual Science, May 2003, Vol. 44, No. 5

which the males are predisposed to spontaneous development of conical corneas.[11] Six, age-matched BALB/c corneas (four male, two female) were similarly collected. Mice were killed with an overdose of intraperitoneal pentobarbital, and, at all times, the ARVO Statement for the Use of Animals in Ophthalmic and Vision Research was adhered to, as were local rules. Corneas, typically measuring 3 mm in diameter, were carefully excised by one of the authors (WA). Immediately after excision, specimens were wrapped in clear plastic wrap and placed in a freezer at −80°C. A few days later, they were shipped via express carrier in dry ice to Cardiff and stored at −80°C before x-ray-scattering experiments at the synchrotron, a large-particle accelerator that generates intense electromagnetic radiation. Previous work has shown that the x-ray diffraction patterns and the data obtained from them are unchanged after freezing and thawing.[15]

X-ray Data Collection

All the x-ray diffraction work was performed at the Synchrotron Radiation Source (SRS; Daresbury Laboratory, Cheshire, UK). Low-angle x-ray-scattering patterns (for fibril diameter and interfibrillar spacing measurements) were collected on station 2.1; high-angle patterns (for orientation measurements) on station 14.1. More details of the approach can be found in a recent review.[10]

Low-Angle X-ray Diffraction

All BALB/c and SKC corneas were individually mounted in a specimen chamber between two sheets of mylar and allowed to thaw as they were positioned in the path of a monochromatic x-ray beam (λ = 0.154 nm) focused to 1 × 0.5 mm (horizontal × vertical) at the specimen. Low-angle x-ray diffraction patterns were recorded by opening the shutters for 2 minutes so that the x-rays passed through the center of each specimen. After passing through the tissue, the main beam was blocked by a lead "backstop," and the scattered x-rays recorded on a multiwire, gas-proportional area detector situated directly behind the cornea, 6.25 m away. An evacuated tube with mylar windows occupied the space between the specimen and the detector to minimize air scatter.

High-Angle X-ray Diffraction

For this portion of the study, six corneas (one male and one female BALB/c and two male two female SKC) were investigated. As for the low-angle work, corneas were individually mounted between mylar in the path of a monochromatic x-ray beam, this time with a wavelength of 0.1488 nm, and focused so that it measured 200 × 200 μm (vertically × horizontally) at the specimen. Again, the straight-through beam was stopped by a lead backstop, and this time wide-angle diffraction patterns were recorded on a CCD x-ray detector located 20 cm from the specimen. All exposures lasted 3 minutes. To obtain collagen orientation data as a function of position across the cornea, we generated a series of x-ray patterns across a complete vertical meridian of the specimen. (Here, the tissue is mounted in the x-ray beam in no particular orientation, and therefore the vertical-horizontal terms used herein refer to experimental details, not to anatomic meridians in situ). A dedicated translation stage interfaced with the x-ray shutter was used to move the specimen vertically between x-ray exposures, and, to scan the whole length of the vertical meridian, we obtained diffraction patterns at 200-μm intervals with the 200-μm x-ray beam from the lower edge of the corneal specimen to its upper edge.

Data Analysis

Low-Angle X-ray Diffraction. Low-angle x-ray patterns (512 × 512 pixels) were analyzed with purpose-written Unix software and statistics and graphics packages (Statistica; Statsoft, Tulsa, OK; and Excel; Microsoft Corp., Redmond, WA) to obtain the average collagen fibril diameter and mean center-to-center collagen fibril Bragg spacing.

X-ray patterns were first normalized by using readings taken by an ion chamber located between the incident x-ray beam pipe exit and the specimen. This was intended to correct for the natural decay of x-ray intensity and/or its increase after a scheduled synchrotron refill. To correct for any nonlinearities in the detector, each normalized image was then divided, pixel by pixel, by a detector response pattern obtained from a 420-minute exposure to a radioactive source (Fe^{55}). Next, a vertical scan, 48 pixels wide, of x-ray intensity versus radial position was generated across the center of each pattern to produce an intensity profile of the first-order equatorial (i.e., collagen interfibrillar) x-ray reflection. The x-ray intensity profile was then summed about its center and multiplied by radial position. The multiplication accounted for the fact that a linear scan had been taken across a circular x-ray pattern, with the result that x-ray reflections farther from the centers of the patterns were spread over greater arcs. Finally, background x-ray scatter from nonfibrillar material was subtracted. From the position of the interfibrillar reflection and after calibration of the system with meridional reflections from rat tail tendon (D = 67 nm), we obtained a measure of the average center-to-center collagen fibril Bragg spacing for a 1 × 0.5-mm region in the center of each cornea. The first subsidiary maximum in the low-angle patterns was also analyzed, as described previously,[10,16] to provide the mean diameters of the stromal collagen fibrils.

High-Angle X-ray Diffraction. As for the low-angle work, high-angle x-ray patterns (again, 512 × 512 pixels) were analyzed with Unix-based software followed by statistics and graphics programs (Statistica, MS Excel, and Optimas, Bothell, WA). In these patterns, x-ray reflections are generated by regularly spaced collagen molecules within fibrils. These intermolecular reflections are generally circular, and any variation in x-ray intensity around the reflection is indicative of a preferred orientation of collagen molecules within the plane of the cornea (a matter that will be addressed in greater depth later). All intermolecular reflections were evaluated to generate a parameter that is indicative of the amount of preferentially aligned corneal collagen in the region of the cornea from which that particular x-ray pattern had been obtained.

To achieve this we first normalized the x-ray patterns to account for beam decay, by using the measured intensity of x-ray scatter produced by mylar. Next, we computed the x-ray intensity at 256 points around the center of each x-ray pattern and repeated this for 80 concentric circles on all x-ray diffraction patterns examined (circles were chosen to encompass the region of the x-ray pattern containing the collagen intermolecular reflections). Background scatter caused by flare from the backstop, as well as by x-ray scatter from nonfibrillar material, was then removed by subtracting a power law fitted to either side of the collagen intermolecular peak on the plot of scattering intensity versus radial position. This was repeated for all 256 radial intensity points, to account for the uneven flare from the backstop and the changes in background with radial direction. Next, a 360° radial integration was produced around each interfibrillar reflection, and from it a numerical orientation index was calculated defined as the amount of aligned collagen divided by the amount of total fibrillar (i.e., aligned plus isotropic) collagen, as described previously.[17]

Results

Fibril Size and Separation

Statistical analyses by ANOVA and separation-of-means tests revealed that the average diameter of corneal collagen fibrils in SKC mice calculated from low-angle x-ray diffraction patterns is significantly higher than the average diameter in BALB/c mice for both SKC males ($P < 0.001$) and females ($P < 0.001$; Table 1). Fibril diameters in male and female SKC corneas are not significantly different ($P = 0.766$). X-ray data also indicates that the average center-to-center collagen interfibrillar Bragg spacing in 3-month-old BALB/c mice measures approximately 50 nm (Table 1), with no appreciable difference between males and females. This is similar to previously quoted data

TABLE 1. Average Collagen Fibril Diameter and Interfibrillar Spacing in 3-Month-Old BALB/c and SKC Mouse Corneas

Mouse Strain	Fibril Diameter	Interfibrillar Bragg Spacing
BALB/c (n = 6)	35.5 ± 0.3	49.7 ± 1.3
SKC male (n = 6)	36.9 ± 0.2	64.5 ± 3.8
SKC female (n = 6)	37.0 ± 0.2	59.9 ± 0.9

Data are mean nanometers ± SE.

(≈48 nm) for 6-month-old mice calculated in the same manner.[14]

The average fibril spacing quoted herein (Table 1) is for the interfibrillar Bragg spacing, a value that does not take into account the mode of packing of the stromal collagen fibrils. If, like Worthington and Inouye,[16] we assume liquidlike packing of fibrillar collagen in cornea, we must multiply the Bragg spacing by a factor of 1.12 to arrive at the actual center-to-center interfibrillar collagen spacing. In the SKC phenotype, collagen interfibrillar Bragg spacing was consistently higher than in BALB/c mice, and this was the case in females (P = 0.008) and males ($P < 0.001$; Table 1). As was the case for fibril diameters, there was no difference in collagen interfibrillar spacing between male and female SKC groups (P = 0.156). We should point out, however, that corneas of male SKC mice exhibited a considerably higher variation in interfibrillar spacing than did corneas from female SKC and BALB/c mice, as indicated by the standard errors in the respective data sets (Table 1).

Fibril Orientation

An intermolecular x-ray reflection was identified on x-ray patterns from all corneas examined. This reflection arises because of interference between x-rays scattered by collagen molecules within fibrils, and an appreciation of how it is formed allows us to elicit information about how many collagen molecules as a proportion of the total number of collagen molecules lie in a particular orientation in the plane of the cornea.

First, because the long, thin collagen molecules that make up the corneal collagen fibrils as a whole tend to lie along the fibrillar axis, we take collagen molecular alignment to reflect collagen fibrillar alignment. An intermolecular x-ray reflection from a single, isolated lamella in the corneal stroma in which all collagen fibrils run in the same direction would appear as two fairly well-defined diffraction maxima located either side of a line that runs in the same direction as the collagen fibrils. It follows that a stack of lamellae with a totally heterogeneous radial distribution—that is, constructed so that, when averaged throughout the whole depth of the cornea, no direction in the plane of the cornea contains more fibrils than any other direction—gives rise to a circular intermolecular reflection of uniform intensity around its circumference. The upshot is that corneas in which some directions possess proportionally more collagen fibrils than other directions give rise to lobed intermolecular x-ray reflections, and these reflections, by definition, contain information about the relative overall orientation of collagen fibrils in the plane of the cornea.

It was immediately evident that intermolecular reflections obtained from 200 × 200 μm regions at the upper and lower edges of the corneal specimens from BALB/c mice were not of uniform intensity. Intermolecular reflections obtained from central regions of these same corneas, however, were (Fig. 1).

Invariably, x-ray reflections from the 200 × 200 μm areas just inside the upper and lower edges of the BALB/c corneas possessed two lobes at the 12 and 6 o'clock positions. This indicates that proportionally more collagen fibrils in these regions of the tissue run horizontally—an observation that is consistent with the existence of a circumferential annulus of collagen near the limbus, given that the tangential components of a vertical circle at its top and bottom edges are horizontal.

To quantify the level of fibrillar orientation indicated by each x-ray pattern, we generated a circular integration of x-ray intensity around each 360° intermolecular reflection. Clearly, a simple, flat trace with no peaks above the noise threshold would be expected by the integration around a perfectly uniform intermolecular reflection, but if regions of elevated x-ray intensity existed in the intermolecular reflection, they would be denoted by peaks in the circular integration trace. All circular integrations generated from x-ray patterns taken near the edges of the specimens contained two peaks. In contrast, high-angle diffraction patterns obtained from more central regions possessed intermolecular reflections that appeared uniformly homogeneous on visual inspection, and the circular integrations confirmed this fact. Representative traces are shown in Figure 2 and are consistent with the presence of circumferential collagen near the corneal limbus in the eyes of BALB/c mice.

To discover by how much intermolecular reflections from different 200 × 200 μm regions of a cornea were lobed, we calculated a numerical index of intensity, by dividing the area under the peaks in the circular integrations but above homogeneous x-ray scatter by the total area under the peaks, including homogeneous scatter (Fig. 2). In effect, we divided x-ray

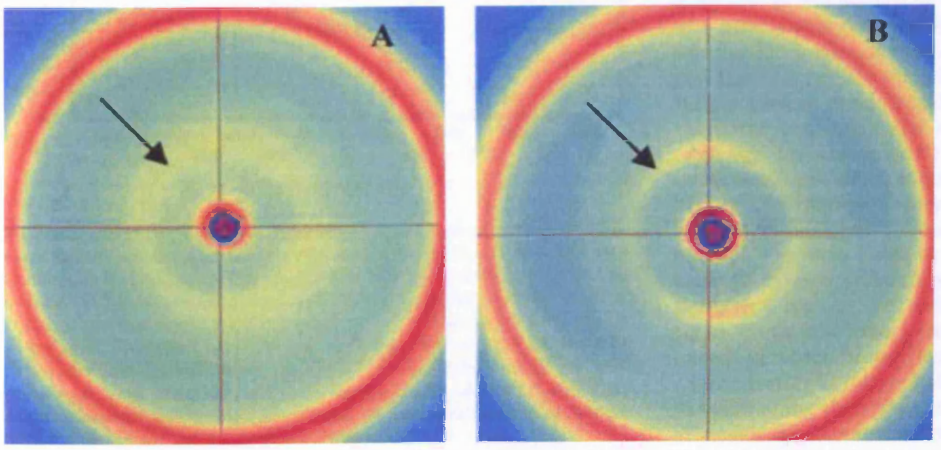

FIGURE 1. High-angle synchrotron x-ray diffraction patterns from 200 × 200 μm regions near the center (**A**) and edge (**B**) of a 3-month-old BALB/c cornea. The *central circle* is the shadow of a lead backstop used to prevent the main x-ray beam from hitting the x-ray detector. Outside this, regions where scattered x-rays were more intense are indicated in *yellow-orange*. *Arrows*: intermolecular reflections. The reflection from the center of the cornea (**A**) was fairly homogeneous circularly, whereas that from the edge of the cornea (**B**) displayed twofold rotational symmetry.

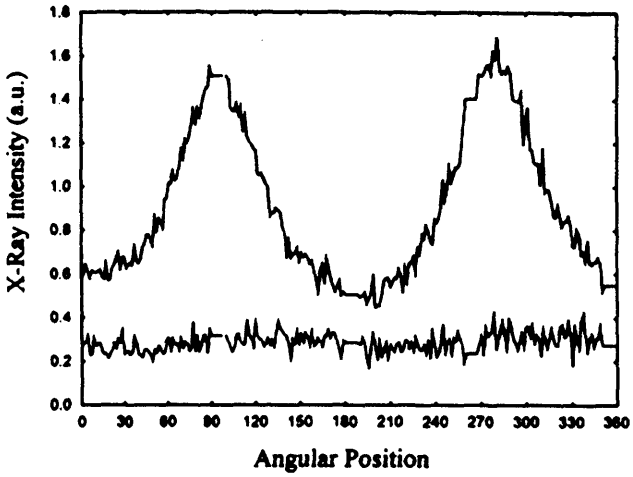

FIGURE 2. Circular 360° integrations around the intermolecular reflections shown in Fig. 1, taken from the 3 o'clock position in a counterclockwise direction. *Bottom trace*: reflection from the central cornea (Fig. 1A); *top trace*: reflection from the edge of the cornea (Fig 1B). The nonuniformity in Fig 1B is clearly recognizable.

scatter from preferentially aligned collagen molecules by the x-ray scatter from all fibrillar collagen molecules. As a result, the more lobed an intermolecular x-ray reflection, the higher its numerical index, and the higher the index, the higher the proportion of preferentially aligned collagen fibrils in that particular region of that particular cornea. Our finding of higher orientation indices at the upper and lower edges of two BALB/c corneas is consistent with the existence of an annulus of circumferentially aligned collagen (Fig. 3). Furthermore, orientation intensity maxima lay eleven 200-μm steps apart, supportive of a corneoscleral annulus in the mouse cornea 2.2 mm in diameter. Equivalent information from two male (Fig. 4A) and two female (Fig. 4B) SKC corneas points to a breakdown in this arrangement in three of the four animals investigated.

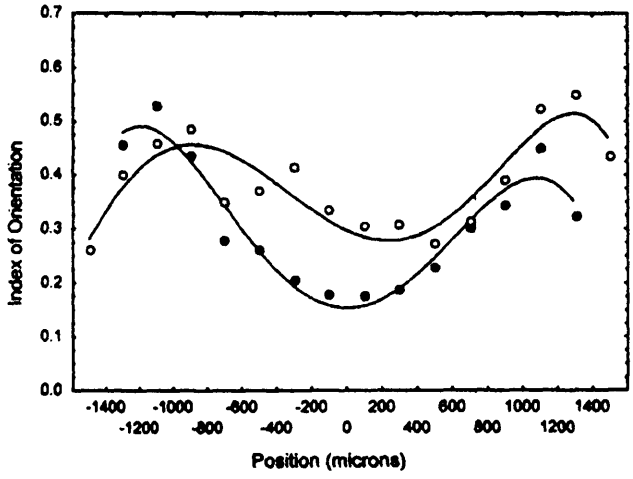

FIGURE 3. Numerical indices reflecting the extent of collagen alignment in 200-μm steps across the corneas of 3-month-old male (●) and female (○) BALB/c mice. The index was higher near the edge of the cornea, indicative of proportionally more circumferentially aligned collagen and consistent with the existence of a circumcorneal annulus of collagen. That the traces are not in register simply reflects the fact that individual corneas were dissected with slightly more or less peripheral tissue intact and that x-ray images were taken until the edge of the specimen was reached (i.e., until no x-ray pattern was recorded because the specimen was missed altogether).

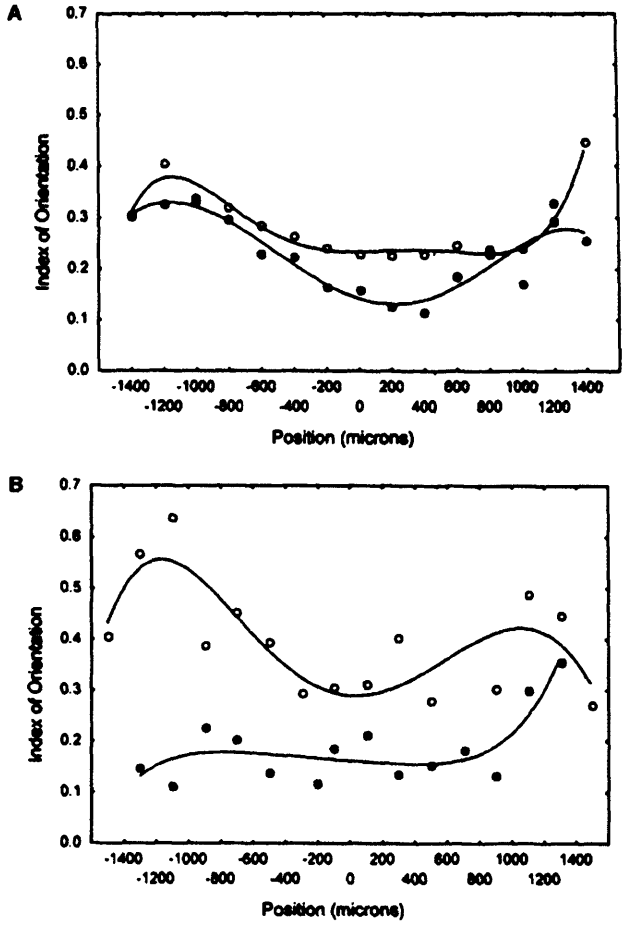

FIGURE 4. Numerical indices reflecting the extent of collagen alignment in 200-μm steps across the corneas of two 3-month-old female (**A**) and two 3-month-old male (**B**) SKC mice. The tendency in normal cornea (see Fig. 3) for the index to be higher just inside the edge of the specimen seemed to break down in at least three of the four animals investigated, suggesting a possible alteration in the structural integrity of the circumcorneal annulus of collagen.

DISCUSSION

X-ray-scattering studies in the late 1980s uncovered evidence of a preferential organization of collagen fibrils in central portions of the human cornea wherein proportionally more collagen fibrils lay in the superior-inferior and medial-lateral meridians than in other meridians.[18] This preferential alignment was later confirmed and quantified.[19] Current x-ray images (e.g., Fig. 1A) indicate that the central mouse cornea, like the corneas of most other species we have studied over the years, but unlike human cornea, does not contain a significant amount of collagen preferentially aligned in an orthogonal manner. Our data point to a commonality between the structures of human and mouse corneas, however, in the more peripheral regions. Recently, a circumcorneal annulus of collagen fibrils was discovered near the limbus in the human cornea in which proportionally more collagen fibrils than elsewhere run circumferentially.[7-9] Because collagen fibrils are stronger along their axes, a situation can be readily envisaged in which the biomechanical stability of the cornea is contin-

gent on the orientation of the fibrils within the plane of the cornea, and it is thought that the fibrillar annulus may well be responsible for the elevated circumferential tension at the limbus.[6] The present data identified a preponderance of circumferentially aligned collagen fibrils at two opposing edges of isolated, BALB/c mouse corneas (Figs. 1, 3). Such a finding is supportive of the concept of a peripheral circumcorneal annulus of fibrillar collagen in mice, 2.2 mm in diameter.

Recently, an inbred line of mice was established (the SKC strain) in which conical corneas tend to develop in adult males. Initially, parallels were drawn with the human condition keratoconus,[11] but the SKC keratopathy is now thought to represent a distinct form of murine corneal ectasia. Reasons for this include the fact that average collagen fibril diameter in the SKC corneas is marginally, but significantly, larger than in BALB/c corneas (Table 1), whereas previous corneal x-ray diffraction experiments by Fullwood et al.[20] found that the average collagen fibril diameter in the corneas of humans with keratoconus was essentially unchanged. They also discovered that in human corneas with keratoconus the average collagen interfibrillar spacing was no different from normal and went on to conclude that any corneal thinning that might be seen in keratoconus should not be attributed to the close packing of the population of collagen fibrils as a whole. Our current measurements indicate that the average collagen interfibrillar Bragg spacing in SKC males measured 64.5 nm, whereas in SKC females it averaged 59.9 nm. Both spacings are significantly wider ($P < 0.001$ and $P = 0.008$, respectively) than the 49.7 nm recorded in the corneas of BALB/c mice of the same age.

It might be reasonably expected that, unless there is a reduction in the amount of fibrillar collagen present, SKC corneas with wider interfibrillar spacing would be unusually thick. In fact, previous studies of the female SKC mouse[11] indicate that corneas are invariably thinner than normal. Such observations are indirectly supportive of a reduction in the amount of fibrillar collagen at the centers of female SKC corneas. In SKC males, too, corneas are generally thin, and a reduction in the amount of fibrillar collagen in the center of the cornea can be envisaged. Some male SKC corneas, in contrast, are thicker than normal because of marked stromal edema.[11] With this in mind, we note the high variability in the male SKC interfibrillar measurements (SE ±3.8 nm), and point out that one individual cornea had a remarkably high average interfibrillar spacing of 82.5 nm. Presumably, this particular cornea was edematous, but additional experiments that directly relate corneal thickness to interfibrillar spacing are required to resolve this matter. The initial report of the SKC strain[10] highlighted similarities with keratoconus in humans, but mentioned that there were distinctions—not least, the likelihood that inflammatory changes may be at play in the SKC mouse cornea. The present work indicates that from a structural viewpoint, too, the SKC strain should not act as a direct animal model of keratoconus in humans. Rather, it and similar strains, such as the JKC mouse[21] hold promise for further studies of the supposed dependence of corneal shape on the collagenous architecture of the corneal stroma.

The ultrastructural changes in SKC mice compared with BALB/c mice are clear, but represent something of a dilemma if we are trying to hold alterations in collagen packing responsible for corneal shape changes. This is simply because previous work has shown that the corneas of female SKC mice are less likely to become misshapen than are the corneas of male SKC mice,[11] but the current findings point to ultrastructural alterations in the stromal matrix in both male and female SKC corneas that are of similar magnitudes. Indeed, neither the collagen diameter measurements nor the interfibrillar measurements are significantly different between male and female SKC groups ($P = 0.766$ and $P = 0.156$, respectively). Taken together, these results seem to suggest that any predisposition of SKC males over SKC females toward development of a misshapen cornea is probably not a direct result of more widely spaced collagen fibrils that are marginally larger than normal.

The idea that collagen fibrillar orientation in the cornea might impinge on tissue stability and shape was the basis for the investigations of Daxer and Fratzl,[5] who discovered that in human keratoconus buttons obtained after surgery the typical inferior-superior/medial-lateral arrangement of corneal collagen in the central cornea[18] breaks down. They reasonably concluded that structural alterations may lead to tissue instability and the formation of a misshapen cornea. Of course, there are important structural differences between the corneas of mice and humans—not least, size and the considerable lamellar interweaving in the anterior stroma in humans, and it is unlikely that the shape mediation of the cornea is borne solely by the limbal annulus. Nevertheless, we believe that current evidence for the likely presence in normal murine cornea of a circumcorneal annulus of fibrillar collagen, 2.2 mm in diameter, identifies the mouse as a legitimate animal model for future investigations into these issues.

The present work revealed no clear, quantitative differences in the alignment of collagen in the central corneas of BALB/c and SKC mice. It did, however, suggest that the structural integrity of the circumcorneal annulus may have been altered in three of the four SKC corneas investigated. Previous work[11] has indicated that male mice of the SKC strain are predisposed to corneal shape changes, but the structural changes in the corneal annulus that we report were manifest in SKC females, even though these mice do not tend toward development of misshapen corneas as often. Thus, the definitive establishment of a causal relationship between corneal shape and the integrity of the circumcorneal annulus awaits further investigation.

Acknowledgments

The authors thank Gunter Grossmann, Mike McDonald, and Rob Keyhoe for help at the SRS, Daresbury Laboratory and Morio Ueno and Chikako Mochida for assistance with tissue collection.

References

1. Komai Y, Ushiki T. The three-dimensional organization of collagen fibrils in the human cornea and sclera. *Invest Ophthalmol Vis Sci.* 1991;32:2244-2258.
2. Maurice DM. The structure and transparency of the cornea. *J Physiol (London).* 1957;186:263-286.
3. Benedek GB. Theory of transparency of the eye. *Appl Opt.* 1971; 10:459-473.
4. Farrell RA. Corneal transparency. In: Albert DM, Jacobiec SA, eds. *Principles and Practice of Ophthalmology.* Philadelphia: WB Saunders; 1994:64-81.
5. Daxer A, Fratzl P. Collagen fibril orientation in the human corneal stroma and its implications in keratoconus. *Invest Ophthalmol Vis Sci.* 1997;38:121-129.
6. Maurice DM. The cornea and sclera. In: Davson H, ed. *The Eye.* London: Academic Press; 1969:489-600.
7. Newton RH, Meek KM. Circum-corneal annulus of collagen fibrils in the human limbus. *Invest Ophthalmol Vis Sci.* 1998;39:1125-1134.
8. Newton RH, Meek KM. The integration of the corneal and limbal fibrils in the human eye. *Biophys J.* 1998;75:2508-2512.
9. Meek KM, Newton RH. Organisation of collagen fibrils in the corneal stroma in relation to mechanical properties and surgical practice. *J Refract Surg.* 1999;15:695-699.
10. Meek KM, Quantock AJ. The use of x-ray scattering techniques to determine corneal ultrastructure. *Prog Retinal Eye Res.* 2001;20: 95-137.

Appendix 10

11. Tachibana M, Adachi W, Kinoshita S, et al. Androgen-dependent hereditary mouse keratoconus: linkage to an MHC region. *Invest Ophthalmol Vis Sci.* 2002;43:51-57.
12. Gyi TJ, Meek KM, Elliott GF. Collagen interfibrillar distances in corneal stroma using synchrotron X-ray diffraction: a species study. *Int J Biol Macromol.* 1988;10:265-269.
13. Meek KM, Leonard DW. The ultrastructure of the corneal stroma: a comparative study. *Biophys J.* 1993;64:273-280.
14. Quantock AJ, Meek KM, Chakravarti S. An x-ray diffraction investigation of corneal structure in lumican-deficient mice. *Invest Ophthalmol Vis Sci.* 2001;42:1750-1756.
15. Fullwood NJ, Meek KM. An ultrastructural, time-resolved study of freezing in the corneal stroma. *J Mol Biol.* 1994;236:749-758.
16. Worthington CR, Inouye H. X-ray diffraction study of the cornea. *Int J Biol Macromol.* 1985;7:2-8.
17. Quantock AJ, Boote C, Siegler V, Meek KM. Collagen organization in the secondary chick cornea during development. *Invest Ophthalmol Vis Sci.* 2003;44:130-136.
18. Meek KM, Blamires T, Elliott GF, Gyi T, Nave C. The organisation of collagen fibrils in the human corneal stroma: a synchrotron X-ray diffraction study. *Curr Eye Res.* 1987;6:841-846.
19. Daxer A, Misof K, Grabner B, Ettl A, Fratzl P. Collagen fibrils in the human corneal stroma: structure and ageing. *Invest Ophthalmol Vis Sci.* 1998;39:644-648.
20. Fullwood NJ, Tuft SJ, Malik NS, Meek KM, Ridgway AEA, Harrison RJ. Synchrotron X-ray diffraction studies of keratoconus corneal stroma. *Invest Ophthalmol Vis Sci.* 1992;33:1734-1741.
21. Tachibana M, Okamoto M, Sakamoto M, Matsushima Y. Hereditary keratoconus-like keratopathy in Japanese wild mice mapped to mouse chromosome 13. *Mamm Genome.* 2002;13:692-695.

Bibliography

Aakre, B.M. and Doughty, M.J. 1997. In vitro hydration kinetics of recent post-mortem tissue versus pre-dried corneal stromal tissue. *Experimental Eye Research* 65, 127-133.

Abahussin, M. 2005. *Personal communication.*

Aghamohamadzadeh, H., Newton, R.H. and Meek, K.M. 2004. X-ray scattering used to map the preferred collagen orientation in the human cornea and limbus. *Structure* 12, 249-256.

Al-Yousuf, N., Mavrikakis, I., Mavrikakis, E. *et al.* 2004. Penetrating keratoplasty: Indications over a 10 year period. *British Journal of Ophthalmology* 88, 998-1001.

Anders, N., Pham, D.T., Antoni, H.J. *et al.* 1997. Postoperative astigmatism and relative strength of tunnel incisions: a prospective clinical trial. *Journal of Cataract and Refractive Surgery* 23, 332-336.

Appelbaum, A. 1936. Keratoconus. *Archives of Ophthalmology* 15, 900-921.

Arffa, R.C., Klyce, S.D. and Busin, M. 1986. Keratometry in epikeratophakia. *Journal of Refractive Surgery* 2, 61-64.

Arntz, A., Duran, J.A. and Pijoan, J.I. 2003. Diagnostico del queratocono sublinico por topogrfica de elevacion. *Archivos de la Sociedad Espanola de Oftalmologia* 78, 659-664.

Auffarth, G.U., Wang, L. and Volcker, H.E. 2000. Keratoconus evaluation using the orbscan topography system. *Journal of Cataract Refractive Surgery* 26, 222-228.

Bibliography

Aurell, G. and Holmgren, H. 1953. On the metachromatic staining of corneal tissue and some observations on its transparency. *Acta Ophthalmologica* 31, 1-27.

Axelsson, I. and Heinegard, D. 1978. Characterization of the keratan sulfate proteoglycans from bovine corneal stroma. *Biochemical Journal* 169, 517-530.

Bains, R.A., Anderson Penno, E.E. and Gimbel, H.V. 2000. Corneal topography. In: Gimbel, H.V. and Anderson Penno, E.E. ed./eds. *Refractive surgery: a manual of principles and practice*. Thorofare, USA: SLACK Inc. pp. 39-62.

Baum, J. 1995. On the location of the cone and the etiology of keratoconus. *Cornea* 14, 142-143.

Bawazeer, A.M., Hodge, W.G. and Lorimer, B. 2000. Atopy and keratoconus: a multivariate analysis. *British Journal of Ophthalmology* 84, 834-836.

Benedek, G.B. 1971. Theory of transparency of the eye. *Applied Optics* 10, 459-472.

Ben-Zvi, A., Rodrigues, M., Krachmer, J.H. *et al.* 1986. Immuno-histochemical characterisation of extracellular matrix in the developing human cornea. *Current Eye Research* 5, 105-117.

Bettleheim, F.A. and Kumbar, M. 1977. An interpretation of small-angle light scattering patterns in the human cornea. *Investigative Ophthalmology and Visual Science* 16, 233-236.

Bigi, A. and Roveri, N. 1991. Fibre diffraction: collagen. In: Ebashi, M.K. and Rubenstein, E. ed./eds. *Handbook on synchrotron radiation.* Italy: Elsevier Science Publisher. pp 199-238.

Bibliography

Birk, D.E., Fitch, J.M. and Linsenmayer, T.F. 1986. Organisation of collagen types I and V in the embryonic chick cornea. *Investigative Ophthalmology and Visual Science* 27, 1470-1477.

Biscleglia, L., Ciaschetti, M., Bonis, P.D. *et al.* 2005. VSX1 mutational analysis in a series of Italian patients affected by keratoconus: detection of a novel mutation. *Investigative Ophthalmology & Visual Science* 46, 39-45.

Blochberger, T.C., Vergnes, J.P., Hempel, J. *et al.* 1992. cDNA to chick lumican (corneal keratan sulphate proteoglycan) reveals homology to the small interstitial proteoglycan gene family and expression in muscle and intestine. *Journal of Biological Chemistry* 267, 347-352.

Boote, C., Dennis, S., Huang, Y. *et al.* 2004a. Lamellar orientation in human cornea in relation to mechanical properties. *Journal of Structural Biology* 149, 1-6.

Boote, C., Dennis, S. and Meek, K.M. 2004b. Spatial mappping of collagen fibril organisation in primate cornea- an x-ray diffraction investigation. *Journal of Structural Biology* 146, 359-367.

Boote, C., Dennis, S., Newton, R.H. *et al.* 2003. Collagen fibrils appear more closely packed in the prepupilliary cornea- optical and biomechanical implications. *Investigative Ophthalmology and Visual Science* 44, 2941-2948.

Borcherding, M.S., Balccik, L.J., Sittig, R.A. *et al.* 1975. Proteoglycans and collagen fibre organisation in human corneoscleral tissue. *Experimental Eye Research* 21, 59-70.

Brancati, F., Valente, E.M., Sarkazy, A. *et al.* 2004. A locus for autosomal dominant keratoconus maps to human chromosome 3p14-q13. *Journal of Medical Genetics* 41, 188-192.

Bron, A.J. 1988. Keratoconus. *Cornea* 7, 163-169.

Bibliography

Bron, A.J. 2001. Editorial: The architecture of the corneal stroma. *British Journal of Ophthalmology* 85, 379-383.

Bron, A.J., Tripathi, A.C. and Tripathi, B.J. 1997. *The cornea and sclera.* London: Chapman and Hall.

Brookes, N.H., Loh, I.P., Clover, G.M. *et al.* 2003. Involvement of corneal nerves in the progression of keratoconus. *Experimental Eye Research* 77, 515-524.

Bruce, V., Green, P.R. and Georgeson, M.A. 1996. *Visual perception: physiology, pshycology and ecology.* East Sussex, UK: Psychology Press/ Taylor and Francis Group.

Buxton, J.N. 1978. Contact lens in keratoconus. *Contact and Intraocular Lens Medical Journal* 4, 73-85.

Caroline, P.J. and Norman, C.W. 1992. Corneal topography in the diagnosis and management of keratoconus. In: Schanzlin, D.J. and Robin, J.B. ed./eds. *Corneal topography: measuring and modifying the cornea.* New York: Springer. pp. 76-78.

Caspersson, T. and Engstrom, A. 1946. Hornhinnevavnadens transparens. *Nordisk Medicin* 30, 1279.

Castoro, J.A., Bettelheim, A.A. and Bettleheim, F.A. 1988. Water gradients across the bovine cornea. *Investigative Ophthalmology and Visual Science* 29, 963-968.

Chakravarti, S., Petroll, W.M., Hassel, J.R. *et al.* 2000. Corneal opacity in lumican-null mice: defects in collagen fibril structure and packing in the posterior stroma. *Investigative Ophthalmology and Visual Science* 41, 3365-3373.

Chapman, J.A., Tzaphlidou, M., Meek, K.M. *et al.* 1990. The collagen fibril-a model system for studying the staining and fixation of a protein. *Electron Microscopy Review 3,* 143-182.

Bibliography

Cheng, E.L., Maruyama, I., SundarRaj, N. *et al.* 2003. Expression of type XIII collagen and hemidesmosome-associated proteins in keratoconus corneas. *Current Eye Research* 22, 333-340.

Cintron, C., Gregory, J.D., Dalme, S.P. *et al.* 1990. Biochemical analysis of proteoglycans in corneal rabbit scars. *Investigative Ophthalmology and Visual Science* 31, 1975-1981.

Comper, W.D. 1996. *Extracellular matrix.* Amsterdam: Harwood Academic.

Connon, C.J., Marshall, J., Patmore, A.L. *et al.* 2003. Persistent haze and disorganisation of anterior stromal collagen appear to be unrelated following phototherapeutic keratectomy. *Journal of Refractive Surgery* 19, 323-332.

Corbett, M.C., Rosen, E.S. and O'Brart, D.P.S. 1999. *Corneal Topography: principles and applications.* London: BMJ Books.

Corpuz, L.M., Funderburgh, J.L., Funderburgh, M.L. *et al.* 1996. Molecular cloning and tissue distribution of keratocan. Bovine corneal keratan sulphate proteoglycans 37a. *Journal of Biological Chemistry* 271, 9759-9763.

Coster, D. 2002. *Cornea.* London: BMJ Books.

Coulombre, A.J. and Coulombre, J.L. 1958. Corneal development. *Journal of Cellular and Comparative Physiology* 51, 1-11.

Craig, A.S. and Parry, D.A.D. 1981. Collagen fibrils of the vertebrate corneal stroma. *Journal of Ultrastructure Molecular Structure Research* 74.

Craig, A.S., Robertson, J.G. and Parry, D.A. 1986. Preservation of corneal fibril structure using low-temperature procedures for electron microscopy. *Journal of Ultrastructure Molecular Structure Research* 96, 172-175.

Bibliography

Daxer, A. and Fratzl, P. 1997. Collagen fibril orientation in the human corneal stroma and its implications in keratoconus. *Investigative Ophthalmology and Visual Science* 38, 121-129.

Dingeldein, S.A. and Klyce, S.D. 1989. The topography of normal corneas. *Archives of Ophthalmology* 107, 512-518.

Dogru, M., Karakaya, H., Ozcetin, H. *et al.* 2003. Tear function and ocular surface changes in keratoconus. *Ophthalmology* 110, 1110-1118.

Duke-Elder, W.S. 1932. *Textbook of ophthalmology*. London: Kimpton.

Edmund, C. 1988a. Corneal elasticity and occular rigidity in normal and keratoconic eyes. *Acta Ophthalmologica* 66, 134-140.

Edmund, C. 1988b. Corneal tissue mass in normal and keratoconic eyes. *Acta Ophthalmologica* 66, 305-308.

Edwards, M., McGhee, C.N.J. and Dean, S. 2001. The genetics of keratoconus. *Clinical and Experimental Ophthalmolgy* 29, 345-351.

Farell, R.A. 1994. Corneal transparency. In: Albert, D.M. and Jacobiec, S.A. ed./eds. *Principles and practice of ophthalmology*. Philadelphia: Saunders.

Farrell, R.A., McCally, R.L. and Tatham, P.E.R. 1973. Wavelength dependencies of light scattering in normal and cold swollen rabbit corneas and their structural implications. *Journal of Physiology* 233, 589-612.

Fatt, I. and Weissman, B. 1992. *Physiology of the eye: an introduction to the vegative functions.* Boston: Butterworth-Heinmann.

Forrester, J.V., Dick, A.D., McMenamin, P. *et al.* 2001. *The eye: basic sciences in practice.* London: WB Saunders.

Forster, W., Kasprzak, H. and Von Bally, G. 1994. Measurement of elastic modulus of the central bovine cornea by means of holographic interferometry. *Optometry and Vision Science* 71, 27-32.

Fortune, B., Cull, G., Wang, L. *et al.* 2002. Factors affecting the use of multifocal electroretinography to monitor function in a primate model of glaucoma. *Documents of Ophthalmology* 105, 151-178.

Francois, J. 1961. Afflictions of the cornea. In: Francois, J. ed./eds. *Hereditary in Ophthalmology*. St Louis: CV Mosby. pp. 297-298.

Freund, D.E., McCally, R.L., Farrell, R.A. *et al.* 1995. Ultrastructure in anterior and posterior stroma of perfused human and rabbit corneas - relation to transparency. *Investigative Ophthalmology and Visual Science* 36, 1508-1523.

Fukuchi, T., Yue, B.Y., Sugar, J. *et al.* 1994. Lysosomal activities in conjunctival tissues of patients with keratoconus. *Archives of Ophthalmology* 112

Fullwood, N.J. and Meek, K.M. 1993. A synchrotron x-ray study of the changes occurring in the corneal stroma during processing for electron-microscopy. *Journal of Microscopy* 169, 53-60.

Fullwood, N.J. and Meek, K.M. 1994. An ultrastructural, time-resolved study of freezing in the corneal stroma. *Journal of Molecular Biology* 236, 749-758.

Fullwood, N.J., Meek, K.M., Malik, N.S. *et al.* 1990. A comparison of proteoglycan arrangement in normal and keratoconus human corneas. *Biochemical Society Transactions* 18, 961-962.

Fullwood, N.J., Tuft, S.J., Malik, N.S. *et al.* 1992. Synchrotron x-ray diffraction studies of keratoconus corneal stroma. *Investigative Ophthalmology and Visual Science* 33, 1734-1741.

Bibliography

Funderburgh, J.L., Corpuz, L.M., Roth, M.R. *et al.* 1997. Mimecan, the 25-kda corneal keratan sulphate proteoglycan, is a product of the gene producing osteoglycin. *Journal of Biological Chemistry* 272, 28089-28095.

Funderburgh, J.L., Hevelone, N.D., Roth, M.R. *et al.* 1998. Decorin and biglycan of normal and pathological human corneas. *Investigative Ophthalmology and Visual Science* 39, 1957-1964.

Funderburgh, J.L., Panjwani, N., Conrad, G.W. *et al.* 1989. Altered keratan sulphate epitopes in keratoconus. *Investigative Ophthalmology and Visual Science* 30, 2278-2281.

Galin and Berger, R. 1958. Atopy and keratoconus. *American Journal of Ophthalmology* 45, 904-906.

Gasset, A.R., Houde, W.L. and Garcia-Bengochea, M. 1978. Hard contact lens wear as an environmental risk in keratoconus. *American Journal of Ophthalmology* 85, 339-341.

Geogiou, T., Funnell, C.L., Cassels-Brown, A. *et al.* 2004. Influence of ethnic origin on the incidence of keratoconus and associated atopic disease in asians and white patients. *Eye* 18, 379-383.

Gipson, I. 1994. Anatomy of the conjunctiva, cornea and limbus. In: Smolin, G. and Throft, R. ed./eds. *The cornea, scientific foundations and clinical practice.* Boston: Little Brown.

Goldman, J.N. and Benedek, G.B. 1967. The relationship between morphology and transparency in the non-swelling corneal stroma of the shark. *Investigative Ophthalmology and Visual Science* 6, 574-600.

Goodfellow, J.M., Elliot, G.F. and Woolgar, A.E. 1978. X-ray diffraction studies of the corneal stroma. *Journal of Molecular Biology* 119, 237-252.

Bibliography

Grewal, S., Laibson, P.R., Cohen, E.J. *et al.* 1999. Acute hydrops in corneal ectasias: associated factors and outcomes. *Transactions of the American Ophthalmological Society* 97, 187-203.

Hamada, R. 1974. Aspect ultrastructural des cellules et du tissu conjonctif corneen normal. In: Hall, C.a. ed./eds. *Wolff's anatomy of the eye and orbit.*

Hart, R.W. and Farrell, R.A. 1969. Light scattering in the cornea. *Journal of the Optical Society of America* 59, 766-774.

Hassell, J.R., Cintron, C., Kublin, C. *et al.* 1983. Proteoglycan changes during the restoration of transparency in corneal scars. *Archives of Biochemistry and Biophysics* 222, 362-369.

Hay, E.D. 1981. *Cell biology of extracellular matrix.* New York: Plenum Press.

Hayashi, T., Huang, J. and Deeb, S.S. 2000. Rinx (VSX1), a novel homeobox gene expressed in the inner nuclear layer of the adult retina. *Genomics* 67, 128-139.

Hedbys, B.O. 1961. The role of polysaccharides in corneal swelling. *Experimental Eye Research* 1, 81-91.

Hedbys, B.O. and Dohlman, C.H. 1963. A new method for the determination of the swelling pressure of the corneal stroma *in vitro*. *Experimental Eye Research* 2, 122-129.

Hedbys, B.O. and Mishima, S. 1962. Flow of water in the corneal stroma. *Experimental Eye Research* 1, 262-275.

Hedbys, B.O. and Mishima, S. 1966. The thickness-hydration relationship of the cornea. *Experimental Eye Research* 5, 221-228.

Heon, E., Greenberg, A., Kopp, K.K. *et al.* 2002. VSX1: A gene for posterior polymorphous dystrophy and keratoconus. *Human molecular genetics* 11, 1029-1036.

Hirano, K., Kobayashi, M., Kobayashi, K. *et al.* 1989. Experimental formation of 100nm periodic fibrils in the mouse corneal stroma and trabecular meshwork. *Investigative Ophthalmology & Visual Science* 30, 869-874.

Hjørtdal, J.O. 1995. Extensibility of the normo-hydrated human cornea. *Acta Ophthalmologica Scandinavica* 73, 12-17.

Hjørtdal, J.O. 1996. Regional elastic performance of the human cornea. *Journal of Biomechanics* 29, 931-942.

Hodson, S., O'Leary, D. and Watkins, S. 1991. The measurement of ox corneal swelling pressure by osmometry. *Journal of Physiology* 434, 399-408.

Hodson, S. and Wigham, C. 1983. The permeability of rabbit and human corneal endothelium. *Journal of Physiology* 342, 409-419.

Hofstetter, H. 1959. Keratoscopic survey of 13395 eyes. *American Journal of Optometry and Archives of American Academy of Optometry* 36, 3-11.

Hogan, M.J., Alvarado, J.A. and Weddell, J.E. 1971. The sclera. In: *Histology of the human eye*. Philadelphia: WB Saunders. pp. 183-201.

Holland, D.R., Maeda, N., Hannush, S.B. *et al.* 1997. Unilateral keratoconus. Incidence and quantitative topographic analysis. *Ophthalmology* 104, 1409-1413.

Hughes, A.E., Dash, D.P., Jackson, A.J. *et al.* 2003. Familial keratoconus with cataract: Linkage to the long arm of chromosome 15 and exclusion of candidate genes. *Investigative Ophthalmology and Visual Science* 44, 5063-5066.

Hukins, D.W.L. and Aspden, R.M. 1985. Composition and properties of connective tissues. *Trends in Biochemical Sciences* 10, 260-264.

Iwamoto, T. and DeVoe, A. 1976. Electron microscopical study of the Fleisher ring. *Archives of Ophthalmology* 94, 1579-1584.

Jakus, M.A. 1962. Further observations of the fine structure of the cornea. *Investigative Ophthalmology and Visual Science* 1, 202-225.

Jeronimidis, G. and Vincent, J.F.V. 1984. Composite materials. In: Huykins, D.W.L. ed./eds. *Connective tissue matrix*. Macmillan. pp. 187-210.

Jester, J.V., Huang, J., Petroll, W.M. *et al.* 1999a. Expression of rabbit corneal crystallins by keratocytes correlates with neonatal development of corneal transparency. *Investigative Ophthalmology and Visual Science* 40, 959.

Jester, J.V., Moller-Pedersen, T., Huang, J.Y. *et al.* 1999b. The cellular basis of corneal transparency: evidence for 'corneal crystallins'. *Journal of Cell Science* 112, 613-622.

Jue, B. and Maurice, D.M. 1986. The mechanical properties of the rabbit and human cornea. *Journal of Biomechanics* 10, 847-853.

Kanai, A. and Kaufman, H.E. 1973. Electron microscopic studies of corneal stroma: ageing changes of collagen fibres. *Annals of Ophthalmology* 5, 285-292.

Kanai, A., Wood, T.C., Polack, F.M. *et al.* 1971. The fine structure of corneosclera. *Investigative Ophthalmology and Visual Science* 10, 687-694.

Kennedy, R.H., Bourne, W.M. and Dyer, J.A. 1986. A 48-year clinical and epidemiologic study of keratoconus. *American Journal of Ophthalmology* 101, 267-273.

Kenney, M., Chwa, M., Opbroek, A.J. *et al.* 1994. Increased gelatinolytic activity in keratoconus cultures. *Cornea* 13, 114-124.

Kenney, M., Nesburn, A., Burgeson, R. *et al.* 1997. Abnormalities of the extra-cellular matrix in keratoconus cornea. *Cornea* 16, 345-351.

Kenney, M.C. and Brown, D.J. 2003. The cascade hypothesis of keratoconus. *Contact Lens and Anterior Eye* 26, 139-146.

Kenyon, K.R. 1975. Mesenchymal dysgenesis in Peter's anomaly, sclerocornea and congenital endothelial dystrophy. *Experimental Eye Research* 21, 125-142.

Kikkawa, Y. and Hirayma, K. 1970. Uneven swelling properties of the corneal stroma. *Investigative Ophthalmology and Visual Science* 9, 735-741.

Kim, W.J., Rabinowitz, Y.S., Meisler, D.M. *et al.* 1999. Keratocyte apoptosis associated with keratoconus. *Experimental Eye Research* 69, 475-481.

Klyce, S.D. and Beuerman, R.W. 1988. Structure and function of the cornea. In: Kaufmann, H.E. ed./eds. *The cornea.* New York: Churchill Livingston.

Kokott, W. 1938. Ubermechanisch-funktionelle strikturen des auges. Albrecht von graefes. *Archives of Ophthalmology* 138, 424-485.

Komai, Y. and Ushiki, T. 1991. The three-dimensional organisation of collagen fibrils in the human cornea and sclera. *Investigative Ophthalmology and Visual Science* 32, 2244-2258.

Korb, D.R., Leahy, C.D. and Greiner, J.V. 1991. Prevalence and characteristics of eye-rubbing for keratoconic and non-keratoconic subjects. *Investigative Ophthalmology and Visual Science* 32, 884.

Krachmer, J.H., Feder, R.S. and Belin, M.W. 1984. Keratoconus and related non-inflammatory corneal thinning disorders. *Survey of Ophthalmology* 28, 293-322.

Laing, R.A., Sandstrom, M.M., Berrospi, A.R. et al. 1979. The human corneal endothelium in keratoconus: A specular microscopic study. *Archives of Ophthalmology* 97, 1867-1869.

Leber, T. 1903. The circulation and nutritional relations to the eye. In: *Graef-saemisch handbuch der gesampten augenheilkunde.* Leipzig: Englemann. pp. 101-491.

Lee, L.R., Hirst, L.W. and Readshaw, G. 1995. Clinical detection of unilateral keratoconus. *Australian and New Zealand Journal of Ophthalmology* 23, 129-133.

Leibowitz, H. 1984. Keratoconus. In: *Corneal disorders: clinical diagnosis and management.* Philadelphia: WB Saunders Company.

Leonard, D.W. and Meek, K.M. 1997. Estimation of the refractive indices of collagen fibrils and ground substance of the corneal stroma using data from x-ray diffraction. *Biophysical Journal* 72, 1382-1387.

Li, Y., Vergnes, J.P., Cornvet, P.K. *et al.* 1992. cDNA clone to chick corneal chrondroitin/dermatan sulphate proteoglycan reveals identity of decorin. *Archives of Biochemistry and Biophysics* 296, 190-197.

Lim, L., Pesudovs, K. and Coster, D.J. 2000. Penetrating keratoplasty for keratoconus: visual outcome and success. *Ophthalmology* 107, 1125-1131.

Bibliography

Lim, N. and Vogt, U. 2002. Characteristics and functional outcomes of 130 patients with keratoconus attending a specialist contact lens clinic. *Eye* 16, 54-59.

Lin, H.C., Chang, J.H., Jain, S. *et al.* 2001. Matrilysin cleavage of corneal collagen type XVIII nc1 domain and generation of a 28-kda fragment. *Investigative Ophthalmology and Visual Science* 42, 2517-2524.

Marchini, M., Morocutti, M., Ruggeri, A. *et al.* 1986. Differences in the fibril structure of corneal and tendon collagen -an electron microscopy and x-ray diffraction investigation. *Connective Tissue Research* 15, 269-281.

Marchini, M., Ortolani, F. and Raspanti, M. 1993. Collagen-glutaraldehyde interaction as revealed by the d-banding of negatively stained fibrils and computer-drawn band patterns. *European Journal of Histochemistry* 37, 363-373.

Marshall, G.E., Kanstas, A.G. and Lee, W.R. 1991a. Immunogold fine structural localisation of extracellular matrix components in aged human cornea. II. Collagen types V and VI. *Graefe's Archives for Clinical and Experimental Ophthalmology* 229, 164-171.

Marshall, G.E., Konstas, A.G.P. and Lee, W.R. 1991b. Immounogold fine structural localization of extracellular matrix components in aged human cornea. I. Types I-IV collagen and laminin. *Graefe's Archives for Clinical and Experimental Ophthalmology* 229, 157-163.

Maurice, D.M. 1957. The structure and transparency of the cornea. *Journal of Physiology* 136, 263-286.

Maurice, D.M. 1969. The cornea and sclera. In: Davson, H. ed./eds. *The eye.* New York: Academic Press. pp. 489-599.

Bibliography

Maurice, D.M. 1984. The cornea and sclera. In: Davson, H. ed./eds. *The eye.* New York: Academic Press. pp. 1-158.

McCally, R.L. and Farell, R.A. 1982. Structural implications of small-angle light scattering from cornea. *Experimental Eye Research* 34, 99-113.

McCally, R.L., Grebe, R., DeLaCruz, A. *et al.* 2005. Light scattering calculations from TEM of healed penetrating corneal wounds. *Investigative Ophthalmology and Visual Science* 46, E-Abstract 2182.

McMonnies, C.W. and Boneham, G.C. 2003. Keratoconus, allergy, itch, eye-rubbing and hand dominance. *Clinical and Experimental Ophthalmolgy* 86, 376-384.

McTigue, J.W. 1967. The human cornea: a light and electron microscopic study of the normal cornea and its alterations in various dystrophies. *Transactions of the American Ophthalmological Society* 65, 591-660.

Meek, K., Blamires, T., Elliot, G. *et al.* 1987. The organisation of collagen fibrils in the human corneal stroma: a synchrotron x-ray diffraction study. *Current Eye Research* 6, 841-846.

Meek, K. and Boote, C. 2004. The organisation of collagen in the corneal stroma. *Experimental Eye Research* 78, 503-512.

Meek, K.M., Dennis, S. and Khan, S. 2003a. Changes in the refractive index of the stroma and the extrafibrillar matrix when the cornea stroma swells. *Biophysical Journal* 85, 2205-2212.

Meek, K.M., Elliot, G.F., Sayers, Z. *et al.* 1981. Interpretation of the meridional x-ray diffraction pattern from collagen fibrils in corneal stroma. *Journal of Molecular Biology* 149, 477-488.

Bibliography

Meek, K.M., Elliott, G.F. and Nave, C. 1986. A synchrotron x-ray-diffraction study of bovine cornea stained with cupromeronic blue. *Collagen and Related Research* 6, 203-218.

Meek, K.M., Fullwood, N.J., Cooke, P.H. *et al.* 1991. Synchrotron x-ray-diffraction studies of the cornea, with implications for stromal hydration. *Biophysical Journal* 60, 467-474.

Meek, K.M., Hayes, S. and Boote, C. 2005a. The effect of swelling on the lamellar arrangement of the corneal stroma. *Investigative Ophthalmology and Visual Science* 46, E-Abstract 2183.

Meek, K.M. and Leonard, D.W. 1993. Ultrastructure of the corneal stroma - a comparative study. *Biophysical Journal* 64, 273-280.

Meek, K.M., Leonard, D.W., Connon, C.J. *et al.* 2003b. Transparency, swelling and scarring in the corneal stroma. *Eye* 17, 927-936.

Meek, K.M. and Newton, R.H. 1999. Organization of collagen fibrils in the corneal stroma in relation to mechanical properties and surgical practice. *Journal of Refractive Surgery* 15, 695-699.

Meek, K.M. and Quantock, A.J. 2001. The use of x-ray scattering techniques to determine corneal ultrastructure. *Progress in Retinal and Eye Research* 20, 95-137.

Meek, K.M., Tuft, S.J., Huang, Y. *et al.* 2005b. Changes in collagen orientation and distribution in keratoconus corneas. *Investigative Ophthalmology and Visual Science* 46, 1948-1956.

Melles, G.R., Eggink, F.A., Lander, F. *et al.* 1998. A surgical technique for posterior lamellae keratoplasty. *Cornea* 17, 618-626.

Michelacci, Y.M. 2003. Collagens and proteoglycans of the corneal extracellular matrix. *Brazilian Journal of Medical and Biological Research* 36, 1037-1046.

Miller, E.J. and Gay, S. 1982. Collagen: an overview. *Methods in Enzymology* 82, 3-32.

Mishima, S. 1968. Corneal thickness. *Survey of Ophthalmology* 13, 57-96.

Moller-Pedersen, T. 2004. Keratocyte reflectivity and corneal haze. *Experimental Eye Research* 78, 553-560.

Moller-Pedersen, T., Cavanagh, H.D., Petroll, W.M. *et al.* 1998. Corneal haze development after PRK is regulated by volume of stromal tissue removal. *Cornea* 17, 627-639

Muller, L.J., Pels, E. and Vrensen, G.F.J.M. 2001. The specific architecture of the anterior stroma accounts for maintenance of corneal curvature. *British Journal of Ophthalmology* 85, 437-443.

Muller, L.J., Pels, L. and Vrensen, G.F.J.M. 1995. Novel aspects of the ultrastructural organization of human corneal keratocytes. *Investigative Ophthalmology and Visual Science* 36, 2557-2567.

Myint, E., Brown, D.J., Ljubimov, A.V. *et al.* 1996. Cleavage of human corneal type VI collagen alpha 3 chain by matrix metalloproteinase-2. *Cornea* 15, 490-496.

Nakayasu, K., Tanaka, M., Konomi, H. *et al.* 1986. Distribution of types I, II, III, IV and V collagen in normal and keratoconus corneas. *Ophthalmic Research* 18, 1-10.

Newsome, D.A., Gross, J. and Hassel, J.R. 1982. Human corneal stroma contains three distinct collagens. *Investigative Ophthalmology and Visual Science* 22, 376-381.

Bibliography

Newton, R.H. and Meek, K.M. 1998a. Circumcorneal annulus of collagen fibrils in the human limbus. *Investigative Ophthalmology and Visual Science* 39, 1125-1134.

Newton, R.H. and Meek, K.M. 1998b. The integration of the corneal and limbal fibrils in the human eye. *Biophysical Journal* 75, 2508-2512.

Newton, R.H. and Meek, K.M. 2001. Mapping the orientations of the collagen fibrils in human cornea and sclera. *Investigative Ophthalmology and Visual Science* 42, 1517.

Niederkorn, J.Y. (1999) The immune privilege of corneal allografts. *Transplantation.* 67, 1503-1508.

Nieduszynski, I.A., Brown, G.M., Ellis, T.S. *et al.* 2004. Dermatopontin interactions with keratan sulphate proteoglycans (abstract). *Ophthalmic Research 36, 285*

Olivares Jimenez, J.L., Guerrero Jurado, J.C., Bermudez Rodriguez, F.J. *et al.* 1997. Keratoconus: age of onset and natural history. *Optometry and Vision Science* 74, 147-151.

Ollivier, F.J., Brooks, D.E., Komaromy, A.M. *et al.* 2003. Corneal thickness and endothelial cell density measured by non-contact specular microscopy and pachymetry in rhesus macaques (macaca mulatto) with laser induced ocular hypertension. *Experimental Eye Research* 76, 671-677.

Owens, H. and Gamble, G. 2003. A profile of keratoconus in New Zealand. *Cornea* 22, 122-125.

Owens, H. and Watters, G.A. 1996. Evaluation of keratoconic cornea using computerised corneal mapping and ultrasonic measurements of corneal thickness. *Opthalmic and Physiological Optics* 16, 115-123.

Bibliography

Ozanics, V., Rayborn, M. and Sagun, D. 1977. Observations on the morphology of the developing primate cornea: epithelium, its innervation and anterior stroma. *Journal of Morphology* 153, 263-298.

Parry, D.A. and Craig, A.S. 1979. Electron microscope evidence for an 80a unit in collagen fibrils. *Nature* 282, 213-215.

Patel, S., Marshall, J. and Fitzke, F.W. 1995. Refractive index of the human corneal epithelium and stroma. *Journal of Refractive Surgery* 11, 100-105.

Patel, S.V., McLaren, J.W., Hodge, D.O. *et al.* 2001. Normal human keratocyte density and corneal thickness measurement by using confocal microscopy in vivo. *Investigative Ophthalmology and Visual Science* 42, 333-339.

Patel, S.V., Tester, R., Soong, H.K. *et al.* 2005. Recurrent ectasia after penetrating keratoplasty for keratoconus. *Investigative Ophthalmology and Visual Science* 46, E-Abstract 4948.

Patey, A., Savoldelli, M. and Pouliquen, Y. 1984. Keratoconus and normal cornea: a comparative study of collagenous fibers of the corneal stroma by image analysis. *Cornea* 3, 119-124.

Pearson, A., Sarvananthan, N., Soneji, B. *et al.* 1999. Does ethnic origin influence the incidence or severity of keratoconus? *Investigative Ophthalmology and Visual Science* 40, 7610.

Peiffer, R.L., Werblin, T.P. and Patel, A.S. 1987. Keratoconus in a rhesus monkey. *Journal of Medical Primatology* 16, 403-406.

Pepose, J. and Ubels, J. 1992. The cornea. In: Hart, W. ed./eds. *Adler's physiology of the eye*. St Louis: Mosby-Year Book. pp. 29-70.

Bibliography

Perry, H.D., Buxton, J.N. and Fine, B.S. 1980. Round and oval cones in keratoconus. *Ophthalmology* 87, 905-909.

Petroll, W.M., New, K., Sachdev, M. *et al.* 1992. Radial keratomy III. Relationship between wound gape and corneal curvature in primate eyes. *Investigative Ophthalmology & Visual Science* 33, 3283-3291.

Peyman, G.A., Sanders, D.R. and Goldberg, M.F. 1980. Corneal disease. In: *Principles and practice of ophthalmology.* Philadelphia, USA: Saunders. pp. 440-445.

Pinsky, P.M., Van der Heide, D. and Chernyak, D. 2005. Computational modeling of mechanical anisotropy in the cornea and sclera. *Journal of Cataract and Refractive Surgery* 31, 136-145.

Plessy, F. and Bettelheim, F.A. 1975. Water vapor sorption of keratan sulfate. *Molecular and Cellular Biochemistry* 6, 85-91.

Polack, F.M. 1961. Morphology of the cornea. *American Journal of Ophthalmology* 51, 179-184.

Polack, F.M. 1976. Contributions of electron microscopy to the study of corneal pathology. *Survey of Ophthalmology* 20, 375-414.

Quantock, A.J., Dennis, S., Adachi, W. *et al.* 2003. An annulus of collagen fibrils in the mouse cornea and structural matrix alterations in a murine specific keratopathy. *Investigative Ophthalmology and Visual Science* 44, 1906-1911.

Quantock, A.J., Kinoshita, S., Capel, M.S. *et al.* 1998. A synchrotron x-ray diffraction study of developing chick corneas. *Biophysical Journal* 74, 995-998.

Bibliography

Quantock, A.J., Kratzowens, K.L., Leonard, D.W. *et al.* 1994. Remodeling of the corneal stroma after lamellar keratoplasty - a synchrotron x-ray-diffraction study. *Cornea* 13, 20-27.

Quantock, A.J., Meek, K.M. and Chakravarti, S. 2001. An x-ray diffraction investigation of corneal structure in lumican-deficient mice. *Investigative Ophthalmology and Visual Science* 42, 1750-1756.

Rabinowitz, Y.S. 1998. Keratoconus. *Survey of Ophthalmology* 42, 297-319.

Rabinowitz, Y.S. and McDonell, P.J. 1989. Computer-assisted corneal topography of keratoconus. *Refractive Corneal Surgery* 5, 400-408.

Rada, J.A., Cornuet, P.K. and Hassell, J.R. 1993. Regulation of corneal collagen fibrillogenesis in vitro by corneal proteoglycan (lumican and decorin) core proteins. *Experimental Eye Research* 56, 635-648.

Radner, W. and Mallinger, R. 2002. Interlacing of collagen lamellae in the midstroma of the human cornea. *Cornea* 21, 598-601.

Radner, W., Zehetmayer, M., Aufreiter, R. *et al.* 1998a. Interlacing and cross-angle distribution of collagen lamellae in the human cornea. *Cornea* 17, 537-543.

Radner, W., Zehetmayer, M., Skorpik, C. *et al.* 1998b. Altered organization of collagen in the apex of keratoconus corneas. *Ophthalmic Research* 30, 327-332.

Rawe, I.M., Meek, K.M., Leonard, D.W. *et al.* 1994. Structure of corneal scar tissue - an x-ray-diffraction study. *Biophysical Journal* 67, 1743-1748.

Reichel, E., Miller, D., Blanco, E. *et al.* 1989. The elastic modulus of central and perilimbal bovine cornea. *Annals of Ophthalmology* 21, 205-208.

Roberts, C. 1994. The accuracy of 'power' maps to display curvature data in corneal topography systems. *Investigative Ophthalmology and Visual Science* 35, 3525-3532.

Robertson, I. 1975. Keratoconus and Ehler's Danlos syndrome: a new aspect of keratoconus. *The Medical Journal of Australia* 1, 571-573

Sandberg-Lall, M., Hägg, P.O., Wahlström, I. *et al.* 2000. Type XIII collagen is widely expressed in the adult and developing human eye and accentuated in the ciliary muscle, the optic nerve and the neural retina. *Experimental Eye Research* 70, 401-410.

Saude, T. 1993. *Ocular anatomy and physiology*. Oxford: Blackwell Science.

Sawada, H., Konomi, H. and Hirosawa, K. 1990. Characterisation of collagen in the hexagonal lattice of Descemet's membrane: its relation to type VIII collagen. *Journal of Cell Biology* 110, 219-227.

Sawaguchi, S., Fukuchi, T., Abe, H. *et al.* 1998. Three dimensional electron microscopic study of keratoconus. *Archives of Ophthalmology* 116, 62-98.

Sawaguchi, S., Twining, S.S., Yue, B.Y.J.T. *et al.* 1994. Alpha-2-macro-globulin levels in normal and keratoconus corneas. *Investigative Ophthalmology and Visual Science* 35, 4008-4014.

Sawaguchi, S., Yue, B.Y., Sugar, J. *et al.* 1989. Lysosomal enzyme abnormalities in keratoconus. *Archives of Ophthalmology* 107, 1507-1510.

Schwartz, W. and Graf-Keyserlingk, D.G. 1969. Macromolecular organisation of a connective tissue. In: Langham, M.E. ed./eds. *The cornea.* Baltimore: John Hopkins Press. pp. 123-132.

Bibliography

Scott, J.E. and Haigh, M. 1985a. Proteoglycan-type I collagen fibril interactions in bone and non-calcifying tissue. *Bioscience Reports* 5, 71-81.

Scott, J.E. and Haigh, M. 1985b. Small proteoglycan collagen interactions. Keratan sulphate associates with rabbit corneal collagen fibrils at the 'a' and 'c' bands. *Bioscience Reports* 5, 71-81.

Seiler, T., Matallana, M., Sendler, S. *et al.* 1992. Does Bowman's layer determine the biomechanical properties of the cornea? *Refractive Corneal Surgery* 8, 139-142.

Semina, E.V., Mintz-Hittner, H.A. and Murray, J.C. 2000. Isolation and characterization of a novel human paired-like homeodomain-containing transcription factor gene, VSX1, expressed in ocular tissues. *Genomics* 63, 289-293.

Sherwin, T., Brookes, N.H., Loh, I.P. *et al.* 2002. Cellular incursion into Bowman's membrane in the peripheral cone of the keratoconic cornea. *Experimental Eye Research* 74, 473-482.

Smelser, G.K. 1960. *The transparency of the cornea.* Oxford: Blackwell.

Smith, M.E., Kincaid, M.C. and West, C.E. 2002. *Basic science, refraction, and pathology*. Missouri: Mosby Inc. pp.30-31.

Smith, V.A., Mol, H.B., Littleton, M. *et al.* 1995. Over expression of a gelatinase activity in keratoconus. *Eye* 9, 429-433.

Smith, V.A., Rishmawi, H., Hussein, H. *et al.* 2001. Tear film MMP accumulation and corneal disease. *British Journal of Ophthalmology* 85, 147-153.

Smolek, M. 1993. Interlamellar cohesive strength in the vertical meridian of human eyebank corneas. *Investigative Ophthalmology and Visual Science* 34, 2962-2969.

Smolek, M.K., Klyce, S.D. and Sarver, E.J. 2002. Inattention to non-superimposable midline symmetry causes wavefront analysis error. *Archives of Ophtalmology* 120, 439-447

Smolin, S. and Thoft, R.A. 1987. *The cornea.* Little, Brown and Company.

Snell, R. and Lemp, M. 1998. *Clinical anatomy of the eye.* Oxford: Blackwell Science.

Somodi, S., Hahnel, C., Slowik, C. *et al.* 1996. Confocal in vivo microscopy and confocal laser-scanning fluorescence microscopy in keratoconus. *German Journal of Ophthalmology* 5, 518-525.

Soriano, E.S., Campos, M.S. and Michelacci, Y.M. 2000. Effect of epithelial debridement on glycosaminoglycan synthesis by human corneal explants. *Clinica Chimica Acta* 295, 41-62.

Spoerl, E., Wollensak, G. and Seiler, T. 2004. Increased resistance of crosslinked cornea against enzymatic digestion. *Current Eye Research* 29, 35-40.

Stachs, O., Bochert, A., Gerber, T. *et al.* 2004. The extracellular matrix structure of keratoconus. *Ophthalmologe* 101, 384-389.

Steimke, M.M., Roman, R.J., Palmer, M.L. *et al.* 1992. Sodium activity in the aqueous humour and corneal stroma of the rabbit. *Experimental Eye Research* 55, 425-433.

Sturbaum, C. and Peiffer, R. 1993. Pathology of corneal endothelium in keratoconus. *Ophthalmolgica* 206, 192-208.

Tachibana, M., Adachi, W., Kinoshita, S. *et al.* 2002. Androgen-dependent hereditary mouse keratoconus: linkage to an MHC region. *Investigative Ophthalmology and Visual Science* 43, 51-57.

Takahashi, T., Nakayasu, K., Okisaka, S. *et al.* 1990. Quantitative analysis of collagen fibres in keratoconus. *Acta Societatis Ophthalmologicae Japonicae* 90, 1068-1073.

Tasheva, E.S., Koester, A., Paulsen, A.Q. *et al.* 2002. Mimecan/osteoglycin-deficient mice have collagen fibril abnormalities. *Molecular Vision* 8, 407-415.

Teng, C.C. 1963. Electron microscope study of the pathology of keratoconus: Part 1. *American Journal of Ophthalmology* 55, 18-47.

Troilo, D., Howland, H.C. and Judge, S.J. 1993. Visual Optics and Retinal Cone Topography in the Common Marmoset (Callithrix jacchus). *Vision Research* 33, 1301-1310.

Tsubota, K., Mashima, Y., Murata, H. *et al.* 1995. Corneal epithelium in keratoconus. *Cornea* 14, 77-83.

Tsuchiya, S., Tanaka, M., Konomi, H. *et al.* 1986. Distribution of specific collagen types and fibronectin in normal and keratoconus corneas. *Japanese Journal of Ophthalmology* 30, 14-31.

Tuori, A., Virtanen, I., Aine, E. *et al.* 1997. The immunohistochemical composition of corneal basement membrane in keratoconus. *Current Eye Research* 16

Turss, R., Friend, J., Reim, M. *et al.* 1971. Glucose concentration and hydration of the corneal stroma. *Ophthalmic Research* 2, 253-260.

Bibliography

Tyynismaa, H., Sistonen, P., Tuupanen, S. *et al.* 2002. A locus for autosomal dominant keratoconus: linkage to 16q22.3.Q23.1 in Finnish families. *Investigative Ophthalmology and Visual Science* 43, 3160-3164.

Walls, G.S. 1942. *The vertebrate eye and its adaptive radiation.* New York: Haffner.

Waring III, G.O. 1989. Making sense of keratospeak II: Proposed conventional terminology for corneal topographyy. *Refractive and Corneal surgery* 5, 362-367.

Weale, R.A. 1982. *A biography of the eye.* London: H.K. Lewis. pp74, 140

Wentz-Hunter, K., Cheng, E.L., Ueda, J. *et al.* 2001. Keratocan expression is increased in the stroma of keratoconus corneas. *Molecular Medicine* 7, 470-477.

Werblin, T.P. 1992. Astigmatism after cataract extraction: 6 year follow up of 6.5 and 12-millimeter incisions. *Refactive Corneal Surgery* 8, 448-458.

Wessel, H., Anderson, S., Fite, D. *et al.* 1997. Type XII collagen contributes to diversities in human corneal and limbal extracellular martrices. *Investigative Ophthalmology and Visual Science* 38, 2408-2422.

Whitelock, R.B., Fukuchi, T., Zhou, L.L. *et al.* 1997. Cathepsin G, acid phosphatase and alpha1-proteinase inhibitor messenger RNA levels in keratoconus corneas. *Investigative Ophthalmology and Visual Science* 38, 529-534.

Williams, K.A., Muehlberg, S.M., Lewis, R.F. *et al.* 1997. *The australian corneal graft registry 1996 report.* Adelaide: Mercury Press.

Wolfe, E. 1968. *Anatomy of the eye and orbit.* London.

Bibliography

Wollensak, G., Sporl, E. and Seiler, T. 2003. Treatment of keratoconus by collagen cross linking. *Ophthalmologe* 100, 44-49.

Wollensak, J. and Buddecke, E. 1990. Biomechanical studies on human corneal proteoglycan- a comparison of normal and keratoconic eyes. *Graefe's Archives for Clinical and Experimental Ophthalmology* 228, 517-523.

Woodward, E.J. and Morris, M.T. 1990. Joint hypermobility in keratoconus. *Ophthalmic and Physiological Optics* 10, 360-362

Worthington, C.R. and Inouye, H. 1985. X-ray diffraction study of the cornea. *International Journal of Biological Macromolecules* 7, 2-8.

Yamamoto, S., Hashizume, H., Hitomi, J. *et al.* 2000. The subfibrillar arrangement of corneal and scleral collagen fibrils as revealed by scanning electron and atomic force microscopy. *Archives of Histology and Cytology* 63, 127-135.

Zadnik, K., Barr, J.T., Edrington, T.B. *et al.* 1998. Baseline findings in the collaborative longitudinal evaluation of keratoconus (CLEK) study. *Investigative Ophthalmology and Visual Science* 39, 2537-2546.

Zimmermann, D.R., Trueb, B., Winterhalter, K.H. *et al.* 1986. Type VI collagen is a major component of the human cornea. *FEBS Letters* 197, 55-58.